State-of-the-Art Review on Ferroelectric Ceramic Materials

R. M. Gruver, W. R. Buessem, C. W. Dickey, et al.
Linden Laboratories, Inc.
State College, Pennsylvania

TECHNICAL REPORT AFML-TR-66-164

May 1966

Air Force Materials Laboratory
Research and Technology Division
Air Force Systems Command
Wright-Patterson Air Force Base, Ohio

DISCLAIMER NOTICE

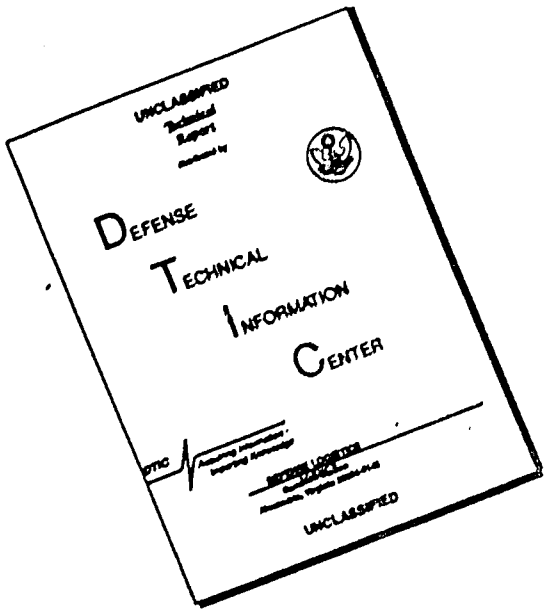

THIS DOCUMENT IS BEST QUALITY AVAILABLE. THE COPY FURNISHED TO DTIC CONTAINED A SIGNIFICANT NUMBER OF PAGES WHICH DO NOT REPRODUCE LEGIBLY.

STATE-OF-THE-ART REVIEW ON

FERROELECTRIC CERAMIC MATERIALS

R. M. Gruver, W. R. Buessem, C. W. Dickey, et al.

FOREWORD

This final report covers work performed during the period from February 1965 to March 1966. This contract was prepared by Linden Laboratories, Inc. for the United States Air Force under Contract No. AF 33(615)-2432. The work was initiated under Project No. 7381, "Materials Application", Task No. 738109, "Ceramics and Graphite Information". This program was technically administered under the direction of the Ceramics and Graphite Information Center, Materials Information Branch, Materials Applications Division, Air Force Materials Laboratory, Research and Technology Division at Wright-Patterson Air Force Base, Ohio with Mr. Barry P. Emrich serving as project engineer.

This report presents the results of a critical survey of the literature on ferroelectric ceramics and a presentation of the state-of-the-art by R. M. Gruver, W. R. Buessem, C. W. Dickey and J. W. Anderson. Dr. R. M. Gruver was the principal investigator for this project.

The authors gratefully acknowledge the assistance of Mr. Paul A. Marshall, Jr., Dr. H. P. Kirchner, and Mr. B. L. Joyner in discussing problems related to the project. They are indebted to Mrs. Norma Lee Gruver and Mr. Sam Wildstein for performing the library work involved in this survey.

The authors' thanks go also to Dr. L. E. Cross from The Pennsylvania State University, to Dr. R. Auty, Mr. J. Fabricius, Mr. M. Kahn, Mr. T. Prokopowicz and Mr. D. A. Payne of the Sprague Electric Company and Mr. D. W. Hamer of Erie Technological Products, Inc., for reading parts of the manuscript critically and for technical contributions.

Manuscript released by authors 12 May 1966 for publication as an AFML Technical Report.

This technical report has been reviewed and approved.

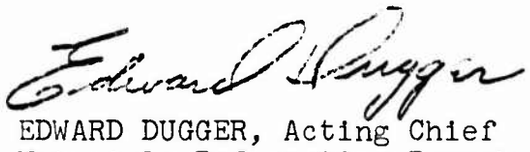

EDWARD DUGGER, Acting Chief
Materials Information Branch
Materials Applications Division
AF Materials Laboratory

ABSTRACT

This report presents a survey of ceramic systems exhibiting ferroelectricity together with fundamental data on ferroelectric crystals. A review of the basic reasons for the occurrence of ferroelectricity as well as for the dependence of the ferroelectric transitions and the properties of ferroelectric materials on the intensive parameters follows. The dielectric, piezoelectric and elastic properties of experimental and commercially available ceramic ferroelectrics are listed. The interpretation of dielectric properties of ceramic ferroelectrics as modified single-crystal properties includes a discussion of dielectric constant, stability, non-linear behavior and domain effects. Techniques for poling and special forming methods for ferroelectrics are described followed by a discussion of the linear and non-linear devices employing ferroelectric materials.

TABLE OF CONTENTS

ILLUSTRATIONS

ILLUSTRATIONS (Cont.)

LIST OF TABLES

STATE-OF-THE-ART REVIEW ON FERROELECTRIC CERAMIC MATERIALS

INTRODUCTION

The purpose and problems considered for this review are discussed below.

In the past twenty years since the discovery of ferroelectricity in barium titanate, many other inorganic ferroelectric materials such as lead titanate, lead metaniobate, potassium niobate, cadmium niobate and various solid solutions of these materials have been discovered and extensively investigated.

Many solid state devices have been proposed to exploit the unique ferroelectric and piezoelectric properties of these materials. The most prominent of these are various types of electro-mechanical transducers, the dielectric amplifier, information storage cell, frequency modulated oscillator, and ferroelectric energy converter. Although many experimental models of such devices have been built and operated, their full potential has not been realized due to several serious materials limitations such as dielectric and mechanical losses, time, temperature and frequency instability of ferroelectric characteristics, and unstable polarization states.

Numerous research programs have been directed toward obtaining a deeper understanding of the physical phenomena responsible for the above limitations. This review and analysis of efforts in this area have been made in order to contribute toward the successful exploitation of ferroelectric materials in Air Force systems.

The state-of-the-art review on ferroelectric ceramic materials attempts to cover the following major aspects of the field in detail:

1. A compilation of compositional, structural, and dielectric studies of ceramic systems exhibiting ferroelectricity.

2. The validity of various theoretical and experimental efforts designed to establish quantitative relationships between

single crystal and polycrystalline ceramic properties - dielectric, piezoelectric, and elastic. Problems and limitations involved in the deduction of ferroelectric and piezoelectric characteristics of ceramic materials from single crystal properties have been explored, and the complex influence of ceramic microstructure and particle size phenomena on polarization and domain dynamics described in all pertinent aspects.

3. A compilation of data on dielectric, piezoelectric, and elastic properties of ferroelectric ceramics, commercially available and experimental.

4. Degradation of ferroelectric ceramics under electrical stress.

5. Evaluations of various special techniques such as poling procedures, formation by devitrification of glass, and thin film fabrication of ferroelectric ceramics.

6. An analysis and characterization of non-linear behavior in ferroelectric ceramics based on work in this area, as well as application of these materials to non-linear devices such as modulators, harmonic generators, dielectric amplifiers and memory storage cells, together with dielectric and mechanical loss phenomena and their effect on device operation.

At an early date it was decided that the boundary of this review is outlined by the subject "ferroelectric ceramic materials". This excludes all materials which show no ferroelectricity over the whole temperature range, but it includes non-linear dielectrics which could possibly be ferroelectric, but for which no proof has been established. The other criterion, "ceramic", is somewhat ambiguous because at the present time the meaning of this word is shifting from "polycrystalline, inorganic, non-metallic materials, formed and densified by ceramic processes" towards the more general meaning "inorganic, non-metallic solid". The new meaning defines single crystals and amorphous thin films as ceramic materials as long as they are not organic or metallic. For the purpose of this review it does not make too much difference which definition is accepted, because single crystals will be discussed in either case.

It is important, however, that both definitions exclude organic ferroelectrics from the survey.

The information collected for this survey is classified roughly into three groups:

1. Research and Development
2. Manufacturing Processes and Commercial Products
3. Application: Design and Devices

The data collected are quite different for each group. In papers of Group 1 all reliable information was collected, especially that on stability which includes temperature range of ferroelectric and nonferroelectric phases as well as on the type of transformation (1st or 2nd order), heat of transformation and all constants of the free-energy function. These include Curie-Weiss constants, elastic constants and piezoelectric constants. In addition, K values as functions of temperature, time and frequency were collected together with data on structure type and lattice constants.

In papers of Group 2 the information extracted was different in quality and quantity. The organization of these data was largely determined (and limited) by whatever data the manufacturer chose to publish.

In Group 3 the information collected was determined by the quantitative tests which can be performed in the range of usability. Of primary interest here was information which could help to decide whether or not measurable material properties (such as the dielectric constants, loss tangent, piezoelectric and elastic constants, porosity, etc.) affect the performance of a device and in what way.

SUMMARY

This State-of-the-Art Review has been written with three groups of users in mind: (1) Designers of components and devices who want to be informed about the general range of properties of available ferroelectric materials. (2) Manufacturers and developers of ferroelectric materials who want to understand better the performance and, perhaps, deficiencies of present materials and who want to develop new and improved materials. (3) Researchers who want information on the amount of reliable experimental data available, where new data are most urgently needed and what level of sophistication and degree of agreement with experimental results has been reached in theoretical treatments.

For the first group data on commercially available dielectric and piezoelectric materials have been compiled with some discussion of their general stability and their use in linear and non-linear devices. For the second group data on the range of ferroelectricity in all known systems are presented and the important compounds in these systems are further characterized by important structural and thermodynamic data. Dielectric and piezoelectric properties of experimental bodies in these systems are presented and a quantitative treatment for deriving the properties of these bodies from the known or computed properties of the single crystals they contain is discussed. The research people will find many useful data, but more empty spaces in the tabulation of measured properties, indicating the great need for more experimental work in this area. A brief survey on the present status of ferroelectric theory shows the achievements as well as the deficiencies and the need for more work.

A few items of special importance have been singled out for a more extensive treatment.

The stability of ferroelectrics with time; i.e., aging and degradation, is discussed in great detail. Aging is defined

as the spontaneous change of all properties under zero external field conditions. It is proposed that aging is a gradual relaxation of mechanical stresses which results in a change in all piezoelectric and dielectric properties. Degradation of titanate dielectrics under dc stress is a slow deterioration process which eventually causes breakdown of the dielectric even under moderate stresses. The main degradation process is ionic in nature.

Thin film ferroelectrics permit the integration of numerous components and circuit elements; however, thin film capacitors show a more erratic performance in yield and stability than thin film resistors.

Devitrified ceramic ferroelectrics, materials with interesting properties, are formed by controlled crystallization during heat treatment of a glass. Details of the formation of silicate-free barium titanate crystals in a crystalline feldspar matrix and their resultant properties are presented.

Poling methods for ceramic ferroelectric materials are given. Barium titanate-type materials are heated to slightly above the Curie temperature and cooled in a dc field; this procedure permits the domains to be aligned as they are being created at the transition temperature. Lead-zirconate-titanate and lead metaniobate materials are poled in the same manner as barium titanate except that high conduction in the materials prevents the poling from being done at the Curie temperature. The field is applied at as high a temperature and for as long a time as necessary in order to align the maximum number of domains.

Non-linear devices that have attained a significant stature include dielectric amplifiers, non-linear capacitors, phase shifters and switches. These devices and the operative effect of mechanical and electrical losses in their piezoelectric ceramic transducers are described.

I. SURVEY OF CERAMIC SYSTEMS EXHIBITING FERROELECTRICITY

A. Introduction

The fundamental structural and dielectric data selected from the literature and arranged according to composition of compounds exhibiting ferroelectricity are presented in this section. Three criteria were used in selecting these data:

1. The data should be judged to be scientifically reliable and sound.

2. The data should be potentially useful in interpreting the behavior of existing ceramic ferroelectric materials or in developing new and improved ceramic ferroelectrics.

3. The data should be characteristic of a crystalline phase of well-defined composition and structure. This would include the basic thermodynamic properties as well as other intrinsic physical properties, but it would exclude properties which are largely "texture" sensitive.

As with all compilations and classifications of this kind, there are many open questions which can be decided upon only in a somewhat arbitrary way, and which are therefore open to criticism.

The following compilations thus are a compromise between the total amount of data available, the available space, the skill of the authors and the present state of the theory which is characterized by a fair success of the phenomenological (thermodynamic) approach.

B. Presentation of Data

In this section, the fundamental data collected during the program have been assembled into various tables and figures for presentation.

In Table I, the chemical formula for each compound is listed together with the temperature of the upper boundary

(Curie temperature) of the ferroelectric range in degrees Kelvin and, also in the last column in this table, the reference from which the data were taken is shown. All these data, in general, are for single crystal ferroelectrics. These compounds have been grouped according to structure type where possible.

The antiferroelectric compounds have been listed in Table II. In this case, the temperature of the upper boundary or transition temperature below which spontaneous antiparallel polarization takes place (similar to Néel temperature of antiferromagnetism) is listed for each compound. Several of these compounds become ferroelectric by application of an applied field.

In Table III, the solid solution systems between two single compounds which show evidence of ferroelectricity are listed. For many of these solid solutions a composition-versus-temperature diagram is given in Figure 1.1-1.29 showing the area where the material is ferroelectric (F), non-ferroelectric or paraelectric (NF) and antiferroelectric (A). In order to show the relationship of the solid solution to the oxide compounds, a ternary phase diagram is also presented for certain systems represented. Figures which are available but not shown may be found by using the reference listed.

In a quaternary phase diagram it is possible to have a series of solid solutions between either three or four single compounds. Table IVa shows the composition of the three-component solid solutions with areas of ferroelectricity at room temperature and Table IVb presents the diagrams showing ferroelectricity between four single compounds. The orientation of the plane of solid solution is shown in the tetrahedron of the oxide system. Table V is for a non-oxide system.

Much of the data presented in Table VI have been compiled in B. Singh's doctoral thesis (S3) and R. Pepinsky's AF-Report (P1) and have been used also by F. Jona and G. Shirane in their book (J1).

TABLE I

Range of Ferroelectricity for Single Compounds in °K

Chemical Formula	Upper Boundary**	Reference
1. Perovskite Type		
$BaTiO_3$	393	(J1)
$SrTiO_3$	≈ 40*	(J1)
$PbTiO_3$	763	(J1)
$CdTiO_3$	≈50-60	(J1)
$KNbO_3$	708	(J1)
$NaNbO_3$	73	(J1)
$AgNbO_3$	613	(P1)
$KTaO_3$	13	(P1)
$NaTaO_3$	<4	(P1)
$AgTaO_3$	758	(J1)
$RbTaO_3$	523	(J1)
2. Related Compounds		
WO_3	50	(J1)
3. Miscellaneous Oxides		
$Cd_2Nb_2O_7$	185	(P1)
$Sr_2Ta_2O_7$	193****	(J1)
$Sr_2(Ta_{0.8}Nb_{0.2})_2O_7$***	673	(J1)
$PbNb_2O_6$	843	(P1)
$PbTa_2O_6$	533	(P1)
$BaNb_2O_6$	343	(C4)

* Curie point obtained by extrapolation from R. T.

** Curie temperature

*** endpoint of solid solution with $Sr_2Ta_2O_7$

**** highest temperature investigated

Ferroelectric crystals with the reference (J1) can be found in the Appendix or Index of that reference.

TABLE I (Cont.)

Chemical Formula	Upper Boundary**	Reference
3. Miscellaneous Oxides (Cont.)		
$LiNbO_3$	1398	(A8)
$LiTaO_3$	723?	(P1)
$AgVO_3$	443-453	(J1)
$PbBi_2Nb_2O_9$	823	(J1)
$PbBi_2Ta_2O_9$	703	(J1)
$SrBi_2Nb_2O_9$	713	(J1)
$SrBi_2Ta_2O_9$	608	(J1)
$BaBi_2Nb_2O_9$	473	(J1)
$BaBi_2Ta_2O_9$	383	(J1)
$Bi_4Ti_3O_{12}$	948	(J1)
$BaBi_4Ti_4O_{15}$	663	(J1)
$SrBi_4Ti_4O_{15}$	803	(J1)
$PbBi_4Ti_4O_{15}$	843	(J1)
$Na_{0.5}Bi_{4.5}Ti_4O_{15}$***	928	(J1)
$K_{0.5}Bi_{4.5}Ti_4O_{15}$***	788	(J1)
$Pb_2Bi_4Ti_5O_{18}$	583	(J1)
$Sr_2Bi_4Ti_5O_{18}$	588	(J1)
$BaBi_3Ti_2NbO_{12}$	543	(P1)
$PbBi_3Ti_2NbO_{12}$	563	(P1)
$Pb_2(FeNb)O_6$	385	(J1)
$Pb_2(FeTa)O_6$	243	(J1)
$Pb_2(ScNb)O_6$	363	(J1)
$Pb_2(ScTa)O_6$	299	(J1)
$Pb_2(YNb)O_6$	580+	(J1)
$Pb_2(MgW)O_6$	310	(J1)

** Curie temperature
*** may not represent single compound
+ probably non-ferroelectric

TABLE I (Cont.)

Chemical Formula	Upper Boundary**	Reference
3. Miscellaneous Oxides (Cont.)		
$Pb_3(MgNb_2)O_9$	265	(J1)
$Pb_3(NiNb_2)O_9$	123	(J1)
$Pb_3(Fe_2W)O_9$	193++	(J1)
$Ba(Al_{1.4}Li_{0.6})(O_{2.8}F_{1.2})$***	423	(J1)
$Ba(Al_{1.7}Li_{0.3})(O_{3.4}F_{0.6})$	413	(J1)
$Pb_3V_2O_8$	373	(I8)
$AlNb_3O_9$		(C4)
Soluble Ferroelectric Compounds		
4. Sulfates		
$(NH_4)_2SO_4$	223.5	(J1)
$(ND_4)_2SO_4$	≈223	(P1)
NH_4HSO_4	270	(J1)
$RbHSO_4$	258	(J1)
$Li(N_2H_5)SO_4$		(J1)
$(NH_4)_2Cd_2(SO_4)_3$	95	(J1)
5. Phosphates		
KH_2PO_4	123	(J1)
KD_2PO_4	213	(J1)
KH_2AsO_4	97	(P1)
KD_2AsO_4	162	(J1)
RbH_2PO_4	147	(J1)
RbD_2PO_4	218	(J1)
RbH_2AsO_4	110	(J1)
RbD_2AsO_4	178	(J1)
CsH_2PO_4	159	(J1)
CsH_2AsO_4	143	(J1)
CsD_2AsO_4	212	(J1)

** Curie temperature
*** may not represent single compound
++ probably also antiferromagnetic

TABLE I (Cont.)

Chemical Formula	Upper Boundary**	Reference
6. Related Compounds		
$(NH_4)_2BeF_4$	176	(J1)
$(ND_4)_2BeF_4$	≈179	(J1)
$LiH_3(SeO_3)_2$	≈363	(P1)
$NaH_3(SeO_3)_2$	194	(J1)
7. Other Ferroelectrics		
$K_4Fe(CN)_6 \cdot 3H_2O$	248.5	(J1)
KNO_3	397	(J1)
$NaNO_2$	433	(J1)
$CaB_3O_4(OH)_3 \cdot H_2O$	270.5	(J1)
SbSI	295	(F1)
8. Questionable Ferroelectrics		
$Mg_3B_7O_{12}Cl$	538	(J1)
MnO_2	323	(J1)

** Curie temperature

TABLE II

Range of Antiferroelectricity for Single Compounds in °K

Chemical Formula	Upper Boundary**	Reference
1. Perovskite		
$NaNbO_3$***	627	(J1)
$PbZrO_3$***	503	(J1)
$PbHfO_3$***	488	(J1)
$PbTiO_3$	173	(J1)
2. Other Compounds		
Pb_2MgWO_6	312	(P1)
$CsH_3(SeO_3)_2$	145	(P1)
$(NH_4)_2H_3IO_6$	253	(P1)
$(ND_4)_2D_3IO_6$	260	(P1)
$Ag_2H_3IO_6$	≈205-245	(P1)
$Ag_2D_3IO_6$	≈245-285	(P1)
NH_4I	231	(P1)
$NH_4PF_6NH_4PF$	228	(P1)
3. Phosphates and Related Compounds		
$NH_4H_2PO_4$	148	(P1)
$ND_4D_2PO_4$	230	(P1)
$NH_4H_2AsO_4$	216	(P1)
$ND_4D_2AsO_4$	299	(P1)

** "Néel temperature"
*** can be driven into ferroelectric phase by application of electric field

TABLE II (Cont.)

Chemical Formula	Upper Boundary**	Reference
4. Sulfates and Related Compounds		
$(NH_4)_2SO_4$	223.5	(J1)
$(NH_4)_2BeF_4$	176	(J1)
NH_4HSO_4	154	(J1)
NH_4LiSO_4	283	(J1)
$(NH_4)_3H(SO_4)_2$	284	(J1)

** "Néel temperature"

TABLE IIIa

Solid Solutions Between Two Compounds
Containing Three Oxides

Figure No.	Solid Solution Composition	Reference, Page No.
1.1	$(Pb\text{-}Ba)TiO_3$	J1, (N5,36)
1.2	$(Pb\text{-}Sr)TiO_3$	J1, (N4,109)
1.3	$(Pb\text{-}Ca)TiO_3$	J1, I6,339
1.4	$(Sr\text{-}Ba)TiO_3$	J1, G9,502
1.5	$(Ca\text{-}Ba)TiO_3$	J1, 249
1.6	$(Ca\text{-}Sr)TiO_3$	J1, G9,502
1.7	$(Ba\text{-}Pb)ZrO_3$	J1, S13,221
1.8	$(Pb\text{-}Sr)ZrO_3$	J1, S13,224
1.9	$Pb(Zr\text{-}Ti)O_3$	J1, (D3,385)
1.10	$Pb(Ti\text{-}Sn)O_3$	I1, 1293(N1,113)
1.11	$Pb(Ti\text{-}Hf)O_3$	I1,1293 H4,261
1.12	$Pb(Zr\text{-}Sn)O_3$	I1, 1293
1.13	$Ba(Ti\text{-}Zr)O_3$	K1, 238
1.14	$Ba(Ti\text{-}Sn)O_3$	J1, (N1,114)
1.15	$K(Nb\text{-}Ta)O_3$	J1, (R2,1881)
1.16	$(K\text{-}Na)NbO_3$	J1, 266 (C8b,179)
1.17	$(Cd\text{-}Pb)_2Nb_2O_7$	J1, 266
1.18	$(Cd\text{-}Ca)_2Nb_2O_7$	J1, 266
1.19	$(Pb\text{-}Ba)Nb_2O_6$	J1, (S4,230)
1.20	$(Bi\text{-}La)FeO_3$	R1, 493
1.21	$Ba_{1-0.5x}(Ti_{1-x}\text{-}Nb_x)O_3$	J1, 255
Available	$(NH_4)_2(BeF_4\text{-}SO_4)$	J1, 343
"	$(Pb\text{-}Ba)HfO_3$	W1, 346
"	$NaNbO_3\text{-}SrNb_2O_6$	T1, 53
"	$NaNbO_3\text{-}Cd_2Nb_2O_7$	(L1,661), W2
"	$BaTiO_3\text{-}Bi_4Ti_3O_{12}$	A1, 895
"	$Na(Nb\text{-}Sb)O_3$	I2, 738
"	$Pb(ZrO_3\text{-}Nb_2O_6)$	D3, 385
"	$Pb(Ta_2\text{-}Nb_2)O_6$	S4, 230

TABLE IIIa (Cont.)

Figure No.	Solid Solution Composition	Reference, Page No.
Available	$(Ba\text{-}Y_{2/3})Nb_2O_6$	M3, 325
"	$(Ba\text{-}Sm_{2/3})Nb_2O_6$	M3, 325,326
"	$(Ba\text{-}La_{2/3})Nb_2O_6$	M3, 325
"	$Na(Nb\text{-}Ta)O_3$	I3, 162
Unavailable	$Cd_2(Nb\text{-}Ta)_2O_7$	J1
"	$Sr(Ti\text{-}La_{2/3})O_3$	T2

TABLE IIIb

Solid Solutions Between Two Single Compounds
Containing Four Oxides (in some cases
fifth oxide is present at a constant per cent)

Figure No.	Solid Solution Composition	Reference, Page No.
Available	$(PbTiO_3)$ - $(BiFeO_3)$	F5, 729 F6, 65
"	$(PbTiO_3)$ - $(NaNb_2O_6)$	T3, 574 B3, 139
"	$(BiFeO_3)$ - $(LaAlO_3)$	F7, 430
"	$(PbTiO_3)$ - $(KNbO_3)$	T3, 574
"	$(BaTiO_3)$ - $(Mn_2Nb_2O_7)$	K2, 569
"	$(PbZrO_3)$ - $(NaNbO_3)$	K3, 636
"	$(KSbO_3)$ - $(NaNbO_3)$	I2, 738
"	$(PbTiO_3)$ - $Pb(FeTa)_{0.5}O_3$	N2, 573
"	$(PbZrO_3)$ - $Pb(FeTa)_{0.5}O_3$	N2, 573
"	$[(PbHfO_3) - (PbTiO_3)] + 0.0125(PbNb_2O_6)$	H4, 261
"	$[(PbZrO_3) - (PbTiO_3)] + 0.025(PbNb_2O_6)$	D3, 385
"	$(PbTiO_3)$ - $(Sr_{0.3}La_{0.7}MnO_3)$	T4, 2238
"	$(Pb(Zr_{0.5}Ti_{0.5})O_3)$ - $(BiFeO_3)$	I4, 63
"	$[(PbZrO_3) - (PbTiO_3)] + 0.01(BiFeO_3)$	I4, 63
"	$[(PbHfO_3) - (PbTiO_3)] + 0.25PbSnO_2 + 0.0125PbNb_2O_6$	H4, 261
"	$PbTiO_3$ - $LaMnO_3$	H18, 51
"	$PbTiO_3$ - $PbMn_{1/2}Nb_{1/2}O_3$	H18, 51

TABLE IVa

Solid Solutions Between Three Single Compounds

Figure No.	Solid Solution Composition	Reference, Page No.
1.22	$Pb(Ti\text{-}Zr\text{-}Sn)O_3$	I1, 1293
1.23	$(Pb\text{-}Ba\text{-}Ca)TiO_3$	I1, 1293
1.24	$(Ba\text{-}Sr\text{-}Ca)TiO_3$	I1, 1293
Available	$Pb(Zr\text{-}Ti)O_3\text{-}PbNb_2O_6$	D3, 384
"	$Pb(Hf\text{-}Ti\text{-}Sn)O_3+0.0125PbNb_2O_6$	H4, 261
"	$Ba(Ti\text{-}Zr\text{-}Sn)O_3$	N3, 1522
"	$Pb(Ti\text{-}Zr)O_3\text{-}BiFeO_3$	I4, 63

TABLE IVb

Solid Solutions Between Four Single Compounds

Figure No.	Solid Solution Composition	Reference, Page No.
1.25	$(Ba\text{-}Ca)(Ti\text{-}Zr)O_3$	I1, 1293
1.26	$(Pb\text{-}Ba)(Ti\text{-}Zr)O_3$	I1, 1293
1.27	$(Pb\text{-}Sr)(Ti\text{-}Zr)O_3$	I1, 1293
1.28	$(Pb\text{-}Ba)(Ti\text{-}Sn)O_3$	I1, 1293
Available	$(Ba\text{-}Pb)(Ti\text{-}Nb)O_3$	S5, 256
"	$(Na\text{-}K)(Nb\text{-}Ta)O_3$	I3, 162
"	$(BaTiO_3)\text{-}(LaTiO_3)$	M5, 82

TABLE V

Non-Oxide System

Figure No.	Solid Solution Composition	Reference, Page No.
1.29	$(NH_4)_2(BeF_4\text{-}SO_4)$	J1, 343

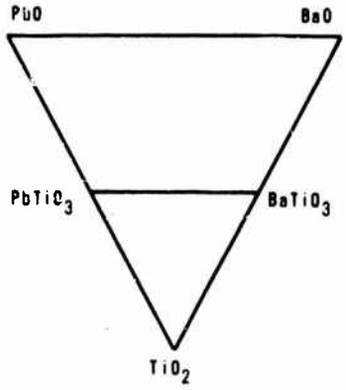

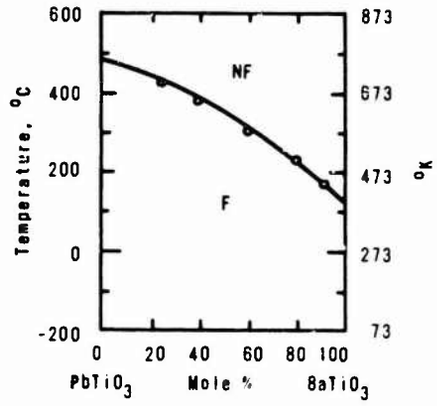

Fig. 1.1 System PbO-BaO-TiO_2

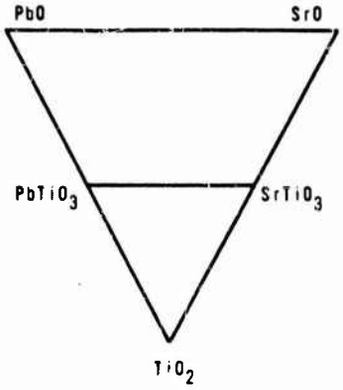

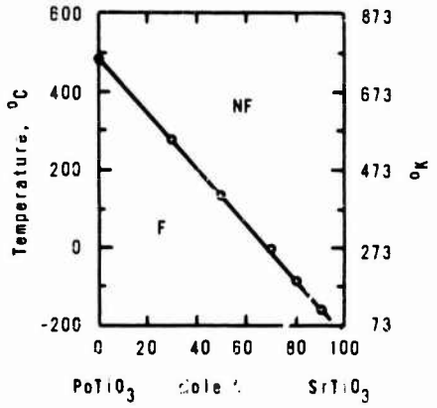

Fig. 1.2 System PbO-SrO-TiO_2

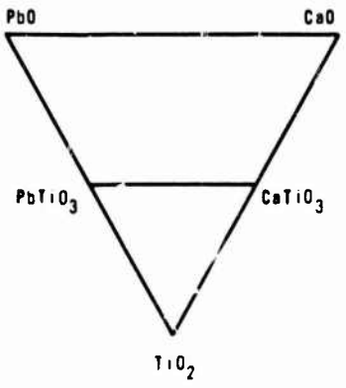

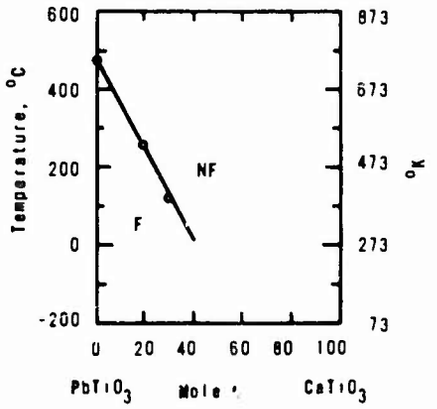

Fig. 1.3 System PbO-CaO-TiO_2

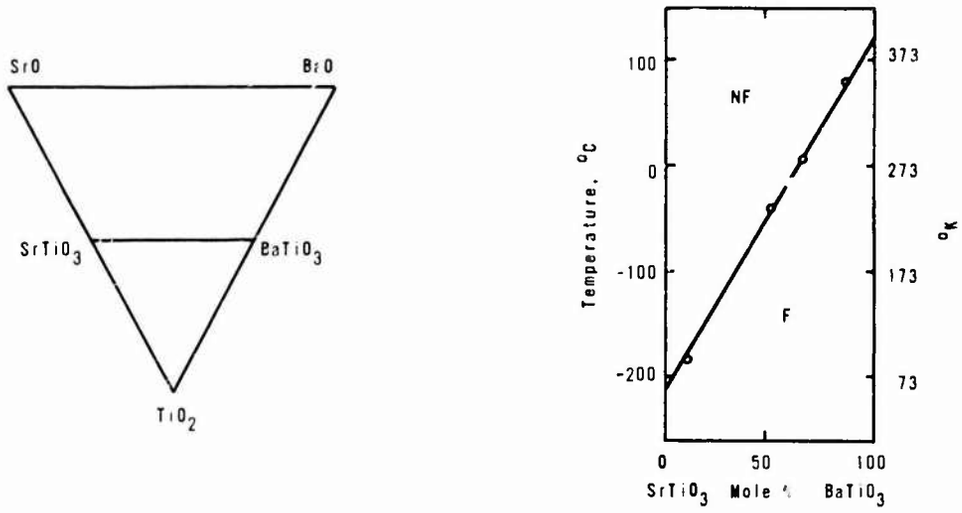

Fig. 1.4 System SrO-BaO-TiO_2

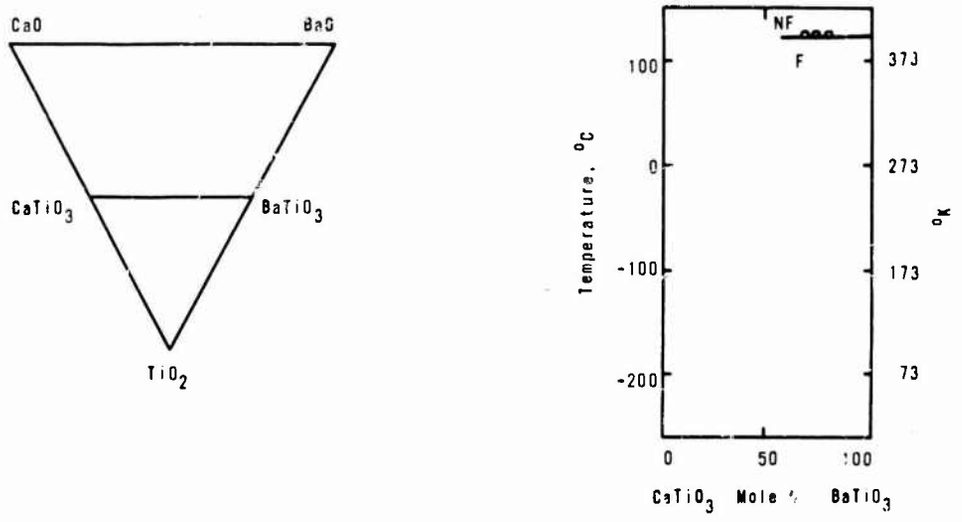

Fig. 1.5 System CaO-BaO-TiO_2

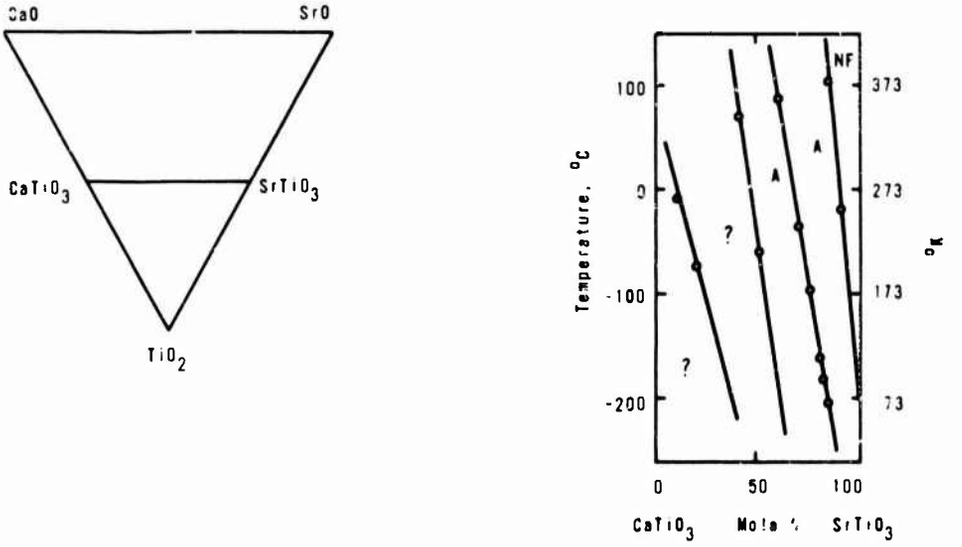

Fig. 1.6 System CaO-SrO-TiO_2

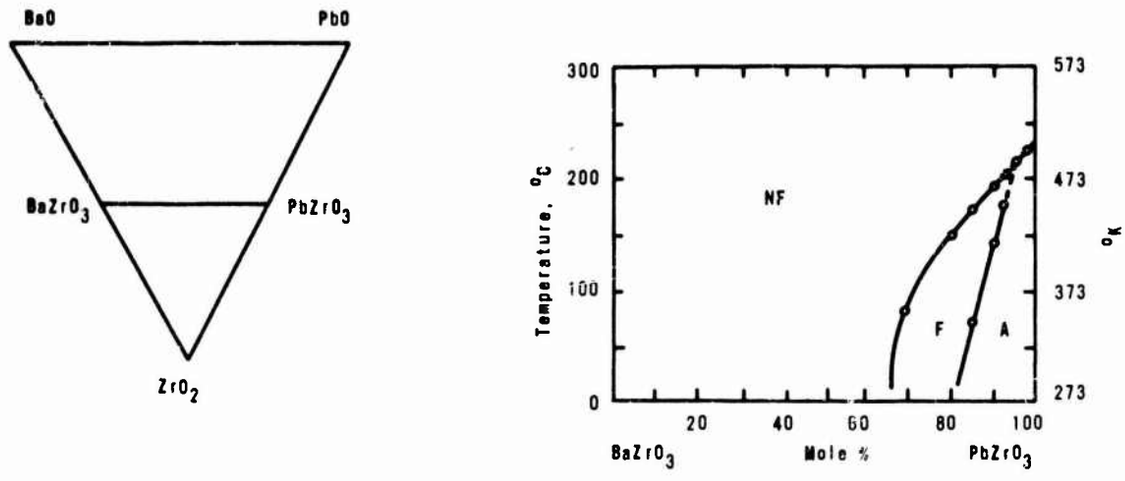

Fig. 1.7 System BaO-PbO-ZrO_2

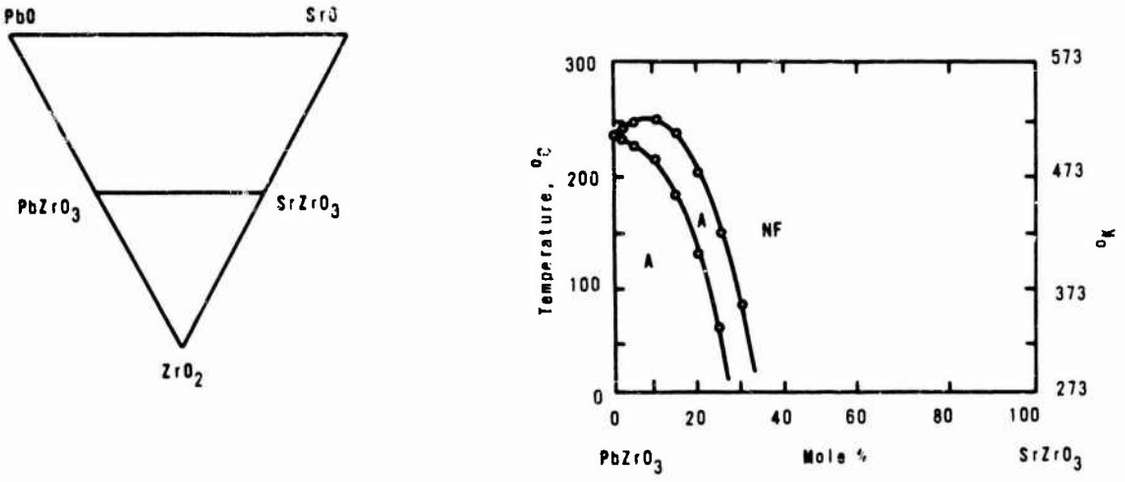

Fig. 1.8 System PbO-SrO-ZrO_2

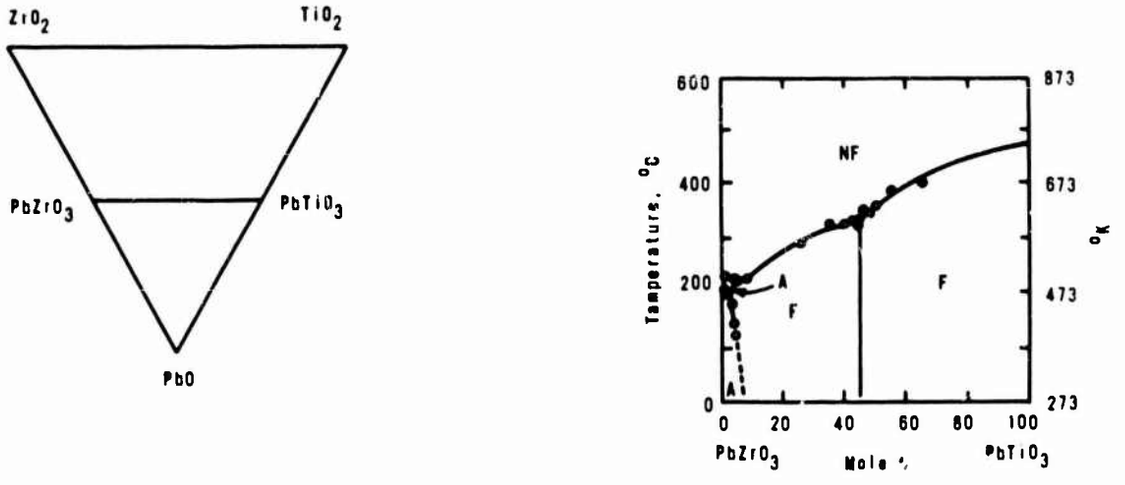

Fig. 1.9 System PbO-ZrO_2-TiO_2

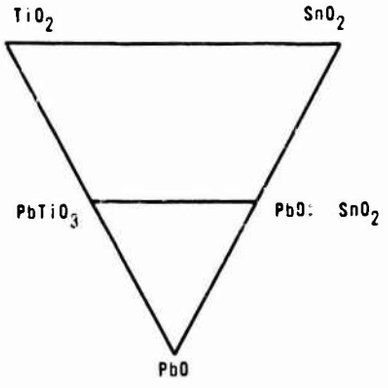

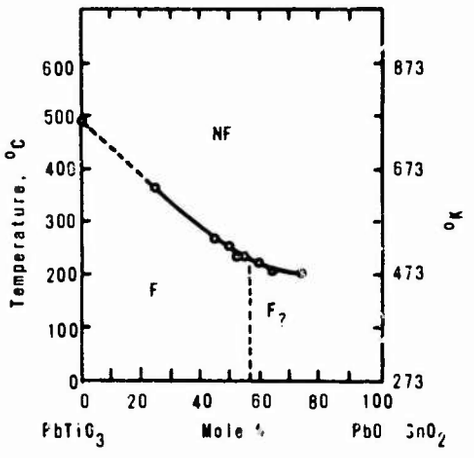

Fig. 1.10 System $PbO-TiO_2-SnO_2$

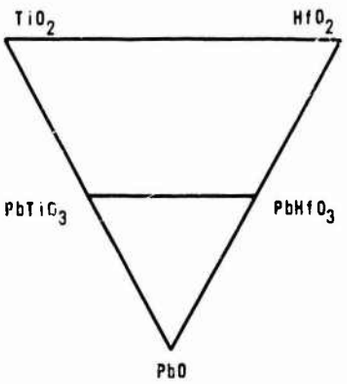

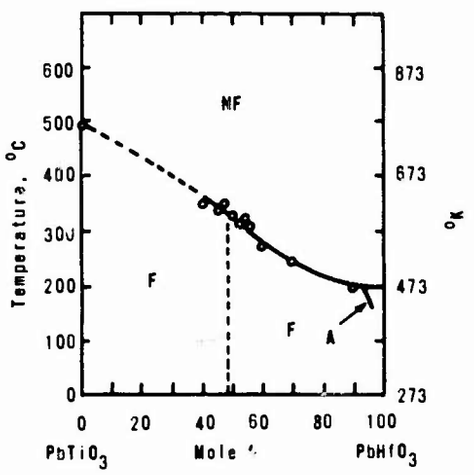

Fig. 1.11 System $PbO-TiO_2-HfO_2$

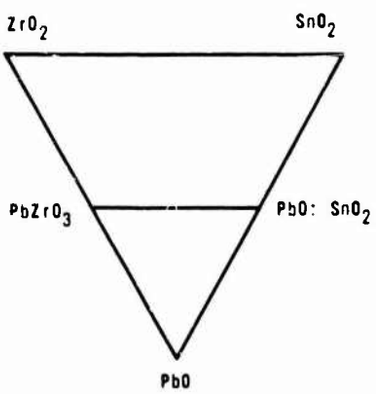

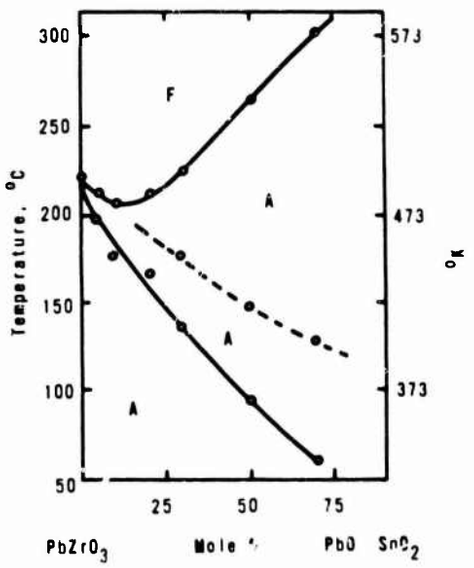

Fig. 1.12 System $PbO-ZrO_2-SnO_2$

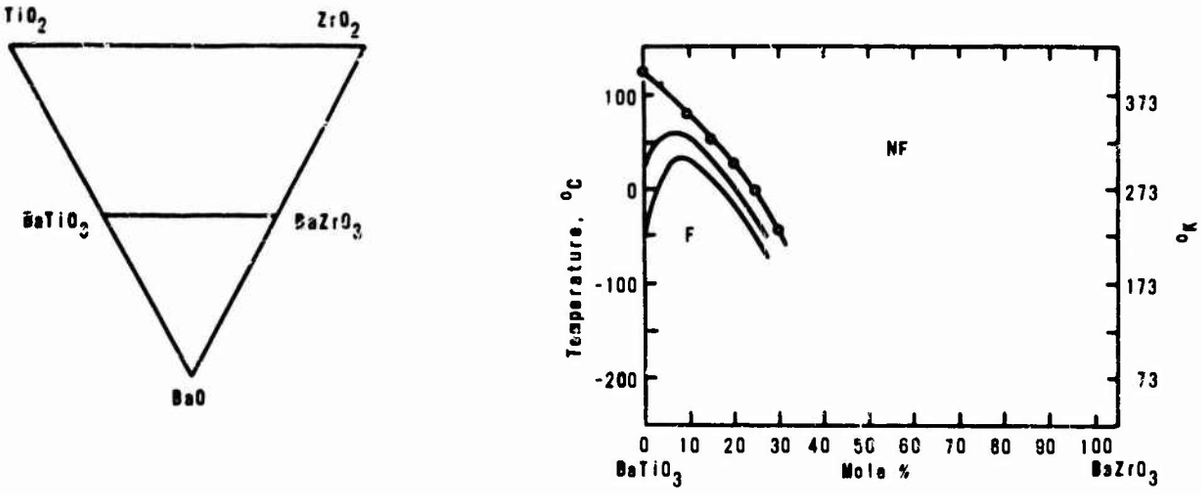

Fig. 1.13 System $BaO-TiO_2-ZrO_2$

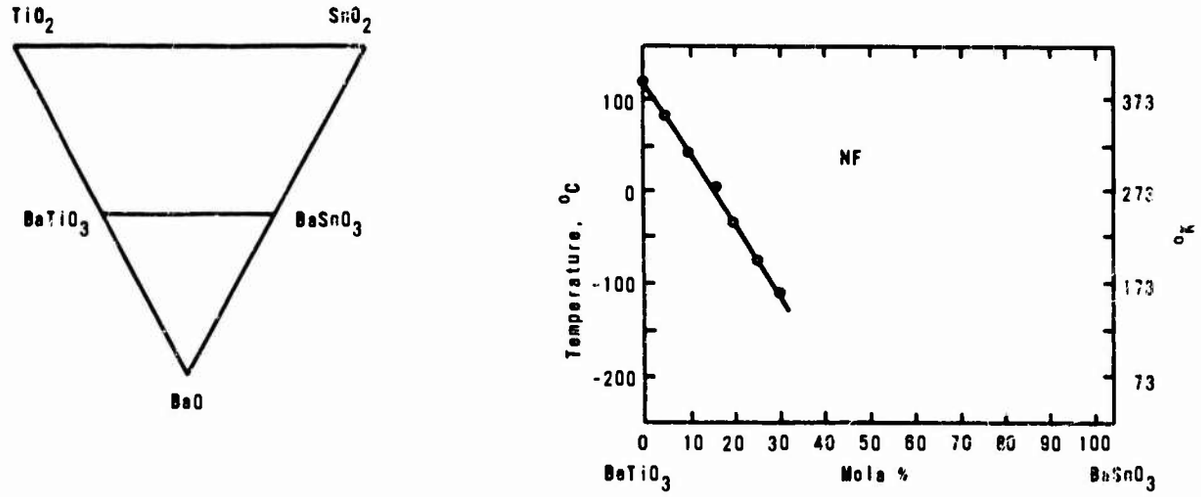

Fig. 1.14 System $BaO-TiO_2-SnO_2$

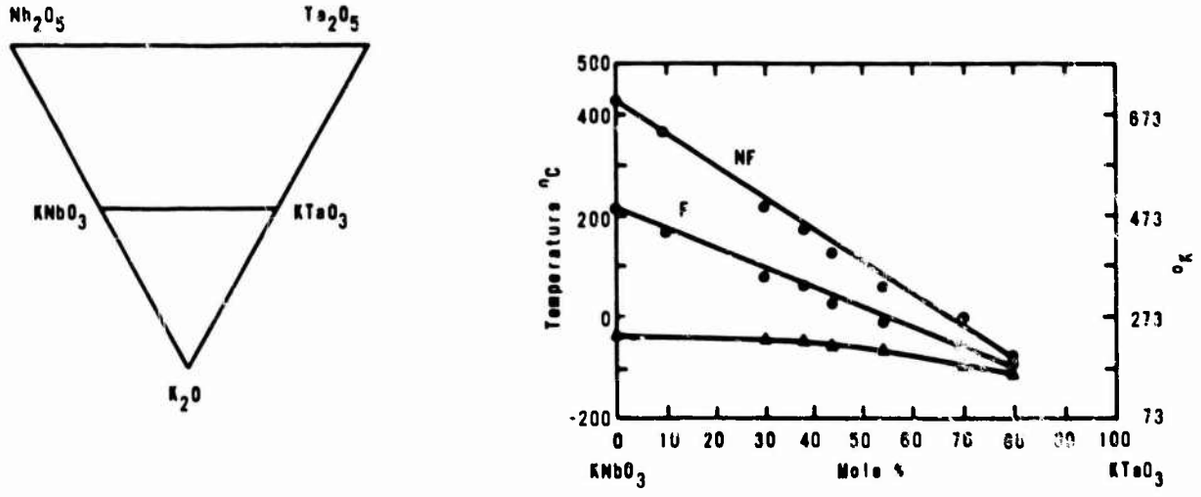

Fig. 1.15 System $K_2O-Nb_2O_5-Ta_2O_5$

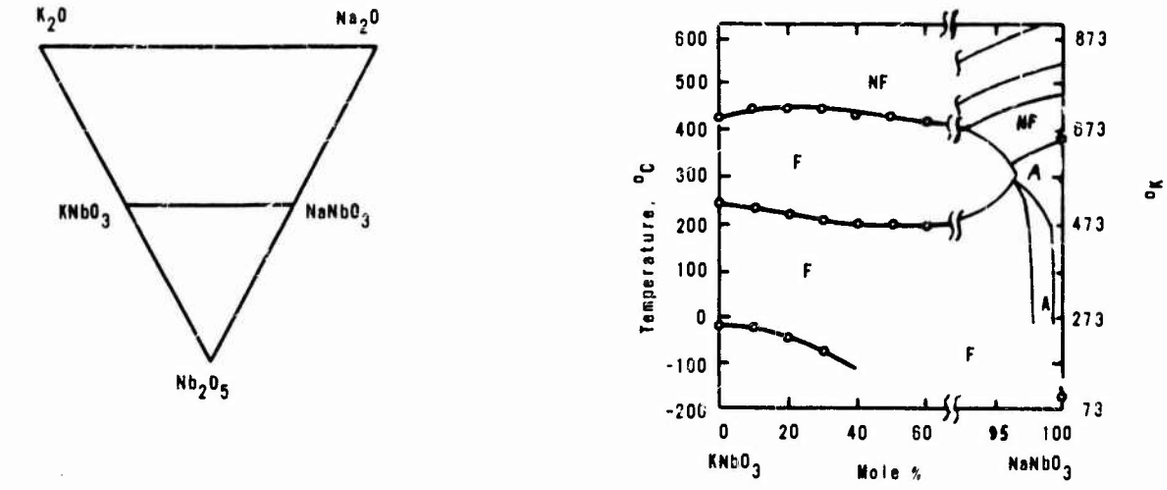

Fig. 1.16 System K_2O-Na_2O-Nb_2O_5

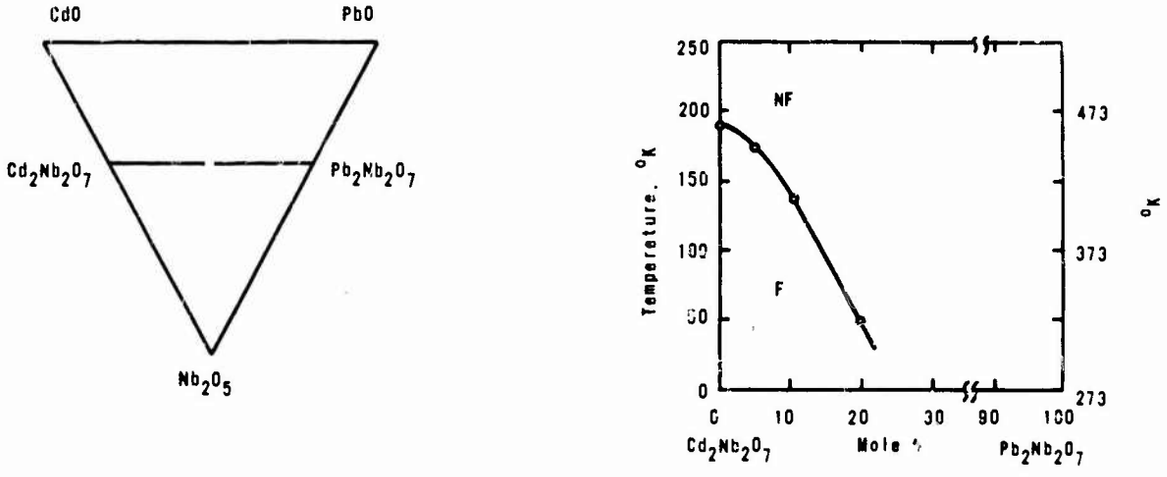

Fig. 1.17 System CdO-PbO-Nb_2O_5

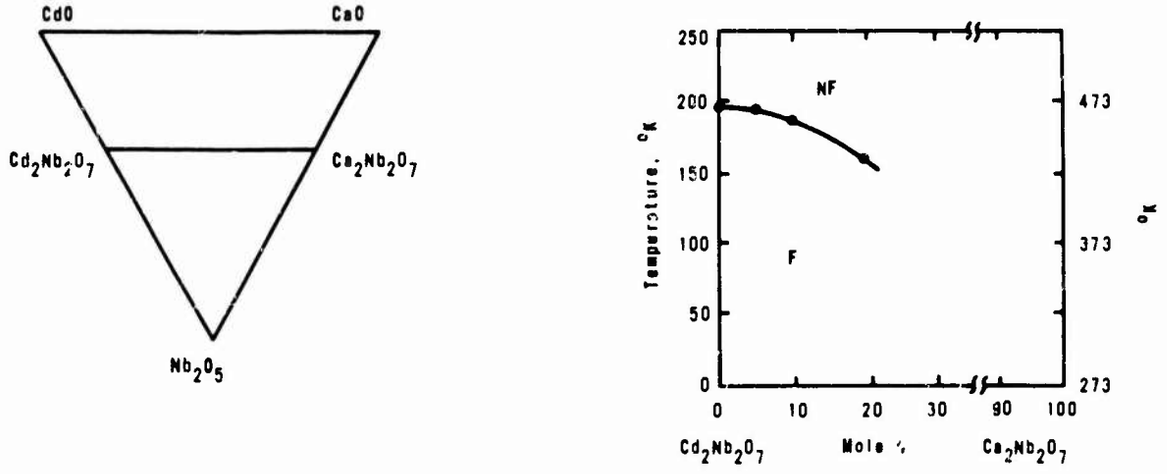

Fig. 1.18 System CdO-CaO-Nb_2O_5

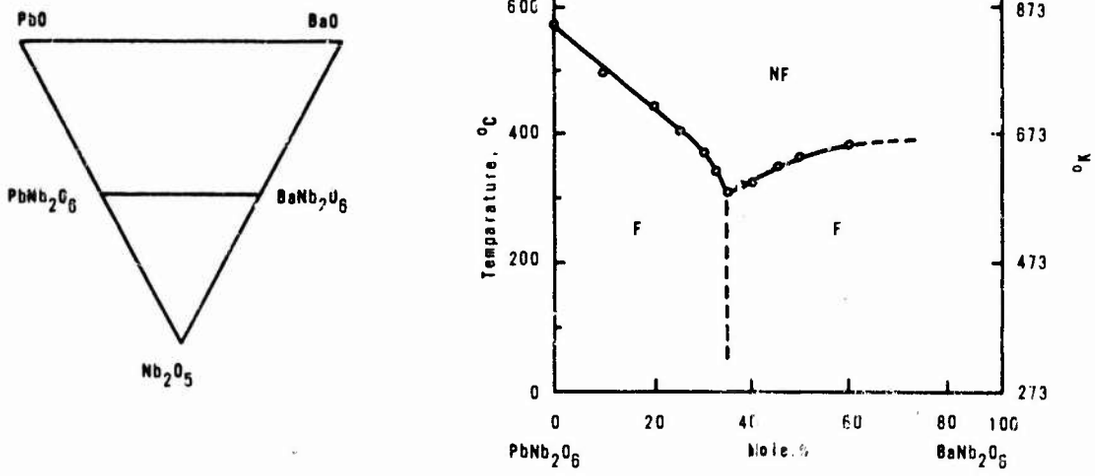

Fig. 1.19 System $PbO-BaO-Nb_2O_5$

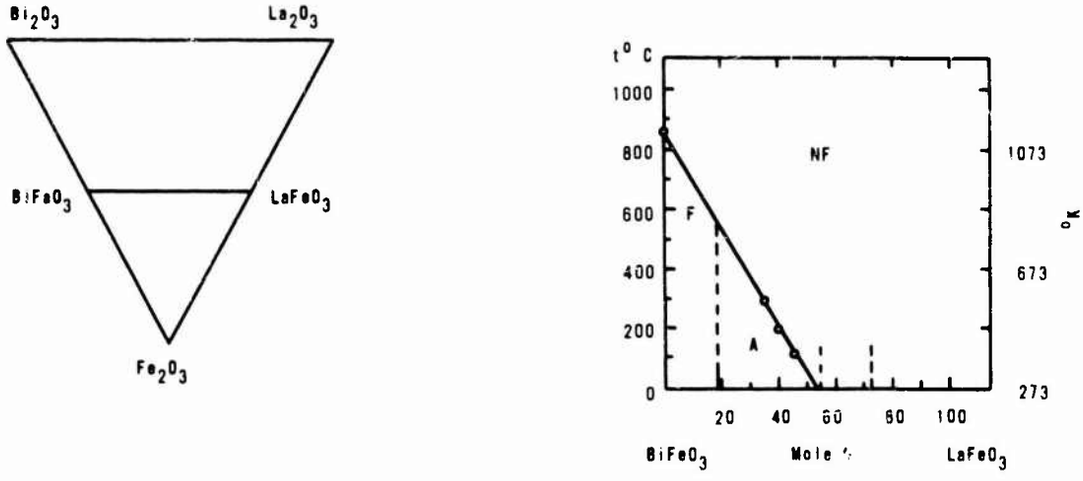

Fig. 1.20 System $Bi_2O_3-La_2O_3-Fe_2O_3$

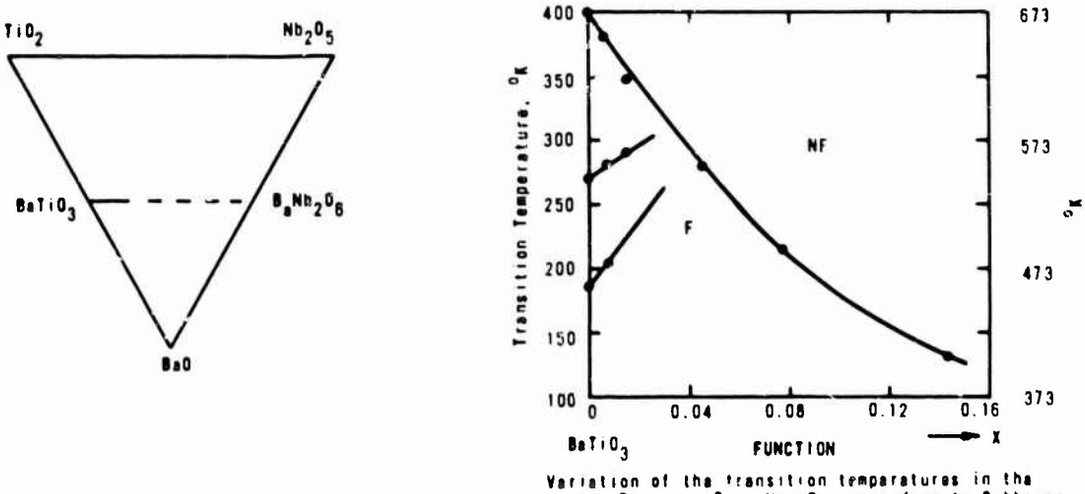

Variation of the transition temperatures in the system $Ba_{1-0.5x}(Ti_{1-x}Nb_x)O_3$ (according to Subbarao and Shirane (S48)).

Fig. 1.21 System $BaO-TiO_2-Nb_2O_5$

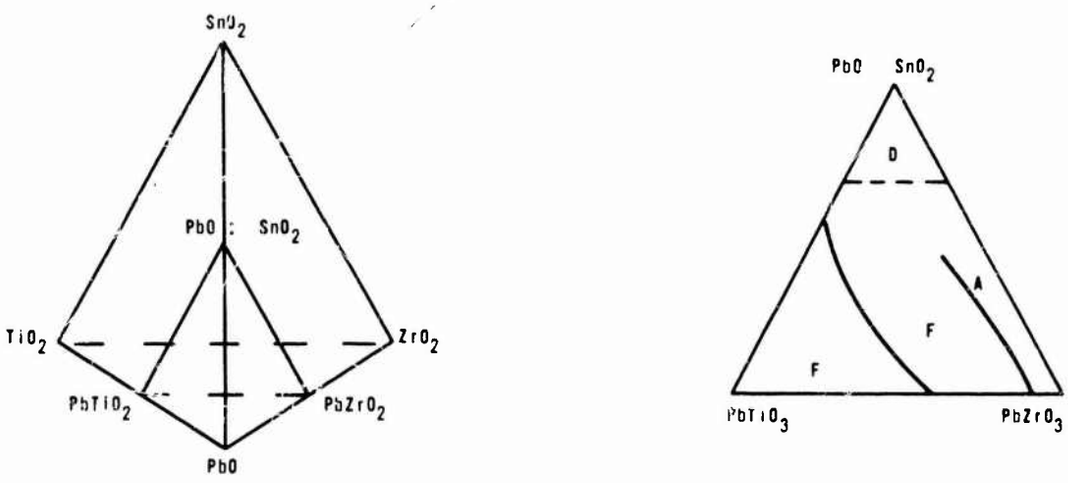

Fig. 1.22 System $PbO-TiO_2-ZrO_2-SnO_2$

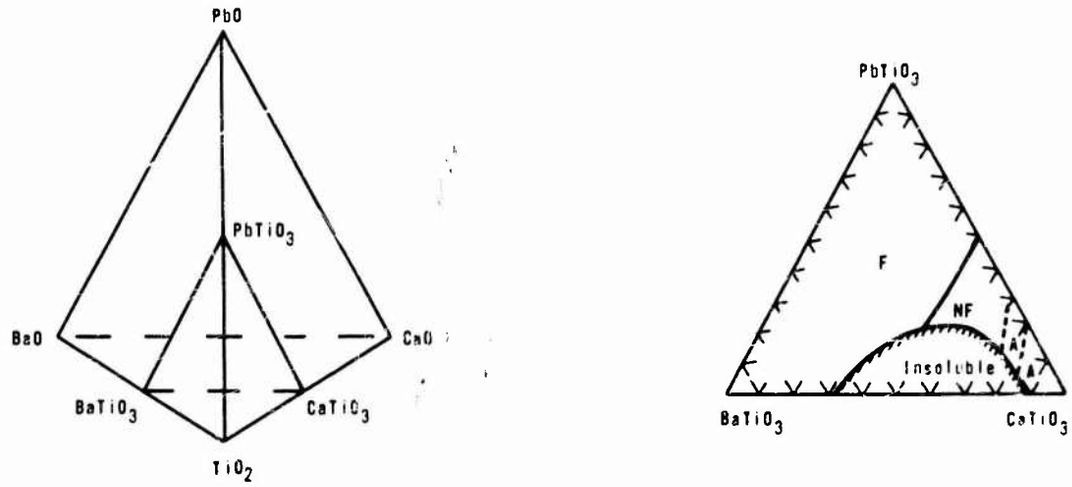

Fig. 1.23 System $PbO-BaO-CaO-TiO_2$

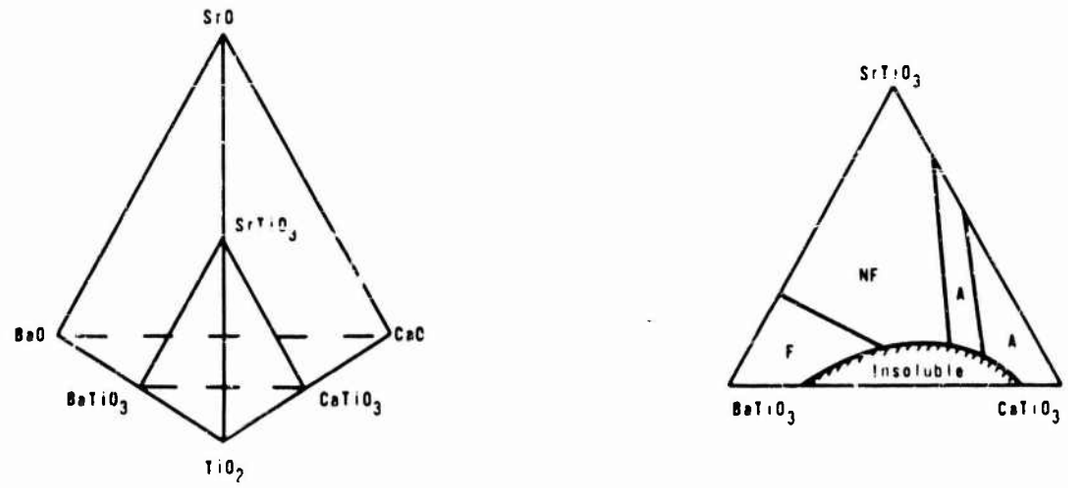

Fig. 1.24 System $Ba?-SrO-CaO-TiO_2$

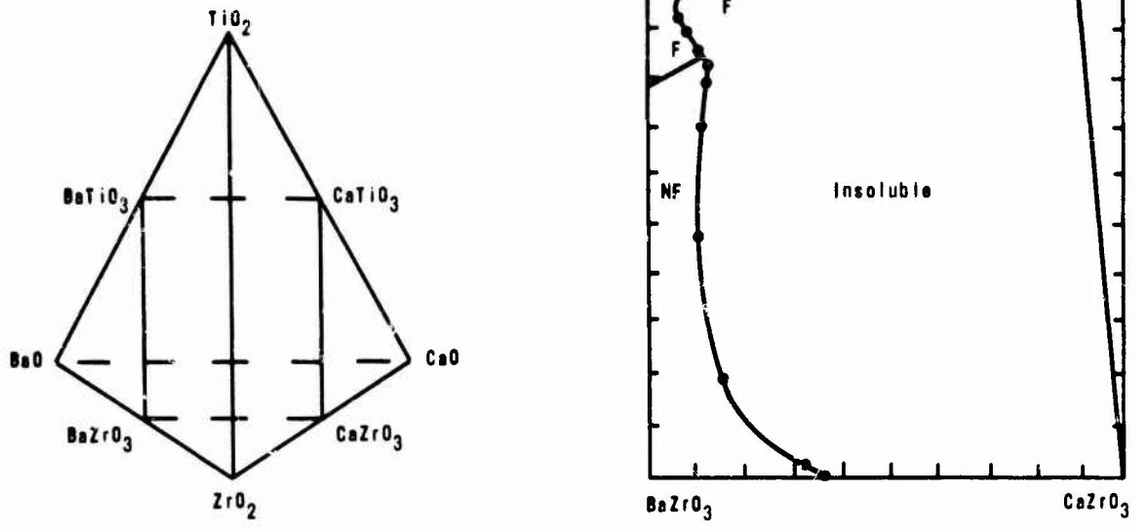

Fig. 1.25 System BaO-CaO-TiO_2-ZrO_2

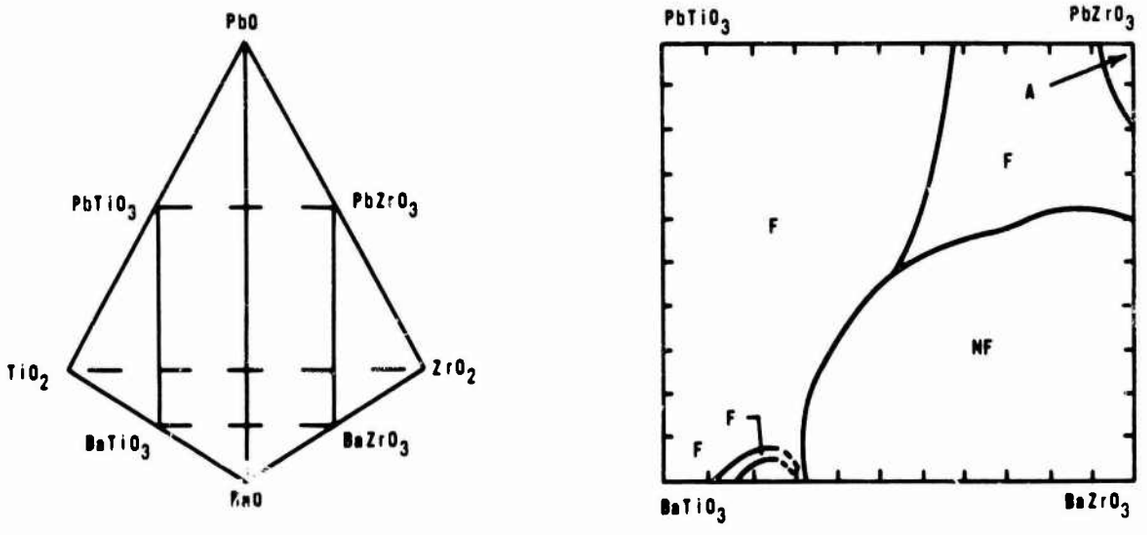

Fig. 1.26 System PbO-BaO-TiO_2-ZrO_2

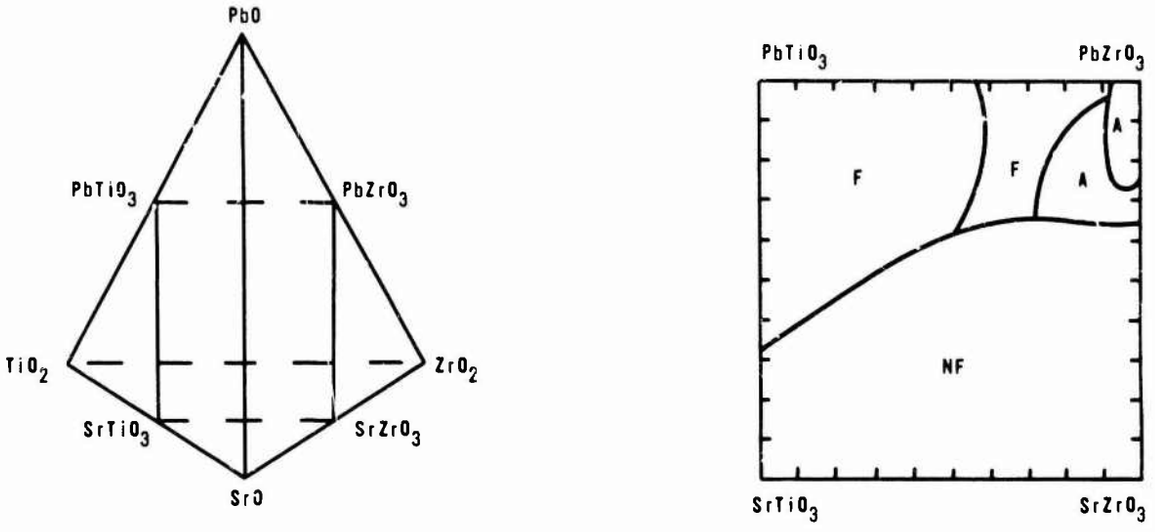

Fig. I.27 System PbO-SrO-TiO_2-ZrO_2

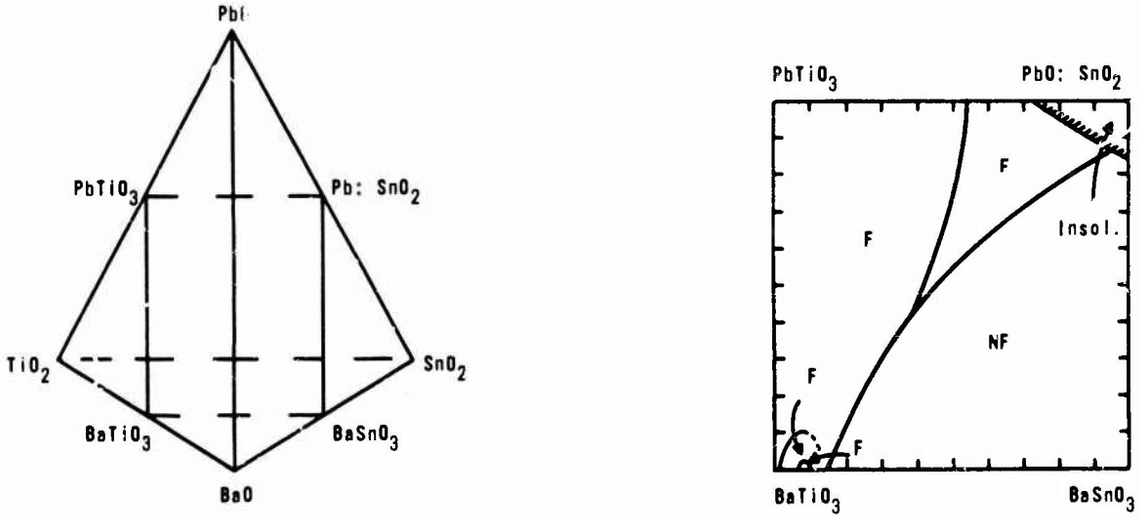

Fig. I.28 System PbO-BaO-TiO_2-SnO_2

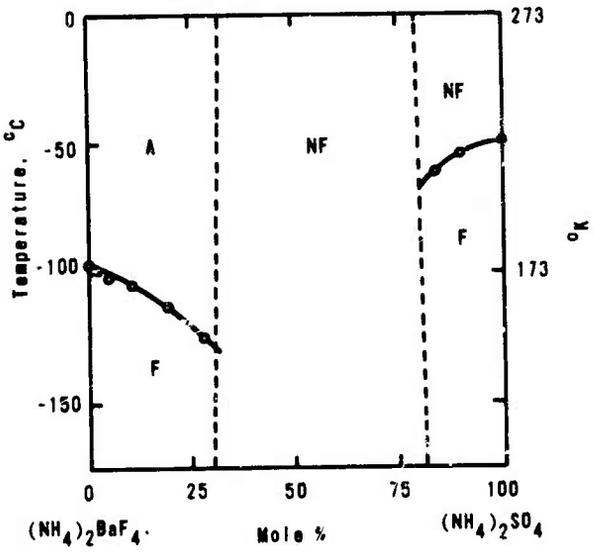

Fig. 1.29 System $(NH_4)_2\ BeF_4$ - $(NH_4)_2\ SO_4$

Symbols used in Table VI :

Lattice parameters are given in Ångstrom units. c/a is the axial ratio followed by the temperature at which the data were obtained in degrees Kelvin. The Curie constant ($C \times 10^{4}$°) and Curie-Weiss temp. difference ($T_c - T_o$) are given in °K. T indicates the transition temperature for each compound and includes the Curie temperature where reported. When known, the order of the transition (1st or 2nd order) follows the T temperature. P_s is the maximum spontaneous polarization expressed in units of 10^{-6} coulombs/centimeter squared. It is followed by the temperature in degrees Kelvin at which the maximum occurs. ϵ, the dielectric peak, is given at the temperature in degrees Kelvin where it occurs. The crystallographic axis of the measurement, the frequency in cycles per second and the external field in volts/mil are given when reported. (K equals one thousand cycles/second, M equals one million cycles/second and v equals volts/mil). E_c, the coercive field, is given in kilovolts/centimeter. The small signal dielectric constants, ϵ_a, ϵ_b and ϵ_c, are given at room temperature.

TABLE VI

Structural Data

Composition	Symmetry		Lattice Parameters						Curie-Weiss Law	
Perovskite Type	Class	Group	a Å	b Å	c Å	c/a	°K	References	$x10^4$ C	T_c-T_o
$BaTiO_3$	cubic	m3m	4.01				473			
	tetra	4mm	3.992		4.036	1.010	293	P1	17.3	11
	ortho	mm	5.682	5.669	3.990	1.006	263	J1		
	rhomb	3m	3.998				173			
$SrTiO_3$	cubic		3.905					J1	8.3	38
$PbTiO_3$	cubic	m3m						P1		
	tetra	4mm	3.904		4.150	1.063	293	M1	11.0	
$CdTiO_3$	ortho		10.834	10.695	7.615		293	J1	4.5	
$KNbO_3$	cubic	m3m	4.021							
	tetra	4mm	3.997		1.017	1.017		P1		
	ortho	mm2	4.038		3.971	0.983		J1	24.0	58
	rhomb	3m	4.016					M1		
$NaNbO_3$	cubic		3.942					P1		
	tetra		2x3.933		4x3.942	1.0015		J1		
	tetra		2x3.924		4x3.924	1.0023		M1		
	ortho	222	5.568	5.505	15.518	1.009	293	M21		
	monoc		5.564	5.548	7.812		113			
$AgNbO_3$	cubic		3.96				923	P1		
	tetra		3.95		3.96		823	J1	18	
	ortho		3.944	3.944	3.926	0.993	393			
$KTaO_3$	cubic	m3m	3.989					P1	6.1	14
								J1		
$NaTaO_3$	ortho		5.513	5.494	2x3.875		293	P1		
	ortho		3.890			0.998		M21		
$AgTaO_3$	ortho		3.931			0.992	293	J1		
$RbTaO_3$	tetra							M21		
$LiTaO_3$	trig	3m						P1		
								J1		
$NaVO_3$								J1		
$AgVO_3$								J1		
Complex Perovskite Type										
WO_3	tetra	4/mmm	5.272		3.920		1223	M21		
	monoc	2	7.274	7.501	3.824		293	P1		
								J1		
$Pb(Sc_{0.51}Nb_{0.5})O_3$	tetra		4.074		4.082	1.002		J1		
$BaNb_{1.5}Zr_{0.25}O_{5.25}$	tetra		12.670		4.017			G10		
	ortho	222								
Misc. Oxides										
$Sr_2Ta_2O_7$	tetra		10.63		10.91			P1		
$PbNb_2O_6$	tetra		12.46		3.907			P1	30	
	ortho		17.51	17.82	2x3.86	1.017	298	J1		
								M1		
$PbTa_2O_6$	ortho							P1		
	ortho		17.68	17.72	2x3.877	1.002		J1	15	
								M1		
$LiNbO_3$	rhomb	3	5.492					P1		
								M21		

Thermodynamic Data at Transition Temperature				Dielectric Data						
Phase Change		Entropy Change	Enthalpy Change	Spontaneous Polarization		Dielectric Peak		Coercive Field	Dielectric Constant (at Room Temp.)	
T °K	Order	ΔS Cal/mol°C	ΔH Kcal/mol	Polar Axis	Maximum Ps		Temp. °K	Ec	ϵ_a/ϵ_o ϵ_b/ϵ_o	ϵ_c/ϵ_o
393	1	0.12-0.13	0.049	[001]	26	$\epsilon_a \approx 10,000$	393	0.5	≈5,000 ≈5,000	≈160
278	1	0.06-0.09	0.021	[110]	at 29€°	7,000	278			
183	1	0.04-0.07	0.011	[111]		4,000 10K	183	at 298°		
82					3	2,000			≈250	
43					at 4.2°					
763	1	1.51	1.51	[001]	80	$\epsilon_c \approx 800$				
173		1.51		[001]	at 173°	1M at 2v			≈50	
50-60									≈250	
708	1	0.19-0.27	0.19	[001]	26	$\epsilon_a \approx 4,500$		0.5		≈500
498	1	0.17	0.085	[110]	at 683°	2,000				
						900				
263	1	0.14	0.032	[111]		10K at 5v				
913	1	0.7	0.050			$\epsilon_a \approx 2.700$	835	≈60		
835	1								76 76	≈670
627	1					10K at 5v				
73				A [001]	12					
823				[001]	very	900	613			
598					small	400	333	30		
						500K				
708						$\epsilon \approx 6,000$				
13						1K at 10v				
903										
853										
753										
758										
643										
523										
(723)				trig c	12 at 573°	≈300		10 at 573°		≈170
(653)										
(448)										
1183		0.24	0.280	NF		$\epsilon_a \approx 90,000$				
1013		0.45	0.450	A						
603				A		$\epsilon_a \approx 40,000$				
223				F	10 at 223°					
363										
						≈20,000				
193										
843	1			[010]	Pr≈0.6	$\epsilon_c \approx b$ 22,000 500K		17		
533				_ to c	8 -10	$\epsilon_c \approx 4,000$ 10K		25	≈300	
(723)										

TABLE VI (Cont.)

Structural Data

Composition	Symmetry		Lattice Parameters						Curie-Weiss Law	
Misc. Oxides	Class	Group	a Å	b Å	c Å	c/a	°K	References	$\times 10^4$ C	$T_c - T_o$
$Cd_2Nb_2O_7$	cubic tetra tetra	m3m	10.372 10.364 10.378			1.0005 1.0011	298 123 133	P1 M21 M1	7	
$Sr_2Ta_2O_7$	tetra		10.63		10.91			P1		
$PbNb_2O_6$	tetra ortho		12.46 17.51	17.82	3.907 2x3.86	1.017	298	P1 J1 M21	30	
$PbTa_2O_6$	ortho ortho		17.68	17.72	2x3.877	1.002		P1 J1 M1	15	
$LiNbO_3$	rhomb	3	5.492					P1 M1		
$Pb_2Ta_2O_9$	tetra							P1		
$Pb_3(MgNb_2)O_9$	tetra							P1		
$PbBi_2Ta_2O_9$	tetra				25.4			P1		
$BaBi_3Ti_2NbO_{12}$	tetra							P1		
$PbBi_3Ti_2NbO_{12}$	tetra							P1		
$BaBi_4Ti_4O_{15}$	tetra							P1		
$PbBi_4Ti_4O_{15}$	tetra				41.4			P1		
$BiFeO_3$	rhomb		3.963					R1		
$Ba(Al_{1.4}Li_{0.6})(O_{2.8}F_{1.2})$	hex		10.44		8.77		298	J1		
$BaThO_3$	cubic		4.497					B1		
MnO_2	tetra							P1		
$Bi_4Ti_3O_{12}$	ortho		5.411		32.83	1.007	298	S20		
$PbBi_2Nb_2O_9$	tetra		5.492	5.503	25.53			J1		
Sulfates										
$(NH_4)_2SO_4$	ortho ortho	mmm mm	7.729	10.560	5.951		298	P1 J1 M1		
NH_4HSO_4	monoc monoc tric	2/m m 1	14.51 14.26 14.24	4.54 4.62 4.56	14.90 14.80 14.81			P1 J1 M1		
$RbHSO_4$	monoc monoc	2/m m	14.36	4.62	14.81			P1 J1, M1		
$LiH(N_2H_5)SO_4$	ortho	mm	8.97	9.91	5.18			P1 J1		
$(NH_4)_2Cd_2(SO_4)_3$	monoc cubic	2(?) 23	10.360					P1 J1		
$(NH_4)Fe(SO_4)_2 \cdot 12H_2O$	cubic monoc	23 2	12.318				298	P1 J1		
Phosphates										
KH_2PO_4	tetra tetra ortho	42m 42m mm	7.453 10.495 10.458	7.453 10.540	6.959 6.919 6.918		273 123 77	P1 J1	0.33	0
KD_2PO_4	tetra	42m	7.453		6.930		273	M1, P1 J1, M21		
$(NH_4)_2BeF_4$	ortho	mm	7.49	10.39	5.89		298	P1 J1, M1		

Thermodynamic Data at Transition Temperature				Dielectric Data							
Phase Change		Entropy Change	Enthalpy Change	Spontaneous Polarization		Dielectric Peak		Coercive Field	Dielectric Consta (at Room Temp.)		
T °K	Order	ΔS Cal/mol°C	ΔH Kcal/mol	Polar Axis	Maximum Ps		Temp. °K	Ec	ϵ_a/ϵ_o	ϵ_b/ϵ_o	ϵ_c/ϵ_o
185	1	0.09	0.018	[111]	6 at 88° 10K at 5v	ϵ_{111}≈1200		10 at 89°		≈310	
193											
843	1			[010]	Pr=0.6	$\epsilon_{c\approx b}$ 22,000 500K		17			
533				1 to c	8-10	ϵ_c≈4000 10K		25		≈300	
(723)											
703											
543											
563											
663											
843											
1123											
(423)					0.1 at 298°			5 at 298°		10	
260											
323				tetra c		ϵ_c 20x10^5 20K at 5v					
948				ortho b	6 at 498°	ϵ_b 570 10K at 10v		30 at 498°			
823											
223	1	4.2	0.93	ortho c	0.45 <223°	$\epsilon_{c\approx155}$ 10K at 5v	223	4 at 213° 12 at 200°	10	9	9
270	2	0.5	0.12	monoc c	0.87 >154°	$\epsilon_{c\approx1420}$ 16-6	270	0.15 at 260°			16
154	1	2.1	0.34			10K	154	1.1 at 154°			
258	2			monoc c	0.65 at 107°	$\epsilon_{c\approx240}$ 10K at 5v		3 at 173° 22 at 123°	7	8	10
None (77 to 413)				ortho c [001]	0.3 at 298°	none 77°-413°		0.32 at 298°			14
95	1		1.00	[100]	0.5 at 93°	$\epsilon_{100\approx40}$ 10K		15 at 93°			
88					0.4			33			
123	2	0.74	0.087	tetra c	4.6 <125°	$\epsilon_{c\approx47,500}$ 800 at 200v		(see J1)			50
213		0.47	0.100	tetra c	4.8				88	88	90
176	1	1.90	0.31	ortho b	0.22 at 153°	$\epsilon_{b\approx55}$ 10K at 5v		1.6 at 153° 12 at 135°	9	10	9

TABLE VI (Cont.)

Structural Data

Composition	Symmetry		Lattice Parameters						Curie-Weiss Law		
Phosphates (Cont.)	Class	Group	a Å	b Å	c Å	c/a	°K	References	$\times 10^4$ C	T_c	T_o
$(ND_4)_2BeF_4$	ortho							P1 J1, M1			
$LiH_3(SeO_3)_2$	monoc	m	6.26	7.89	5.43			P1 J1, M1			
$NaH_3(SeO_3)_2$	monoc	2/m						P1 J1, M1			
Miscellaneous Ferroelectrics											
$K_4Fe(CN)_6 \cdot 3H_2O$	monoc	2/m	9.38	16.84	9.40			P1 J1, M1			
KNO_3	rhomb ortho	3m mmm	4.365 6.431	9.164	5.414		299	P1 J1, M1			
$RbNO_3$	cubic trig		4.36 10.48		7.45			D1			
$NaNO_2$	ortho ortho	mmm mm	5.33 5.390	5.68 5.578	3.69 3.570			P1 J1, M1			
$Ca_2B_6O_{11} \cdot 5H_2O$	monoc	2/m	8.743	11.264	6.102 $\beta=110°7'$			P1 J1, M1	0.05		
SbSI								F1			
Questionable Ferroelectrics											
$Mg_3B_6O_{12}Cl$	cubic ortho	43m mm						P1 J1			
Antiferroelectrics											
$PbZrO_3$	ortho		5.88	11.76	8.20	0.988		P1 J1, M1	12	185	
$PbHfO_3$	ortho		4.136		4.099	0.991		P1 J1, M1			
Pb_2MgWO_3								P1			
$(NH_4)_3H(SO_4)_2$	monoc	2/m m 1	14.51	4.54	14.90			P1 J1 M1			
$NH_4H_2PO_4$	tetra ortho	42 222	7.479		7.516		273	P1 J1 M21			

Thermodynamic Data at Transition Temperature				Dielectric Data							
Phase Change		Entropy Change	Enthalpy Change	Spontaneous Polarization		Dielectric Peak		Coercive Field		Dielectric Constant (at Room Temp.)	
T °K	Order	ΔS Cal/mol°C	ΔH Kcal/mol	Polar Axis	Maximum Ps		Temp. °K	Ec	ϵ_a/ϵ_o	ϵ_b/ϵ_o	ϵ_c/ϵ_o
179		2.27	0.38	ortho c	0.19 at 163°				9	10	9
none				⊥ to [001]	15 (363-77°)	none		1.4 at 293° 27 at 73°	29	13	30
194	1	0.97	0.19	[103]	6.5 >94° 4.3 <94°	$\epsilon_{132} \approx 250$	194	32 at 183° 22 at 80°			
248	2			[101]	1.4 at 233°	$\epsilon_{101} \approx 1500$ 1M					
397 383	1		≈1.1	trig ortho b	6.3 at 394°	$\epsilon_c \approx 44$ 1M		4.5 at 394°		7	
437				trig c							
433	1			ortho b	6.4 at 416°			2.3		7.4	
270	2			monoc b	0.65 at 203°	$\epsilon_b > 700$ 1K		2 at 203°		20	
295					25	50,000		100 at 0°			
538				c	0.002	$\epsilon \approx 25$ 1M		20		≈10	
503	1	0.87	0.44	tetra a		$\epsilon_a \approx 2500$ 1M at 10v					
488 436 298	1			ortho a		550					
312											
247 143				b		65 49	247 143				16
148	1	1.05	0.154	tetra a		$\epsilon_a \approx 85$ $\epsilon_c \approx 30$ 800 at 200v					

II. THEORY OF CERAMIC FERROELECTRICS

A. Single Crystal Theory

1. Introduction

The useful application of the data collected in this survey requires a general understanding of the stability and the properties of ferroelectric bodies and how they are affected by changes in composition and structure as well as by changes in the intensive parameters: temperature, pressure, stresses and electric fields. Such an understanding can only be gained in the framework of a theory. Although all ferroelectric theories use drastic simplifying assumptions, they are rather lengthy and complicated and cannot be treated here in detail.

For a deeper understanding, it is therefore necessary to consult textbooks and review articles*. On the other hand, some parts of the theory; i.e., the basic reasons for the occurrence of ferroelectricity as well as the dependence of the ferroelectric transitions and the properties of ferroelectric materials on the intensive parameters can be presented in rather brief form. This part of the theory should become a working tool for people working in the field and is therefore included in this survey.

The presentation will be given in three steps which do not necessarily represent three different levels of sophistication. The first two steps deal with static and dynamic model theories; the third step deals with the thermodynamic treatment.

2. Static model theories

The classical model of a dielectric is an assembly of N atoms per unit volume of polarizability α: α is defined as the induced dipole moment p_e divided by the local field E_{loc} times the dielectric constant of the vacuum ϵ_o

---

* See Jona and Shirane (J1) page 27 for references

$$\alpha = \frac{p_e}{\epsilon_o \cdot E_{loc}} \tag{1}$$

In this way the macroscopic polarization P becomes

$$P = N \cdot \alpha \cdot E_{loc} \cdot \epsilon_o \tag{2}$$

Using the Clausius-Mosotti field

$$E_{loc} = \frac{P}{3\,\epsilon_o} \tag{3}$$

as the local field in addition to the applied field and dividing the polarizability into an electronic part (α_{el}) and an ionic part (α_{ion}) one obtains for the dielectric constant K

$$K = \frac{\epsilon}{\epsilon_o} = 1 + \frac{N(\alpha_{el} + \alpha_{ion})}{1 - \frac{N(\alpha_{el} + \alpha_{ion})}{3}} \tag{4}$$

One sees immediately that, if

$$\frac{N(\alpha_{el} + \alpha_{ion})}{3} = 1 \tag{5}$$

K goes to infinity and a discontinuity in properties (and structure) must occur.

For $BaTiO_3$; e.g., the electronic polarizability leads to a term (Slater (S25))

$$\frac{N\,\alpha_{el}}{3} = 0.61 \tag{6}$$

so that only a contribution of

$$\frac{N\,\alpha_{ion}}{3} = 0.39 \tag{7}$$

from the ionic polarization is necessary to produce the dielectric instability; one can suspect that this instability indicates the ferroelectric transition.

A somewhat different way to visualize the possibility of a stable ferroelectric arrangement; i.e., one with a spontaneous polarization, is the following (Beam (B39)).

Assume a situation such as that pictured in Figure 2 where the polarizability is rather high and P is a <u>non-linear</u> function of the local field (E_{loc}). This non-linear relation is given by Curve I. On the other hand, any polarization P will produce a local Clausius-Mosotti field of magnitude $\frac{P}{3\epsilon_o}$ if there is no applied external field; i.e., either for a toroidal arrangement of the material or for an electroded arrangement with short circuited electrodes. This local field $E_{loc} = \frac{P}{3\epsilon_o}$ is represented by Straight Line II in Figure 2. The point where the straight line crosses Curve I presents a stable situation where there is a remanent polarization (spontaneous polarization) as well as a remanent internal local field.

The question is how one can visualize the large values of the ionic polarization which are necessary to produce the dielectric instability as expressed in the breakdown of formula (5) or the occurrence of a spontaneous polarization as pictured in Figure 2.

The most obvious way, naturally, is to visualize the ionic polarizability as being due to the existence of permanent dipoles in the material; these dipoles partially orient themselves with their moment parallel to the local field and this dependence has a non-linear character (Langevin function). The contribution of the orientation to the ionic polarizability can be given by a term

$$\alpha_{orient} = \frac{\mu^2}{3kT} \tag{8}$$

where μ is the dipole moment, k is Boltzmann's constant and T is the absolute temperature and, if this is included in formula (4), one obtains

$$K = 1 + \frac{N(\alpha_{el} + \alpha_{ion} + \frac{\mu^2}{3kT})}{1 - \frac{N}{3}(\alpha_{el} + \alpha_{ion} + \frac{\mu^2}{3kT})} \tag{9}$$

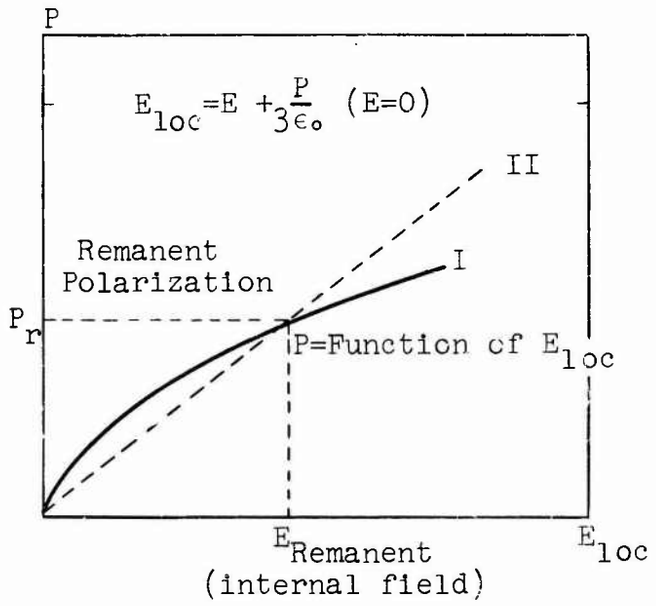

Fig. 2 Polarization P vs Local Field E_{loc} (B39)

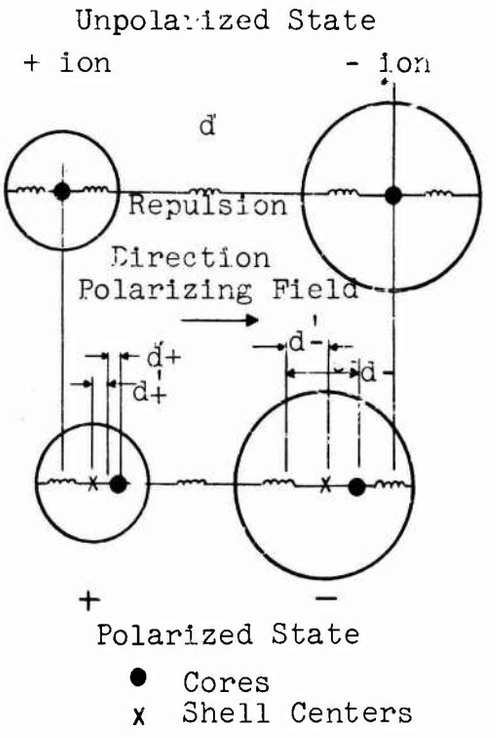

Fig. 3 The short-range interaction polarization. $d\pm$ are the displacements of the shells with respect to the cores in the absence of replusion between the ions. $d'\pm$ are the additional shell displacements resulting from repulsion. (D10)

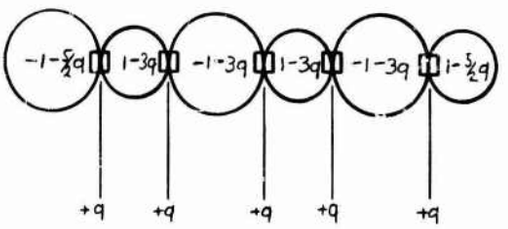

Fig. 4 Chain of positive and negative ions in an unpolarized crystal, showing exchange and electron charge magnitudes and positions. The large circles represent negative ions. (D10)

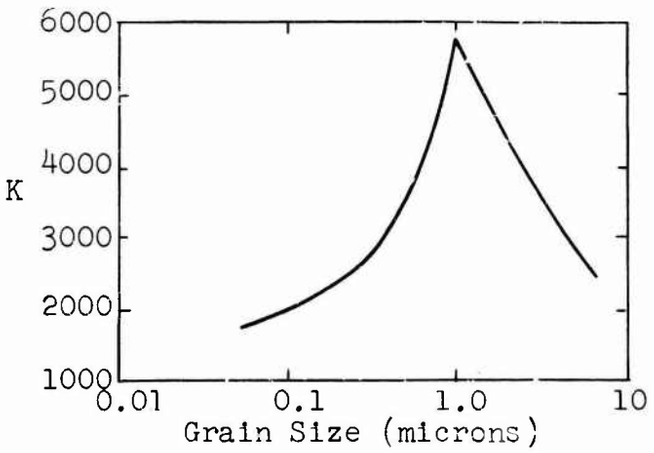

Fig. 5 Dielectric Constant of $BaTiO_3$ vs Grain Size (at 23°C) (B40)

Since T can go to any low value, it is evident that K must become infinite at a certain temperature (Clausius-Mosotti catastrophe). This formula has several flaws which are discussed in all textbooks; it does not hold even in the cases where there are actually permanent dipoles in the material. It is interesting to note that one of the first theories of $BaTiO_3$ was based on the assumption of pre-existing dipoles; it has been shown since that this leads to conclusions which do not agree with the experiments.

One important improvement of the basic formula (4), involving ionic polarization by displacements rather than by dipole orientation came from Slater (S25). Slater found that the local field computed according to Clausius-Mosotti holds for some points of the perovskite unit cell but needs drastic correction factors at other points. Especially he found a very strong interaction between the Ti- ion and the O_I-ion. As a result of this it was possible to formulate equation (4) as follows:

$$K = 3.84 + \frac{1.93}{1 - 16.19 \frac{N \alpha_{ion}}{3}} \qquad (10)$$

in which equation the values for the electronic polarizabilities already have been included.

Equation (10) implies that, if

$$\frac{N \alpha_{ion}}{3} = 0.062 \qquad (11)$$

(as compared with 0.39 in (7)) ferroelectricity is obtained. This result is especially important because it proves that with the perovskite structure and with a combination of cations and anions of large electronic polarizability, only a very small contribution from the ionic polarizability is needed to bring about ferrcelectricity.

Other static models have been proposed by Tagaki (T11), Kinase (K15), Triebwasser (T10) and Hagedorn (H14). Some of

these computations reveal that $BaTiO_3$ must be considered largely as a non-ionic crystal. This points to the importance of covalent bonds as emphasized by Megaw (M21) and Smolenskii (S26). Smolenskii (S27) formulates the condition for ferroelectricity as one "where the strength of the dipole-dipole interaction must be greater than that of the restoring elastic force". Summarizing the results of this chapter one can say that the strength of the dipole-dipole interaction is due to strong electronic polarizability plus the enhancement of this interaction in certain directions and in certain structures, whereas the weakening of the restoring elastic force might be due to covalent effects. Whereas the first two factors, electronic polarizability and dipole-dipole interaction, allow a fair quantitative formulation, the treatment of the covalent forces is not developed to the point that one could predict ferroelectricity on the basis of a model treatment alone. However, study of short-range interaction and exchange forces, which is the basis of anharmonicity of lattice forces, is a very active field of research; e.g., in the study of the higher order of the elastic constants, etc. It can be expected that eventually a quantitative treatment of this part of the model theory will be feasible.

3. Dynamic model theories

The dynamic model theories of ferroelectrics are based on lattice dynamics and have been developed gradually from the theory of the dielectric constant of alkali halides. The following presentation is taken largely from the pioneering paper of Dick and Overhauser (D10) which introduced the so-called shell model of dielectrics that was, in turn, the starting point for Cochran's (C10) successful dynamic model theory of $BaTiO_3$.

The simple classical theory of the dielectric constants of ionic crystals considers the following model: The crystal lattice is occupied by polarizable ions in static equilibrium of charge $\pm Ze$ and polarizability $\alpha\pm$. This theory gives expressions for the extrapolated high-frequency dielectric

constant K_∞, the low-frequency dielectric constant K_o, and the characteristic frequency of transverse lattice polarization waves (the reststrahlen frequency) ω_T:

$$\frac{K_\infty - 1}{K_\infty + 2} = \frac{N(\alpha_+ + \alpha_-)}{3\epsilon_o} \tag{12}$$

$$\frac{K_o - 1}{K_o + 2} = \frac{N}{3\epsilon_o}\left[(\alpha_+ + \alpha_-) + \frac{(Ze)^2}{A}\right] \tag{13}$$

$$\overline{M}\,\omega_T^2 = A - \frac{N(Ze)2/3\,\epsilon_o}{1 - \frac{N(\alpha_+ + \alpha_-)}{3\epsilon_o}} \tag{14}$$

Here $\overline{M}$ is the reduced mass of the positive and negative ions; N is the number of ion pairs per unit volume; and A is the harmonic restoring force constant related to the short-range repulsion between the ions which in the simple theory for NaCl type alkali halides is given by $A = 6\,R_o/K^*$, R_o being the nearest neighbor distance and K^* the compressibility.

Of the parameters appearing in these expressions $\overline{M}$, N and Z are known if the crystal is specified and is assumed to be completely ionic. The polarizabilities α_+ and α_- for, say, the alkali metal ions and the halogen ions in alkali halides are known neither in vacuum nor in a crystal environment and are to be regarded as adjustable parameters in the simple classical theory.

Equation (12) can be used to express $N(\alpha_+ + \alpha_-)$ in terms of K_∞. Substituting this $N(\alpha_+ + \alpha_-)$ into (13) and (14) two expressions are obtained from which the adjustable parameters α_+ and α_- have been eliminated:

$$K_\infty = G[K_\infty,\ A,\ N(Ze)^2] \tag{15}$$

$$\overline{M}\omega_T^2 = H[K_\infty,\ A,\ N(Ze)^2] \tag{16}$$

If A is expressed in terms of the lattice constant and the compressibility, (15) and (16) contain experimental quanti-

ties only. By eliminating alternately A or $N(Ze)^2$ between (15) and (16) these two relations can be written

$$\bar{M}\omega_T^2 (K_o + 2)/(K_\infty + 2) = A = 6 R_o/K^* \qquad (17)$$

$$K_o - K_\infty = (K_\infty + 2)^2 [\frac{N(Ze)^2}{\epsilon_o}]/9 \bar{M}\omega_T^2 \qquad (18)$$

In this form (17) and (18) are called the first and second Szigeti relations, respectively (Szigeti (S28,S29)). The failure of the experimental data to satisfy (17) and (18) demonstrates the inadequacy of the model on which the classical theory is based.

The first Szigeti relation depends for its validity on both the classical theory of the dielectric constants and the theory of the compressibility which associates A with experimental data. If, by definition

$$K_c^* \equiv 6 R_o(K_\infty + 2)/\bar{M}\omega_T^2 (K_o + 2) \qquad (19)$$

then a comparison of K_c^* with the observed compressibility K^* gives a check on the validity of the first Szigeti relation. If the relation were satisfied, $K_c^*/K^* = 1$. Values of K_c^*/K^* derived from the experimental data show deviations of K_c^*/K^* from unity of both signs and as great as 34%.

The second Szigeti relation gives the difference between the high-frequency and the low-frequency or static dielectric constants. It is a relation that does not contain A and so does not depend in this classical theory on the validity of the theory of the compressibility as did the first Szigeti relation. As is the case with the first Szigeti relation, the second relation is not satisfied by the experimental data. Accordingly Szigeti introduced a quantity e* in place of e in (18): e*/e is defined by

$$(e^*/e)^2 \equiv 9 \bar{M} \omega_T^2 \epsilon_o (K_o - K_\infty)/Ne^2(K_\infty + 2)^2, (Z = 1) \qquad (20)$$

If (18) were satisfied, e*/e would be unity. The values of e*/e derived from experimental data are always less than unity (0.69-0.93).

The shortcoming of the classical theory as proven by the fact that it does not give the correct value for $\frac{e^*}{e} = 1$ according to the second Szigeti equation has induced Dick and Overhauser (D10) to develop a new theory of the dielectric constant of alkali halides, based on the shell model (Figure 3). The physical idea is that in ions with a closed-shell electron configuration the outer electrons retain their spherical symmetry and move in a field as an undistorted sphere against the rest of the ion (core) to which the sphere is bound by a rather small isotropic force constant. The rest of the ion, the core, on the other hand, is rigid and does not deform appreciably. Figure 3 depicts a mechanical model with the isotropic force constants symbolized by a chain of linear springs, showing the short range forces between cores and shells of cation as well as anion and, in addition, the repulsive forces between the shells. Other force constants such as those between the two nuclei and those between the nuclei and the shells of the other ions are not shown. The shell model leads to two new types of polarization which are foreign to the classical model, but which have to be understood if one wants to understand dielectrics.

First one must consider what happens due to the short-range interaction when pairs of ions are moved together as is the case in that polarization of a crystal due to the motion of the positive and negative ions. The shells of the ions repel one another and tend to become displaced with respect to the ion cores because of this repulsion. This is equivalent to a polarization of the ions. The restoring spring between the shell and the core is in general weaker in the negative ion than it is in the positive ion, and hence one would expect the polarization of the negative ion due to the repulsion of the shells to exceed that of the positive ion if the shell charges were the same. Referring to Figure 3, it is seen that the polarization due to the short-range interaction is in the

direction of the applied field for the positive ion and against the direction of the field for the negative ion. If the negative-ion "short-range interaction polarization" exceeds that of the positive ion, it is seen that there is a resulting net dipole per ion pair directed opposite to the applied field. Whether it will in fact be a net dipole directed opposite to the field depends, of course, both on the spring constants k and on the shell charges ne. For the NaCl-type alkali halides, the polarization due to this mechanism is indeed negative. This is the sort of contribution to the polarization that serves to reduce e*/e to values less than unity. The short-range interaction polarization arises from a coupling of the ionic displacement polarization and the electronic polarization of the ions, a coupling beyond that which exists because of the Lorentz field (Clausius-Mosotti field).

There is another sort of polarization which is a consequence of the overlap of the ions and the resulting exchange charge. When the repelling ions are moved with respect to one another there is a change in the overlap integrals and a consequent change in the exchange charge distribution. This change is responsible for the repulsive force between the ions at short distances. In a crystal the displacement of the ions in the polarization process causes such redistributions of exchange charges and the resulting forces cause the ionic displacement polarization to be finite. Associated with these charge redistributions is a net dipole moment per unit volume. This will be called the exchange charge polarization.

A chain of ions in a NaCl-type alkali halide crystal in equilibrium (no field) with their associated exchange charges is shown in Figure 4.

It is seen that in the overlap region between the interacting shells there is a positive charge q (exchange charge) between each pair and the ions themselves have acquired an increased negative charge which is "excavated" from the overlap region to make the exchange charge. Without a polarizing field the dipoles formed by the exchange positive charges and the

extra negative charges on the ions do not lead to a static polarization; i.e., the dipole moments cancel each other in the same way as do the dipole moments which one can formally build up from an array of positive and negative ions.

As soon as a field is applied, however, two types of exchange charge polarization appear: one is a dipole moment per ion pair due to the changes in magnitude of the exchange charges (q in Figure 4); the other one is due to the movement of the exchange charges.

The shell model was applied to ferroelectrics by Cochran (C10). He treats first the case of diatomic crystals which shows basically the same features as crystals with a larger number of atoms such as $BaTiO_3$.

The theory leads to two expressions for the frequency of the transverse optical (= polarization) mode ω_T, which is the reststrahlen frequency of the classical theory (see above equation (14)), and for the frequency ω_L for the longitudinal optical mode:

$$\bar{M}\omega_T^2 = R_o' - \frac{(K_\infty + 2)}{9\, v\, \epsilon_c} (Z'e)^2 \qquad (21)$$

$$\bar{M}\omega_L^2 = R_o' + \frac{2(K_\infty + 2)}{9\, v\, \epsilon_\infty} (Z'e)^2 \qquad (22)$$

R_o' is the short range restoring force related to A in equation (14); v is the volume of the unit cell related to 1/N in equation (12). The shell model is used here in such a way that only the negative ion is taken as polarizable and the non-Coulomb forces act through the shell rather than through the core.

Ze, Xe and Ye are the charges of the positive ion, the core of the negative ion and the shell of the negative ion, respectively; X + Y + Z = 0. The forces have been separated into Coulomb forces which depend on the polarization P and on the short range forces specified by the force constant R_o

between shells and positive ions and a force constant k between shell and core of the negative ion (see Figure 3).

The constants R_o' and Z' in equations (21) and (22) depend on R_o, k, Y and Z in the following way:

$$R_o' = \frac{k\,R_o}{k + R_o} < R_o \tag{23}$$

$$Z' = Z + \frac{Y\,R_o}{k + R_o} < Z \tag{24}$$

Both Z', R_o and v depend linearly on temperature due to the anharmonicity of the lattice vibration. One can, therefore, rewrite (21) as:

$$\bar{M}\omega_T^2 = 1 - \frac{(K_\infty + 2)(Z'e)^2}{9\,v\,\epsilon_o} = \delta\,(T-T_c) \tag{25}$$

where δ is a temperature coefficient of the same order as the volume coefficient of expansion.

Using the second Szigeti equation in a slightly different form (Z' instead of Z) and introducing (25) into it, one gets:

$$K_o = K_\infty + \frac{(K_\infty + 2)^2\,(Z'e)^2}{9\,v\,R_o'\,\delta\,(T-T_c)\epsilon_o} \tag{26}$$

This is the Curie-Weiss law of ferroelectricity:

$$K_o = K_\infty + \frac{C}{T-T_c} \tag{27}$$

where

$$C = \frac{(K_\infty + 2)^2\,(Z'e)^2}{9\,v\,R_o'\,\epsilon_o\,\delta} \tag{28}$$

The physical reason for the appearance of ferroelectricity is contained in Equation (21) which states that (for wave vector $q \longrightarrow 0$, i.e., for very long waves) the transversal optical mode, i.e., the transversal polarization waves, can go towards

zero frequency; that is, freeze in. This phenomenon can occur when the two terms on the right side become equal and it gives a good picture of ferroelectricity in that it states that the particular polarization corresponding to the transversal optical mode exists already in the paraelectric state as transient mode. In fact, this polarization exists in all ionic crystals, alkali halides and others, but, due to the temperature dependence of the two terms on the right side of (21) - especially the last term - only in certain crystals can its frequency go to zero, and the polarization corresponding to this mode becomes permanent.

The theory of ferroelectricity for $BaTiO_3$ (with five atoms instead of the two which have been considered above) is in principle the same; only the number of the force constants R is much larger as one has to consider interaction between all the shells, between all the cores, and between all cores and all shells. In spite of formidable and cumbersome computations, this problem has been solved and it has been shown that this theory can be brought into a form in which its agreement with important experimental facts can be checked. An interesting fact might be mentioned concerning the frequency which is assumed to go to zero. It seems that this frequency, which is normally in 10^{13} cps range, drops 1-2 orders of magnitude upon approach of the ferroelectric transition but does not actually become zero: before this happens the material becomes unstable and transforms into the ferroelectric state.

An important contribution to the question of the parallelism of the ferroelectric transition to the frequency of the transverse optical mode becoming abnormally low has been made by Cowley (C12). Cowley has measured the frequency of this mode in $SrTiO_3$ at 90°K and 296°K, using inelastic scattering of slow neutrons, as function of the wave vector. At wave vector zero the frequency drops indeed to abnormally low values (10^{12} c/s). A plot of the reciprocal dielectric constant and of the square of the (q=0) transverse optical mode frequency as function of

temperature gives two straight lines which both give a Curie temperature of 32°K. This is an experimental confirmation of Cochran's equations (25) and (26).

Theoretical investigations into the temperature dependence of the transverse optical mode have been made by several authors, e.g., Silverman and Joseph (S30).

4. Thermodynamic theory

The usefulness of the static and dynamic model theories lies in the fact that they show all the factors which are at work to make a crystal ferroelectric. Some of these factors can be brought into a quantitative form and one can estimate the relative influence of structure, electronic and ionic charge, and electronic polarizability; however, when it comes to a precise prediction of which compounds can become ferroelectric, at what temperatures and of the values of their dielectric, piezoelectric and elastic properties, the model theories fail. The reason is that in a true model theory all the force constants, the R's and the k's should be computed from first principles and this cannot be done at present. Here is where the phenomenological thermodynamic theory comes in. This theory sets up a free energy function as a power series of the polarization, the coefficients of which are determined by comparison with experimental data. If the function is properly chosen, mainly in regard to the number of terms and the temperature dependence of the coefficients, one can derive all other interesting properties of the materials from it.*

The free energy function generated by any model theory may then be compared directly with the phenomenological function, and provided an agreement is achieved, it is then certain that the model theory will describe the whole range of observed properties.

---

* The following presentation is taken verbally from Goswami (G5).

Following the method suggested by Müller for Rochelle salt, Devonshire (D5 a,b) expanded the free energy of barium titanate as a function of polarization and strain and, using an expression consistent with the original cubic symmetry with relatively few parameters, was able to describe:

(1) variations of spontaneous strain and spontaneous polarization with temperature,

(2) variation of permittivity with temperature,

(3) piezoelectric constant d_{ij} and the elastic compliances s_{ij} as functions of temperature, and

(4) dielectric susceptibilities at constant stress and at constant strain as functions of temperature.

No attempt was made to determine the free energy function in terms of stresses and polarization, so that one could use this function to determine the variation of permittivity under different types of mechanical stresses in the ferroelectric state. Previous workers have attempted to correlate the dielectric properties under mechanical stresses but only in the paraelectric state. To study the influence of mechanical stresses on the dielectric properties in the ferroelectric state, the free energy function in terms of stresses and polarization is necessary. The method of obtaining this function follows. Devonshire's expression for Gibbs' free energy function of the unstressed crystal has the form

$$G_1 = A(P_x^2 + P_y^2 + P_z^2) + B(P_x^4 + P_y^4 + P_z^4) + C(P_x^6 + P_y^6 + P_z^6) + D(P_x^2P_y^2 + P_y^2P_z^2 + P_z^2P_x^2) \qquad (29)$$

and the Helmholtz free energy is given by an expression of the form:

$$
\begin{aligned}
A_1 = {} & 1/2c_{11}(x_x^2 + y_y^2 + z_z^2) + c_{12}(y_y z_z + z_z x_z + x_x y_y) \\
& + 1/2c_{44}(x_y^2 + y_z^2 + z_x^2) + g_{11}(x_x P_x^2 + y_y P_y^2 + z_z P_z^2) \\
& + g_{12}[x_x(P_y^2 + P_z^2) + y_y(P_z^2 + P_x^2) + z_z(P_x^2 + P_y^2)] \\
& + g_{44}[y_z P_y P_z + z_x P_z P_x + x_y P_x P_y] + A'(P_x^2 + P_y^2 + P_z^2) \\
& + B'(P_x^4 + P_y^4 + P_z^4) + D'(P_y^2 P_z^2 + P_z^2 P_x^2 + P_x^2 P_y^2) \\
& + C'(P_x^6 + P_y^6 + P_z^6) + A_{10} \qquad (30)
\end{aligned}
$$

where A is related to the dielectric stiffness in the paraelectric state, decreasing linearly with temperature; B, C, D are constants; the corresponding primed quantities stand for the constants of the Helmholtz free energy function; c_{ij}'s are the appropriate elastic constants; g_{ij}'s are the electrostrictive constants.

With increasing precision in experimentation, efforts have been made to improve the formula by increasing the number of terms and by using better constants than those used in the original treatment. Perhaps the most reliable expression is that due to Huibregtse et al (H15) which is

$$
\begin{aligned}
A_1 = {} & 1/2c_{11}(x_x^2 + y_y^2 + z_z^2 + 1/2c_{44}(x_y^2 + y_z^2 + z_x^2) \\
& + c_{12}(x_x y_y + y_y z_z + z_z x_x) + g_{11}(x_x P_x^2 + y_y P_y^2 + z_z P_z^2) \\
& - g_{12}[x_x(P_y^2 + P_z^2) + y_y(P_z^2 + P_x^2) + z_z(P_x^2 + P_y^2)] \qquad (31) \\
& + g_{44}(x_y P_x P_y + y_z P_y P_z + z_x P_z P_x) + A(P_x^2 + P_y^2 + P_z^2) \\
& + B(P_x^4 + P_y^4 + P_z^4) + C(P_x^6 + P_y^6 + P_z^6) \\
& + D(P_x^2 P_y^2 + P_y^2 P_z^2 + P_z^2 P_x^2) \\
& + G(P_x^2 P_y^4 + P_x^4 P_y^2 + P_y^2 P_z^4 + P_y^4 P_z^2 + P_z^2 P_x^4 + P_z^4 P_x^2)
\end{aligned}
$$

From this Helmholtz free energy function, an expression for the Gibbs free energy function G_1 has been derived in terms of stress and polarization by Goswami (35). This function takes the form

$$\begin{aligned} G_1 = {} & 1/2s_{11}(X_x^2 + Y_y^2 + Z_z^2) - s_{12}(X_xY_y + Y_yZ_z + Z_zX_x) \\ & - 1/2s_{44}(X_y^2 + Y_z^2 + Z_x^2) + Q_{11}X_x + Q_{12}Y_y + Q_{12}Z_z)P_x^2 \\ & + (Q_{12}X_x + Q_{11}Y_y + Q_{12}Z_z)P_y^2 + (Q_{12}X_x + Q_{12}Y_y + Q_{11}Z_z)P_z^2 \\ & + Q_{44}(X_yP_xP_y + Y_zP_yP_z + Z_xP_zP_x) + A(P_x^2 + P_y^2 + P_z^2) \\ & + B(P_x^4 + P_y^4 + P_z^4) + C(P_x^6 + P_y^6 + P_z^6) \\ & + D(P_x^2P_y^2 + P_y^2P_z^2 + P_z^2P_x^2) \\ & + G(P_x^2P_y^4 + P_x^4P_y^2 + P_y^2P_z^4 + P_y^4P_z^2 + P_x^2P_x^4 + P_z^4P_x^2) \end{aligned} \qquad (32)$$

where X_x, Y_y, Z_z are the normal stress components,
Y_z, Z_x, X_y are the shear stress components,
s_{11}, s_{12}, s_{44} are the elastic compliances,
P_x, P_y, P_z are the components of polarization,
and Q_{11}, Q_{12}, Q_{44} are the electrostrictive coefficients.

Numerical values for these coefficients are listed in Table VII.

The field components may be readily obtained from the free energy function by

$$E_x = \frac{\partial G_1}{\partial P_x} \qquad E_y = \frac{\partial G_1}{\partial P_y} \qquad E_z = \frac{\partial G_1}{\partial P_z} \qquad (33)$$

and the strain components by

$$x_x = \frac{\partial G_1}{\partial X_x} \qquad y_y = \frac{\partial G_1}{\partial Y_y} \qquad z_z = \frac{\partial G_1}{\partial Z_z} \qquad (34)$$

The permittivities are given by

$$\frac{4\pi}{\epsilon_{xx}} = \frac{\partial^2 G_1}{\partial P_x^2} \qquad \frac{4\pi}{\epsilon_{yy}} = \frac{\partial^2 G_1}{\partial P_y^2} \qquad \frac{4\pi}{\epsilon_{zz}} = \frac{\partial^2 G_1}{\partial P_z^2} \qquad (35)$$

For non-orthogonal stress systems one must also consider the off diagonal terms: ϵ_{xy} ϵ_{yz} ϵ_{zx}.

The usefulness of the thermodynamic theory is manifold. First, by investigating the free function (29) as a function of temperature and polarization, it gives direct insight into the nature of the ferroelectric transition. If all coefficients of (29) are positive, the free energy function has a minimum at P = 0, corresponding to the paraelectric state. If A, the first coefficient, goes through zero and becomes negative, A(P) has two minima, corresponding to a ferroelectric state. In this case, the spontaneous polarization changes smoothly from the zero value above the Curie temperature to the finite values below it; the susceptibility (1/A) becomes infinite at the Curie point. The smooth transition of the polarization at the Curie point is indicative of a second order transition.

If, however, the coefficient B in (29) is negative, then the A(P) curve already has three minima above the Curie point which become equal at this transition. In this case, the spontaneous polarization changes abruptly from the central minimum into one of the side minima and one has a phase transition of the first order. The susceptibility, however, does not become infinite in this case but changes abruptly from one finite value to another.

The usefulness of the thermodynamic theory as a means of checking model theories has already been pointed out. This has been done with the Devonshire-Slater static model theory as well as with Cochran's dynamic model theory.

One of the main advantages of the phenomenological theory, especially in the form (32), is that it allows one to compute any changes of spontaneous polarization or dielectric constants as a function of stresses which is important for an estimate of the effect of internal and external stresses on the properties of ceramic ferroelectrics. An example of this application will be given below.

B. Polycrystal Theory

1. Passive interaction between grains (dielectric mixing rules)

A ceramic is an assembly of crystallites which are usually randomly oriented and which are strongly bound to each other through grain boundaries. If the phase present is of cubic symmetry there is no direct active interaction between grains besides the grain boundary stresses which affect only small regions near the boundaries. If there are several phases present which have the same thermal expansion coefficient, the same situation exists, i.e., there is no active stress interaction. In the following discussion of the dielectric properties of mixtures of several phases, it will be assumed that there is no active (stress) interaction between grains, or, if there is, due to differences in thermal strain, that this interaction does not affect the dielectric constants appreciably.

If two or more phases are present which have different dielectric constants, the problem of computing the resulting dielectric constant of the mixture ($\overline{K}$) can be solved exactly only for a few cases. If the boundaries between the phases are planes parallel to the field, a simple linear mixing rule holds:

$$\overline{K} = \sum_{1}^{n} v_n K_n \qquad (1)$$

where n is the number of phases, v_n is the volume fraction of phase n and K_n is the dielectric constant of phase n.

Similarly, if the plane boundaries of the n phases are perpendicular to the field, the resulting $\overline{K}$ is computed from:

$$1/\overline{K} = \sum_{1}^{n} v_n/K_n \qquad (2)$$

The so-called logarithmic mixing rule is:

$$\log \overline{K} = \sum_{1}^{n} v_n \log K_n \qquad (3)$$

Only equations (1) and (2) hold exactly for the geometries given, whereas (3) is an arbitrary - if very convenient - interpolation formula between the two extremes which has no physical foundation and should be used only for very quick, rough estimates.

A much more reliable approximate interpolation formula for the case of phase mixing and other cases has been developed by Bruggemann (B43)(B44) and Niesel (N8). The following presentation follows Niesel's arguments.

Two cases have been treated:

1. Particles of Phase I are completely embedded in a continuous Phase II.

2. Both phases consist of particles which completely fill the space; this is possible if the space between particles is always filled with finer particles.

The first case is realized by pores in a dielectric or by an exsolved second phase in a continuous first phase. The second case is realized by a eutectic mixture of two phases; it is distinguished from the first case in that <u>both</u> phases are interconnected. The second case contains as a limiting condition the random arrangement of one single anisotropic phase which can be considered as a case of self-mixing.

Niesel's deductions are based on an axiom which had already been used by Bruggemann; if one is willing to accept this axiom, everything else follows logically and is convincing. The axiom goes as follows: If particles of identical shape and orientation (ellipsoids) with the dielectric constant K_i are embedded in a <u>homogeneous</u> medium of dielectric constant K_a, the aggregate has a dielectric constant K'. If now the same particles of dielectric constant K_i in the same shape, orientation and concentration are embedded in a <u>quasihomogeneous</u> medium (made up in a different way) of dielectric constant K_a, the axiom postulates that this aggregate also has a resulting dielectric constant of value K'. In the derivation K' is computed as

$$K' = \frac{D_z}{E_z} \qquad (4)$$

where both $\overline{D}_z$ and $\overline{E}_z$ are the spatial averages over the whole dielectric with the field assumed to be in the z-direction. For small concentrations of the embedded ellipsoids with dielectric constant K_1, the fields inside the ellipsoids are homogeneous and the problem consists in computing the average of the disturbed, inhomogeneous field outside the ellipsoids. Since the sum of all surface charges (interfacial divergence of D) is zero, the average component $\overline{E}_z$ due to these charges is also zero. If this field (stray field or depolarizing field) is designated by E_{st} one has:

$$\delta_1 \overline{E}_{st,1} + \delta_a \overline{E}_{st,a} = 0 \qquad (5)$$

where δ_1 is the volume fraction of the ellipsoids and δ_a, the volume fraction of the homogeneous medium with dielectric constant K_a.

The result is for small concentrations of δ_1:

$$K' = K_a [1 + \delta_1 F(K,L,M,N)] \qquad (6)$$

where F is a simple function of the three dielectric constants of the ellipsoid, the dielectric constant K_a of the homogeneous medium and of the three depolarization factors L,M,N of the ellipsoid.

The computation of K' for large values of δ_1 consists then in applying formula (6) in infinitesimal steps, taking the resulting mixture as a quasihomogeneous medium and proceeding with the next infinitesimal step according to the axiom stated at the beginning. This leads to a differential equation for K' which can be integrated. The result is computed for spherical, platelike and cylindrical aggregates of isotropic substances. The formula for spherical aggregates is:

$$1 - \delta_1 = \frac{K_1 - K'}{K_1 - K_a} \sqrt[3]{\frac{K_a}{K'}} \qquad (7)$$

For anisotropic materials the formulae become unwieldy; Niesel has treated only the case of a spherical aggregate of a uniaxial crystal; he asserts that the results are practically identical with those obtained with Equation (7), using for K_i the linear average of the dielectric constants of the uniaxial crystal.

The procedure for case 2, i.e., mixtures of anisotropic ellipsoids in which both phases are interconnected, is similar to the procedure in case 1. For two isotropic substances with dielectric constants K_1 and K_2 and spherical particles one obtains:

$$\overline{K} = 1/4 \left[(2 E_p - E'_p) + \sqrt{(E'_p - 2 E_p)^2 + 8 K_1 K_2} \right] \qquad (8)$$

where $E_p = \delta_1 K_1 + \delta_2 K_2$

and $E'_p = \delta_1 K_2 + \delta_2 K_1$

Especially important is the case of one single anisotropic phase so that $\delta_2 = 0$; this is the case called "self-mixing".

For a uniaxial material in spherical particles and with the dielectric constants $K_x = K_y$ and K_z, one has:

$$\overline{K} = \frac{K_x}{4} (1 + \sqrt{9 - 8\tau}) \qquad (9)$$

where

$$\tau = 1 - \frac{K_z}{K_x} \qquad (10)$$

Valid evidence that the Bruggeman-Niesel formulae come closer to reality than the logarithmic mixing rule (3) has been produced by Herczog (H5) and will be discussed under V-B (Devitrified Ceramics); see especially Figure 15 in that chapter.

2. Active interaction between grains

Active interaction between grains is the interaction by which the grains exert stresses of such magnitude upon each other that the intrinsic dielectric properties are changed.

The treatment of such pre-existing internal stresses due to mutual clamping is only in the beginning stages and needs much more theoretical and experimental work for its solution. As an initial approximation one can assume that there is a uniform strain in the polycrystalline body corresponding to the macroscopically observed strain, i.e., each distance during a temperature or a phase change in each crystallite experiences the same relative length change as that observed with the body as a whole. This corresponds to the so-called Voigt approximation in the theory of elastic constants of polycrystalline bodies and suffers from the same flaw; i.e., that the stresses across grain boundaries are not in equilibrium. In this approximation Laszlo's (L5) formulae hold for the maximum tensile and compressive stresses:

$$\sigma_b = (\alpha_b - \bar{\alpha}) \frac{\Delta T E}{1+v} \qquad (11)$$

$$\sigma_c = (\alpha_c - \bar{\alpha}) \frac{\Delta T E}{1+v}$$

where α_b is the thermal expansion coefficient in the b-direction of an orthorhombic crystal and α_c is the coefficient for the c-direction. Here α_b is assumed to be the largest coefficient and α_c the smallest as; e.g., in aluminum titanate. $\bar{\alpha}$ is the average expansion coefficient, E is Young's modulus, v Poisson's ratio and ΔT the temperature change measured from the state of zero stress. In the case of phase changes, e.g., at the Curie point of $BaTiO_3$, the product $\alpha\Delta T$ has to be replaced by the corresponding conversion strain term. The Laszlo formulae (11) give a fair idea what the maximum stresses in an anisotropic polycrystalline body are.

As a second approximation Buessem (B45) has introduced the idea that not all distances in the crystals but only the distances between the center points of the grains experience the macroscopic length changes. Each grain has an average of 14 neighbors; i.e., it forms a tetrakaidekahedron which is easily visualized as a penetration of a cube with an octahedron.

The 14 vector forces due to the expansion incompatibility have a vector sum which is zero. The centerpoints of the grains are farthest away from the points of attack of these 14 forces and it is not unreasonable to assume that they are the least affected by individual forces and that their movement conforms most closely with that of the body as a whole.

If one makes this assumption, one can allow for changes in strain near the grain boundaries which gives the possibility of satisfying the condition of stress equilibrium across grain boundaries.

The stresses at both sides of the grain boundary are then given by the expression:

$$\sigma = \left[\frac{(\alpha_n + \alpha_{n'})}{2} - \bar{\alpha}\right] \frac{\Delta TE}{1+\nu} \qquad (12)$$

where α_n and $\alpha_{n'}$ are the normal expansion coefficients on both sides of the grain boundary. Since one can compute the frequency of all normal expansion coefficients if the three principal values are known, one can also compute the frequency with which a certain combination n/n' occurs on both sides of the grain boundary. This then gives the possibility of computing a stress distribution curve and deriving from it average stress values. It can be shown that these average stress values are considerably below the maximum values which are computed from the original Laszlo formula; in other words, there is considerable stress relief due to the probability that a high expanding direction in a grain will have a neighbor with a low expansion coefficient in this direction so that the full Laszlo stresses are not developed.

The active interaction of grains due to anisotropy of strain developing at a phase change or during temperature changes is an important feature in all ferroelectric ceramics.

In large-grain materials there exists a mechanism which can lead to substantial stress relief far beyond that which has been discussed in the last paragraphs. This mechanism is the formation of a 90° domain by means of which a tetragonal grain can simulate a shape corresponding to the original shape

of the grain in the cubic state. One has to remember, however, that this stress relief is not complete. A laminated aggregate of (101) twins does not have exact 90° angles between the twinned polar axes; there is a deficit of about 36'. If the laminated slab was completely free, the outside surface perpendicular to the twinning plane would be zigzagged and there would be no stress besides the usual stress around a 90° domain wall. If this slab is built into a polycrystalline matrix, however, there must be stresses where the twinning plane meets the grain boundaries - stresses which tend to straighten out the zigzag shape. One could assume pure shear forces through all twinned lamellae to make the angle exactly 90°, but this would require much too high strain energies. One has to assume, therefore, that the areas at those lines where the twinning planes meet grain boundaries are areas of high local stresses; these stresses might even be so large that dislocations are formed near these lines.

For small grains the formation of 90° domains becomes energetically unfavorable. With decreasing grain size the wall energy decreases only with the second power of the grain diameter, whereas the strain energy decreases with the third power; below a critical size the strained single-domain particle becomes more stable. The theoretical computation of the 90° wall energy is still disputed, but from experimental observation it has been found that the critical diameter must be about one micron.

The effect of the internal stresses on the dielectric properties can be computed using the formulae of the phenomenological theory (32). In principle one could proceed in two ways: either one could compute some average stresses from the frequency distribution of the normal stresses and compute from them with the help of (32) the resulting dielectric constants, or one can start from the measured dielectric constant and get an estimate of the stresses. Goswami (G5) and Buessem, Cross and Goswami (B46) have used the second approach.

3. Grain size effects

Besides the grain size effects in ferroelectrics and especially in $BaTiO_3$ which have been discussed at the end of the last chapter, there exist other grain size effects which are not fully understood. If, as Brandmayr, Brown and Dunlap (B40) have shown, the grain size of $BaTiO_3$ is below 1 micron, the dielectric constant is falling off again (Figure 5). This cannot be understood from the standpoint of the phenomenological theory because the stresses in a single domain particle should not depend on its absolute size.

The phenomenon is reminiscent of the phenomenon of superparamagnetism in ferromagnetics; however, the onset of superparamagnetism is at particle sizes much below 1 micron and occurs from 0.05 micron down. It is possible that, since ferroelectricity is a cooperative phenomenon due to long range Coulomb forces, the cooperation begins to fall off from 1 micron on down. Another possibility is that below 1 micron the surface areas play a greater role. It is well known that there are strong surface fields due to Schottky exhaustion layers which are estimated to extend down to 0.1-1 micron depth. It can only be decided by future research what causes loss in dielectric constant at these very small grain sizes.

TABLE VII Values of Constants Used for Modified Free Energy Function (G5)

Constant	Value used	Reference
s_{11}	0.833×10^{-12} cm^2/dyne	(B41)
s_{12}	-0.268×10^{-12} cm^2/dyne	(B41)
s_{44}	0.924×10^{-12} cm^2/dyne	(B41)
Q_{11}	1.23×10^{-12} cgs	(B41) and (T10)
Q_{12}	-0.48×10^{-12} cgs	(B41) and (T10)
Q_{44}	0.65×10^{-12} cgs	(B41) and (T10)
A	$3.7\times10^{-5}(T-108)$ cgs	Modified from (H15) and (D11)
B	$0.58\times10^{-14}(T-120)-2.5\times10^{-13}$ cgs	Modified from (H15) and (D11)
C	$-7.41\times10^{-25}(T-120)+3.7\times10^{-23}$ cgs	Modified from (H15) and (D11)
D	4.0×10^{-3} cgs	Modified from (H15) and (D11)
G	6.0×10^{-23} cgs	Modified from (H15) and (D11)
T_o	108°C	Modified from (H15) and (D11)

III. DIELECTRIC, PIEZOELECTRIC AND ELASTIC PROPERTIES OF CERAMIC FERROELECTRICS

A. Introduction

In this section the properties of polycrystalline ferroelectric ceramic materials are listed according to composition for experimental compounds and according to piezoelectric and dielectric properties for commercially available bodies.

B. Experimental Bodies

1. Dielectric-constant-versus-temperature data

The curves which are available in the literature for dielectric constants plotted against temperature according to compositions are listed in Table VIII with the references.

Representative curves for some of these data are shown in Figure 6.

2. Piezoelectric data

In this section on properties of experimental bodies, a compilation of coupling factors, piezoelectric d and g constants, and elastic constants together with the dielectric constant at room temperature, mechanical Q, Curie point and density are listed according to composition.

In Table IX, a list of the compounds for which these data are available together with their references is given. The numerical values of the properties found in the literature for compounds of known chemical composition are listed in Table X.

C. Commercially Available Bodies

1. Piezoelectric transducer bodies

The compilation of piezoelectric and dielectric properties of commercially available ceramic ferroelectric transducer materials is given in Table XI. Figure 7 shows the variation with temperature for several properties listed in Table XI for ferroelectrics from the Clevite Corporation.

These data were compiled from bulletins and literature distributed by the companies represented.

2. Capacitor dielectrics

The important properties of ceramic ferroelectric capacitor dielectrics are: (1) variations in permittivity with temperature, frequency and applied field, (2) change in power factor with temperature (3) insulation resistance, (4) dielectric strength and (5) life test rating.

Information in company literature on body compositions and the values of the above listed properties is very limited as shown by Table XII. Typical curves for capacitance data with temperature are presented in Figures 8 and 9 for bodies from American Lava Corporation, Gulton Industries, Sprague Electric Company and Erie Technological Products, Inc.

TABLE VIII

A List of Dielectric-Constant versus Temperature Curves that are Available in the Literature According to Composition

I. ABO_3 Compounds	Figure 6	References
A. $BaTiO_3$	-	B35, P8, R5, R4, E2, M7, J3, J8, E26, B36
Solid Solutions of $BaTiO_3$ Including Exsolved Phases		
$(Ba-Pb)TiO_3$	6.1	S14, N5
$(Ba-Sr)TiO_3$	6.2	D9, B35, R5, G9, P2, B36
$(Ba-Ca)TiO_3$	-	B34, M19
$Ba(Ti-Zr)O_3$	6.3	K1
$Ba(Ti-Hf)O_3$	-	P4
$Ba(Ti-Sn)O_3$	6.4	N1
$Ba(Ti-Mn)O_3$	-	B37
$Ba(Ti-Ge)O_3$	-	P6
$Ba(Ti-Si)O_3$	-	P6
$(Ba-Pb-Ca)TiO_3$	6.5	I6
$(Ba-Ca-Co)TiO_3$	6.6	S8
$(Ba-Sr-Ni)TiO_3$	-	B36
$(Ba-Pb)(Ti-Zr)O_3$	-	I5, B25
$(Ba-Mg)(Ti-Sn)O_3$	-	P2
$BaTiO_3 + La_2O_3$	-	J3
$BaTiO_3 + Y_2O_3$	-	B18
$BaTiO_3 + Y_2TiO_3$	-	B18
$BaTiO_3 + Ta_2O_5$	-	S24
$BaTiO_3 + NaNbO_3$	-	B7
$BaTiO_3 + Nb_2O_5$	-	S24
$Ba(KLa)_{1/2}TiO_3$	-	G9
$Ba(KNd)_{1/2}TiO_3$	-	G9
B. $SrTiO_3$	-	T2
Solid Solutions of $SrTiO_3$		
$(Sr-Ca)TiO_3$	-	M19, G9
$SrTiO_3 + Bi_{2/3}TiO_3$	-	C8
$SrTiO_3 + La_{2/3}TiO_3$	-	T2

TABLE VIII (Cont.)

C. $PbTiO_3$	-	B37
Solid Solutions of $PbTiO_3$		
$(Pb\text{-}Ca)TiO_3$	-	S6
$(Pb\text{-}Sr)TiO_3$	6.7	B38, N4, B36
$Pb(Ti\text{-}Zr)O_3$	-	S6, K1, J4
$Pb(Ti\text{-}Zr)O_3 + Nb_2O_5$	-	K8, D3
$Pb(Ti\text{-}Zr)O_3 + Ta_2O_5$	-	K8
$Pb(Ti\text{-}Zr)O_3 + La_2O_3$	-	K8
$Pb(Ti\text{-}Zr)O_3 + Y_2O_3$	-	K8
$Pb(Ti\text{-}Zr)O_3 + Nd_2O_3$	-	K8
$Pb(Ti\text{-}Sn)O_3$	6.8	N1
$(Pb\text{-}Bi)(Ti\text{-}Fe)O_3$	-	F6
$Pb(Ti\text{-}Fe\text{-}Ta)O_3$	6.9	N2
$Pb(Sc\text{-}Nb\text{-}Ti)O_3$	6.10	J7
$PbTiO_3 + PbNb_2O_6$	-	S23
$PbTiO_3 + NaNbO_3$	-	B3
$PbTiO_3 + KNbO_3$	-	T3
$PbTiO_3 + Sr_{0.3}La_{0.7}MnO_3$	-	T4
D. $KNbO_3$	-	E1
Solid Solutions of $KNbO_3$		
$(K\text{-}Na)NbO_3$	-	E1, J2
$(K\text{-}Na)(Nb\text{-}Ta)O_3$	6.11	I9
E. $NaNbO_3$	-	T1, W2, E1, D7
Solid Solutions of $NaNbO_3$		
$Na(Nb\text{-}Ta)O_3$	-	I3
$Na(Nb\text{-}Sb)O_3$	6.12	I2
$Na(Nb\text{-}V)O_3$	-	P10
$NaNbO_3 + PbZrO_3$	-	B3, K3
$NaNbO_3 + CdNb_2O_6$	6.13	L1, W2
$NaNbO_3 + Sr_{1/2}NbO_3$	6.14	T1
$NaNbO_3 + (Sr_{1/4}Cd_{1/4})NbO_3$	6.15	T1

TABLE VIII (Cont.)

F. $KTaO_3$	-	H11
G. $BiFeO_3$	-	F6
Solid Solutions of $BiFeO_3$		
$(Bi\text{-}La)FeO_3$	-	R1
$(Bi\text{-}La)(Fe\text{-}Al)O_3$	6.16	F7
H. Antiferroelectric $PbZrO_3$ and $PbHfO_3$		
$PbZrO_3$	6.17	S7, R4
$PbHfO_3$	-	W1
Solid Solutions of $PbZrO_3$ and $PbHfO_3$		
$(Pb\text{-}Ba)ZrO_3$	-	R4, S13
$(Pb\text{-}Sr)ZrO_3$	-	S13
$Pb(Ti\text{-}Zr)O_3$	6.17	S7
$Pb(Ti\text{-}Nb\text{-}Zr)O_3$	-	D3
$Pb(Sc\text{-}Nb\text{-}Zr)O_3$	6.18	J7
$PbZrO_3 + PbNb_2O_6$	-	D3
$PbZrO_3 + NaNbO_3$	6.19	K3
$(Pb\text{-}Ba)HfO_3$	-	C2, W1
$(Pb\text{-}Sr)HfO_3$	-	W1
$Pb(Sc\text{-}Nb\text{-}Hf)O_3$	6.20	J7
II. $A_2B_2O_7$ Compounds		
A. $Cd_2Nb_2O_7$	-	L1, S12, H10, S17, D8
B. $Sr_2Ta_2O_7$	-	S17
III. AB_2O_6 Compounds		
A. $PbNb_2O_6$	-	F10, G4
Solid Solutions of $PbNb_2O_6$		
$Pb(Ta\text{-}Nb)_2O_6$	6.21	F10
$Pb(Ti\text{-}Nb)_2O_6$	-	S22, S23

TABLE VIII (Cont.)

$(Pb\text{-}Ba)Nb_2O_6$	-	B6
$(Pb\text{-}Sr)Nb_2O_6$	-	B6
$(Pb\text{-}Ca)Nb_2O_6$	-	B6
$(Pb\text{-}Cd)Nb_2O_6$	-	B6
$PbNb_2O_6 + BaTiO_3$	-	B6
$PbNb_2O_6 + BaZrO_3$	-	B6
$PbNb_2O_6 + Bi_{2/3}Nb_2O_6$	-	S20
B. $\underline{BaNb_2O_6}$	6.22	C4
Solid Solutions of $\underline{BaNb_2O_6}$		
$(Ba\text{-}Sr)Nb_2O_6$	-	B6
C. $\underline{PbTa_2O_6}$	6.23	C4, S4
D. $\underline{AlNb_3O_9}$	6.24	C4
IV. Complex and Miscellaneous Compounds		
$PbBi_2Nb_2O_9$	6.25A	S19
$SrBi_2Nb_2O_9$	6.25B	S19
$BaBi_2Nb_2O_9$	6.25C	S19
$PbBi_2Ta_2O_9$	6.26A	S19
$SrBi_2Ta_2O_9$	6.26B	S19, S20
$BaBi_2Ta_2O_9$	6.26C	S19
$PbBi_4Ti_4O_{15}$	6.27A	S19, S21
$SrBi_4Ti_4O_{15}$	6.27B	S19
$BaBi_4Ti_4O_{15}$	6.27C	S19, S21
$Sr_2Bi_4Ti_{15}O_{18}$	6.28A	S19
$Pb_2Bi_4Ti_{15}O_{18}$	6.28B	S19
$Ba_2Bi_4Ti_{15}O_{18}$	-	A1
$K_{0.5}Bi_{4.5}Ti_4O_{15}$	6.29A	S19
$Na_{0.5}Bi_{4.5}Ti_4O_{15}$	6.29B	S19
$Bi_4Ti_3O_{12}$	-	S20
$Bi_3PbTi_2NbO_{12}$	-	S20
$Bi_{2.2}Sr_{0.8}Ti_{0.2}Nb_{0.8}O_9$	6.30	S19
$Pb_3V_2O_8$	-	I8

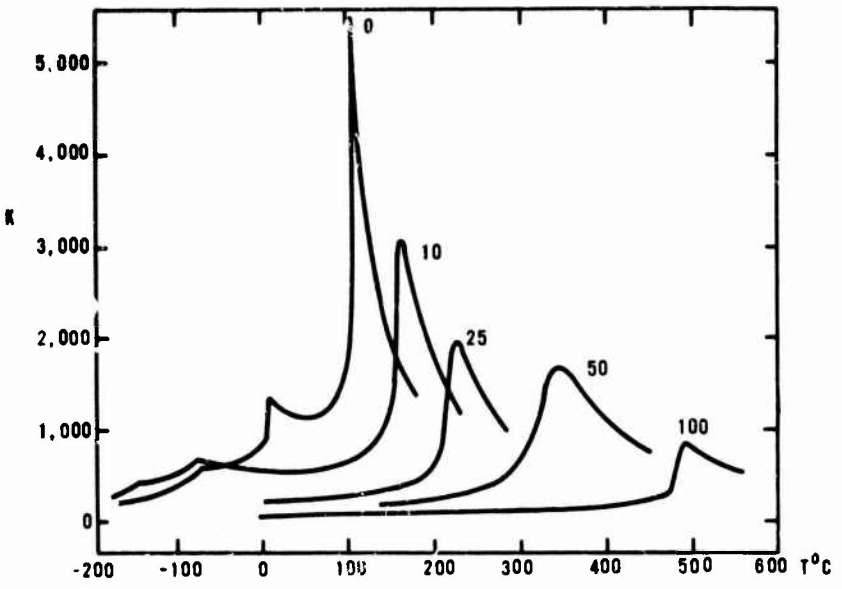

FIG. 6.1 M% $PbTiO_3$ IN $BaTiO_3$

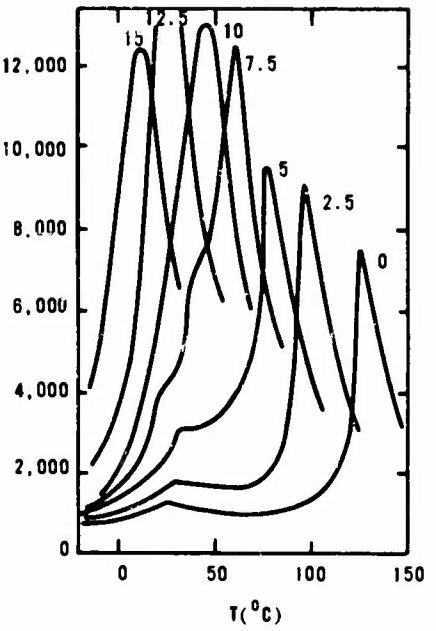

FIG. 6.4 M% $BaSnO_3$ IN $BaTiO_3$

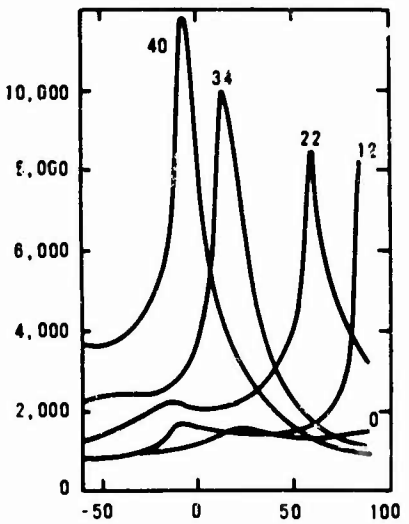

FIG. 6.2 M% $SrTiO_3$ IN $BaTiO_3$

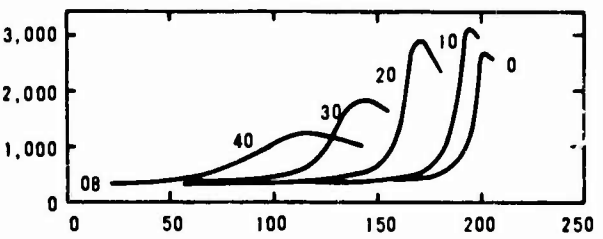

FIG. 6.5 M% $CaTiO_3$ IN $Ba_{0.8}Pb_{0.2}TiO_2$

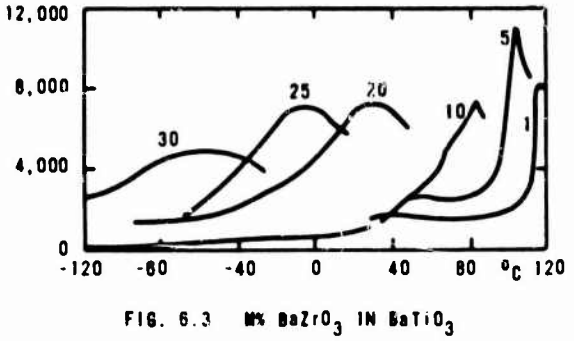

FIG. 6.3 M% $BaZrO_3$ IN $BaTiO_3$

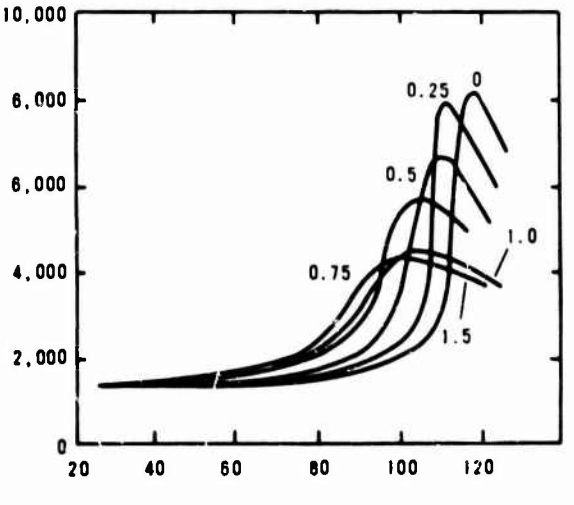

FIG. 6.6 M% Co IN $Ba_{0.95}Ca_{0.05}TiO_2$

Fig. 6 Dielectric Constant of Ferroelectrics vs Temperature

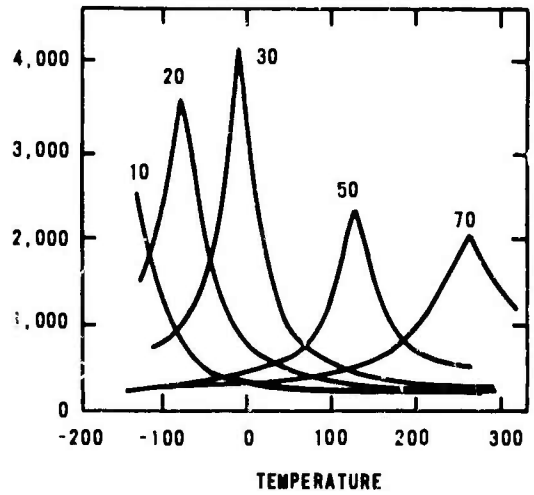

FIG. 6.7 M% $PbTiO_3$ IN $SrTiO_3$

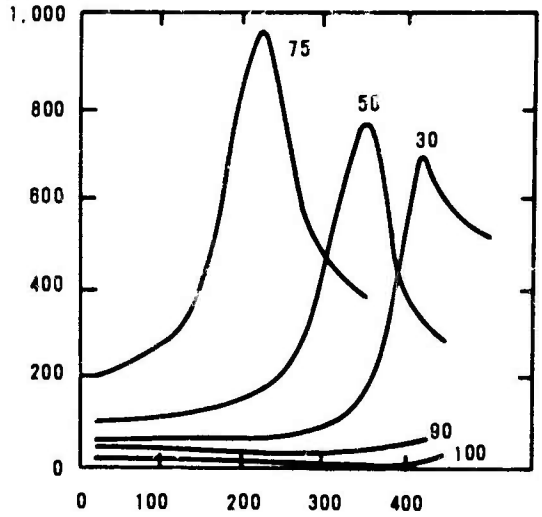

FIG. 6.8 M% $PbSnO_3$ IN $PbTiO_3$

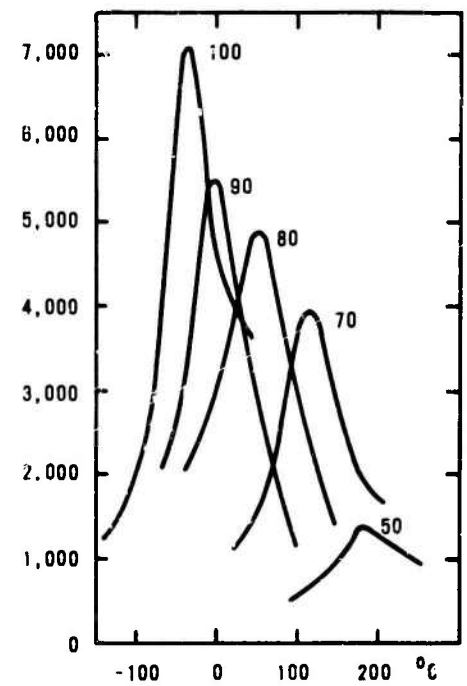

FIG. 6.9 M% $Pb(FeTa)_{\frac{1}{2}}O_3$ IN $PbTiO_3$

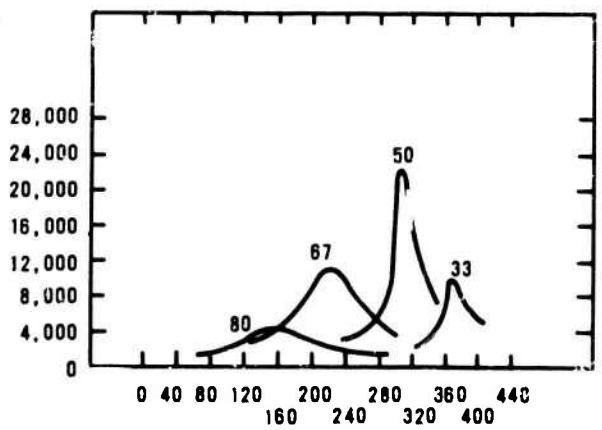

FIG. 6.10 M% $Pb(Sc_{\frac{1}{2}}Nb_{\frac{1}{2}})\ O_3$ IN $PbTiO_3$

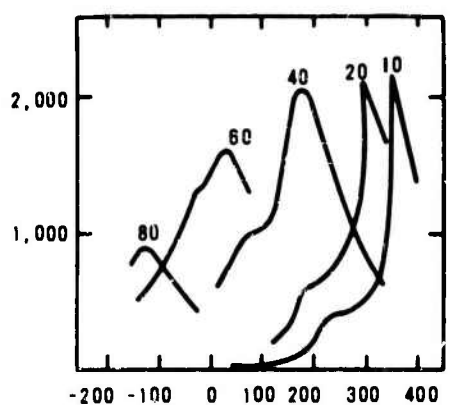

FIG. 6-11 M% $KTaO_3$ IN $NaNbO_3$

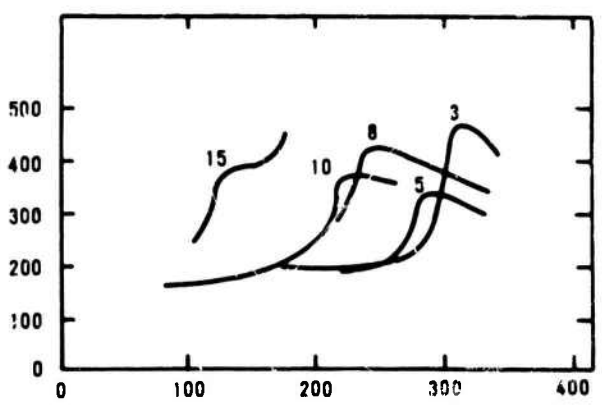

FIG. 6.12 M% $NaSbO_3$ IN $NaNbO_3$

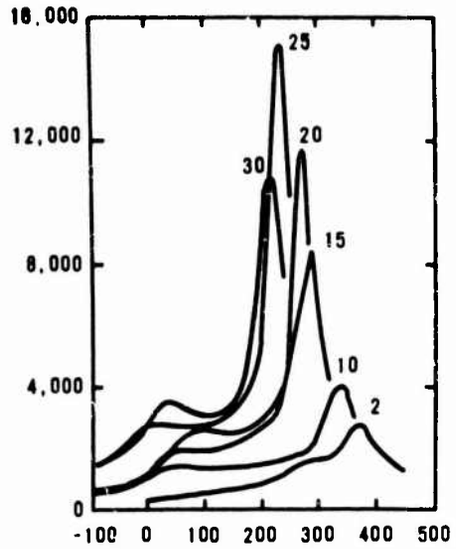

FIG. 6.13 M% $Cd_{\frac{1}{2}}NbO_3$ IN $NaNbO_3$

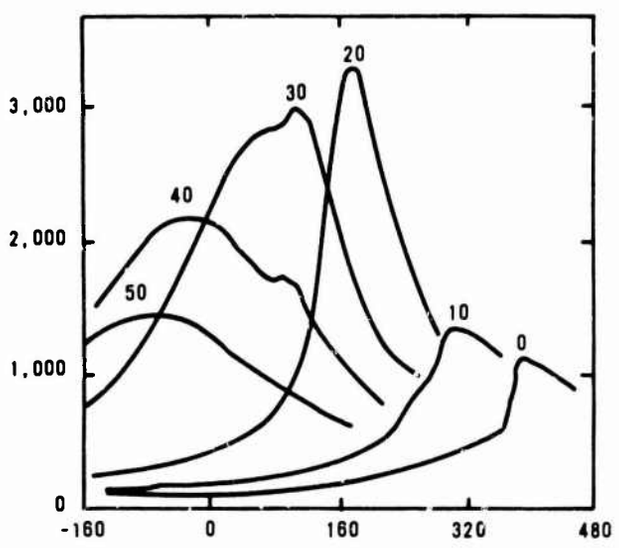

FIG. 6.14 M% $Sr_{\frac{1}{2}}NbO_3$ IN $NaNbO_3$

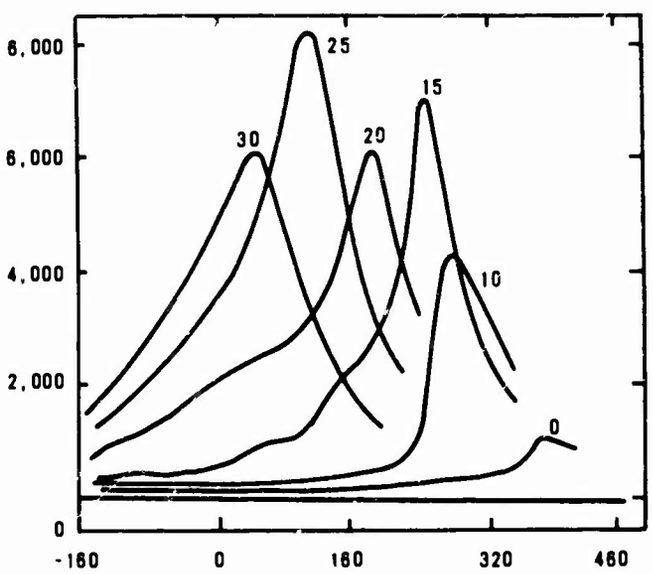

FIG. 6.15 M% $(Sr_{\frac{1}{2}}Cd_{\frac{1}{2}})NbO_3$ IN $NaNbO_3$

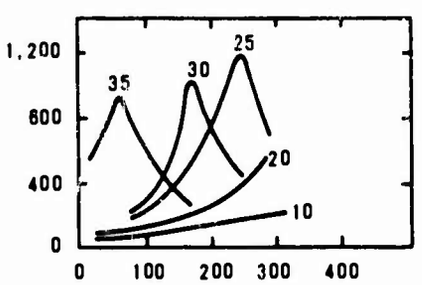

FIG. 6.16 M% $LaAlO_3$ IN $JiFeO_3$

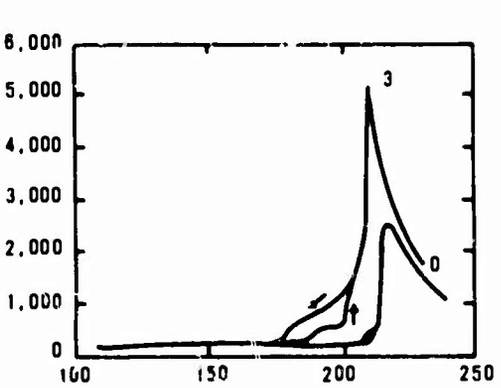

FIG. 6.17 M% $PbTiO_3$ IN $PbZrO_3$

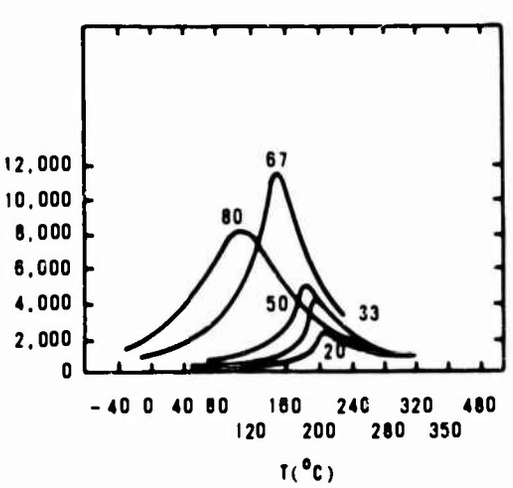

FIG. 6.18 M% $Pb(Sc_{\frac{1}{2}}Nb_{\frac{1}{2}})O_3$ IN $PbZrO_3$

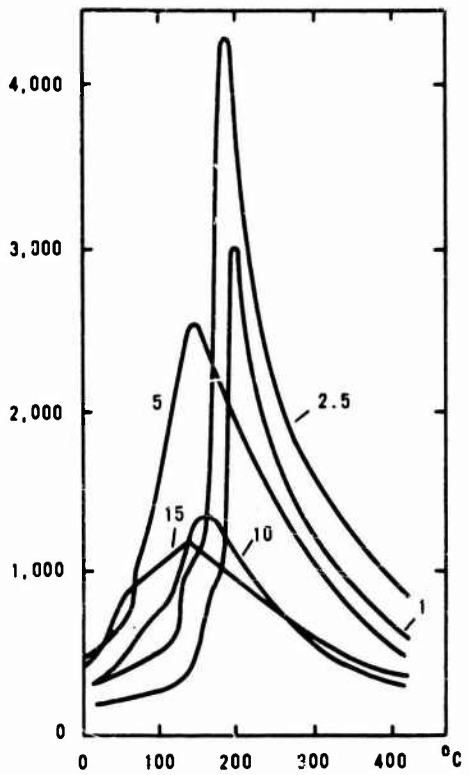

FIG. 6.19 M% $NaNbO_3$ IN $PbZrO_3$

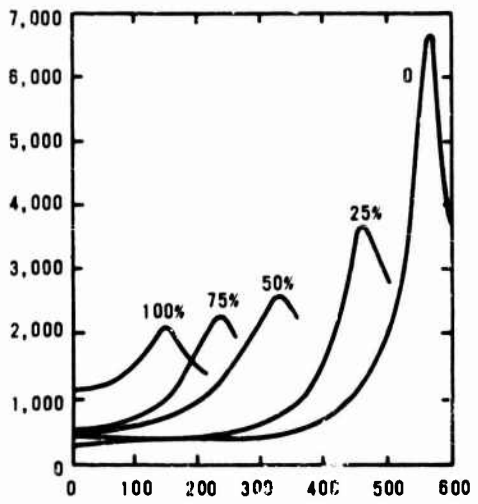

FIG. 6.21 M% $PbTa_2O_6$ IN $PbNb_2O_6$

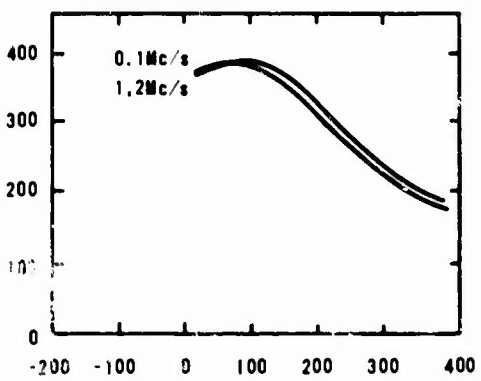

FIG. 6.23 $PbTa_2O_6$

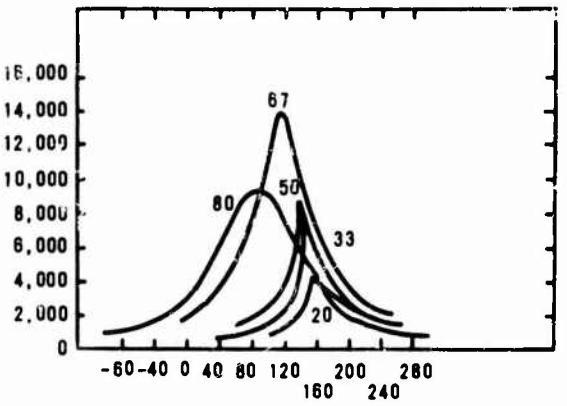

FIG. 6.20 M% $Pb(Sc_{\frac{1}{2}}Nb_{\frac{1}{2}})O_3$ IN $Pb\ HfO_3$

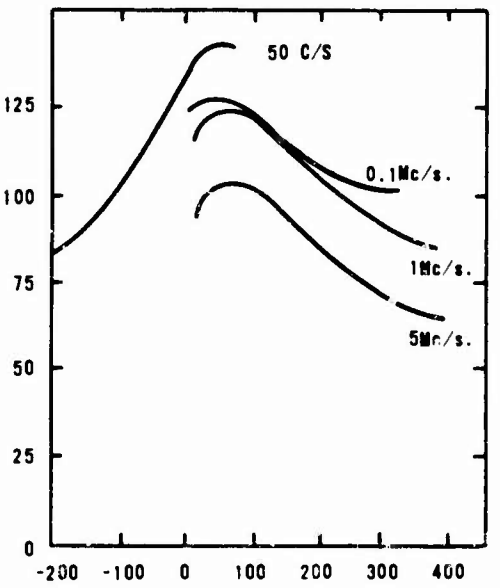

FIG. 6.22 $BaNb_2O_6$

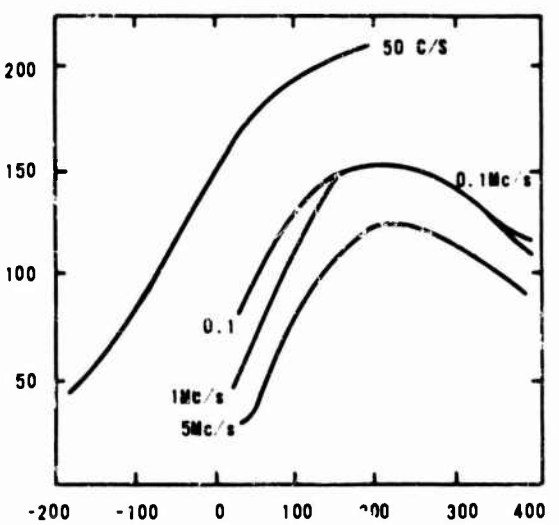

FIG. 6.24 $AlNb_3O_9$

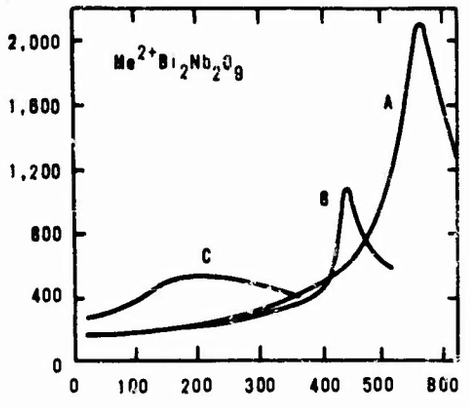

FIG. 6.25 A = $PbBi_2Nb_2O_9$
B = $SrBi_2Nb_2O_9$
C = $BaBi_2Nb_2O_9$

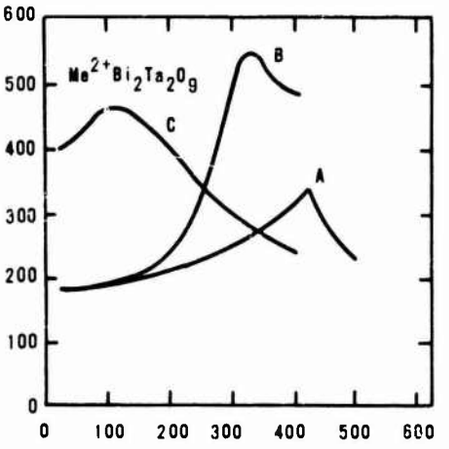

FIG. 6.26 A = $PbBi_2Ta_2O_9$
B = $SrBi_2Ta_2O_9$
C = $BaBi_2Ta_2O_9$

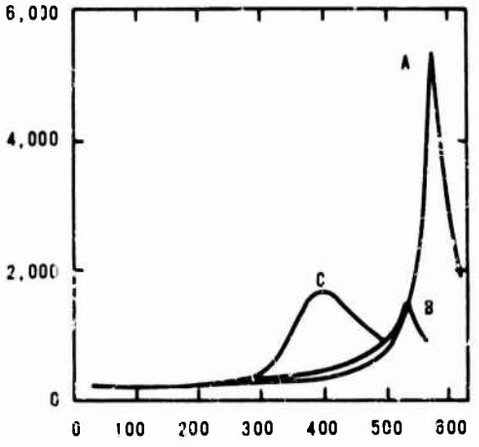

FIG. 6.27 A = $PbBi_4Ti_4O_{15}$
B = $SrBi_4Ti_4O_{15}$
C = $BaBi_4Ti_4O_{15}$

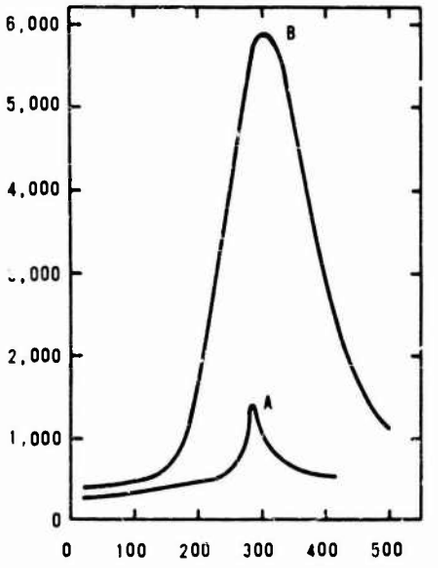

FIG. 6.28 A = $Sr_2Bi_4Ti_5O_{18}$
B = $Pb_2Bi_4Ti_5O_{18}$

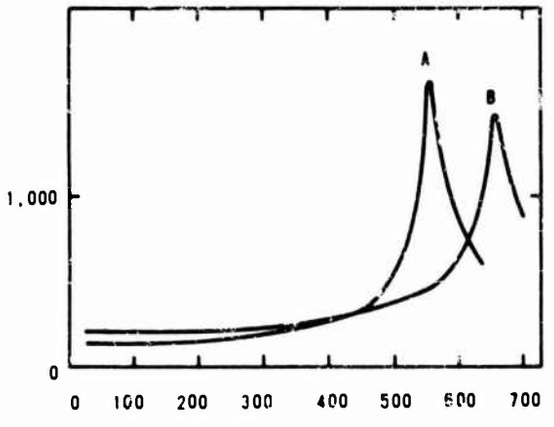

FIG. 6.29 A = $K_{0.5}Bi_{4.5}Ti_4O_{15}$
B = $Na_{0.5}Bi_{4.5}Ti_4O_{15}$

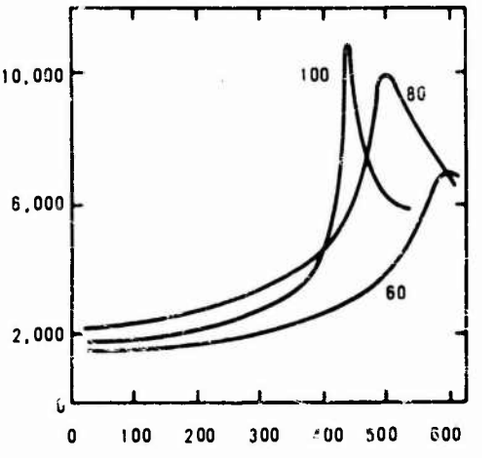

FIG. 6.30 M% $SrNbO_3$ IN $BiTiO_3$

TABLE IX

Ferroelectric Ceramic Compounds
According to Composition with References
Containing Coupling Factors, Piezoelectric
Constants, Elastic Constants, etc.

I. ABO_3 Compounds	References
A. $BaTiO_3$	B8, M8, J3, B9, B18
Solid Solutions of $BaTiO_3$	
$(Ba\text{-}Pb)TiO_3$	B18, J3, K6
$(Ba\text{-}Ca)TiO_3$	B18, B12, B6
$(Ba\text{-}Ni)TiO_3$	B7
$Ba(Ti\text{-}Zr)O_3$	K1, B26
$(Ba\text{-}Pb\text{-}Ca)TiO_3$	M12, B13, B26, B9
$(Ba\text{-}Ca\text{-}Co)TiO_3$	S9, B13
B. $PbTiO_3$ + Additives	T3
Solid Solutions of $PbTiO_3$	
$Pb(Ti\text{-}Zr)O_3$	J5, J4, J3, K8, K9, B14, D3, B9
$Pb(Ti\text{-}Zr)O_3$ + Additives	K8, K9, K7
$Pb(Ti\text{-}Hf)O_3$	J4
$Pb(Ti\text{-}Zr\text{-}Sn)O_3$	J4
$(Pb\text{-}Sr)(Ti\text{-}Zr)O_3$	K9
$(Pb\text{-}Sr)(Ti\text{-}Zr)O_3$ + Additives	K8, K9
$(Pb\text{-}Ca)(Ti\text{-}Zr)O_3$	K9
$(Pb\text{-}Ba)(Ti\text{-}Zr)O_3$	B25
C. Solid Solutions of $KNbO_3$	
$(K\text{-}Na)NbO_3$	E1, J2, B9, D7
D. $NaNbO_3$	D7
Solid Solutions of $NaNbO_3$	
$(Na\text{-}Cd)Nb_2O_6$	J3
E. Solid Solutions of Antiferroelectric $PbZrO_3$ and $PbHfO_3$	
$Pb(Zr\text{-}Ti)O_3$	T
$Pb(Zr\text{-}Ti)O_3 + PbNb_2O_6$	D
$Pb(Zr\text{-}Ti)O_3 + Pb(Mg_{1/3}Nb_{2/3})O_3$	O
$PbZrO_3 + PbNb_2O_6$	D
$PbZrO_3 + PbO:SnO_2$	J
$Pb(Hf\text{-}Ti\text{-}Sn\text{-}Nb)O_3$	H
II. AB_2O_6 Compounds	
A. $PbNb_2O_6$	J
Solid Solutions of $PbNb_2O_6$	
$(Pb\text{-}Ba)Nb_2O_6$	B
III. Complex Compounds	
$(B^{+3}_2O_3)^{+4}(Me_{m-1}R_mO_{3m+1})^{-4}$	

TABLE X

Piezoelectric Properties of Experimental Bodies

C	$BaTiO_3$					$(Ba_{1-x}-Pb_x)TiO_3$		
R	B8	B18	M8	J5	B9	B18	J3	K6
x						0.05w	0.1	0.12
y								
k_{33}	0.493		0.52		0.50		0.36	0.365
k_{31}	0.208	0.214	0.22		0.212	0.193	0.12	0.125
k_{15}	0.476				0.48			
k_p	0.354		0.37		0.36		0.20	0.210
d_{33}	191			190	190		70	90
d_{31}	-79	-78		-78	-78	-58	-23	-30
d_{15}	270				260			
g_{33}	11.4				12.6			
g_{31}	-4.7	-5.2			-5.2	-5.5		
g_{15}	18.8				20.8			
E_{33}	1680	1700	1600		1700	1190	500	850
E_{11}	1436				1450			
S_{11}	8.55	9.1	7.8	9.1	9.1	9.1	8.3	7.8
S_{33}	8.93				9.5			8.1
S_{44}	23.3		21		22.8			
Q				400	300		800	1200
p	5.72	5.7			5.7	5.5		5.7
T_c				115	115			150

C	$(Ba_{1-x}-Ca_x)TiO_3$			$(Ba_{1-x}-Ni_x)TiO_3$						
R	B18	B12	B9	B7						
x	0.05w	0.05w	0.05w	0	0.05	0.01	0.02	0.03	0.04	0.05
y										
k_{33}		0.49	0.48							
k_{31}	0.193	0.19	0.19							
k_{15}		0.495	0.48							
k_p		0.325	0.33	0.35	0.32	0.23	0.15	0.15	0.13	0.11
d_{33}		150	149							
d_{31}	-58	-58	-58							
d_{15}		257	242							
g_{33}			141							
g_{31}	-5.5		-5.5							
g_{15}			210							
E_{33}	1190	1200	1200	1500	1750	1850	1850	1850	1800	1650
E_{11}		1280	1300							
S_{11}	8.6	8.6	8.6	9.2	8.3	8.2	8.1	8.1	8.2	8.2
S_{33}		9.0	9.1							
S_{44}		22.7	22.2							
Q		500	400	200						
ρ	5.5	5.5	5.55	57	5.68	5.65	5.67	5.60	5.55	5.55
T_c		115	115	120	100	88	68	69	70	71

TABLE X (Cont.)

C	$Ba(Ti_{1-x}-Zr)O_3$										
R	K1										B26
x	0	0.01	0.02	0.05	0.075	0.10	0.15	0.20	0.25	0.30	0.05
y											
k_{33}											0.40
k_{31}											0.15
k_{15}											
k_p	0.298	0.351	0.360	0.387	0.220	0.167	0.04	--	--	--	0.35
d_{33}											150
d_{31}											-60
d_{15}											
g_{33}											12.1
g_{31}											-4.8
g_{15}											
E_{33}	1355	1350	1350	1100	1350	1450	2700	6750	5000	3200	1400
E_{11}											
S_{11}											9.1
S_{33}											
S_{44}											
Q											200
ρ	5.21	5.64	5.64	5.44	5.50	5.54	5.55	5.62	5.24	5.50	544
T_c											105

C	$(Ba_{1-(x+y)}-Pb_x-Ca_y)TiO_3$				
R	M12		B13	B26	B9
x	8w	12w	12w	8	12w
y	8w	8w	8w	12	8w
k_{33}			0.34	0.30	0.34
k_{31}			0.113	0.12	0.113
k_{15}			0.30		
k_p	0.252	0.217	0.19	0.22	0.19
d_{33}			60	90	60
d_{31}			-20	-35	-20
d_{15}					
g_{33}				18	15.1
g_{31}				-7.3	-5.0
g_{15}					
E_{33}	574	470	400	600	450
E_{11}					
S_{11}	7.65	7.83	7.8	7.7	7.8
S_{33}					8.1
S_{44}					
Q	578	570	1200	350	1200
ρ			5.4	5.3	5.4
T_c			140	160	140

TABLE X (Cont.)

C	$(Ba_{1-(x\ y)}\text{-}Ca_x\text{-}Co_y)TiO_3$							
R	B13	S9						
x	0.05w	0.05w	0.05w	0.05w	0.05w	0.05w	0.05w	0.05w
y	0.0075w	0	0.0025w	0.0050w	0.0075w	0.010w	0.0125w	0.015w
k_{33}								
k_{31}	0.182							
k_{15}								
k_p	0.31	0.34	0.33	0.32	0.31	0.28	0.29	0.29
d_{33}								
d_{31}	-59	-61	-60	-59	-59	-56	-55	-59
d_{15}								
g_{33}								
g_{31}		-5.2	-5.3	-5.0	-4.7	-4.4	-4.1	-4.4
g_{15}								
E_{33}	1420	1320	1270	1340	1420	1500	1500	1500
E_{11}								
S_{11}	8.1	8.1	8.6	8.2	8.1	8.5	7.8	8.6
S_{33}								
S_{44}								
Q								
ρ	5.7	5.74	5.61	5.65	5.69	5.73	5.70	5.71
T_c	105	118	111	110	105	104	100	100

C	$Pb(Ti_{1-x}Zr_x)O_3$											
R	J5	J4										J3
x	0.55	0.3	0.4	0.5	0.525	0.55	0.575	0.60	0.70	0.80	0.90	0.55
y												
k_{33}	0.5											0.55
k_{31}	0.22											0.23
k_{15}												
k_p	0.37	0	0.07	0.27	0.39	0.39	0.35	0.30	0.19	0.18	0.14	0.39
d_{33}	130											130
d_{31}	-50				-67	-56						56
d_{15}												
g_{33}	29											
g_{31}	-11				-9.8	-11.7						
g_{15}												
E_{33}		221	338	641	782	606	533	524	388	375	322	500
E_{11}												
S_{11}	7.5											13.3
S_{33}												
S_{44}												
Q												300
ρ		7.3	7.3	7.1	7.2	7.2	7.2	7.3	7.5	7.4	7.2	
T_c		420	405	400	370	330	350	350	320	280	235	350

TABLE X (Cont.)

C	$Pb(Ti_{1-x}Zr_x)O_3$ (Cont.)									
R	K8		K9		P3					
x	0.54	0.54	0.53	0.53	1	0.95	0.94	0.93	0.92	0.90
y										
k_{33}										
k_{31}										
k_{15}										
k_p	0.49	0.50	0.48	0.47	--	--	0.105	0.105	0.76	0.105
d_{33}					--	--	47	56	55	56
d_{31}	-71	-69	-71	-69						
d_{15}										
g_{33}										
g_{31}			-14.7	-14.4						
g_{15}										
E_{33}	537	513	544	542	109	333	423	430	485	450
E_{11}										
S_{11}			7.7	7.8						
S_{33}										
S_{44}										
Q										
ρ	7.41	7.29	7.40	7.39	7.77	7.69	7.70	7.73	7.58	7.68
T_c	390	387	385							

C	$(Pb(Ti_{1-x}-Zr_x)O_3$ (Cont.)							
R	B14							B9
x	0.48	0.50	0.52	0.54	0.56	0.58	0.60	0.54
y								
k_{33}	0.435	0.546	0.670	0.626	0.619	0.607	0.585	0.626
k_{31}	0.170	0.230	0.313	0.280	0.267	0.254	0.238	0.208
k_{15}	0.408	0.504	0.694	0.701	0.657	0.646	0.625	0.701
k_p	0.289	0.397	0.529	0.470	0.450	0.428	0.400	0.47
d_{33}	110	173	223	152	142	129	117	152
d_{31}	-43.0	-70.0	-93.5	-60.2	-54.3	-48.9	-44.2	-60.2
d_{15}	166	251	494	440	357	325	293	440
g_{33}	18.7	23.1	34.5	38.1	37.8	36.7	35.2	38.1
g_{31}	-7.3	-9.3	-14.5	-15.1	-14.5	-13.9	-13.3	-15.1
g_{15}	28.4	33.2	47.2	50.3	48.0	48.8	49.3	50.3
E_{33}	666	846	730	450	423	397	376	450
E_{11}	663	855	1180	990	840	751	672	990
S_{11}	10.8	12.4	12.8	11.6	11.0	10.5	10.4	11.6
S_{33}	10.9	13.3	17.1	14.8	14.0	12.8	12.0	14.8
S_{44}	28.3	32.8	48.2	45.0	39.8	37.7	36.9	45.0
Q	1170	950	860	680	490	500	600	680
ρ	7.59	7.55	7.55	7.62	7.59	7.64	7.60	7.62
T_c			350					370

TABLE X (Cont.)

C	$Pb(Ti_{0.46}\text{-}Zr_{0.54})O_3 + y(x)$							$Pb_{0.988}Th_{0.006}(Zr_{0.52}Ti_{0.48})O_3$
R	K9				K7			K7
x	0	Y_2O_3	La_2O_3	Nd_2O_3	Nb_2O_5	La_2O_3	W	--
y	0	0.01w	0.01w	0.01w	0.01w	0.01w	0.015	--
k_{33}								
k_{31}								
k_{15}	0.49	0.34	0.53	0.52	0.53	0.53	0.56	0.56
k_p								
d_{33}								
d_{31}	-76	-66	-138	-130				
d_{15}								
g_{33}								
g_{31}								
g_{15}								
E_{33}	537	841	1483	1387	1371	1483	1500	1560
E_{11}								
S_{11}								
S_{33}								
S_{44}								
Q					61			90
ρ	7.41	7.26	7.47	7.43	7.43	7.46		783
T_c	390	374		339				

C	$Pb(Ti_{1-x}\text{-}Zr_x)O_3 + y(Nb_2O_5)$								- +y(Ta_2O_5)				
R	K8												
x	0.54	0.54	0.54	0.54	0.54	0.54	0.54	0.54	0.54	0.54	0.54	0.54	0.54
y	0	0./w	0.5w	0.8w	1.0w	1.2w	1.4w	1.7w	2.0w	1.0w	2.0w	2.5w	5.0w
k_{33}													
k_{31}													
k_{15}													
k_p	0.50	0.38	0.46	0.48	0.53	0.48	0.50	0.47	0.50	0.49	0.49	0.36	0.33
d_{33}													
d_{31}	-70	-54	-94	-105	-125	-104	-113	-105	-115	-112	-112	-82	-76
d_{15}													
g_{33}													
g_{31}													
g_{15}													
E_{33}	525	598	790	1166	1275	1167	1218	1218	1202	1154	1250	1112	1052
E_{11}													
S_{11}													
S_{33}													
S_{44}													
Q					61	70	69		48	61		28	
ρ	7.35	7.26	6.96	7.36	7.48	7.34	7.37	7.39	7.39	7.27	7.45	7.23	6.75
T_c	388				361			344	369	368	364		

TABLE X (Cont.)

C	$Pb(Ti_{1-x}-Zr_x)O_3$ + 1 weight % Nb_2O_5									$Pb(Ti_{1-x}-Hf_x)O_3$	
R	K8									J4	
x	0.50	0.51	0.52	0.53	0.54	0.55	0.56	0.57	0.58	0.475	0.50
y											
k_{33}											
k_{31}											
k_{15}											
k_p	0.42	0.45	0.45	0.53	0.54	0.56	0.56	0.50	0.49	0.37	0.38
d_{33}											
d_{31}										-59	-54
d_{15}											
g_{33}											
g_{31}										-8.8	-10.3
g_{15}											
E_{33}	1041	1188	1200	1371	1296	973	745	684	630	764	672
E_{11}											
S_{11}											
S_{33}											
S_{44}											
Q	81	73	76	61	62	55	56	60	62		
ρ	7.38	7.31	7.39	7.43	7.44	7.40	7.38	7.41	7.41	8.5	8.4
T_c										350	330

C	$Pb(Ti_{1-x}-Sn)O_3$		$Pb(Ti_{1-(x+y)}-Zr_x-Sn_y)O_3$							
R	J4		J4							
x	0.55	0.60	0.40	0.43	0.32	0.34	0.23	0.25	0.14	0.15
y			0.10	0.10	0.20	0.20	0.30	0.30	0.40	0.40
k_{33}										
k_{31}										
k_{15}										
k_p	0.25	0.20	0.33	0.39	0.39	0.38	0.40	0.38	0.36	0.36
d_{33}										
d_{31}	-46	-28	-60	-52	-72	-61	-74	-65	-63	-61
d_{15}										
g_{33}										
g_{31}	-5.1	-5.0	-7.8	-9.7	-9.2	-9.5	-7.7	-9.1	-8.2	-8.9
g_{15}										
E_{33}	1260	776	815	827	976	836	1110	941	962	910
E_{11}										
S_{11}										
S_{33}										
S_{44}										
Q										
ρ	8.0	8.2	7.2	7.6	7.7	7.7	7.8	7.8	7.6	7.8
T_c	235	225	330	320	300	270	250	260	250	270

TABLE X (Cont.)

C	$(Pb_{1-x}\text{-}Sr_x)Ti_{1-y}\text{-}Zr_y)O_3$							
R	K9							
x	0.01	0.05	0.08	0.1	0.13	0.13	0.13	0.13
y	0.53	0.53	0.53	0.53	0.47	0.50	0.52	0.53
k_{33}								
k_{31}								
k_{15}								
k_p	0.49	0.50	0.50	0.49	0.28	0.33	0.44	0.47
d_{33}								
d_{31}	-75	-101	-103	-103	-40	-57	-91	-100
d_{15}								
g_{33}								
g_{31}	-14.5	-11.4	-10.6	-10.3	-6.8	-7.3	-9.0	-9.1
g_{15}								
E_{33}	584	1002	1094	1129	663	880	1149	1237
E_{11}								
S_{11}	7.7	7.6	7.9	7.9	9.9	9.0	8.3	8.1
S_{33}								
S_{44}								
Q								
ρ	7.42	7.47	7.29	7.22	7.09	7.11	7.10	7.14
T_c				290				265

C	$(Pb_{1-x}\text{-}Sr_x)Ti_{1-y}\text{-}Zr_y)O_3$ (Cont.)								
R	K9								
x	0.13	0.13	0.13	0.15	0.20	0.20	0.20	0.20	0.20
y	0.54	0.56	0.59	0.53	0.50	0.53	0.54	0.55	0.56
k_{33}									
k_{31}									
k_{15}									
k_p	0.51	0.51	0.45	0.43	0.29	0.34	0.35	0.34	0.35
d_{33}									
d_{31}	-119	-116	-66	-97	-56	-86	-91	-86	-81
d_{15}									
g_{33}									
g_{31}	-10.1	-10.8	-12.7	-8.7	-6.5	-7.8	-7.7	-7.3	-8.2
g_{15}									
E_{33}	1325	1210	585	1260	970	1257	1341	1337	1113
E_{11}									
S_{11}	7.5	7.3	9.2	7.7	8.1	7.1	6.2	6.4	6.5
S_{33}									
S_{44}									
Q									
p	7.16	7.14	7.17	6.90	6.56	6.48	6.36	6.36	6.35
T_c				242					

TABLE X (Cont.)

	$(K_{1-x}\text{-}Na_x)NbO_3$				$NaNbO_3$	$(Na_{1.6}\text{-}K_{0.2})Nb_2O_6$
	E1	D7	J2		D7	
x	0.5	0.5	0.5	0.5		
y			(air-fired)	(hot-pressed)		
k_{33}			0.51	0.53		
k_{31}			0.22	0.27		0.18
k_{15}						
k_p	0.37	0.17	0.36	0.45	0.15	
d_{33}	80		80	160		175
d_{31}	-32	-9	-32	-49	-9	70
d_{15}						
g_{33}	31.5		31.5	43		
g_{31}	-12.6	-10	-12.6	-13.1	-10	
g_{15}						
E_{33}	290	110			120	2000
E_{11}						
S_{11}	104	12.3	9.6	8.7	12.9	11
S_{33}						
S_{44}						
Q	130		130	240		300
ρ	4.25		4.25	4.46		
T_c			290	420		220

C	$Pb(Zr_{1-x}\text{-}Ti_x)O_3$						$Pb_{1-(y/2)}(Zr_{1-(x+y)}Ti_xNb_y)O_3$				
R	D3						D3				
x	0	0.05	0.06	0.07	0.08	0.10	0.03	0.05	0.088	0.065	0.01
y							0.025	0.025	0.025	0.01	0.06
k_{33}											
k_{31}											
k_{15}											
k_p			0.10	0.10	0.08	0.10	0.116	0.150	0.160	0.105	0.080
d_{33}							81	103	89	80	66
d_{31}			-47	-56	-55	-56					
d_{15}											
g_{33}											
g_{31}											
g_{15}											
E_{33}	109	332	423	430	485	454	317	275	350	226	454
E_{11}											
S_{11}											
S_{33}											
S_{44}											
Q											
ρ	7.77	7.69	7.70	7.73	7.58	7.68	7.69	7.70	7.63	7.15	7.51
T_c							208	218			

TABLE X (Cont.)

	$(xPbZrO_3 + yPbNb_2O_6)$			$Pb_{0.988}(Hf_{0.975-(x+y)}Ti_xSn_yNb_{0.025})O_3$				
R	D7			H4				
x	0.97	0.95	0.90	0.03	0.10	0.10	0.05	0.04
y	0.03	0.05	0.10	0	0	0.25	0.15	0.05
k_{33}								
k_{31}								
k_{15}								
k_p	0.07	0.10	0.05	0.102	0.156	0.091	0.058	0.076
d_{33}	100	80	20	65	77	90	54	65
d_{31}								
d_{15}								
g_{33}								
g_{31}								
g_{15}								
E_{33}	390	615	422	475	500	555	610	520
E_{11}								
S_{11}								
S_{33}								
S_{44}								
Q								
ρ	7.42	7.58	7.39					
T_c	186	170	181	163	174	140	155	164

C	$[xPb(Mg_{1/3}Nb_{2/3})O_3 + yPbTiO_3 + [1-(x+y)]PbZrO_3]$						$(1-x)PbNb_2O_6 \cdot xBaNb_2O_6$			$PbNb_2O_6$
R	02						E6			J3
x	0.75	0.50	0.5	0.25	0.25	0.01	.2	.4	.6	
y	0.25	0.40	0	0.50	0.25	0.45				
k_{33}										0.42
k_{31}										0.045
k_{15}										
k_p	4.6	30.4	7.5	29.0	29.5	33.6	0.20	0.38	0.16	0.07
d_{33}										80
d_{31}										-11
d_{15}										
g_{33}										
g_{31}										
g_{15}										
E_{33}	2689	1481	330	920	566	514				225
E_{11}										
S_{11}										3.5
S_{33}										
S_{44}										
Q	404	146	568	126	221	186	20	250	1000	11
ρ	7.27	7.55	7.23	7.50	7.46	7.12	5.9	5.9	5.6	
T_c							340	260	300	570

TABLE X (Cont.)

C R x y	$SrBi_2Nb_2O_9$ S19	$SrBi_2Ta_2O_9$ S19	$PbBi_2Nb_2O_9$ S19	$Na_{0.5}Bi_{4.5}Ti_4O_{15}$ S19
k_{33}				
k_{31}				
k_{15}				
k_p				
d_{33}	10	23	15	10
d_{31}				
d_{15}				
g_{33}				
g_{31}				
g_{15}				
E_{33}	190	180	170	200
E_{11}				
S_{11}				
S_{33}				
S_{44}				
Q				
p	6.9	7.5	7.6	6.3
T_c	440	335	560	655

TABLE XI

Piezoelectric and Dielectric Properties of Commercially Available Materials

Company	Trade Name	Type	T_c	Max. Temp.	ρ	E	Qm	K	tan δ
Bausch & Lomb	-	F	195	160	4.5	11.0	240	400	1.5
Centralab	KD-10	C	115		5.5	11.6	400	1200	3.0
"	KD-13	A	125		5.3	10.6	400	1600	3.0
"	KE-12	B	300		7.5	8.2	600	1200	1.0
"	KE-14	B	360		7.6	6.6	80	1600	3.0
"	KG-25	B	180		7.3	7.0	70	3000	3.0
Clevite	Ceramic "B"	C	115		5.6	11.6	400	1200	0.8
"	PZT-4	B	325		7.6	8.2	500	1300	
"	PZT-5A	B	365		7.7	6.1	75	1700	
"	PZT-5H		193		7.5	6.1	65	3400	2.0
"	PZT-8		300		7.6	9.0	1000	1000	0.4
Commander Labs	#100	E	140		5.4	12.8	1200	400	
"	#300	C	115		5.5	11.6	500	1200	
"	#400	B	340		7.5	8.2	600	1200	
"	#500	B	360		7.5	6.8	75	1500	
Erie Tech	Ceramelec 1005	A	120	95	5.6	10.2	380	1700	0.8
"	Ceramelec 1006	C	120	90	5.5	11.5	360	1200	0.9
"	Ceramelec 1007			45	5.4	10.1		1200	2.5
"	Ceramelec 1008	C	115	90	5.4	9.4	600	1200	0.5
"	Ceramelec 1009	D	135	100	5.6	11.0	360	1400	0.8
"	Ceramelec 1011	E	145	125	5.4	11.2	350	700	0.6
"	Ceramelec 2001	B	300	150	7.5	7.8	200	1150	0.5
"	Ceramelec 2003	B	300	150	7.6	7.0	85	1600	1.5
Gulton Ind	Hi-T	B	280		7.5	7.3		1700	2.0
"	Glennite		130		5.6	11.5		1250	1.5
Linden Labs	Sonotite 101	B	350	150	7.6	7.1	80	1700	1.5
"	Sonotite 102	B	310	150	7.5	7.6	230	1200	0.5
"	Sonotite 501	A	120	95	5.6	10.4	400	1800	0.9
"	Sonotite 502	A	120	95	5.6	10.2	650	1800	0.6
"	Sonotite 601	C	120	90	5.5	11.5	350	1200	0.9
"	Sonotite 602	C	120	90	5.5	10.0	580	1200	0.7
"	Sonotite 701	D	133	100	5.6	11.0	350	1400	0.9
"	Sonotite 702	D	133	100	5.6	10.0	550	1400	0.8
"	Sonotite 801	E	145	120	5.3	11.2	350	730	0.7
"	Sonotite 802	E	145	120	5.3	12.0	500	730	0.5
"	Sonotite 803	E	145	120	5.3	11.2	400	600	0.7
Solidtronics	BT-10	C	120		5.5	12.1	600	1150	
"	BT-15	D	130		5.5	12.2	500	1250	
"	BT-20	E	140		5.3	12.4	1200	550	
"	LZ-30	B	350		7.4	8.2	700	600	
"	LZ-40	B	330		7.6	7.9	600	1200	
"	LZ-50	B	330		7.6	7.2	75	1500	
TAMCO	5205	B	350		7.6		75	1650	1.5
"	5204	B			7.6			1380	0.3
UPI	401	B	350		7.6	8.0	625	1375	0.4
"	501	B	360		7.6	6.9	85	1625	1.2
"	601	B	340		7.5	8.6	375	1050	1.6
"	701	B	340		7.4	11.0	1300	400	1.0
"	702	B	340		7.3	9.5	1025	500	1.0
"	901	B	340		7.25	7.3	75	1850	1.2

Coupling Coefficients				Frequency Constants		Piezoelectric Constants			
k_p	k_{15}	k_{31}	k_{33}	N_1	N_3	d_{31}	d_{33}	g_{31}	g_{33}
0.45	0.60	0.27	0.53	69	122	- 49	160	-14	45
0.30		0.18	0.46	125	108	- 57	150	- 5.4	14
0.31		0.18	0.41	118	99	- 65	150	- 4.7	11
0.53		0.31	0.64	88	79	-110	250	-10.0	24
0.56		0.32	0.66	82	71	-160	330	-12.0	24
0.60		0.34	0.71	85	75	- 25	34	- 9.4	14
0.33	0.48	0.19	0.48	90	108	- 58	139	- 5.5	14.0
0.58	0.71	0.33	0.70	65	79	-122	285	-10.0	24.9
0.60	0.69	0.34	0.71	55	70	-171	374	-11.4	24.8
0.65	0.68	0.39	0.68	56	79	-274	593	- 9.1	19.7
0.50		0.30		67		- 93	218	-10.5	24.5
0.19	0.30	0.11	0.34	96	90	- 20	68	- 5.6	19
0.32	0.49	0.19	0.49	90	116	- 58	150	- 5.5	14
0.52	0.65	0.31	0.64	65	79	-110	255	-10.4	24
0.54	0.65	0.32	0.68	59	74	-140	320	-10.6	24
0.33		0.20	0.47	116	97	- 77	188	- 4.9	11.9
0.31		0.18	0.48	123	103	- 56	146	- 5.2	13.6
0.37		0.22	0.55	115	96	- 71	177	- 6.7	16.7
0.32		0.19	0.65	118	101	- 60	154	- 6.4	16.4
0.32		0.19	0.52	118	101	- 62	160	- 5.1	13.1
0.27		0.16	0.51	121	98	- 38	107	- 6.1	17.2
0.50		0.30	0.65	87	79	-108	245	-10.6	25.0
0.53		0.31	0.67	82	77	-140	320	- 9.9	22.6
0.54		0.31	0.56	83	59	-140	320	- 9.0	21
0.33		0.20	0.51	103	91	- 62	155	- 6.1	14
0.55		0.32	0.69	81	78	-150	340	-10.8	23
0.51		0.31	0.67	85	80	-112	260	-10.6	25
0.35		0.22	0.50	115	97	- 80	190	- 4.6	12
0.34		0.21	0.48	115	97	- 78	188	- 4.7	11.9
0.32		0.18	0.47	123	102	- 56	145	- 5.1	13.2
0.32		0.18	0.50	119	100	- 60	150	- 6.2	15.9
0.32		0.18	0.50	118	101	- 60	150	- 5.0	12.8
0.32		0.18	0.52	116	100	- 65	160	- 5.8	14.5
0.28		0.16	0.44	120	98	- 40	110	- 6.2	17.0
0.26		0.16	0.50	123	100	- 38	120	- 5.9	18.6
0.28		0.16	0.50	123	100	- 36	112	- 6.8	21.2
0.36		0.18	0.47	122	89	- 64	164	- 6.1	15.0
0.33		0.18	0.46	118	85	- 62	158	- 5.8	14.0
0.28		0.14	0.36	122	84	- 30	91	- 7.3	18.0
0.52		0.30	0.63	90	75	- 94	223	-14.5	34.5
0.53		0.32	0.64	90	65	-110	255	-10.4	24.0
0.55		0.31	0.68	88	63	-145	330	-10.6	25.0
0.54									
0.53				90					
0.53		0.32	0.64	88	76	-125	275	-10.5	24.5
0.55		0.32	0.68	82	71	-145	330	-10.3	25.0
0.42		0.26	0.52	94	81	- 82	195	- 8.8	21.0
0.25		0.14	0.31	104	90	- 27	70	- 7.6	19.0
0.28		0.16	0.34	100	88	- 36	83	- 8.5	20.0
0.50		0.42	0.61	83	72	-140	340	- 8.5	23.0

Description of Symbols and Units Used in Tables X and XI

C = Compound formula $[(A_{1-(x+y)}-B_x-C_y)D\ O_3]$

R = References

x = Mole ratio B_x in compound (w = weight ratio)

y = Mole ratio of C_y in compound

k = Coupling Coefficients

d = Piezoelectric constant ($x10^{-12}$ Coulomb/Newton)

g = Piezoelectric constant ($x10^{-3}$ volt meter/Newton)

E = Relative dielectric constant, free (E^T/E_o) (= K)

s = Elastic compliance at constant electric field ($x10^{-3}$ volt meter/Newton)

Q = Mechanical Q

ρ = Density ($x10^3$ kg/m^3)

T_c = Curie temperature (°C)

Y = Young's Modulus (10^{10} Newton/meter^2)

Tan δ = Dissipation Factor at 1 kcps (%)

N_1 = Radial Frequency Constant (Kilocycle-inches)

N_3 = Thickness Frequency Constant (Kilocycle-inches)

Type = Material Composition Type

A. Pure Barium Titanate
B. Lead-Zirconate-Titanate
C. Barium-Calcium-Titanate
D. Barium-Lead-Titanate
E. Barium-Lead-Calcium-Titanate
F. Sodium-Potassium-Niobate
G. Lead-Metaniobate

TAMCO = National Lead Company

UPI = Ultrasonic Powders, Inc.

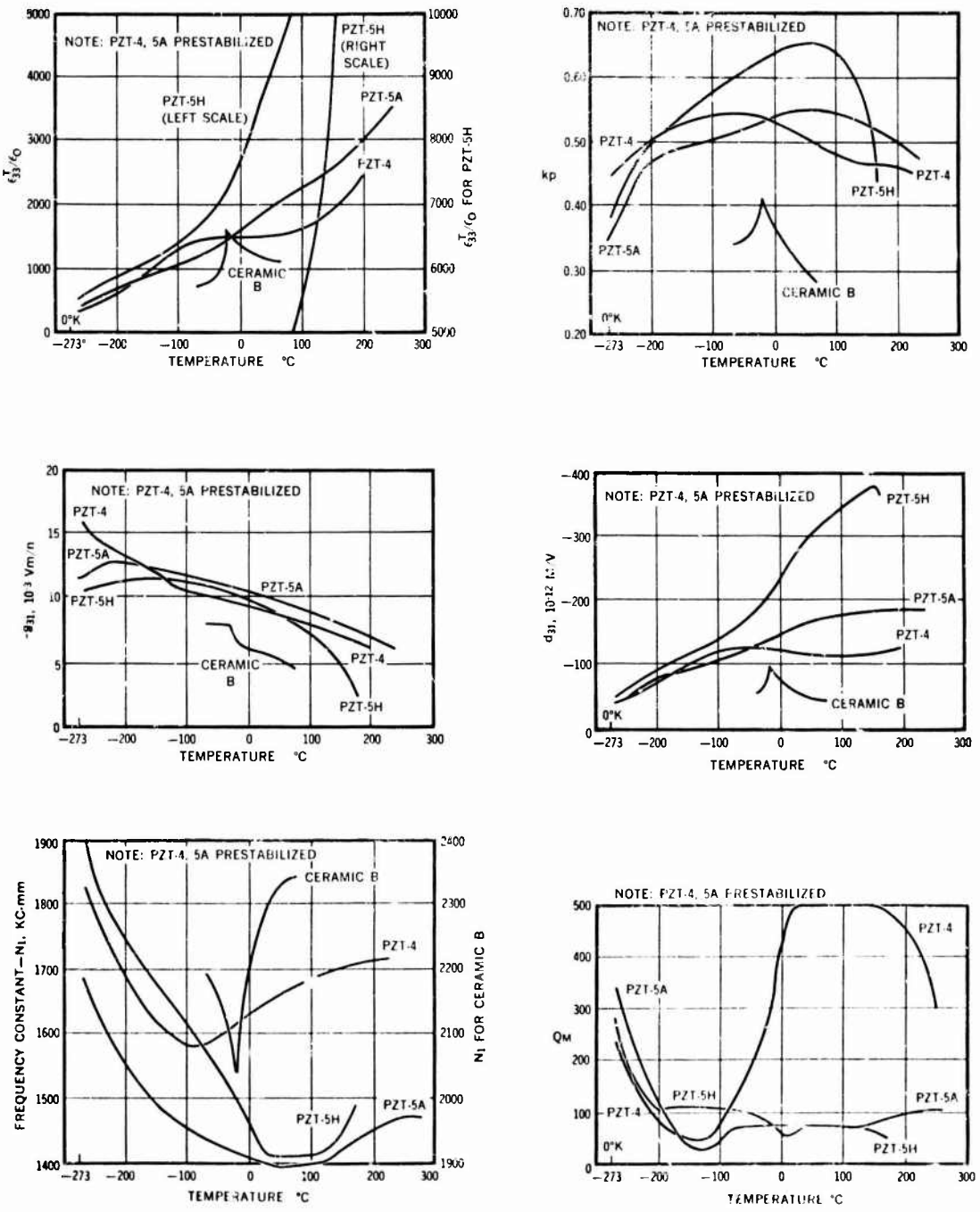

Fig. 7 Dielectric and Piezoelectric Properties vs. Temperature of Clevite Ferroelectric

TABLE XII

Properties of Commercially Available Capacitor Dielectrics

Trade Designation	Insulation Resistance ($\times 10^3$ megohm.)	Dielectric Constant	Dielectric Strength (volt per mil at thickness in inches)				Life Test Rating (volt per mil at °C)		
Company Name	Typical		0.02	0.03	0.04	0.05	85°	125°	250°
American Lava									
ALSIMAG									
T-106-J	750	1650	350	275	225	175	63	40	
T-128-B	125	9000	160	125	100	85	50	25	
T-153-A	225	825	325	275	225	200	50		
T-157-A	400	290	300	275	250	225	50		
T-158-A	400	2150	175	150	125	125	80	40	
T-158-B	500	2100	175	160	125	125	80		
T-164-E	1000	1300	300	250	200	175	100	63	40
T-171-A	150	3000	225	200	175	150	70	40	20
T-172-A	150	1900	230	200			50		
T-176-A	300	5250	175	165	150	140	75	40	
T-183-A	125	6250					50		
T-185-A	150	11500	75				35		

TABLE XII (Cont.)

Properties of Commercially Available Capacitor Dielectrics

Trade No.	24 Hr K (min)	Aging %/Decade (max)	D.F. Max 1KC	Min RC Product Megohm MFD	Life Test Rating Vdc/mil in °C			Voltage Sensitivity (at 25°C) 25 Vdc/mil	Temperature Characteristics in °C							
Company Name					85°	125°	150°	Typical	-55°	-30°	+10°	45°	65°	85°	125°	150°
Erie Technological Products, Inc.																
K025021	250	3.0	1.5	500	100	63		+2.2%	+5.0 -7.5	+5.0 -7.5	+5.0 -7.5	+5.0 -7.5	+5.0 -7.5	+5.0 -7.5	±10	+5 -15
K060011	700	4.0	1.0	200	50	32		-5.0%	-10	-9	±5.0		-10	-10	+30 -10	
K110021	1050	1.0	1.7	500	100	63		+0.3%	±4.7	±3 3	±3.3	±3.3	±3.3	±3.3	+15 -5	+10 -20
K120071	1200	2.0	1.5	600	100	63	50	-4.5%	±7.5	±6.0	±5.0		±7.5	±7.5	+40 -8	+20 -15
K200011	2000	4.0	1.7	500	100	75	50	-13.0%	-15	-10	+10 -5.0		-12	-15	-40	-60
K260011	2600	4.0	2.0	500	100	50		-17.5%	-30	-25	±7.5	±7.5	±7.5	±7.5	+10 -22	-50
K450011	4500	3.0	1.5	500	63	40		-37.0%	-56	+22 -33	+22 -15	-25	-40	-56	-80	
K520011	5100	4.0	1.0	500	63	40		-29.0%	-56	+22 -33	±15	-25	-40	-56	-80	
K900011	8000	5.5	2.5	500	63			-55%	-90	-80	+10 -45	±20	-45	-56	-80	
K1000Q11	10000	10.0	2.5	500	50	20		-70%	-90	-80	+15 -50	-60	-80	-90	-95	

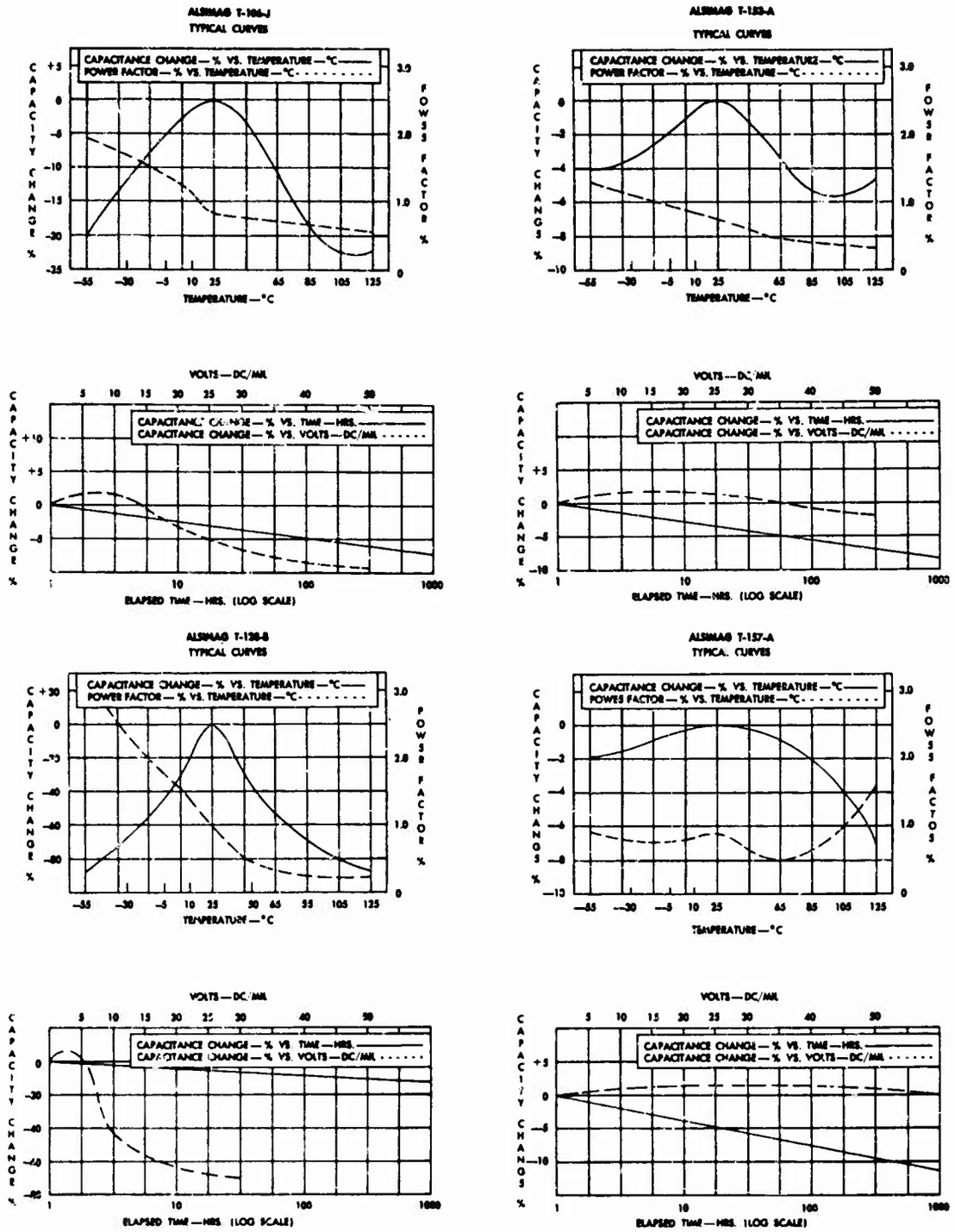

Fig. 8.1 Dielectric Properties of American Lava Capacitor Ferroelectric Bodies

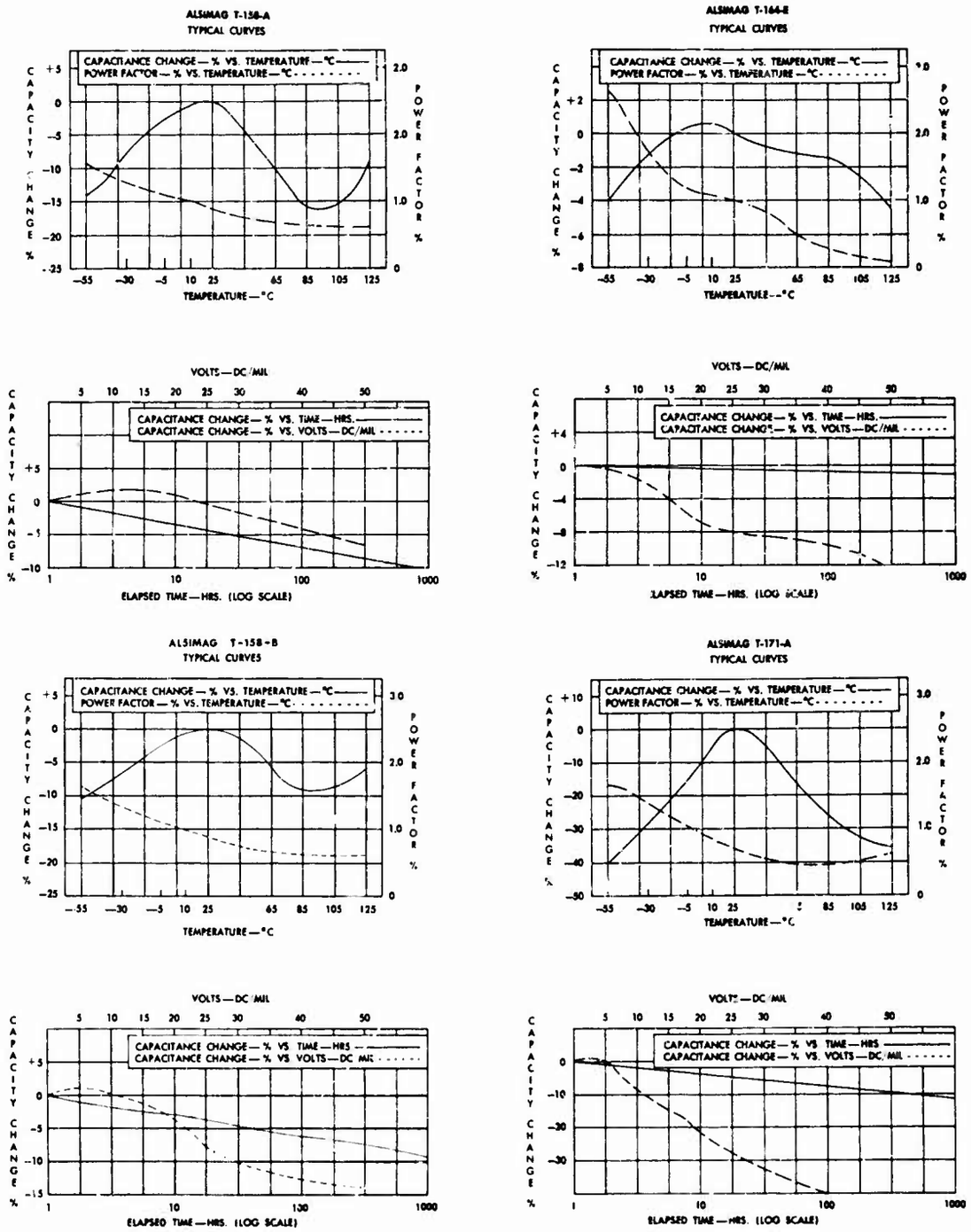

Fig. 8.2 Dielectric Properties of American Lava Capacitor Ferroelectric Bodies (Cont'd)

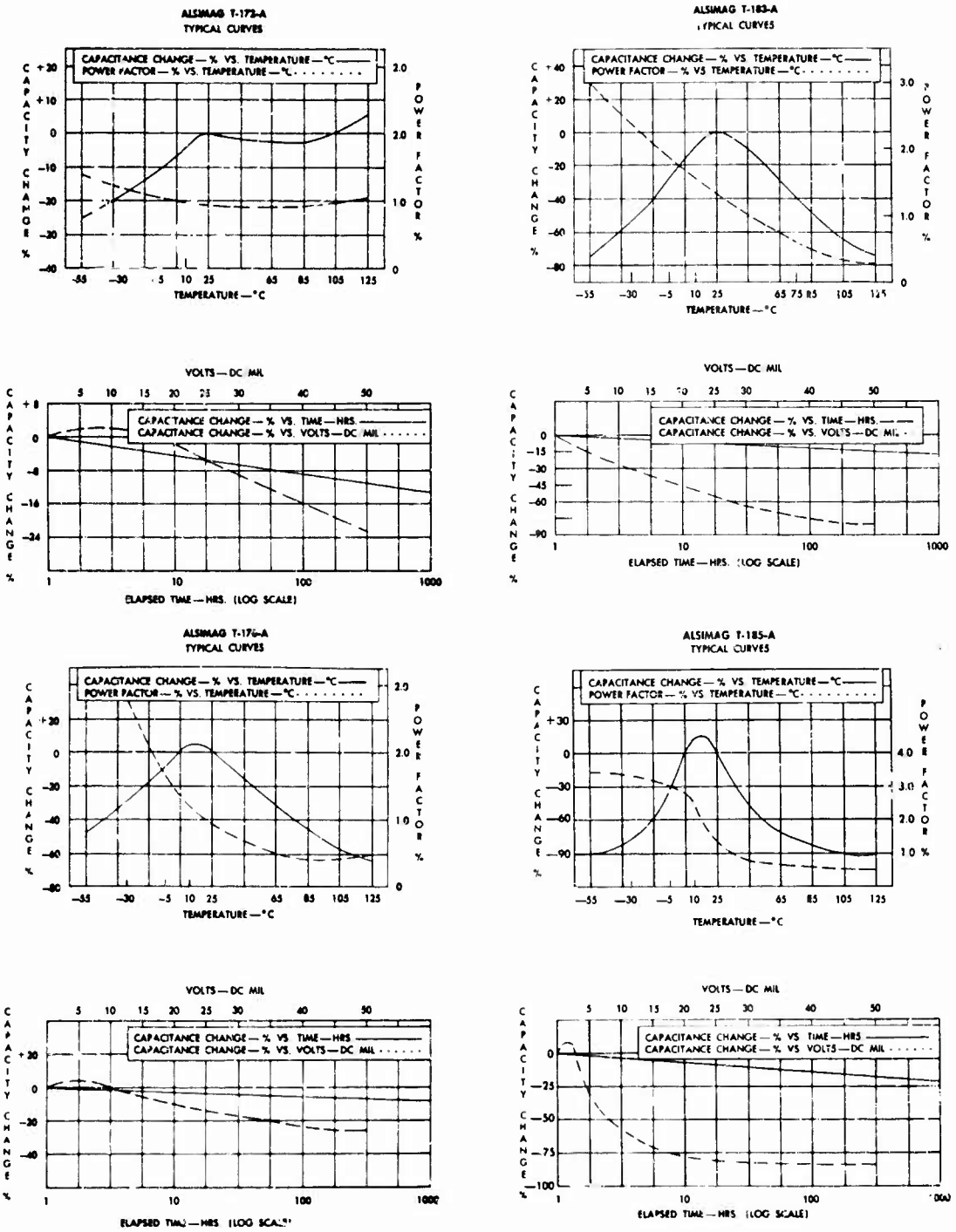

Fig. 8.3 Dielectric Properties of American Lava Capacitor Ferroelectric Bodies (Cont'd)

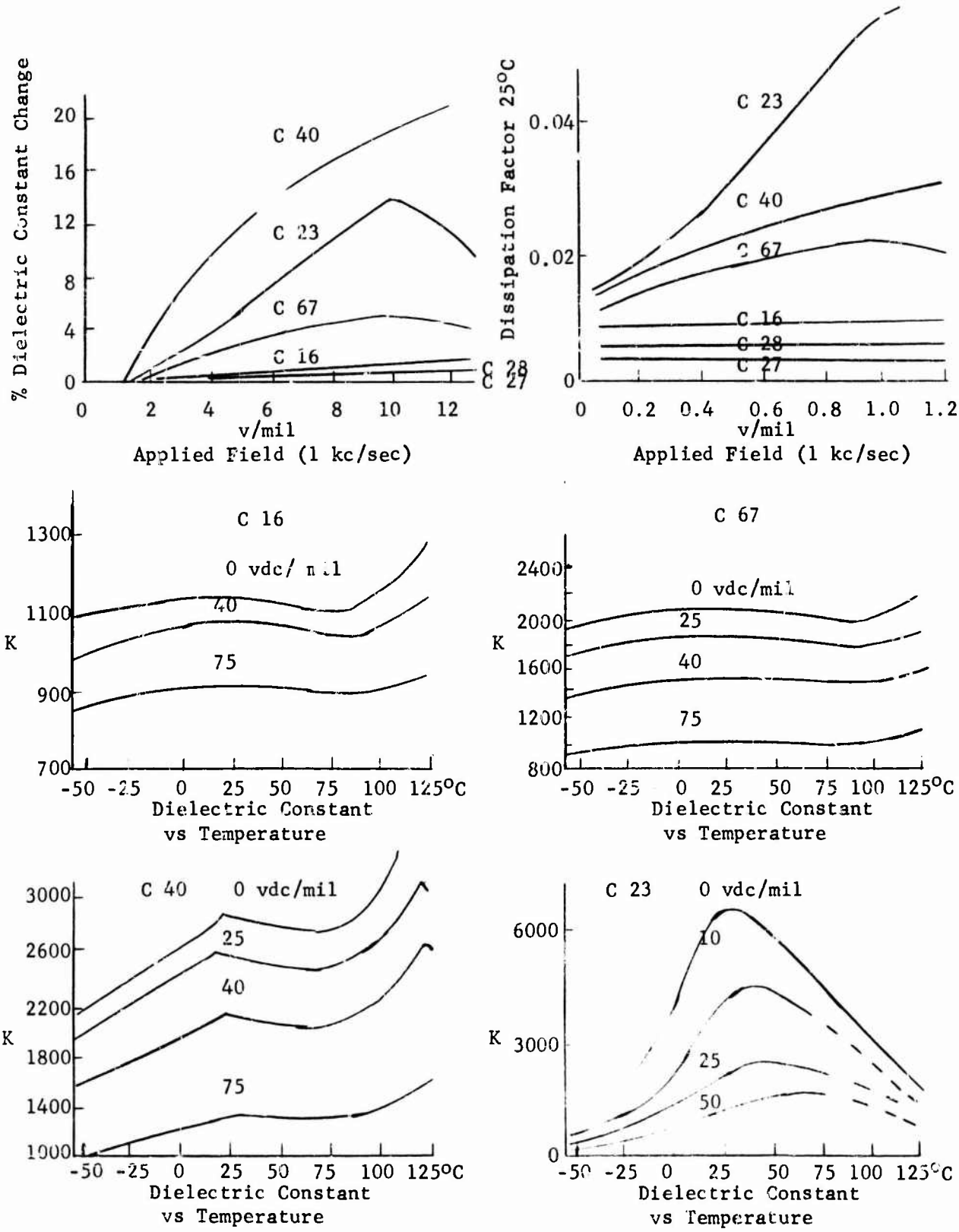

Fig. 8.4 Dielectric Properties of Sprague Capacitor Bodies (Cont'd)

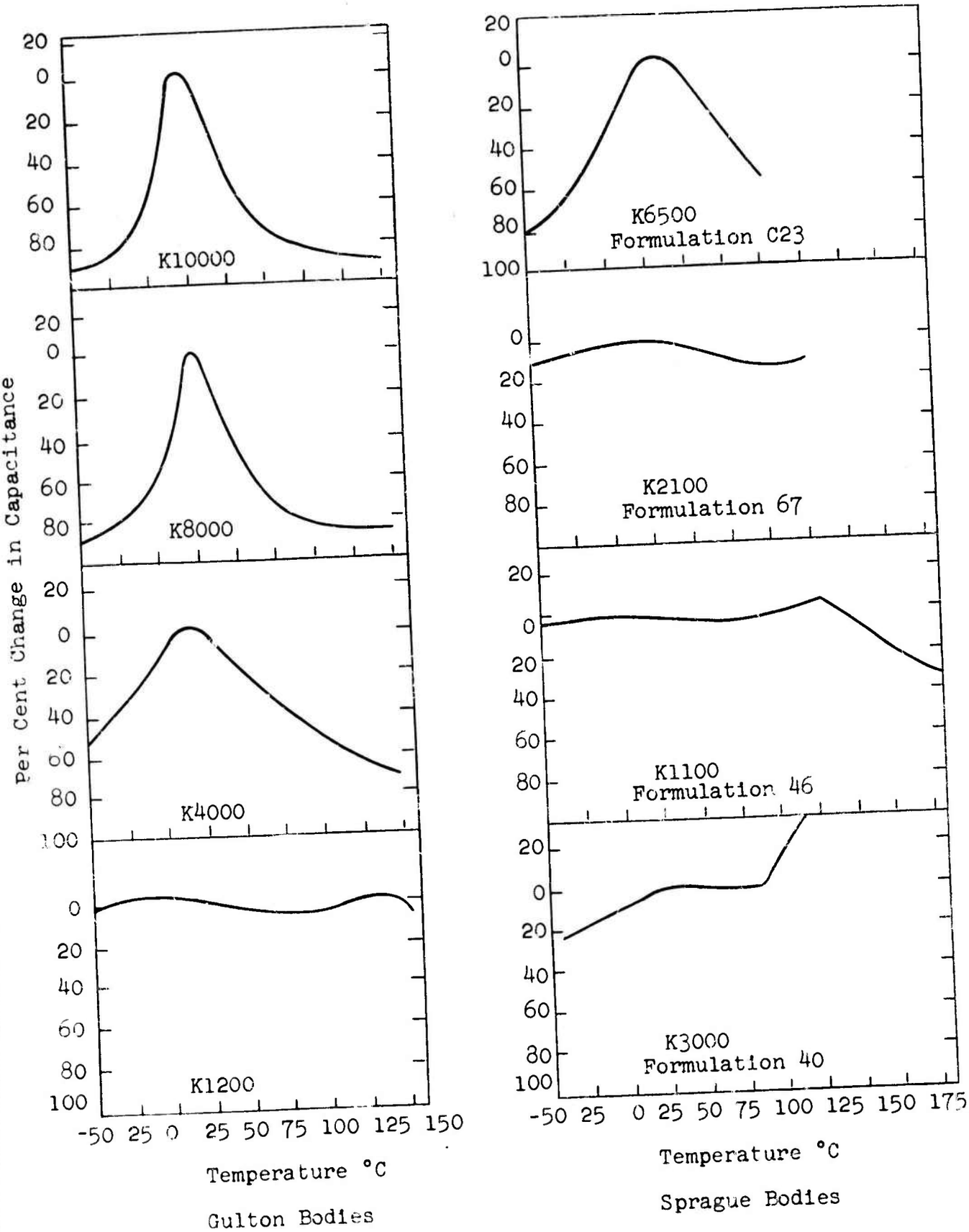

Fig. 9 Capacitance Change with Temperature

IV. INTERPRETATION OF DIELECTRIC PROPERTIES OF CERAMIC FERROELECTRICS AS MODIFIED SINGLE CRYSTAL PROPERTIES

A. Dielectric Constant

1. Room temperature values

Given the isotropic dielectric constant of a polycrystalline, ceramic ferroelectric, it should be possible to correlate it with the single crystal dielectric constants of the compounds of which it is composed. The questions which arise in this respect, are the following:

(a) Is the dielectric constant of the crystallites intrinsic, i.e., is it due to the volume polarizability of the constituent crystals?

(b) If the dielectric constant is intrinsic, what is the texture of the crystallites (grain structure)? This determines which averaging formula has to be used (see II-B-1).

(c) What is the concentration of pores and what is the concentration and nature of second phases?

(d) What is the internal stress distribution?

(e) Are all or part of the grains of "subcritical size" (see IV-B-3) so that "superparaelectric" effects have to be expected?

(f) Is there any contribution of extrinsic polarization mechanisms such as domain wall motions, jumping ions, rotating defect pairs or Maxwell-Wagner effects?

Only if the crystalline phases in a polycrystalline material can be identified with well known single crystal phases and only if the texture of the polycrystalline material is carefully studied, can these questions, or at least some of them, be answered. Assuming the absence of extrinsic effects, of "superparaelectric" effects and of stresses other than those due to point defects, dislocations, grain boundaries and 90° domain wall zigzag stresses, assuming furthermore a spherical

grain and pore structure, the dielectric constant of pure $BaTiO_3$ can be computed with formula (6) in II-B-1. With $K_x = K_y = 4100$ and $K_z = 160$ (J1, page 112), one computes

$$\overline{K} = 2210$$

A 5% porosity gives, with formula (4) in II-B-1,

$$\overline{K} = 2040$$

Values like this are frequently observed; however, most observers cite $\overline{K}$ = 1400-2000 as the most frequent range of K of ceramic $BaTiO_3$ at room temperature. It is difficult to decide how much of the differences between observers are due to differences in impurities, grain size and shape, pore concentration, size and shape, etc. Plessner (P5) goes so far as to believe that the intrinsic value of polycrystalline $BaTiO_3$ is about 300 due to complete clamping in the ceramic, and that the observed values of 1500 and more are due to extrinsic effects, i.e., mainly domain wall motion.

As to clamping, there will be little clamping due to the electrostrictive effect because it is a quadratic effect and each domain expands with an applied field the same way as the antidomain. With the piezo-effect, this is different and in the same field in which the domain expands the antidomain will contract. This clamping will be 100% close to the 180° domain wall and will be much less at a distance of the wall. In single crystals, a reduction of K of about 18.35% has been found by Drougard and Young (D13) for the same kind of clamping and this value seems reasonable as an order of magnitude value for the polycrystal, too. If this reduction factor would be applied to the above average of $\overline{K}$ = 2040, one would get

$$\overline{K} = 1665$$

which is not too different from the value Marutake (M8) has observed and slightly higner than the one which he has computed by actually taking the piezoelectric interaction into account.

There is still the possibility of a contribution of oscillating domain walls to K as it is well known from the ferromagnetic case. However, ferroelectric domain walls are very different from ferromagnetic domain walls; whereas, the ferromagnetic walls behave almost like rubber membranes, the ferroelectric walls do not easily move sideways, apparently only by a partial nucleation process. The present author has formed the opinion that there will be a side movement but not 90° ahead of the electric field as the other polarization processes but only in phase with the field and, therefore, contributing mainly to K" and not the K'.

2. Temperature dependence of K

The first problem which the ceramists working with pure $BaTiO_3$ and other single compound ferroelectrics had to solve was to find means to smooth out the high peaks of the dielectric (and other) constants near the ferroelectric transformation temperatures. There is no problem in shifting these peaks up and down by incorporating other components in solid solution. The classical examples are the addition of $SrTiO_3$ for a downmovement of the Curie peak and $PbTiO_3$ for an upmovement.

The flattening of the peaks was a much more difficult problem. There is first a small flattening effect by mixing with another phase without active interaction. Then there is the possibility that the single crystal peaks can be broadened themselves by solid solutions in which the constants A, B, C, D and G of the thermodynamic function and their temperature dependence is changed which might result in broader peaks. In the same way, the stress and strain distribution of single phase solid solutions might be changed so that a wider range of stresses results.

The most effective mechanism, however, of broadening seems to be that of having a second phase, usually not ferroelectric, and having some active, i.e., stress interaction, between the two phases. If this second phase is produced in

the body by exsolution from the main phase, it is possible that non-equilibrium compositions are obtained by cooling down from the firing temperature, so that there are actually regions with different composition and, therefore, different Curie-points present.

Another type of broadening is that of joining together the different peaks corresponding to the different ferroelectric transitions; e.g., in pure $KNbO_3$ the 3 peaks are 450°C apart, whereas in the 80% $KTaO_3$ solid solution, they are only 40°C apart. In other systems, the lower transformation temperatures move up when the Curie temperature is moved down; this happens by addition of $Ba_{(1-x/2)}Ti_{(1-x)}Nb_xO_3$ to $BaTiO_3$ (Subbarao and Shirane)(S24).

3. Frequency dependence of K

Single crystals of $BaTiO_3$ have a small loss of K of 20-50% at the piezoelectric resonance frequency, e.g., 10 Mcps for a plate of 1 cm diameter and .1 cm thickness; they retain the lower value (clamped value) up to frequencies of perhaps 50 Gc/s.

Ceramic samples, on the other hand, show a drop from about 1500 to 300 at 1-10 Gc/s, a phenomenon which is not quite understood.

Several authors, e.g., Merz (M1) ascribe this drop to domain wall relaxation because a similar drop has been found by Fousek (F11) in multidomain single crystals of $BaTiO_3$, whereas single domain single crystals as mentioned above experience only the 20-50% drop (Benedict and Durand) (B47). The picture is not very consistent: If the drop from 1500 to 150 in ceramics and that from 2000 to 150 in Fousek's multidomain crystal is due to domain wall relaxation, one should assume that the low frequency value, i.e., the excess over 150 would be due to domain wall oscillations. However, the single crystal without domain walls has the same value of 2000 after the piezoelectric resonance which is, in fact, halfway between the intrinsic value for the free crystal and that for the completely clamped crystal, according to Devonshire's theory.

In the ceramic, one can visualize the drop due to a transition from the partially clamped state into the total clamping due to piezoelectric resonance of the grains; however, there are other processes which might produce relaxation.

There are, e.g., the currents due to changes in internal fields caused by the divergence P-charges; they will occur on all domain and grain boundaries which are not traversed by the polarization vector P in a symmetrical head-to-tail fashion. Depending on the actual value of dielectric constant and resistivity, these charging-discharging currents will have relaxation times from microseconds to seconds and might affect the frequency dependence of the dielectric constant as well as that of the losses.

It seems that in this area much more research is needed to establish reliable experimental facts as well as to give consistent explanations. One of the discrepancies which might be mentioned here is that ceramic $BaTiO_3$ dielectrics show the sharp drop from the 1.5 Mc/s to the 9.54 Gc/s value not only at room temperature but also in the cubic phase which seems to rule out the explanation of piezoelectric resonance (P12). For this reason von Hippel (V2) suggests a grain size effect. On the other hand, solid solutions of $BaTiO_3$ with $SrTiO_3$ in the range from about 20 to 60% b.m. do not show the slightest decrease of their 1.5 Mc/s dielectric constant at the 9.54 Gc/s frequency above their Curie point (P12).

B. Non-linear Behavior and Domain-Effects

In ferroelectrics one has to distinguish two types of non-linear behavior: One due to the non-linear character of the P vs E function which according to the phenomenological theory is a function of the 5. order if the free energy function is taken up to the P^6 term.

The other type of non-linear behavior is due to domain switching which occurs as a function of electrical as well as of mechanical stresses.

The poling problem which is treated from a technical viewpoint in part V-C can be looked upon as a problem of domain switching. If a complete reversal of all 180° domains would take place, the P_s-value of the poled ceramic would be 0.5 of the spontaneous polarization of the single crystal; if, in addition, all possible 90° domain switches would occur the value would be 0.84.

The P_s-value of ceramic $BaTiO_3$ is 0.05 Coul/m^2 when measured on a 60 c/s hysteresis loop; this is less than 0.2 of the spontaneous polarization of the single crystal. In the long time poling process a high degree of 180° domain switches can be achieved, and, temporarily, 10-17% of the 90° domains can be switched. Of these, after removal of the poling voltage a portion switches back. Subbarao, McQuarrie and Buessem (S31) measured the length changes during depoling of samples which had been poled with a field of 10 kv/cm. The depoling strain developing at the Curie point was -2.3×10^{-4}, corresponding to about 9% of the 90° domains; i.e., about half of the 90° domains switched back after poling, the other half after depoling. It is possible that a portion of the 90° domains switches back after poling because this removes much of the mechanical stress which comes about when the poling voltage is removed. The electrostrictive effect makes a sphere into a prolate ellipsoid in the field direction and the 90° domain switches with the field to minimize the strain energy with respect to that shape. If the poling field is removed, the ellipsoid tends to go back to the spherical shape and a portion of the 90° domains has to switch back to achieve minimization of strain energy under the new conditions.

A puzzling effect of poling is that the dielectric constant of ceramic $BaTiO_3$ increases, both in the direction of poling and perpendicular to it. There are, perhaps, three effects involved: The immediate effect is usually de-aging due to heating above the Curie point during poling. When this is eliminated as cause of the K-increase by comparing poled and

unpoled samples at the same age, one finds still an increase of about 12% in the poling direction and 3% perpendicular to it (B8) (M20) (M7). Two factors might contribute to this. It might be partly ue to the stresses just described in the last paragraph, which are tending to make the grain more cubic and increase its K slightly (G5) (B46). The main factor, as mentioned by Jona and Shirane (J1),might be that part of the 180° domain clamping might be removed by removal of most of the 180° domain walls. The clamping effect was estimated to be of the order of magnitude of 18%. The K increase, due to the removed clamping, in addition to the stress effect, might overcompensate the slight decrease which would result from the 5-9% 90°-domain switches after poling and which, by themselves, would reduce K correspondingly.

C. Stability

1. Without applied field: aging

Introduction. The instability of all dielectric and piezoelectric properties of ferroelectric ceramics with respect to time; i.e., the spontaneous change (decrease or increase) of all properties under zero external field conditions has been termed "aging". This instability must be distinguished clearly from the changes which occur with time under DC-stress (degradation) or changes which may occur under conditions of AC-stress, mechanical stress or other conditions affecting the initial performance such as atmosphere, humidity, radiation, etc. The literature is not completely unambiguous in this respect, but in most publications the term "aging" or "ageing" is used in the sense defined here. The most powerful criterion which can be applied to distinguish aging from all the other changes is that it occurs only in the ferroelectric state, whereas degradation and most other changes mentioned may occur as well above the Curie temperature.

The practical importance of aging of ferroelectric ceramics cannot be overestimated. The K-aging seriously affects the tolerance problem in production of ferroelectric condensers. The aging of the piezoelectric properties, especially the aging of the frequency constant, is the most serious hindrance to widespread use of IF transformers.

Literature Survey. Table XIII contains references on aging of dielectric and piezoelectric properties of different bodies. Most papers give only aging rates of the properties investigated without going into a theoretical discussion of the possible mechanisms involved. The logarithmic time law for the decrease of the dielectric constant K

$$K_t = K_1[1 - \frac{a}{100} \log t] \qquad (1)$$

was already established by Marks in 1948 (M6); the constant a in this relation is the aging rate per decade of time in %;

TABLE XIII

Literature Survey of Aging

Composition	Unpoled				Poled						
	K	Tan δ	P_R	P_s	K	Tan δ	Frequ. Const.	Coupl. Coef.	d_{31}	s_{31}	P_s
$BaTiO_3$			M16	M16							
$BaZrO_3 \cdot PbTiO_3$	J6	J6			J6			J6			
$BaTiO_3$	M15	M15									
$BaTiO_3 \cdot SrTiO_3$	M15										
$BaTiO_3$(Stoichiom.)	M15										
$80BaTiO_3 \cdot 12PbTiO_3 \cdot 8CaTiO_3$	M12				M12	M12	M12	M12	M12	M12	M12
$93BaTiO_3 \cdot 7CaTiO_3$					G6		G6	G6	G6		
$95BaTiO_3 \cdot 5PbTiO_3$					G6		G6	G6	G6		
$BaTiO_3$	P5	P5									
$85BaTiO_3 \cdot 10SrTiO_3 \cdot 5MgF_2$	P5	P5									
$BaTiO_3 \cdot CaZrO_3$	P5	P5									
$BaTiO_3$ FT*					T6		T6	T6			
$BaTiO_3$(cycling thru T_c)					T6		T6				
$BaTiO_3$(cycling thru T_c)					T5		T5				
$96BaTiO_3 \cdot 4PbTiO_3$					T5		T5				
$BaTiO_3$ + $MgSnO_3$	P3										
$PbZrO_3 \cdot PbTiO_3$(+La,Nb)	G1										
$PbTiO_3 \cdot CaTiO_3$			S6	S6							
$BaTiO_3$ FT*	B31										
$BaTiO_3$ CB**, FT*	B29										
$BaTiO_3$ CB**, K***	D6										

*Fluorine treatment, **Commercial body, ***With different K

e.g., from time one to time ten, e.g., in minutes, if K_1 is K at time one. Many observers have wondered about the unusual form of this law which is inverse to a normal decay function:

$$b = b_o + b_1 e^{-t/t_1} \qquad (2)$$

in which the time t is a function of the log of the property and not the reverse. However, one can approximate (1) by a sum of expressions (2). The important consequence of this form of the aging function is that it allows for a flat portion at very short times and also at very long times, whereas equation (1) implies the nonsensical result of an infinite K at time zero and a zero K at time infinite.

Almost as important as aging is the reverse process, called de-aging (rejuvenation). Complete de-aging is possible by heating above the Curie temperature; partial de-aging by any temperature change, but also by mechanical or electrical stresses. An exact knowledge of the de-aging properties of a body as well as the aging properties is necessary, if one wants to use pre-aging as a means to overcome some of the detrimental effects of aging. For example, with an aging rate of 3% per decade and one minute as the time of the first measurement, the material has aged 15% during the first five decades but the aging rate for the next year is only about 2% per year and for the next ten years only 1/2% per year. In other words, the material is now rather stable, provided that no de-aging occurs. Whether the pre-aging technique can be used successfully depends on the de-aging sensitivity of the material as well as on the magnitude and frequency of thermal, electrical and/or mechanical shocks after pre-aging. The only detailed de-aging study has been published by W. Heywang and R. Schoefer (H17). These authors observed the propeller-shaped hysteresis curves of the aged $BaTiO_3$ which had been described formerly by McQuarrie (M16); they observed also that it disappeared after a certain time of display on the screen. To measure the de-aging time exactly, they introduced a new

method whereby dP/dE vs E was displayed rather than P vs E. A normal hysteresis curve is hereby transformed into a distorted square, the two maxima corresponding to the two steepest slopes on the hysteresis curve. An aged $BaTiO_3$, however, had 4 maxima and the time of disappearance of the two extra maxima was taken as time needed for de-aging. The study was performed on three samples of 100, 80 and 50 micron grain size as a function of temperature between -40°C and 130°C. For each sample it was found that the de-aging time vs temperature curve had two sharp maxima, one about 18°C below the tetragonal/orthorhombic transformation temperature, the other 18°C above it. In the case of the "fine" grain (50μ) material the upper maximum was about one hour, whereas at the transformation temperature itself and also at the Curie point the time it was zero. For the 80 μ grain size material the maximum was 15 minutes, for the 100 μ grain size material two minutes. One can see that even at these large grain sizes the effects are strongly dependent on grain size.

In the following paragraphs, certain important facts are summarized from the papers cited; these are the facts which have to be explained by any theory of aging and which will be used for a discussion of possible and probable aging mechanisms.

(1). The "initial" (= small signal) permittivity of ceramic ferroelectrics decreases according to a log t law (M6).

(2). The aging rate of the tan delta in the intermediate frequency range (1 kc) is typically three to four times greater than that of the real part of the dielectric constant (M15)(P5).

(3). An aged body exhibits a propeller-shaped hysteresis curve, indicating an about equal loss (absolute) in maximum polarization and remanent polarization; de-aging occurs after a few minutes of displaying the propeller-shaped hysteresis curve under the influence of the AC-signal which is used for this display (M16) (H17).

(4). For $BaTiO_3$ bodies with impurities the K-aging rate decreases with increasing c/a ratio (M15).

(5). For $BaTiO_3$ the K-aging rate increases with increasing temperature (M15) (P5) (D12).

(6). The aging rate of K and tan delta of $BaTiO_3$ and of commercial high K-bodies can be lowered substantially by fluorine treatment; the same applies to the frequency constant of poled $BaTiO_3$ and PZT ((B31) (B29) (T6).

(7). The aging rate of K for $BaTiO_3$ bodies can be lowered by exsolution or deposition of second phases (B31) (B29).

(8). Aging rate is low for $BaTiO_3$ bodies with small grain size (G5).

(9). For bodies with large grain size K-aging rate is proportional to K (D6).

(10). Aging of K decreases with concentration of (111)-twins in $BaTiO_3$ (D12).

Possible and Probable Aging Mechanisms. After Mason (M12) and McQuarrie and Buessem (M15) had established that aging occurs only in the ferroelectric state, it was generally assumed that it had to do with a domain reorientation (J1). The only exception is aging of ceramic $Pb_{0.5}Ca_{0.4}TiO_3$ in which aging has been explained by an exsolution of a second phase at room temperature (S6).

The great difficulty in invoking domain reorientation to explain aging is the fact that domain switches can occur in times of the order of a microsecond whereas aging might involve times up to 20 years. This is a difference of 15 orders of magnitude and indicates that quite different domain processes must be involved.

The most detailed proposal of aging as a domain reorientation process has been given by Plessner (P5).

Plessner bases his picture of the unaged ceramic barium titanate on Devonshire's (D5) concept of the clamped dielectric constant; he assumes ceramic $BaTiO_3$ to be 100% clamped. Whereas the linear average of the dielectric constants in the "free" state is about 3100, the "clamped" average may be as low as 300. The difference between 300 and the observed values of 1500-1900 is then ascribed to domain wall motion; it

is pointed out that for a field of 1 volt/cm domain switching of a fraction of only 10^{-5} of all domains would be sufficient to account for the observed permittivity. By use of Figure 10a (P5, page ~~118~~ 109) aging of K can then be explained as follows: After cooling through the Curie temperature a domain wall is fixed in a metastable position at A in which it can move with a small restoring force (shallow potential well) and give a rather large contribution to K. Or a wall might be fixed in a metastable position at C, separated only by a small activation energy H from another position C' to which it might jump under a field with the help of thermal activation. This jump is a typical relaxation process with relaxation time

$$\tau = \tau_o \exp(-H/kT) \qquad (3)$$

and in the neighborhood of the relaxation frequency $\omega = 1/\tau$ contributes greatly to the tan delta. Plessner assumes for τ_o a value of 10^{-9} sec and H values from 0.125 to 0.45 ev. Both domain walls, that at A and that at C', might eventually jump over the barrier E or E' into a well at B where the restoring force is much greater and, therefore, the contribution to K for the same field much less. The much greater value of E as compared with the barrier of type H explains the difference between the fast domain wall movements contributing directly to K and the very slow movements producing K and tan delta aging.

Plessner's picture of the aging mechanism in $BaTiO_3$ seems to recommend itself because it explains not only aging but also the initial high value of tan delta and its constancy over wide ranges of frequency. On the other hand, there are several weak points. First of all, the assumed degree of clamping is unrealistic. Clamping by 180° domains must be a function of height to width ratio of these domains. If the width of a domain is comparable to its height (or depth), the effect of such clamping will be minor and only if the domains are very thin in relation to their height will there be substantial

clamping. The effect is similar to that of stress distribution in sandwiched structures.

Secondly, in single crystals there is no evidence for a sideways movement of 180° domain walls under elastic restoring forces, as it is well known for magnetic domains. There is evidence, however, that existing walls can move by a kind of protuberance process which is actually partial nucleation of a new wall after application of the field (J1). It seems, therefore, that such a movement would be non-elastic and in phase with the field. This domain process could, therefore, explain the high losses in the intermediate frequency range.

The aging itself could then be explained by gradual relaxation of electrical and mechanical stresses* The electrical stresses are depolarizing fields originating from discontinuities in displacement D (div D); they can relax by two processes: either domain formation (mainly 180° domains) or movement of conduction charges annihilating the depolarizing fields. The characteristic relaxation times for both processes are small: microseconds for nucleation of walls and microseconds to seconds for the movement of charges (time constant = resistivity x dielectric constant). The mechanical stresses can relax by dislocation movement, ion or vacancy diffusion and, most important, nucleation and/or growth of 90° domains. The relaxation times of these processes might range from microseconds (dislocation movement) to months (diffusion of ions, nucleation of 90° wall).

Figures 10b and 10c prove that electrical stresses and mechanical stresses of the type occurring in ceramic $BaTiO_3$ produce increased K and that relaxation; i.e., decrease of these stresses with time, will result in decrease of K; that is, in aging (G5) (B46).

---

* McQuarrie who originally (M15) attributed K-aging to the removal of some contribution of 90° domain walls, believes now that aging is due to stress relaxation and its effect on intrinsic K (Personal Communication).

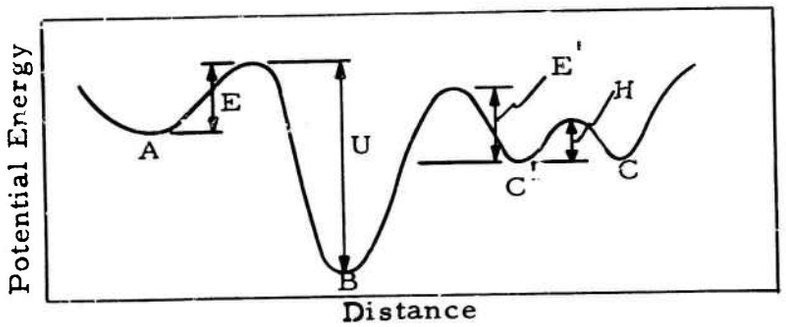

Fig. 10a The potential energy of a domain wall as a function of position.

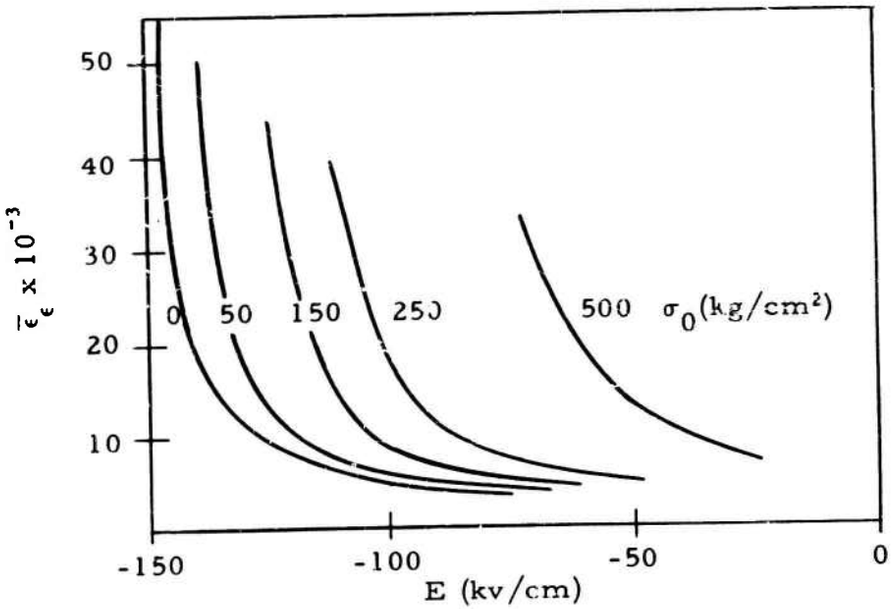

Fig. 10c Variation of arithmetic permittivity with internal field for Barium Titanate over a range of internal stresses σ_i

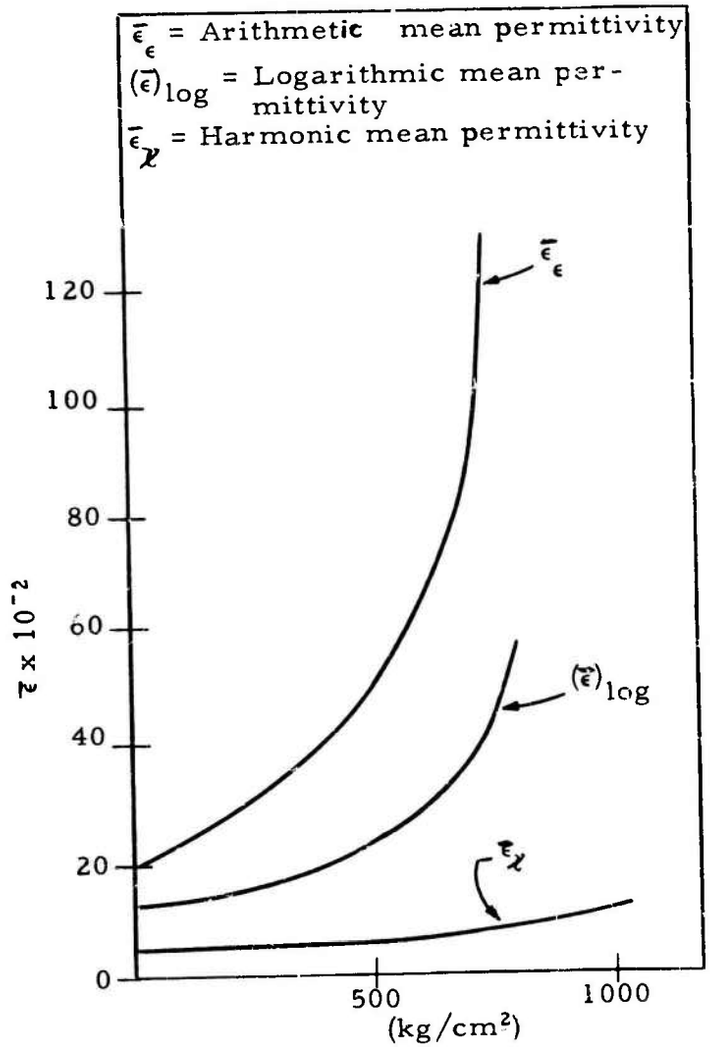

Fig. 10b Variation of average permittivity with internal stress for Barium Titanate

Conclusion. In the foregoing chapter, mainly the aging of the small signal permittivity has been discussed and two very different mechanisms were compared; i.e., deepening of potential wells for elastic domain wall oscillations (Plessner mechanism) and mechanical stress relaxation and reduction of K by nucleation and growth of 90° domains. The second mechanism has the advantage that it also explains automatically the aging of poled ceramics in that nucleation of 90° domains must reduce the remanent polarization P_R; the change of all other piezoelectric properties can be correlated with the decrease in the effective P_R. For this reason, the second mechanism seems to offer the most natural and general explanation of the aging process as a whole. Only future research can prove whether the first mechanism makes any contribution at all.

2. Stability - With long application of DC-Fields: Degradation

Introduction. The word "degradation" has two meanings. The first, derived from "to degrade (v.i.)" means deterioration and degeneration; the second, derived from "to degrade (v.t.)" means reduction in rank and lowering in the scale of classification (Webster). The following discussion is concerned only with the first meaning which is more general and can be applied to the deterioration of experimental and commercial dielectrics as well. The second meaning does not indicate the deterioration process as such, but the action which the testing engineer must take because of its occurrence; it can be applied only to classified, commercial dielectrics. Deterioration implies a loss in quality. To simplify this presentation mainly the ultimate loss in quality, the complete failure, will be discussed.

There are three different failure modes: The first mode is that of dielectric breakdown which is an instantaneous electronic process of weak temperature dependence occurring at high fields. The values of the dielectric breakdown fields (E_{max}) are in the order of 10^8 volts per meter for insulators

with low dielectric constant (e.g., alkali halides). There is some correlation between dielectric constant and breakdown field (B10); titanates and zirconates of low dielectric constant ($K = 200$) have breakdown fields of 25 megavolts per meter whereas those that have a high dielectric constant ($K = 10,000$) have breakdown fields of 5 megavolts per meter.

The second failure mode is that of thermal breakdown; this mode is strongly temperature dependent and is characteristic of failure at higher temperatures. It occurs when heat inside the dielectric (ohmic heat and losses) is produced at a faster rate than can be transferred to the available heat sinks; the sample becomes thermally and electrically unstable. Thermal breakdown is only partly dependent on intrinsic material properties; it depends also on geometry and other design factors, especially on the efficiency of the heat sinks.

For short time DC-fields only the two failure modes of dielectric and thermal breakdown have to be considered. If one plots an E_{max} versus temperature diagram with log E_{max} as ordinate and a $1/T_{abs}$ scale as abscissa, one has a field of allowed conditions of temperature and voltages bounded by two intersecting lines (Fig. 11). The first line contains the E_{max} values for dielectric breakdown and is practically horizontal for many dielectrics. Approaching higher temperatures one has another boundary which is given by the thermal breakdown conditions for short times (0 hrs.); this line also is straight but lies at a slope determined mainly by the activation energy of the conduction process in the dielectric. The position of the thermal breakdown line depends largely on external conditions and can be shifted to higher temperatures with better heat sinks.

For longer application times of DC-stress, there is a third failure mode called failure by degradation. Degradation is a slow process and consists in a steady increase of the conductivity of the dielectric until the ohmic heat production reaches the critical value characteristic of thermal breakdown. This can be shown on the diagram used to delineate the allowed

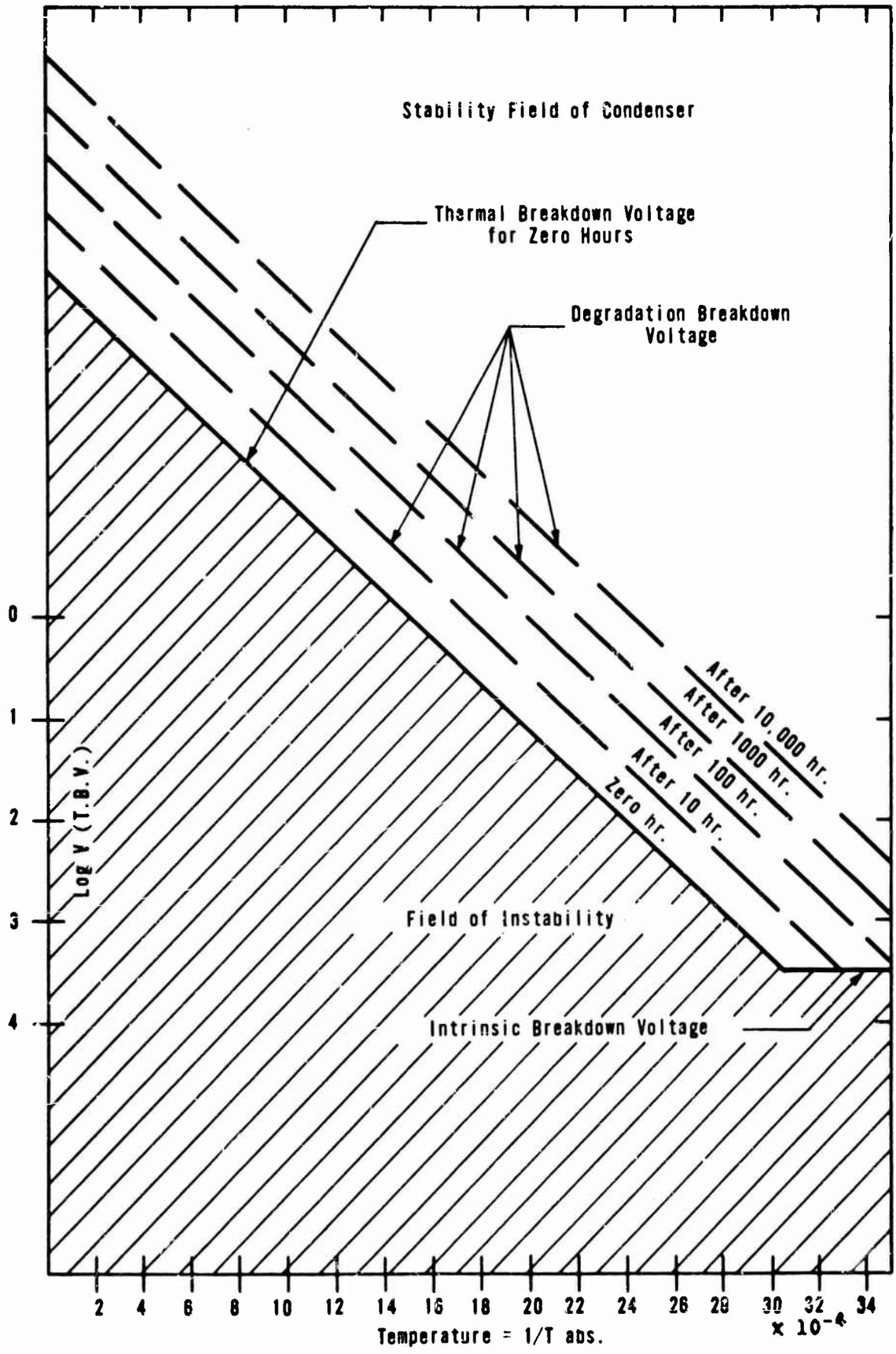

Fig. 11 Breakdown Voltage as Function of (1/T) $^{0}K^{-1}$ (Schematic)

temperature-field combinations for short applications (Fig. 11). The activation energy of conduction is usually not changed by the degradation process and the boundaries for thermal breakdown after lifetimes of, e.g., 100, 1000, 10,000 hours are lines parallel to the initial (zero hour) thermal breakdown line. In other words, with increasing application time the thermal breakdown boundary is continuously shifting to lower temperatures.

Basic Definitions. To facilitate the description of degradation and their explanation, some basic concepts and terms will be defined here at the outset.

1. The changes in conductivity with time are brought about by an electric field and consist either in changes in the carrier concentration or in changes of their mobility. Changes produced by moving ions (or vacancies) will be called degradation by an ionic process. This does not refer to the initial conductivity process (which can be electronic, ionic or mixed), but only to the process which effects the change in conduction. All other processes which do not involve moving ions or vacancies will be termed non-ionic.

2. If the degradation process extends over the dielectric as a whole and can be recognized by discoloration and/or space charges which develop at one electrode and move through the whole dielectric towards the other electrode, it will be termed a macroscopic process. Conversely, if degradation processes have a repetitive pattern from grain to grain with the grain boundaries at the anode side taking on some of the functions of the anode and the grain boundary at the cathode side taking on functions of the cathode, it will be termed a microscopic process.

3. The movements of carriers effecting the degradation can be either through the bulk of the grains or through the grain-boundary zones and are analogous to the material transport in ionic conduction, diffusion or sintering. Depending on the path it takes, the process will be described as a bulk or grain-boundary process.

4. A condenser with cathode and anode consisting of the same material will be termed symmetrical; a condenser with anode and cathode of different material will be termed asymmetrical.

5. A condenser in which both anode and cathode are sealed on the outside by an impervious, inorganic layer of glass or ceramic will be called a closed system; if only one electrode is sealed, it is a partially closed system. If both electrodes are bordering on air or an organic matter, the condenser will be termed an open system.

6. A degradation process which originates visibly (e.g., by discoloration) at the anode or which depends in its degradation characteristics mainly or exclusively on the anode material, will be termed an anodic process. Conversely, if the process originates on the cathode or is controlled by the cathode material, it will be termed a cathodic process.

7. In an ionic degradation process, the migrating species ideally might belong to one of the compounds which make up the material (Ba, Ti, O or their vacancies in $BaTiO_3$); this is termed self-migration. If the migrating species is an impurity ion which is there by design or accident, the term used is impurity-migration. If the species comes from outside, it will be termed in-diffused or injected. Injected species can come either from the electrode or from an absorbed or adsorbed layer at the electrode, or it can be a vacancy injected by an ejection of a lattice ion or impurity ion.

8. A degradation process which involves the migration of one species will be termed single; a process in wnich several species move simultaneously will be termed mixed. If the second process is normally the weaker one, but becomes effective after the first process is eliminated by exhaustion of its migrating species or by stabilizing agents, it will be called residual.

Literature Survey. As far as degradation is concerned, there is no basic difference between a compound in its ferroelectric state or in its paraelectric state. This is under-

standable because the ferroelectric state is only a slightly disturbed paraelectric state and, if there is a heat of transformation at all (as with those ferroelectrics which have a first-order transformation at their Curie point), it is only of the order of one hundred calories as compared with kilocalories in other crystallographic transformations (T9).

What is more, the degradation phenomenon occurs in compounds which are not ferroelectric at all and the degradation of TiO_2 (rutile), which is not ferroelectric, has great similarities to the degradation of $BaTiO_3$. This is useful because many degradation experiments have been performed on TiO_2 or on ferroelectric materials in their paraelectric state, i.e., above their Curie points.

The degradation of TiO_2 single crystals and of TiO_2 ceramics has already been observed by Cronemeyer in 1951 (C6) (C7). He reported increases of the conductivity of single crystals with the DC-field parallel to the c-axis up to four orders of magnitude upon prolonged application of strong fields. Similar values were exhibited by ceramic samples where he used fields up to 300 volts per mil.

Systematic studies on commercial TiO_2 and $BaTiO_3$ ceramics (manufactured by different companies) have been performed by the Erie Resistor Company under Contract W 36-039-SC 44534 (01). A TiO_2-body under a DC-stress of 35 volts/mil dropped its resistivity to one-third in 500 hours at room temperature, whereas the 150°C resistivity changed to one-tenth of its initial value in the same time. Similar values were observed for commercial $BaTiO_3$-bodies.

The first attempt at an explanation of degradation was given by Weyl and Terhune (B32)(W4). These authors considered an anodic process in an open system; the migrating species was protons (H^+) injected from the adsorbed water film at the anode. They considered the action of the protons in two steps. The first step is the incorporation of the protons as $(OH)^-$ groups under reduction of the iron impurity of the rutile which is assumed to be in the Fe^{4+} state; this assumption is based on

Selwood's (S10) magnetic experiments. The protons which are injected after all the Fe^{4+} present is reduced to Fe^{3+} reduce Ti^{4+} to Ti^{3+} and this reduction is, in essence, the degradation process. The electrons which are brought in with the positive protons to maintain electroneutrality are in localized orbitals of Ti^{4+} ions near the (OH)-groups and bonded to them by small energies of 0.1-0.2 electron volts. It takes only small thermal activation to lift these electrons into the narrow 3d-conduction band of the rutile where they increase carrier concentration and conductivity.

The most extensive study of degradation of titanates was undertaken by Linden Laboratories, Inc. (State College, Pa.) during the years 1953 through 1959. A brief report will be given first on the work up to the First Summary Report (15 October 1961) (B30).

Most of the work concerned degradation studies on commercial grade TiO_2 and $BaTiO_3$ bodies in open, symmetrical systems with Ag and Au electrodes. Many properties were measured before, during and after exposure to DC-voltages at intermediate and high temperatures, especially in the range from 150°-300°C. Some of these properties were: changes of resistivities, dielectric constants and loss factors for different frequencies, temperatures, field values and geometries. The goal of this work was threefold: (1) To learn as much as possible about degradation so as to propose and check possible models for this process. (2) To find means of controlling degradation. (3) To help to correlate short life tests under severe conditions of temperature and/or electrical stress with performance under milder conditions for long periods of time. While the results concerning the first two goals were quite satisfactory, the attempts to develop a short testing procedure to predict long life times met only with moderate success. Two criteria were used for this prediction: (1) for moderate electrical stresses: the time to reach maximum resistance; (2) for larger stresses: the negative slope of the log-resistivity-

versus-time curve for the first few hours of life testing. Semi-empirical formulae were developed which predict the average life of the group; however, these formulae were not tested for the prediction of long lives. The main results in regard to the other two goals can be summarized as follows:

1. A very low voltage produces no change in resistivity with time; intermediate voltages give first an increase in resistivity with time and eventually a decrease; higher voltages lead immediately to a decrease in the resistivity with time and, finally, to failure (degradation).

2. The stability of a titanate dielectric towards degradation is increased by many orders of magnitude through the incorporation of cations with valences higher than four, especially U^{6+}, W^{6+}, Ta^{5+} and Nb^{5+}, or by anions with valences lower than two (F^-).

3. In long life experiments at high temperatures (e.g., 150-200°C) the silver metal at the anode is almost completely oxidized, whereas the silver metal at the cathode is not affected.

4. Sealing off the anode side by a thin layer of titanate which contains the additions mentioned under (2) increases the lifetime by a factor of 10^2-10^4 as compared to the lifetime of the same dielectric which has the thin layer at the cathode side.

Based on these facts, the following picture of the degrading titanate and of the degradation process has been developed:

A titanate is appreciably reduced at the firing temperature; the re-oxidation upon cooling in air is rather fast above 1100°C but practically stops at some temperature between 600-900°C. As a consequence, the outside of the sample and, to some extent, of each grain is well oxidized, but the interior still has an oxygen deficiency. The missing oxygen ions ($V_O^{\cdot\cdot}$) carry an effective charge of 2^+, which is neutralized by twice the number of electrons in localized 3d levels of Ti^{4+} ions, forming Ti^{3+} ions. At low temperatures, these Ti^{3+} ions are bound by a small energy of 0.1-0.2 electron volts to individual

(AV); only a small part is separated from (AV). The electrons of the Ti^{3+} ions elevated into the narrow 3d band are responsible for conduction. The $(AV)^{2+}$ also experience a force moving them toward the cathode; their mobility is several orders of magnitude smaller than that of the electrons. The (AV) and Ti^{3+} groups which are not separated cannot participate in the conduction process; however, they experience a torque which leads to a dielectric polarization and a dielectric absorption current.

Due to the difference in (AV) concentration between the surface of each grain and the bulk, brought about by the manufacturing history of the dielectrics, the number of conducting carriers - predominantly electrons - is much larger in the bulk than in the surface. Correspondingly, the conductivity of the bulk is much greater than that of the surface and the resulting conductivity of the sample is intermediate between the two. Upon application of a voltage the field in the surface layers is much greater than that in the bulk. In a surface layer on the cathode side of each grain the free (AV) move out of this layer under the influence of the strong field, thereby further increasing the field. Under these high fields, Zener breakdown may occur and two electrons of the 2p-level on an O^{2-} near the surface might be brought up into the 3d-levels of the 3d band. The strong field will carry the newly formed (AV) immediately toward the cathode and atomic oxygen will emerge at the anode side: a new defect has been born and the degradation process has begun. The actual macroscopic process will depend upon the fate of the atomic oxygen formed. At the anode, it can immediately diffuse into the silver layer and oxidize the silver to silver oxide (see 3. above). If the oxygen formed on inner grain surfaces cannot get out, then the formation of new defects will slow down when a certain O^{2-} and O_2 concentration is reached. In this case the influx of new defects is a macroscopic process starting out from the anode side of the sample. If the anode is sealed off by layers containing U^{6+}, W^{6+}, Nb^{5+} or Ta^{5+}, then the influx of new defects is stopped effectively and the lifetime is increased (see 4. above).

The formation of new (AV) defects is not a necessary feature of every degradation. At higher voltages, approaching the breakdown voltage, a rapid decrease of resistivity sets in immediately (see 1. above). In this case, Zener breakdown may occur right from the start.

The stabilization of titanates by U^{6+}, Nb^{5+}, etc. additions can be visualized as follows: In the first place the additions reduce the (AV) concentrations in the bulk and in the surface layer and reduce the large difference between bulk and surface simply by making the concentration of (AV) very small in both. The remaining difference in (AV) concentration does not result in a great difference in conductivity because the (Ti^{3+}) is connected almost exclusively with the higher-valent cations (e.g., Nb^{5+}) and not with (AV), and the cation concentration is the same in both. One can see that the main reason for degradation, i.e., the difference in conductivity between surface and bulk, is eliminated. The apparent contradiction that the dielectric is greatly improved by making it somewhat semiconducting is dispelled by the observation that even with these additives the overall conductivity is less or at least equal to that without the additions.

The possibility of a Zener breakdown remains to be checked. It has been estimated that, at the outset, the conductivity of the well-oxidized surface layer is about two orders of magnitude higher than the average field across the sample. Applying, for instance, 60 volts/mil or 24,000 volts/centimeter to the sample would result in 2.4 million volts/centimeter across the surface layer. This is in the right order of magnitude for a Zener breakdown to occur (gap 2 ev) and a small movement of (AV) might increase this field strength fast.

As far as boundaries are concerned, one has to distinguish between surfaces and interfaces. The first ones (pores) are the locations where the reactions with the atmosphere take place and the (AV) gradients will be mainly perpendicular to these surfaces. The boundaries between different grains are important during the sintering operation; they are supposed to act as

defect sinks. The main paths of material and defect transport go through these regions (grain-boundary migration) and are the paths of oxygen diffusion during cooling. This is the reason to believe that grain boundaries have a higher electrical resistivity than the bulk of the grain. This would be an essentially chemical explanation of the barriers at the grain boundaries.

Koller and Pospisil (K5) reported on an investigation into the degradation mechanism of two dielectrics; one, a rutile ceramic with 5% additions; the other, a $BaTiO_3$-$SrTiO_3$ ceramic.

Their theory of degradation can be summarized as follows: In a fired titanate there are vacancies with Ti^{3+} attached to them. The presence of vacancies affects the electric properties of the material and its further changes, despite the fact their concentration is so small that they are not shown by a decrease in the mass of the sample. A material containing vacancies in an electric field experiences changes leading to the production of color centers. The mechanism of their production as a result of an electric field is not analogous to their production by irradiation. It depends rather on the passage of the current through the material, but a more exact explanation has not yet been found chiefly on account of the lack of experimental material.

V. Ya. Kunin and A. N. Tsikin (K11) reported on degradation and regeneration of rutile ceramics. Degradation is effected by 800 volt/mm (about 20 v/mil) DC at 150°C and the conductance increases rapidly under these conditions from less than 1.10^{-9} amp/v to 30.10^{-9} amp/v (in 25 minutes). The phenomenon studied by these authors is mainly regeneration at the same temperature where degradation was produced which is either (a) spontaneous regeneration without any voltage applied or (b) forced regeneration by a voltage of opposite sign. The spontaneous regeneration is a rather slow process. The conductivity (measured by a very small measuring voltage) decreases rapidly after the interruption of the degradation voltage of 800 v/mm, but, upon reestablishing the former field, the conductivity increases much faster than with the virgin dielectric.

It takes several days to reestablish the original rate of conductivity increase with time; upon reaching the former rate, the recovery is considered complete. However, regeneration by a reversed voltage is much faster: after a degradation period of 100 minutes at 800 v/mm, it took only 25 minutes at -800 v/mm to reestablish the original degradation rate, i.e., to effect complete regeneration (according to the authors definition).

As to the mechanism of degradation, it is assumed that at higher temperatures new defects are formed in TiO_2 in an electric field, and that they are responsible for local levels in the forbidden band. In this case regeneration of rutile ceramics in a field of reversed polarity can be explained, providing the defects produced in the TiO_2 lattice are paired. It had been formerly suggested (K12)(K13) that in the presence of an electric field and thermal motion, oxygen ions leave the lattice sites and locate themselves interstitially in the vicinity of the anion vacancies formed, without leaving the crystal boundaries. Therefore, when the field is removed or the polarity is reversed they can reoccupy the vacant lattice sites, i.e., the process of recombination of defects takes place. It appears therefore that the authors propose the formation of anti-Frenkel defects in rutile in a DC-field of 20 volt/mil.

A paper of interest because of its bearing on carriers and currents in titanates at higher temperatures is that of J. W. Northrip (N6). The title "High-Temperature Discharge in Ferroelectric Ceramics" is somewhat misleading in that the phenomena in question are found to occur in the same manner in non-ceramics ($BaTiO_3$ single crystal) and in non-ferroelectrics (rutile). The effect consists in a substantial discharge without (and with) preceding charge (poling). With a heating rate of 300°C/hr., the output current into a 100 kohm resistor becomes appreciable above 300°C, reaches a maximum above 400°C and becomes small again at 600°C. At constant temperature (350°C) the current decays from an initial value of 2 microamperes to 0.2 microampere in a few hours. After discussing

earlier observations by Berlincourt (B16), Roberts (B19) and Hurd, Simpson and Tredgold (H12), the author expresses his belief that these effects can best be explained as electrochemical reactions between the electrode metal and the anion-vacancies of the titanate.

Starting with 1962, degradation experiments have become somewhat more sophisticated by measuring the potential distribution in the dielectric and its changes during the passage of DC-current. This is done by probing the surface of the dielectric parallel to the field lines with a point contact and measuring the potential with an electrometer.

V. Ya. Kunin and A. N. Tsikin whose work on degradation of rutile ceramics has been reviewed above, published a paper with L. N. Fomenko (K10). In this second paper they report potential distribution measurements made simultaneously with resistivity measurements. Their experimental conditions were: 87% TiO_2 ceramic, Pd-electrodes, field 2.4 kv/cm, 200°C, 1500 hours.

They distinguish four periods of degradation, characterized by the slope of the current-vs-time curves: period (a) is one of constant current or slight current decrease; period (b), one of strong increase; period (c), one of slow rise or fall and, finally, period (d), one of strong increase ending with breakdown. They mention, however, that with their tubular samples period (c) was missing and that there was only one continuous period of current rise until breakdown occurred. They attribute the absence of the third stage in tubular samples to the considerably smaller surface of the tubes, so that less heat could be transferred to the surrounding medium. They do not give the dimensions of the tubes so one cannct check quantitatively how much smaller the tube area was compared to the slabs.

As far as potential distribution is concerned, they find a very strong positive space charge 1/2-1 mm in front of the cathode which diminishes through the first three hours (period (a)); with the onset of period (b) and the strong current rise the field is almost linear. Period (c) starts after more than

120 hours during which the current increased about two orders of magnitude. Period (c) is characterized by deviations from the linear field distribution, leading to zero field near the cathode. The authors do not explain the mechanism of these changes. They refer to their earlier papers on degradation and state that period (b) is one of homogeneous defect generation throughout the ceramic, according to a relation

$$N_t = N_e - (N_e - N_d) \exp. -t/\tau \qquad (1)$$

where N_t is the defect (donor) concentration at time t, N_e is the equilibrium concentration at temperature T and electric field E, N_d is the defect concentration before applying the field. τ is a relaxation time. They describe the current rise during period (b) by the formula

$$I_n = A\, t^n \qquad (2)$$

where A and n are constants to be taken from the log-log plot. It is not quite obvious how the dependency expressed in (1) should lead to current rise given by (2).

The main feature in which the results of Kunin et al differ from those of other authors is the potential distribution during period (a) with an extremely strong cathode fall. The authors think of this cathode fall as caused by "electronegative impurities" and they call period (a), during which the cathode fall disappears, the period of "electrical cleaning". They do not say what these impurities are or where they go.

As far as period (c) is concerned, the authors state only that it is characterized by an equilibrium concentration of defects ($N_t = N_e$); furthermore, that now other processes are going on which produce layers with differing conductivity; these processes are not clear. In comparing the field distortions which they observe during periods (a) and (c) with the linear distribution which they had during period (b) they more or less imply that the high current increase in period (b) is due to the linear voltage distribution and the slow increases during

periods (a) and (c) are due to the field distortions. This is not completely supported by the results of other authors which indicate that current increases occur during periods of increasing field distortions.

An important paper by Lehovec and Shirn (L4) will be discussed in some detail. The experimental conditions were: commercial high-K-body, electrodes: graphite, electric field 2, 4 and 6 kv/cm, temperature 250°-300°C, 63 hours.

The principal result to be noted is the see-saw effect in most of their current-versus-time curves consisting first in a strong rise in the current, then an even stronger decrease and then another rise. Practically all of the subsequent evaluations in this paper deal with the phases in the current history of their samples in which the current decreases by one or more orders of magnitude. During the decreasing current phase the main space charges are in the interior where they move from the anode towards the cathode. Lehovec and Shirn give detailed discussion of the degradation phenomenon.

They first deduce that the electron mobility must be greater than 0.04 cm^2/volt-sec., which results in transit times through the sample of a few milliseconds at most. This is in obvious disagreement with the time constant of the initial current rise. Thus, while electron injection at the cathode (and space-charge-limited current flow, which was mentioned before) may well be one of the steps initiating the current rise, other slower steps must be involved.

Space-charge-limited currents are the extreme case of uncompensated space charges of carriers; the other extreme case is that where the zero space-charge condition is approximately satisfied for every volume element of the sample. If this extreme case were valid, the conductivity distribution along the sample would be ascribed to a change in the distribution of "donors" (i.e., (AV), protons and other defects).

How can an inhomogeneous distribution of donors (defects) arise after applying the field? Let us assume that defects can be generated or annihilated at the anode and cathode inter-

faces and at grain boundaries of the polycrystalline material.

If the current at the anode and at the cathode were the same, i.e., if there were no space-charge buildup in the sample and if the fraction of the current carried by the defects (vacancies, etc.) were the same for cathode and anode, the defect level in the sample would remain unchanged. However, if these conditions are not satisfied (and we know that space charges build up in the sample) the defect level in the sample will change with time.

Consider, e.g., the case in which the entire current at the cathode is carried by electrons and a small, but finite fraction of the current at the anode is carried by defects (vacancies, etc.). This would lead to a pile-up of defects at the cathode with some of the defects trapping injected electrons. The conductivity at the cathode would increase with time. Alternatively, if defects were removed from the region near the anode by the field faster than they were generated at the anode, a low defect, i.e., high resistivity zone would be generated at the anode.

These examples show that the conductivity level in a reduction semiconductor is a function of the injection (or extraction) efficiency of defect transport across the electrodes (boundary conditions). This efficiency (equal to the defect current/total current) may well be a function of temperature, current density, electric field strength, defect density adjacent to electrodes and chemical constitution of the electrodes. While the motion of ion defects has been considered as an important factor in the phenomena, changes in conductivity by field-induced changes in the electron distribution (without changes in the concentration of donor or trapping centers) are also conceivable. The clear color (bleaching of originally blue regions) would then indicate removal of trapped electrons from defects rather than removal of defects altogether. In view of this, the interpretation of the drift mobility of the conductivity or resistivity pulses (defect mobility or relaxation time of electron transitions in trap levels) is uncertain.

After stating that the drift mobility of the resistivity pulses is estimated for their material to be 10^{-10} cm^2/volt seconds at 250°C and 2.10^{-9} cm^2/volt seconds at 300°C, Lehovec and Shirn describe clearly the different functions which the grain boundaries might have in these processes in polycrystalline materials.

This brings up the important question of whether the degradation is a phenomenon restricted only to polycrystalline materials. Lehovec and Shirn's measurements on a $BaTiO_3$ single crystal (with aquadag electrodes) show no change in current with time under conditions where the polycrystalline materials show drastic changes. Experiments made by Cronemeyer (C6), however, and recent investigations on single crystals have proved that the basic phenomenon of degradation, i.e., resistivity decrease under DC-stress, occurs also in single crystals of TiO_2 as well as $BaTiO_3$.

F. Cardon (C1) investigated rutile single crystals and studied first the discharge phenomenon which he found difficult to explain because of the very large decay time. He writes: "Phenomena with such a great time constant are generally not electronic and one expects also here that the ions, or more exactly, the vacancies play a role. It is, however, generally believed that no measurable ion transport occurs in rutile even at 850°C."

Cardon tried to measure current-voltage relations on thin flakes; no reproducible measurements could be obtained unless the crystals were "normalized". This normalization consisted of a prolonged treatment (100 minutes) with a rather high voltage of 25000 v/cm. A marked reduction in resistance was observed. The effect of normalization disappeared gradually with time and immediately upon heating the sample to 800°C. By grinding the surface of a normalized sample and evaporating new electrodes, it was found that the normalization was not a surface effect but a bulk effect; the sample with the new electrode showed the same low resistance that the sample had after normalization and before grinding.

Cardon then refers to work on CdS where similar phenomena have been observed. It is suggested "that the 'normalization' and associated effects are pre-breakdown effects which result in a change in the distribution of electrons in higher discrete energy levels. Another possibility in TiO_2, although less probable but not impossible, is the migration of anion-vacancies to the cathode ...."

It is obvious that the "normalization" phenomenon with the reduction of resistivity under high DC-stress is very similar to the degradation process in polycrystalline titanates; the slow time changes at low temperatures (recovery) and the immediate restoration by heat treatment at 800°C in O_2 are very suggestive of an ionic defect migration (AV or protons).

Branwood and Tredgold have reported studies of the conductivity of $BaTiO_3$ single crystals in several papers (B24) (B23)(R3). Using gold or silver as electrodes they find a decrease in resistivity (degradation) of about one order of magnitude in 2×10^4 minutes for fields of 10 volts/mil (temperatures 130-150°C). Using radioactive tracers (^{198}Au) they prove that the influence of the gold anode on impurity concentration is confined to a surface layer less than 100 Å thick. The reduction in resistivity does not occur with Al, Cr or Sn electrodes.

As far as the increase in conductivity with time with gold (and silver) anodes is concerned, the authors assume that this is associated with an enhanced hole injection at the anode. It might be mentioned at this point that this assumption is not too different from the picture of the anodic process given by Buessem and Marshall (B30) who have described this process as one whereby one 2p-electron of an O^- at the surface is elevated into the 3d-band of the Ti-ion. The surface oxygen, deprived of its valency electron, can evaporate into the electrode zone and leaves an (AV) behind which has a certain chance to be carried away by the field towards the cathode. This is the creation of an (AV).

The process proposed by Branwood and Tredgold to explain the increase in conductivity of $BaTiO_3$ with time is identical to the one described up to the point of evaporation of the oxygen atom into the electrode space. If one just assumes the elevation of a 2p-electron into a higher level, then one has the formation of a positive hole in the valency band which can move away towards the cathode. This is essentially an electronic process and might lead to difficulties with the time constant.

The work on degradation at Linden Laboratories between 1961 and 1965 is reported in the Second Summary Report (B28). During this time evidence has been produced (Figs. 12 and 14) that the proton can play an important role in the degradation process, as had been proposed by Weyl and Terhune in 1953 (W4). Furthermore, it has been found that hot pressed $BaTiO_3$ made from very pure raw material and pressed to practically theoretical density is very stable, almost as stable as those materials which have been stabilized by dopants. A great amount of effort has been spent on measuring potential distributions during degradation which reveals development of space charges as a function of voltage stress, electrode material, pretreatments with dry or wet air, humidity during testing, etc. Most important is the finding that incorporation of higher valent cations is a very effective means of counteracting the detrimental effects of protons on degradation. The charging-discharging phenomenon in $BaTiO_3$ was studied in great detail in the hope that either the magnitude or the decay constant of the discharge current could be used to detect weak samples and to predict possible breakdown at an early stage. These attempts were not successful in that the discharge current (at least in the time interval studied) is not affected by those features in a sample which determine its eventual breakdown; it indicates only the more severe stages of degradation when the sample is already badly damaged.

D. A. Berlincourt et al (B10) studied a great number of ceramic compositions of perovskites (ABO_3), the B^{4+} ion being Ti and Zr and the A^{2+} ion being Pb, Ba and Sr. Nb^{5+} and Sc^{3+}

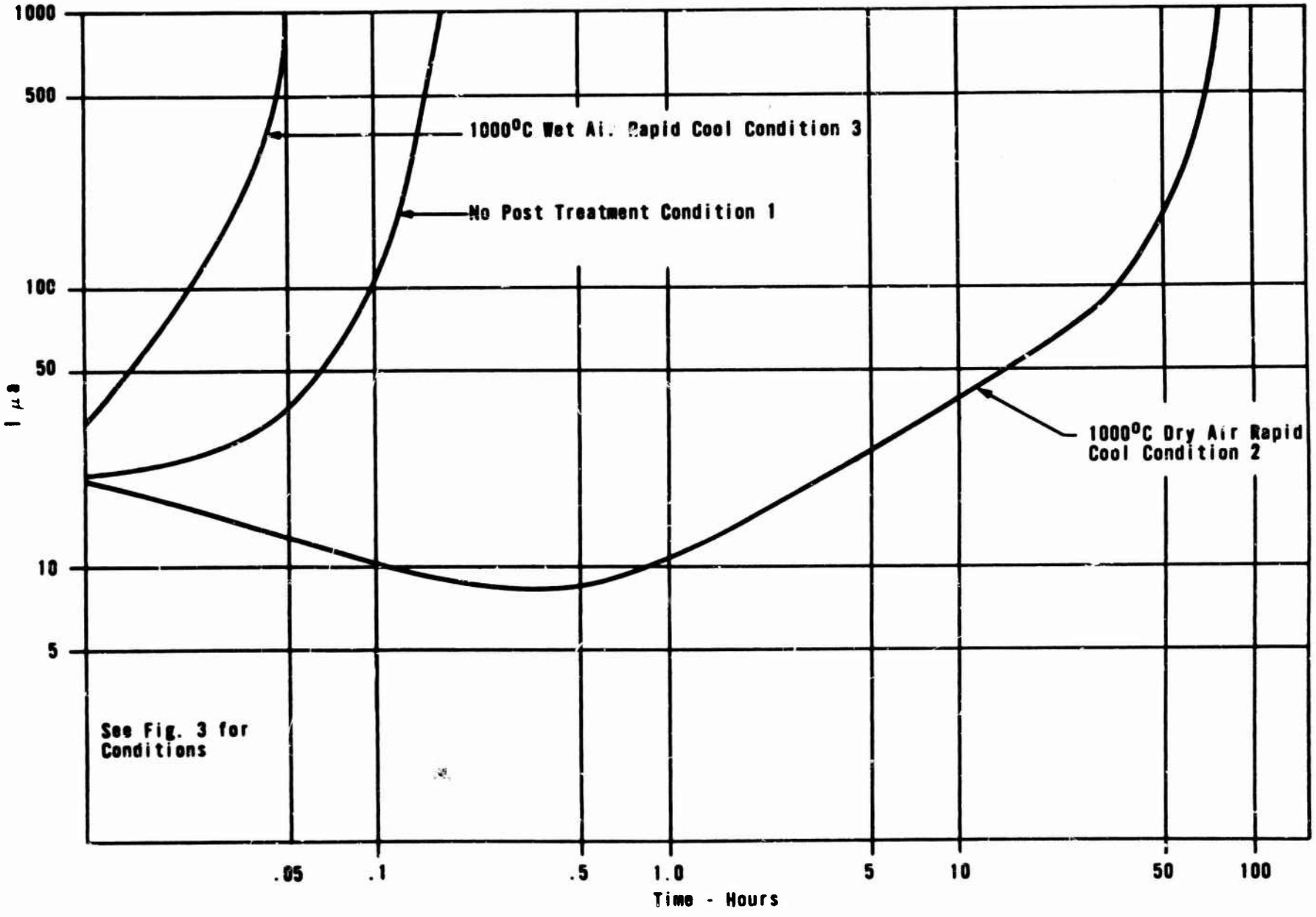

Fig. 12 Current as a Function of Time

were used as dopants. The authors demonstrated that zirconates as a class are far superior with respect to long term degradation which is described as an "electrolysis of oxygen". Ti^{4+} is more easily reduced than Zr^{4+} which explains the greater stability of the latter; the same fact, perhaps, also explains the greater volume resistivity of the zirconates. However, there is no clear-cut difference in dielectric strength. Degradation in dielectrics with p-type conduction (which was found to be the usual case) is generally inhibited by donor doping.

H. H. Barrett et al (B5) report on "Failure Mechanisms in Ferroelectric and Nonlinear Dielectrics". The paper is mainly concerned with the dielectric breakdown aspect of failure and investigates $SrTiO_3$ as a model substance. Of interest in regard to degradation are diffusion studies with O^{18} in which they found that unannealed $SrTiO_3$ with a dislocation density of $1.4 \times 10^6/cm^2$ had an activation energy of 15.5 kcal and a preexponential term $D_o = 1.6 \times 10^{-7}$ cm^2/sec. Extrapolation of these values to the temperature range used for DC-life tests (100-250°C) gives diffusion coefficients which are not incompatible with the idea of an ionic migration in an electric field.

T. Prokopowicz et al (P9) have investigated during 1962-1965 the "Intrinsic Reliability of Subminiature Ceramic Capacitors". The progress which has been made in commercial dielectrics is apparent if one compares the life test results in this report with those reported in 1951 (O1). At this earlier date K100 material (essentially TiO_2) showed degradation of its resistivity by one order of magnitude in 500 hours under 27 volt/mil at 150°C, whereas now the improved K2000 ceramics survive 1000 hours under 160 volt/mil at the same temperature with only a slight decrease in resistance. Prokopowicz et al have develop a life-time formula which allows one to predict the actual performance (without failure) of capacitors at lower voltages and temperatures from measurements at higher voltages and temperatures. The accelerated test conditions are 160 hours at 80 v/mil and 150°C.

The formula reads:

$$t_1 = t_2 \, E_2^n / E_1^n \exp\left(\frac{w}{kT_1} - \frac{w}{kT_2}\right) \qquad (3)$$

t_1 = performance time at low voltage and temperature, to be calculated

t_2 = performance time at high voltage and temperature

E_1 = low voltage, test voltage, e.g., 20 volt/mil

E_2 = high voltage, e.g., 80 v/mil

n = 3

w = 0.9 ev

k = Boltzmann's constant

T_1 = low temperature

T_2 = high temperature, e.g., 150°C

The same group, headed by T. Prokopowicz, has recently made an important discovery which has practical as well as theoretical significance. D. Payne* has found that the steady state current in monolithic capacitors, using a K = 2200 body (Sprague C67) and palladium electrodes, exhibits in certain cases the well known (E4) Schottky emission current-voltage dependence. The following compilation, taken from Emtage and Tantraporn's paper (E4), shows this dependence in comparison with other dependencies which are frequently found:

Mechanism	Current-voltage dependence	Current-temperature dependence
Space charge limited	$I \propto V^2$	$I \propto \mu$ (μ mobility of the electrons in the insulator)
Tunnel emission	$I \propto V$ for $V < \Phi$ $I \propto V^2 \exp(\text{const}/V)$ for high V	None
Schottky emission	$I \propto \alpha \exp(\beta V^{1/2})$	$I \propto T^2 \exp \frac{-\text{const}}{T}$

Here $\alpha = AT^2 \exp(-\Phi/kT)$, $\beta = \left(\frac{q^3/Ka}{kT}\right)^{1/2}$,

* Personal Communication

q is the charge of an electron, a is the thickness, K the relative dielectric constant and A is the Richardson constant.

Figure 13 illustrates a linear relationship existing between steady state current and the square root of the applied voltage (Va), for formulation MD 128 which has been shown to be unreliable. No linearity existed for C67NMX-1 and many others which were extremely reliable.

From the findings, it appears that Schottky emission is initially experienced in unreliable units.

It is proposed that with time and applied-field strength, there is a net drift of vacant-oxygen sites toward the cathode. At some critical distance from the cathode, X_o, these vacancies form an "apparent" anode; the field strength across the gap X_o is increased considerably. This effect can be taken into account by a factor α which expresses the increase in field over the value V/a, where a is the thickness (1-2.5 mil).

For six groups of unreliable units which were first tested at 150°C in regard to the Schottky emission law and which were later subjected to an 85 volt/mil 1000 hour life test at the same temperature, α values of 2000 to 7500 were found; X_o is computed from this to be 84-180 A.U.

The practical importance of Payne and Prokopowicz's findings is that it allows one to predict at an early stage which units are unreliable.

The theoretical implications are far reaching and will be discussed by these authors in a forthcoming report on their results.

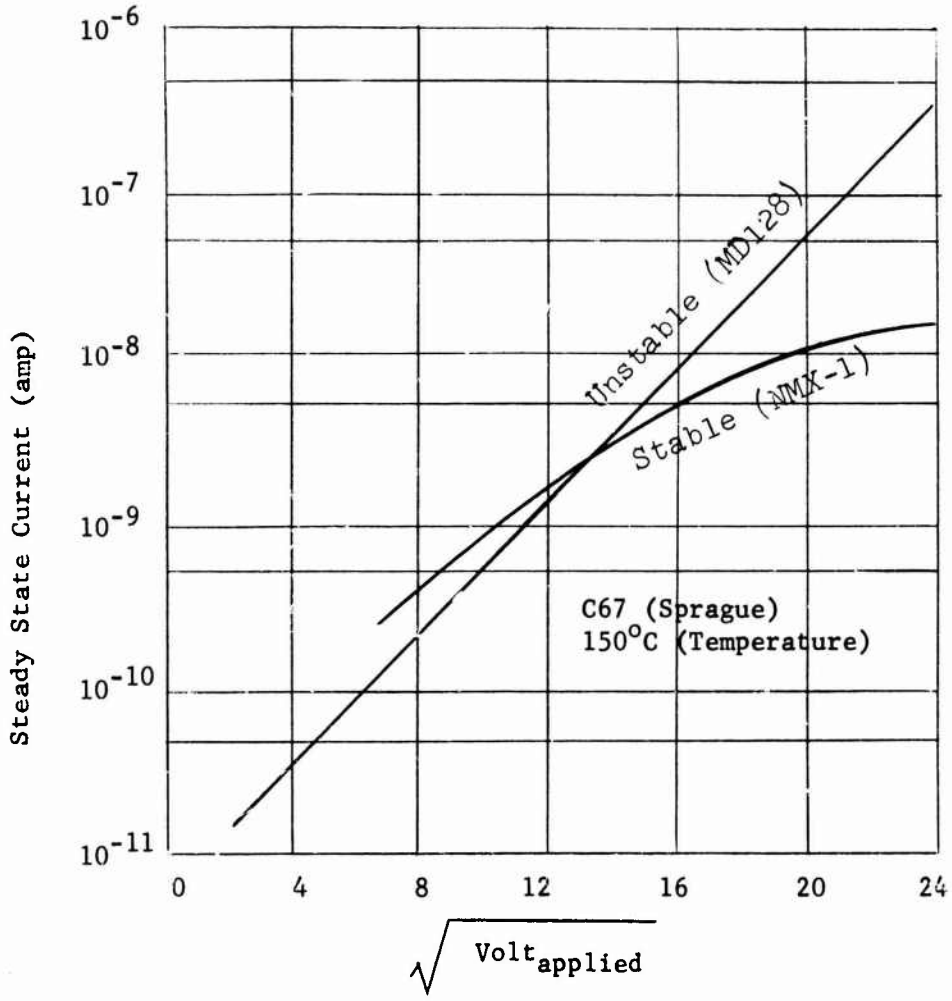

Fig. 13 Steady State Current vs Square Root of Voltage

G. A. Shirn and D. M. Smyth have reported on "Some Failure Mechanisms at Insulator-Conductor Junctions" (S15) which gives data for Ta_2O_5 and $BaTiO_3$ dielectrics. Some of the results for $BaTiO_3$ were reported by G. A. Shirn in a paper with Lehovec which has been reviewed above (L4). In the present paper the study of discoloration under DC-stress at intermediate temperatures is emphasized as a means of following the progress of the degradation process. "By analogy (with the color centers found in alkali halides) it is proposed that the color effects in the ceramic are caused by the presence of oxygen vacancies injected by the anode. Oxygen vacancies having a double charge could accommodate one, two or three electrons, allowing for a variety of color centers. One visualizes the color formation process as follows: Consider the ceramic as a very viscous electrolyte. When the field is applied, oxygen ions migrate to the anode where they are removed (vacancies injected) by either gas evolution or oxidation of the anode. In case of oxidation of the anode the oxide film formed will slow or stop the vacancy injection process. The pulse of vacancies giving the brown color will spread out from the anode and, since the supply is cut off by the oxide film, the area near the anode will return to the original color. If the oxide film is ruptured, a new pulse of vacancies will be injected ....

The oxygen vacancies arriving at the cathode must pile up there, since no oxygen is available from the cathode. The various colors are attributed to the various states of ionization of the oxygen vacancy. Potential probing of the various regions of blue, brown and tan showed high conductivity for the blue and low for the tan. Thus the presence of vacancies increases the conductivity of the device .... The same experiments on single crystals of $BaTiO_3$ indicate .... that the blue color and the extra oxygen vacancies in the ceramic are concentrated in the grain boundaries." These discussions show that the degradation speed is determined not only by the mobility of the migrating species (anion vacancies) but also by the rate of injection at the anode; shutting off the supply by oxide film formation leads to a reversal of the degradation trend and could explain the periods of current decrease which most investigators have found at intermediate conditions. Since the system investigated by Shirn et al is "open" in the sense of the definition given in basic terms, it seems possible that protons also are injected from the anode which would produce effects similar to those caused by anion vacancies.

The missing link in the chain of investigations on degradation is an answer to the question whether an ionic process involving injection and migration of anion vacancies, protons, etc. is <u>possible at all</u> between room temperature and about 250°C.

A positive answer to this question has been given recently by D. D. Glower and R. C. Heckman (G2) using Carl Wagner's (W3) ingenious method of an electrochemical concentration cell. These authors have proven that ceramic $BaTiO_3$ made from pure, spectrographic-grade raw materials and of 95% theoretical density exhibits 100% ionic conductivity between 100°C and about 300°C and they suggest that the conductivity below 100°C down to room temperature is also 100% ionic.

The experiment utilizes the electrical potential of an electrochemical concentration cell.

Figure 14

Discolorations in $BaTiO_3$ Under DC-Stress

From Right to Left:

Test Condition: 125°C, 10 v/mil, In-Ga Electrodes*

Condition	Definition of Post-Treatment	Time Under Stress
1	No Post Treatment	5.9 hrs.
2	1000°C Dry Air Rapid Cool (R.C.)	121.0 hrs.
3	1000°C Wet Air R.C.	2.15 hrs.
4	1000°C Dry Air Slow Cool (S.C.)	121.0 hrs.
5	1000°C Wet Air S.C.	3.8 hrs.
6	500°C Wet Air R.C.	121.0 hrs.
7	500°C Dry Air R.C.	28.2 hrs.
8	1000°C Dry Air R.C., 500°C Dry Air, R.C.	121.0 hrs.
9	1000°C Dry Air R.C., 500°C Wet Air, R.C.	121.0 hrs.
10	1000°C Dry Air R.C., 500°C Dry H_2, R.C.	121.0 hrs.

* Right electrode: Cathode

All treatments for period of one hour

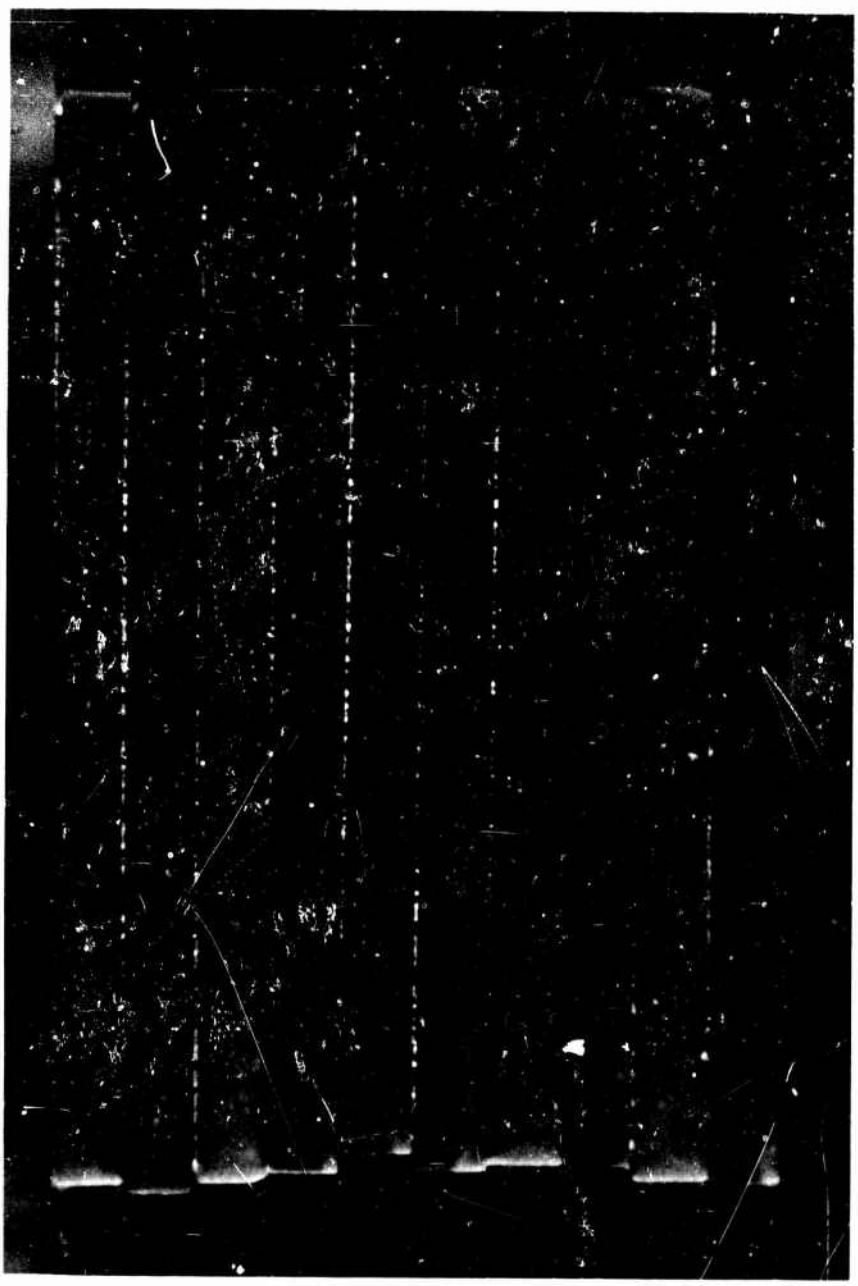

Fig. 14

BLANK PAGE

$$\text{Pt, } O_2(p_1) \left| \begin{array}{c} BaTiO_3 \\ \\ \text{crystal} \end{array} \right| O_2(p_2), \text{ Pt.}$$

The electromotive force E_1 of this cell is determined for a purely ionic conductor by the partial pressures of oxygen p_1 and p_2 and may be calculated from the equation

$$E_1 = (RT/nF) \ln(p_2/p_1) \qquad (4)$$

In this equation R is the gas constant, T the absolute temperature, F the Faraday constant, and n is the number of Faradays of charge transported for each mole of molecular oxygen. In the interpretation of the results n has been taken equal to 4, which is equivalent to assuming the reaction

$$O_2 + 4e = 2\,O^{2-}$$

One can turn Equation (4) around and compute p_2/p_1 - ratios resulting from an applied field E_1. One sees immediately that the usual voltages of 100-1000 v produce very large p_2/p_1 ratios and explain the migration and ejection of oxygen at these low temperatures.

Evaluation and Conclusions. The great progress towards a solution of the degradation problem is demonstrated by a comparison of today's ceramic dielectrics with those manufactured fifteen years ago.

There is no doubt that this progress is due to the discriminate use of certain means of stabilization which are being applied today either singly or in combination:

1. Incorporation of stabilizing agents (dopants), either cations of a valency higher than 4 replacing Ti^{4+} (e.g., Nb^{5+}, U^{6+}) or anions of a valency lower than 2, replacing O^{2-} (F^-)
2. Closed system
3. Purer raw materials
4. Denser fired product

5. Lower firing temperatures (4 and 5 as well as 3 can be achieved by hot pressing)

6. Drying treatments before applying electrodes

The effect of these measures, especially 1, 2 and 6, in conjunction with all other reported effects such as discolorations, injection of space charges, influence of anode material on degradation speed, is positive proof that in an open system without stabilizing agents there are two ionic degradation mechanisms which can occur singly or simultaneously: One is the injection of anion vacancies at the anode and their subsequent migration towards the cathode; the other is the injection of protons at the anode and their migration to the cathode, or the activation of protons which have been incorporated before by a wet treatment. Both defects reduce Ti^{4+} to Ti^{3+} and create new carriers for conduction, which is a prerequisite for eventual thermal breakdown and failure.

In dielectrics in which all means of stabilization have been fully used, degradation will not occur at conditions which would normally, without these means, be beyond the limit of stability. In other words, the thermal breakdown boundary has been shifted considerably towards higher temperatures. However, the degradation process may not be completely eliminated and degradation may still occur if much more severe conditions of temperature and voltage stress are applied. This type of degradation has been termed in the definitions "residual" degradation and it is still an open question whether it is essentially the same process of either anion vacancy injection or proton injection occurring now under conditions of higher thermal and/or electrical activation, or whether it is a completely different process. There is the possibility of field-induced electronic processes or that of a different ionic process involving other migrating species. No such process has yet been proposed. With the great activity which has been induced in the field of stability of dielectrics by the greater demands for reliability as well as by the advent of microelectronics and thin films, it is to be expected that these questions can be answered in the near future.

V. SPECIAL TECHNIQUES

A. Thin Film Ferroelectrics

1. Introduction

The present trend in electronic component development is the fabrication of the numerous components with their functional interconnections into an integral device. The emphasis on miniaturization of circuit assemblies and the rapid development of printed circuit techniques have extended into the field of components. Thin film technology thus has come into focus as a means of obtaining components in miniature sizes accompanied, of course, by major alterations in manufacturing processes. At present, thin film technology has attained nearly universal use since evaporation processes have been developed to obtain films of required thickness.

The fabrication of thin-film resistive components by various methods has advanced to a rather high level of development. The evaporation of thin resistive films and the subsequent etching of specific patterns to yield the appropriate component value has matured into a fully automated manufacturing process which yields precise and reproducible resistor components. Resistor film techniques are generally uncomplicated, and the large variety of stable materials suitable for resistor elements permits considerable latitude in deposition techniques. Dielectric materials for capacitor fabrication present very different problems to the thin film technologist. These will become more apparent in the following sections of this report.

Although considerable advance has been made in the thin-film resistor field, the search for active thin film devices has clouded many of the objectives of the researchers in the field of passive components. The search for thin film counterparts of the transistor has inspired endeavors to fabricate

circuits containing both passive and active components with a compatible set of film technologies. It is generally conceded (L2) that semiconductor films that have been produced are not single crystal, and while device operation has been achieved to a degree, reproducibility and reliability leave much to be desired. A more promising method for obtaining single-crystal thin film semiconductors has been the deposition of silicon on sapphire substrates. In spite of this, however, no active thin-film device performance to date even approaches that of conventional high-frequency bipolar transistors (L2).

The overall picture is much more promising for passive thin films than for active ones, and although researchers have made considerable advances in the resistor field, the capacitor problems have been especially troublesome.

2. Thin film capacitors

The most significant success in thin film dielectrics for capacitor bodies has been in materials having a low dielectric constant. These are generally in the group of materials which includes the oxides of tantalum and other metals; the desire, however, is to make use of materials such as titanium dioxide, barium titanate, and similar dielectrics which have much higher dielectric constants. Thin films of these latter materials have been fabricated, and they invariably have been lossy or have had poor dielectric strength.

Among the factors that must be considered in the fabrication of capacitors are (B2)(H6):

1. the capacitance per unit area,
2. polarization of the capacitor,
3. voltage breakdown,
4. temperature coefficient,
5. cost.

Compromises have been made among the several factors listed above, but the fundamental considerations of dissipation factor, voltage breakdown, and capacitance per unit area are the gravest limitations. The extremely high dielectric constants of the

materials in the barium titanate class of ferroelectrics attract researchers in the thin film field. It is appropriate to review developments in this field and to attempt to present a summary of achievements with these materials.

3. Substrate

The characteristics of the substrate surface are of major importance where the dielectric is deposited in a planar configuration. The surface microfinish is extremely critical and should approach an atomically smooth surface with no sharp discontinuities. Dielectric films are extremely sensitive to small defects since a uniform dielectric strength is required over the entire capacitor area (H6). Other characteristics of the substrate surface which are of equal importance are the chemical composition, stability, thermal conductivity, porosity, working temperature, vacuum degassing, and forming capability. Dielectric films are usually deposited on a metallic substrate which is then used as an electrode; however, there have been some attempts to replace these with metallized ceramic plates (L2). Because of the high temperatures employed in the fabrication of ferroelectric dielectrics, platinum foil and similar high-melting metals are generally used.

4. Thin films of $BaTiO_3$

The present investigation is limited to an evaluation of thin films and thin film technology of $BaTiO_3$, either in single crystal or polycrystalline form. The techniques that have been used to form these films include firing of pressed bodies, slips, vaporization of the oxides, heat treatment of the precipitated Ba-Ti complex from solution (D2)(F3)(F2), growth of thin single crystals (D2)(M2), and thinning of single crystals by etching (S2).

Thick films (several microns) exhibit properties nearly like the bulk material; that is, there is a nearly linear dependence of capacity and breakdown strength on film thickness. With film thicknesses below several thousand Angstroms, the

breakdown strength might be reduced by the presence of film defects and interfacial roughness. At still lower thicknesses, avalanching becomes more pronounced and may lead to non-linear voltage dependence of the leakage current.

The firing of slips has produced film thicknesses as low as 0.3 mil, but the grinding of pressed bodies is limited to thicknesses considerably greater than this because of fragility. The thinnest films are obtained by the growth (and etching) of thin single crystals and by the evaporation of the barium titanate oxides. Of the various methods of producing thin films, the latter two techniques merit strong consideration. This is particularly true in view of recent developments in thin-film electron beam processing as developed by von Ardenne et al (V1).

5. Vaporization of the oxides

$BaTiO_3$ decomposes into the oxides of barium and titanium as it is evaporated in a vacuum. The oxides are evaporated onto an appropriate substrate capable of withstanding the subsequent high firing temperature. The more common technique is that employed by Feldman (F2) wherein a filament is coated with an aqueous solution of $BaTiO_3$, dried, and then evaporated completely in order to maintain the proper ratio of the barium and titanium oxides. The resulting thin film is then fired at temperatures ranging from 800 to 1500°C in an oxidizing atmosphere to reconstitute the $BaTiO_3$ (F3)(F2)(H1).

Many researchers are investigating the effect of the oxidizing atmosphere and firing temperatures on the voltage breakdown and dissipation factors of the resulting films. It has been found (H1) that increasing the oxygen pressure during the evaporation of BaO plus TiO_2 onto a heated substrate has resulted in lowered dissipation factors. Maintaining an external field on the film at temperatures of 600 to 700°C has had little apparent effect although some grain orientation was found (H1).

TABLE XIV

Tabulation of Physical and Electrical Properties of Thin-Film $BaTiO_3$ Single Crystal and Polycrystalline Dielectrics

Process	Film Thickness (in microns)	Dielectric Data: Reproducible	Dielectric	K	Dielectric Data: Dissipation Factor %	Remarks	Reference
Press/Grind	254	yes	$BaTiO_3$, various (polycrystalline)	1900-6600	1 to 3	TC of K investigation	(S1)
Evaporate KF/$BaTiO_3$ (Pt Substrate)	0.1-1	yes	$BaTiO_3$ (single crystal)	?	?	No dielectric properties available	(D2)
Evaporate $BaTiO_3$ and Fire (Pt Substrate)	1-2	yes	$BaTiO_3$ BaO, TiO_2	170-260	5 to 40	Some pinholes, impurities, causing electrode diffusion	(F3) (F2)
Evaporate $BaTiO_3$ and Fire (Pt Substrate)	1-2	uncertain	$BaTiO_3$ BaO, TiO_2	31-1200	27 to 36	Evaluation of dissipation factor vs oxygen, temperature, pinholes	(H1)
Evaporate $BaTiO_3$ (LiF Substrate) (Au Film Substrate)	0.09	yes	$BaTiO_3$ (single crystal with impurity)	500	?	Single crystal growth at reduced substrate temperature (500°C)	(M2)
Evaporate BaO + TiO_2 (60 Pt-40 Rh Substrate) (Electron Beam)	0.12	yes	$BaTiO_3$ (single crystal with some Ba_2TiO_4)	500-1330	4.1	Single crystal growth on heated substrate (950°C), somewhat low breakdown strength	(F4)
Evaporation $BaTiO_3$ (+ additives) by a grain-grain method	0.1-0.3	yes	$BaTiO_3$ + solid solutions of $BaTiO_3$ with $SrTiO_3$ and $BaSnO_3$	400-700 $BaTiO_3$ 250-350 $Ba(Ti_{0.9}Sn_{0.1})O_3$ 200-400 $(Sr_{.73}Ba_{.27})O_3$	2 to 10 ? ?	High breakdown strength in $BaTiO_3$, lowered with Sr and Sn additives	(M4)

6. Thin single-crystal films of $BaTiO_3$

Thin single crystals of $BaTiO_3$ have been grown from a mixture of KF and $BaTiO_3$ heated to a temperature of 1000°C. In this technique, a platinum sheet or foil is lowered into the solution at the reaction temperature and is held stationary or withdrawn by a crystal pulling process. The crystal growth takes place near the interface of the substrate and the surface of the solution. In earlier experiments on fine-grained platinum surfaces, the predominant nucleation sites were the grain boundaries. The effect of grain boundaries was reduced by increasing the size of the platinum grains by grain growth. This was achieved by cold-working the platinum and subsequently annealing it at approximately 1200°C for several hours. This modified technology reduced grain boundary nucleation, but nucleation within the grain was more pronounced. Although the area of the $BaTiO_3$ single-crystal films is small, nevertheless the high degree of perfection and firm attachment of these single-domain crystals to the substrate seem to represent a reproducibility and stability of properties in this high permittivity material.

Thin single crystals of barium titanate have been produced by methods similar to those of Feldman, but differing in that the substrate temperature is maintained at a high value (600 to 980°C) and the material to be evaporated is heated by electron bombardment (F4). The substrate is heated by resistive heating, while adequate vacuum is maintained at the electron guns by a multiple-stage differential pumping system. This technique is considered to be free of many of the possible contaminants in filamentary evaporation techniques. Grain boundary nucleation on the platinum substrate was reduced by increasing the grain size of the substrate by heat treatment. The properties of the $BaTiO_3$ obtained by this method are included in Table XIV.

Thin films of the order of one micron have been produced by a vapor deposition of $BaTiO_3$ using a grain-by-grain evaporation method developed by Müller et al (M4). Contamination of

the material to be evaporated was reduced by use of an iridium boat. This method was also used to obtain compositions of mixed titanates including $SrTiO_3$. High dielectric constants (up to 700) and improved dissipation factors were obtained. Results are shown in Table XIV. Epitaxial $BaTiO_3$ was deposited on a silver substrate on NaCl by a grain-by-grain evaporation process (J9)(J10), and an extension (A4) of the process to include cathodic sputtering of Ba and Ti at controlled rates from each cathode to determine the conditions for the formation of $BaTiO_3$.

Thin barium titanate single crystals were grown successfully by a rather straightforward technique of melting $BaTiO_3$ powder on a thin platinum sheet (L3). The temperature was raised to 1600°C and the resulting thin films were less than 0.2 microns in thickness. Since this work was directed primarily toward polarization of the resulting crystal, no information is available as to the dielectric properties. It is worthy of note that little or no contamination due to platinum occurred, and the utilization of bulk materials produced a high percentage of pseudocubic barium titanate.

Table XIV summarizes the properties of the various thin film ferroelectrics obtained by the methods described above. In several cases, certain specific properties are not given in the reference.

B. Devitrified Ceramic Ferroelectrics

1. Introduction

Devitrified ceramic ferroelectric materials are formed by controlling crystallization during heat treatment of a glass. The formation of silicate-free barium titanate crystals in a crystalline feldspar matrix has been reported by Herczog (H5) (H13) while Anderson and Friedberg (A4) discuss crystallizing lead metaniobate from a (PbO-Nb_2O_3-SiO_2-Al_2O_3) glass.

2. Microcrystalline Barium Titanate

In the development of microcrystalline barium titanate by devitrifying a glass, Herczog found that the composition must be chosen properly to minimize interaction between the desired ferroelectric crystal phase and the glass network-forming oxides during crystallization of the glass. Glass melts with low concentrations of network formers are very fluid and crystallize rapidly on cooling; therefore, these glasses are generally cooled while being formed from the liquid temperature to below 700°C in two to tenseconds to prevent spontaneous crystallization. Because of the need for rapid cooling to retain a glassy substance, articles formed during cooling are limited to one-half inch in thickness. If the melt is allowed to crystallize by moderate cooling from the liquid state to the crystalline state, the barium titanate formed as the main crystalline phase does not have as good mechanical and electrical properties as barium titanate formed by devitrifying the glass product. These poorer properties are reported to be due to the larger crystals and lower yield of barium titanate obtained on slow cooling of the melt.

The composition of a typical devitrified ceramic ferroelectric containing approximately 50 to 75% $BaTiO_3$ by weight is as follows:

Oxide	Mole %
BaO	42.9
TiO_2	35.8
SiO_2	14.2
Al_2O_3	7.1
BaF_2	2.0

The presence of a small amount of fluoride in the glass is reported to give a product with properties more closely related to ceramic barium titanate due to more rapid crystallization at the beginning of the devitrification cycle; its presence also allows the glass to completely crystallize at the end of the cycle. It was not possible to completely devitrify the glass which contained no fluorides.

The dielectric constants of this material according to particle size and per cent by volume of the barium titanate are shown in Figure 15.

The computed ϵ_1-values for the $BaTiO_3$ phase are high for normal large grain $BaTiO_3$, but agree well with the values for fine grained $BaTiO_3$ which is under stress and exhibits increased values of the intrinsic dielectric constant (see Figure 5, B40).

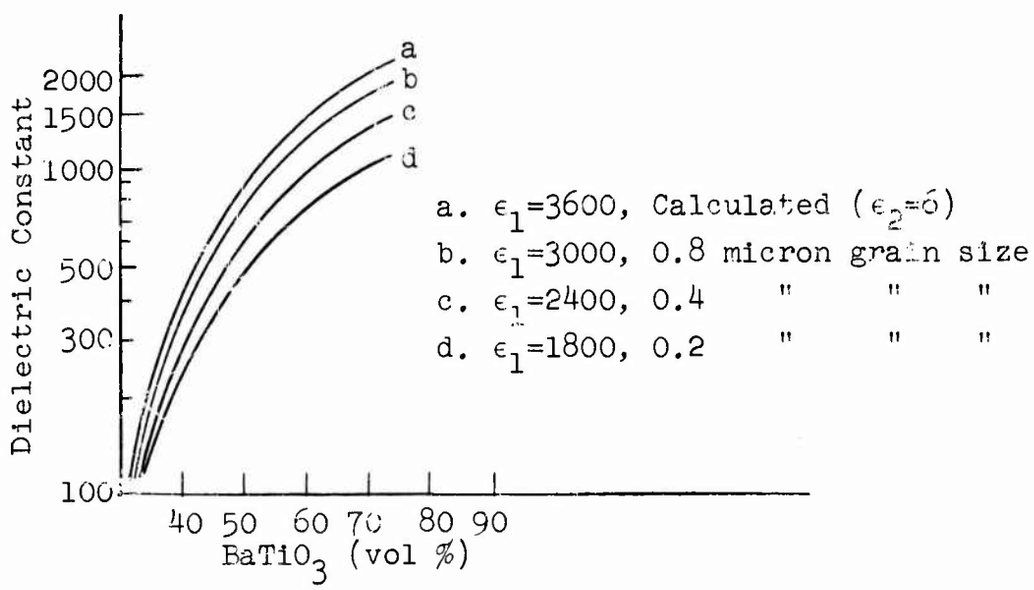

Fig. 15 Dielectric Constant at 25°C as a Function of the $BaTiO_3$ Content

C. Properties of Reduced Ceramic Barrier-Type Capacitors

Relatively large capacitance values are achieved in ferroelectric ceramic capacitors by utilization of thin ceramic surface barrier layers. In the manufacture of such a part the ceramic is made semiconductive by reduction at high temperatures. The removal of some oxygen atoms creates an excess of electrons so that the material attains a resistivity of .5 to 50 ohm cm. A layer on the surface of such a body about 1/2 mil deep is then reconverted to the insulating state by firing in an oxidizing atmosphere and an electrode is applied to the surface. A capacitor is formed thereby between the external electrode and the semiconductive body, so that a finished part consists essentially of two series capacitors.

There is a wide variety of such barrier layer capacitors available depending on the starting material used, the degree of reduction or doping, the reoxidation temperature and procedure and the metal paint applied. The details are largely proprietary and the literature on this subject is scarce. In one patent (C13) it is claimed that high capacitance and low losses can be achieved by separating the application of the metal paint which is done in a neutral atmosphere (N_2) and the reoxidation of the reduced sample which is done in oxygen. In another patent (C14) it is claimed that especially good properties can be obtained if the barrier layer contains a second phase (compounds of higher TiO_2 content than $BaTiO_3$, e.g., $BaO \cdot 2\ TiO_2$) which upon reoxidation of the first phase ($BaTiO_3$) remains partly reduced and acts as an electron yielding impurity center.

These capacitors are normally catalogued by their voltage ratings. These are related to the thickness of the dielectric under the electrodes which, in turn, determines the capacitance per square inch. Table XV shows some industry ratings and the specific capacitances of completed capacitors. These parts are normally rated to withstand life tests of 250 to 1000 hours, at 85°C and at voltages that range from the rated voltage up to

2 times rated voltage. The allowable leakage resistances at end of life go up with higher voltage ratings and with smaller capacitance values. They range from 5000 ohms for 2.2μf, 3V units to 500 megohms for 0.1μf, 25 V units. Figures 16a, 16b, 16c and 16d show how the insulation resistances of the various ratings go up logarithmically when the applied voltage is reduced.

Barrier layer capacitors are made in a wide range of temperature coefficients and Table XVI gives a listing of the capacitance change with temperature as has been observed in parts of the various voltage ratings as made by different manufacturers. Figure 16e shows the shape of these curves for the three sets of voltage ratings. Figures 16f and 16g show how the insulation resistance of parts made to these four voltage ratings varies with temperature.

The semiconducting interior of the barrier layer capacitor represents a low but finite series resistance. As a result, the dissipation factors of these parts increase from 3-6% in the audio range when going to RF frequencies. Figures 16b and 16c show the variation of capacitance and dissipation factor with frequency. The DC-voltage dependence of capacitance is shown in Figure 16j.

TABLE XV

Voltage Ratings and Capacitance of Barrier Layer Capacitors

Voltage Ratings	Specific Capacitance of Completed Capacitors
3V	6-7μf/in^2
10V, 12V	1-1.5μf/in^2
16V	.5-.8μf/in^2
25V, 30V	.3-.6μf/in^2

TABLE XVI

Capacitance Change (in %) from Room Temperature Capacity at Various Ambient Temperatures for Barrier Layer Capacitors

Voltage Rating	Manufacturer	-55°C	+10°C	+85°C
3V	A	-10%	-3%	+12%
10V	A	-23%	-5%	+17%
10V	B	-50%	-7%	-14%
10V	C	-85%	-8%	-60%
12V	D	-71%	-17%	-50%
25V	A	-22%	-4%	+4%
25V	E	-45%	-7%	-25%
25V	F	-75%	-8%	-30%
30V	D	-29%	-11%	+.5%

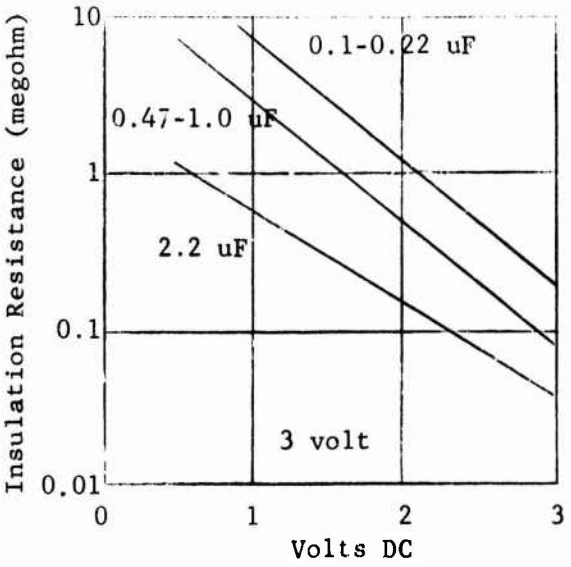

Fig. 16a Insulation Resistance vs DC Voltage

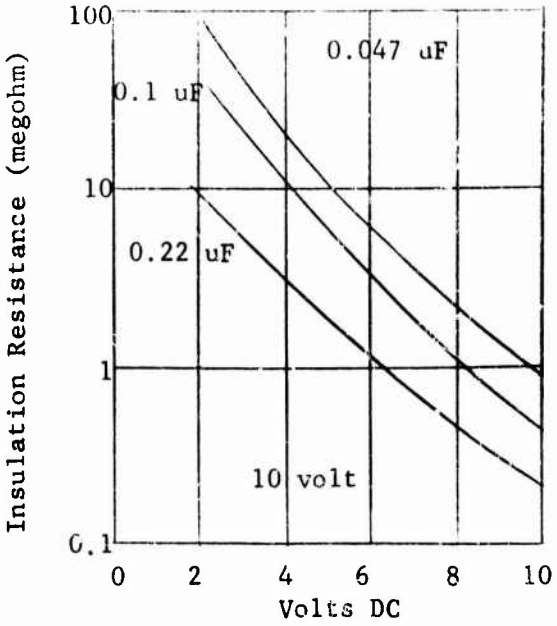

Fig. 16b Insulation Resistance vs DC Voltage

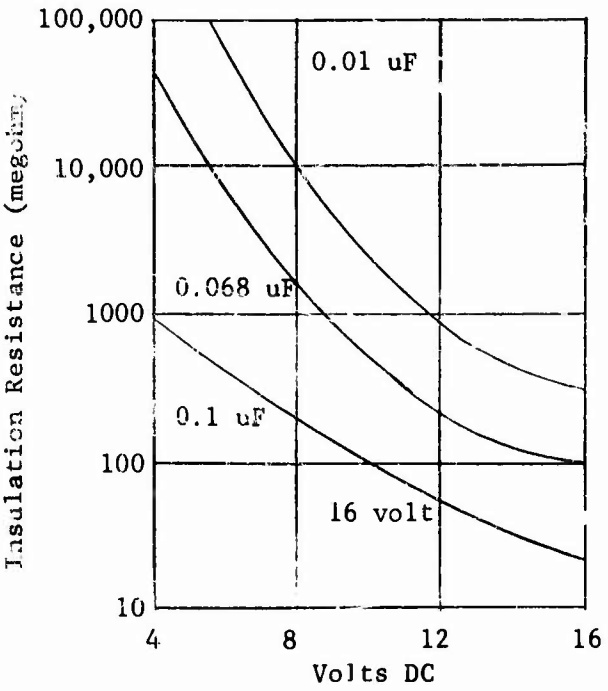

Fig. 16c Insulation Resistance vs DC Voltage

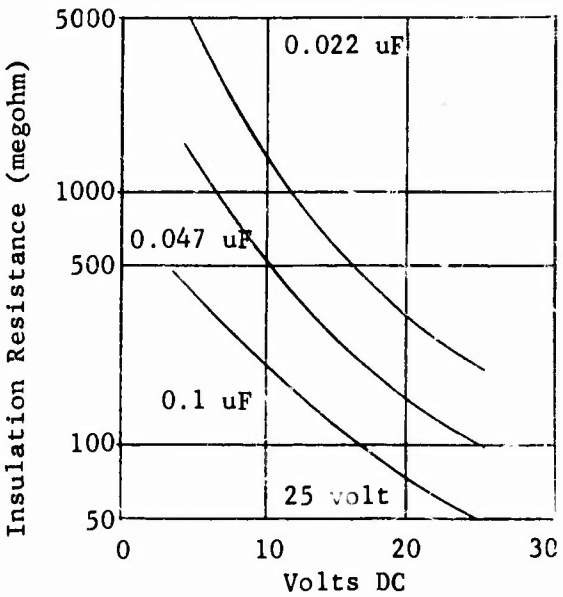

Fig. 16c Insulation Resistance vs DC Voltage

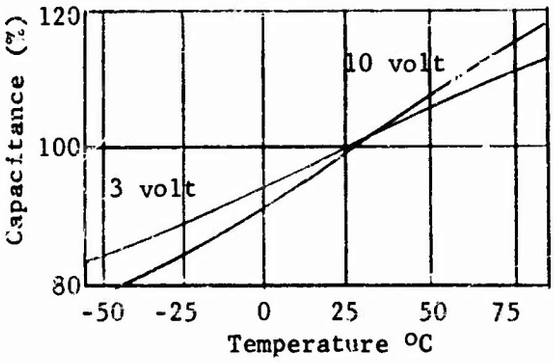

Fig. 16e Capacitance with Temperature

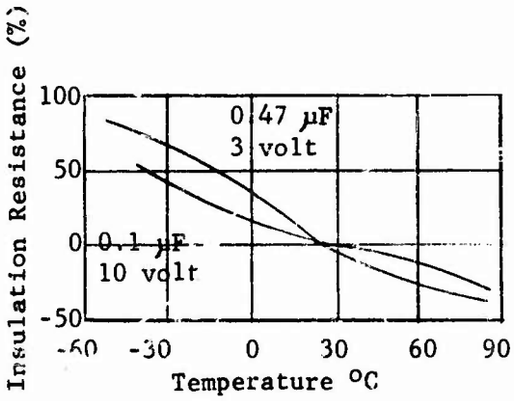

Fig. 16f Insulation Resistance with Temperature

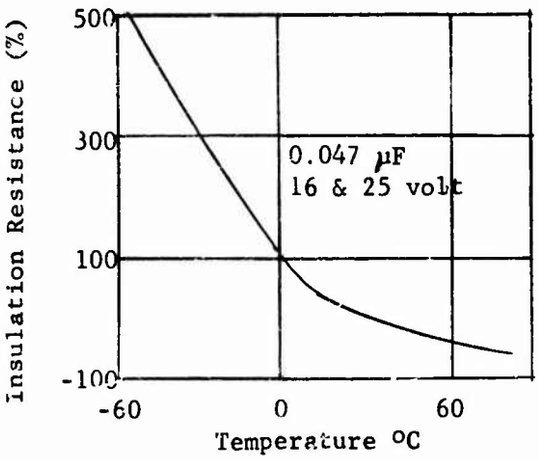

Fig. 16g Insulation Resistance with Temperature

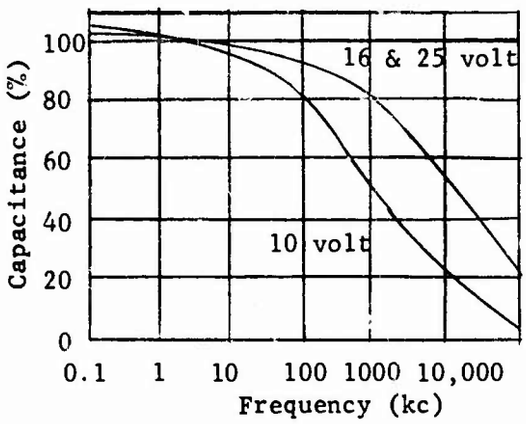

Fig. 16h Capacitance with Frequency

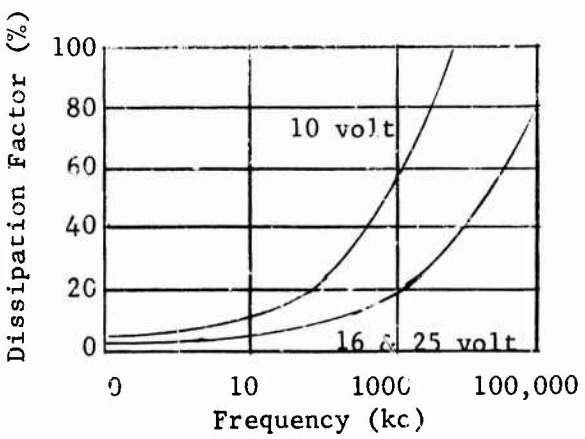

Fig. 16i Dissipation Factor with Frequency

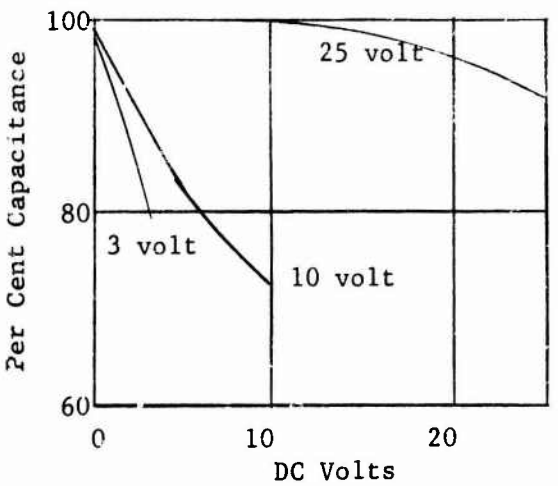

Fig. 16j Capacitance Change with DC Voltage

D. Poling Techniques for Ferroelectric Ceramics

1. Poling Processes

Barium Titanate Types

Temperature - The most common practice in poling barium titanate bodies is to cool them through their Curie point under an applied voltage stress. The shaped material with electrodes in place usually is activated by heating to a temperature approximately five degrees above the Curie point in a poling medium (such as oil), bringing it to thermal equilibrium (G7) and then cooling it to room temperature.

For certain special applications techniques such as "cold-poling" (B12) are used to polarize ceramic compositions at specific activity levels less than those obtainable under optimum poling conditions (D4). Also, some ceramic compositions can be pre-aged to an extent by altering the poling temperature and cycle.

Voltages - The electrical fields generally will range from approximately 15 volts per mil to 40 volts/mil. This variation is due to compositional variations and to the thickness of the ceramic body across which the voltage is applied. As the thickness increases the field which can be applied decreases. This relationship is not linear, but logarithmic (H7).

Time Cycles - The time cycle for heating, cooling and applying the dc field will vary with the size and configuration of the part being poled. However, experience has shown it to be desirable to lower the temperature from maximum to minimum in a time interval of not more than two hours. This statement is a general rule-of-thumb.

Poling Media - The most common poling medium is silicon oil (such as Dow Corning 200 fluid). This oil works well because of its high-voltage breakdown strength, its thermal-voltage stability and its resistance to chemical change. Other poling media have been used over the years; for example, poling has been accomplished in air, in special gaseous atmospheres

such as carbon monoxide, and in a variety of oils. Peanut oil has been recommended by some engineers as a good poling medium.

The arguments against using silicon oil as the poling medium are generally based on subsequent inability to bond the ceramic element to other types of hardware. This problem probably is due to difficulty in removing the silicon oil from the surfaces to be bonded.

Special Poling Techniques such as Poling with Temporary Electrodes, etc.- There are numerous special techniques for poling to produce ceramic piezoelectric elements with a particular set of characteristics (B27). Certain devices operating in the torsional or shear mode of vibration present somewhat difficult poling problems. In this mode of vibration the poling axis is normal to the drive axis. At present, there are three methods of obtaining poled ceramics for this transverse application, depending upon the geometrical configuration of the ceramic body. The most common use of the shear mode in ceramic transducers is in the delay line transducer. Since these are thin film devices utilizing the k_{15} coupling factor, the choice of material is arbitrary for this discussion. The three methods of obtaining transverse poling are: fringe poling, removal and replacement of electrodes, and slicing from poled ceramic bodies. A description of these methods follows:

Fringe Poling - This method (W6) of obtaining ceramics for operation in the k_{15} mode consists of moving two spaced poling electrodes adjacent to the surface of a film of ceramic material in a fringe-like manner. It is not known how effective this method is for thicker bodies.

Removal and Replacement of Electrodes - The method of placing poling electrodes on the edges of thin wafers and, after poling, removing the electrodes by edge grinding and replacing them in other positions on the plane surfaces of the wafers has had mixed success. Attempts to fire electrodes on the major surfaces of poled ceramics result in depoling. The electroless nickel process employed by Bell Laboratories (M14) provides electrodes of good adherence which may be readily soldered.

Shear plates obtained by this method produce excellent transducers having low insertion losses and large bandwidths.

Slicing from Poled Ceramics - This method of obtaining thin shear plates yields transducers of good performance with a high degree of reproducibility. The reproducibility results from slicing or dicing a great quantity of thin wafers from one large block of ceramic material. Slicing may be performed by use of a diamond-charged wheel and coolant or, preferably, by ultrasonic dicing. The latter method allows thinner slices without loss of polarization, while the former results in some loss of polarization adjacent to the surface because of heat generated during the slicing. Subsequent surface grinding and lapping remove the unpoled regions. Electrodes may be placed on the major surfaces by the electroless nickel process or, for many applications, indium-gallium, etc. alloys may be applied by scrubbing techniques.

It should be mentioned that measurements of the coupling coefficient (k_{15}) at random positions over the area of the thin wafers show greater variance for those wafers sliced by use of the diamond wheel.

Torsional Operating Transducer and Poling Method - Transducers operating in the torsional mode are generally cylindrical in shape. Several methods for making them are discussed by Mason (M10), with one method in particular yielding high electromechanical coupling. This method requires cutting a hollow ceramic cylinder in half along the length. Each half is then poled in opposite directions along the length in conventional manner. The poling electrodes are then removed and the two halves are cemented together by a conducting cement. Electrical drive is applied to the cement electrodes resulting in utilization of the k_{15} coupling factor for the thickness shear mode. Maximum efficiency is realized since all of the material is used to drive the transducer.

Poling Under Static Stress - During the poling process, domains within the crystallites of ceramic transducer materials are aligned (switched) to some degree with a dimensional change

in the material taking place. During poling, barium titanate increases in length in the direction of the polar axis by as much as 0.11% and decreases in length perpendicular to this by as much as 0.046% (K6). Lead-zirconate-titanate ceramics with nearly twice the crystal distortion as barium titanate undergo strains approximately four times as great as barium titanate. In view of the dimensional changes noted above it is apparent that a properly oriented stress applied during poling can effectively aid or impede the poling process. Stress alone cannot pole a ceramic but can depole it.

Lead-Zirconate-Titanate Types

Temperature - The temperature requirements for poling the lead-zirconate-titanate bodies vary somewhat from the requirements for the barium titanate types. While the use of the temperature cycle method is sometimes employed in poling the lead-zirconate-titanate bodies, the most common practice is to hold them at a constant elevated temperature, which is generally in the range of 70 to 150°C depending on the composition being poled. When variation in temperature is employed, the common practice is to apply voltage at 150°C and then lower the temperature to approximately 50°C while maintaining a constant applied voltage.

Voltages - The fields employed for poling lead-zirconate-titanate bodies generally range from 40 to 80 volts/mil depending upon body composition. It is common to experience greater difficulty in obtaining the exact required voltage for the lead-zirconate-titanate types which may be due to the wider composition variations that will occur from lot to lot.

Poling Times - The poling times at constant elevated temperatures range from 1 to 20 minutes, in general. The variation in time cycles is again due to the body compositional differences. When a temperature cycle (150° down to 50°C) is employed, it is usually desirable to accomplish this temperature drop within a 20-minute time period or at a rate of approximately 5° per minute.

Poling Media - The poling media described for barium titanate are also used for the poling of lead-zirconate-titanate types.

Special Poling Techniques such as Reverse Poling - Conditioning of the ceramic material by reverse poling is generally beneficial when conduction and shorting are problems. This method results in higher coupling coefficients than is possible with poling in one direction only. In reverse poling, the field is applied in a given direction until conduction becomes too high and then applied in the opposite direction again until conduction becomes too high. For some compositions after a number of reversals, the poled body is able to withstand higher applied fields and accept a higher degree of polarization than the same body after initial poling. An example is given by Berlincourt et al (B12) for $PbZrO_3$:$PbTiO_3$ (53:47 mole ratio) which would initially withstand 40 kv/cm at 100°C only instantaneously. After a number of reversals of the poling field, the specimen would withstand a field of 60 kv/cm for eight minutes before conducting. This higher applied voltage permitted a higher planar coupling factor to be obtained for the sample.

Daniel points out that intermittent unidirectional poling (D4) may produce a higher and more rapid activation in poled ceramic materials by resulting in a shock excitation which puts the body into vibration at its natural frequency every time the potential is applied. Another advantage of intermittent poling is that higher potentials can be used than is possible with continuously applied voltages.

Still another variation of poling, as described by Hansell, is the use of a superimposed alternating ripple of resonant frequency on the poling potential or pulsating the unidirectional poling potential at a similar frequency (H7).

Metaniobate Types - According to Goodman, lead metaniobate materials can be permanently polarized by the methods used for barium titanate (G4); for example, a potential of 20 kv/cm at 200° to 250°C should be applied for 30 minutes. Above 250°C

there is a rapid increase in conduction which prevents maintaining the potential necessary for poling. Polarized samples of $PbNb_2O_6$ have been heated briefly to 550°C with little change in their piezoelectric properties after cooling.

Goodman (G3) also recommends a potential of 750 volts/mm at 250°C for two and one-half hours for poling metaniobates.

Materials having a transformation (sub-Curie) temperature permit the use of a special poling technique. Mason (M11) proposes poling $KNbO_3$ by heating to at least 210°C but not more than 215°C and allowing it to cool under a potential of 9 kv/cm to room temperature. At 210°C the tetragonal form of $KNbO_3$ changes to the orthorhombic structure. Mason indicates that the applied field (9 kv/cm for $KNbO_3$) should be slightly greater than the coercive field at the transition temperature.

2. Problems encountered in the poling process

Arcing through the unit being poled or across its edges can generally be attributed to pores, to edges that have been contaminated with salts or by handling, or to contaminated and/or deteriorated poling media. Rigid quality control must be maintained prior to poling and poling media must also be periodically cleaned or replaced.

Cracking during the poling process is a problem that is generally attributed to the presence of internal stresses in the ceramic body or the generation of excessive internal heat. This internal heat may be due to partial reduction or density variations through the body.

If the desired piezoelectric activity is not achieved during the first poling attempt, the process should be repeated several times.

3. Measuring the degree of poling

The effect of the poling treatment can be determined by use of the IRE Standards on Piezoelectric Crystals: Measurement of Piezoelectric Ceramics (I7); however, in many cases the

efficiency of poling can be determined more economically and more quickly by a simulated service test. In this case, one might not be able to describe the degree of poling in as well-defined parameters as in the IRE tests.

VI. DEVICES

A. Introduction

In this presentation, discussion of the types of "linear" and "non-linear" devices employing ferroelectric materials must necessarily be limited. Nearly all devices having linear design objectives may be operated in such a manner as to render them non-linear in their response, hence this discussion will be restricted to linearity as being that characteristic of a device which responds linearly to the stress applied to the body. Nevertheless, a brief description of the factors that define the linear range of operation of representative devices will be included.

All devices have a dynamic range of operation over which they respond faithfully to the instantaneous input; this is usually referred to as the dynamic range of the device. Although response is obtained beyond this range, the output departs from the original response behavior. In general, nearly all devices having linear design objectives exhibit a dynamic range of approximately 60 decibels (1000/1); beyond this, the response becomes non-linear. This 60-decibel dynamic range (or similar dynamic range) is restricted to definite maximum and minimum values of stress. Any device operated within a range of stress levels which extends either below or above this specific range will result in non-linear output as a function of the input. In order to obtain the maximum linear dynamic range, the following boundary conditions must be observed:

(a) The dynamic range of stress amplitudes applied, electrical and mechanical
(b) The wavelength of the applied stress
(c) The required bandwidth of the device
(d) The environmental conditions present

B. Non-Linear Response of Linear Devices

Frequently a device designed to be linear over a range of input signals will exhibit one or more non-linearities in its instantaneous response. This occurs most frequently in electro-mechanical devices subjected to varying mechanical disturbances in the presence of the desired signal. This can be observed quite frequently in the field of acoustics where input acoustic signals may vary over a range of 160 decibels as, for example, from the whisper of a voice to the blasts of small-arms fire. It is quite obvious that a transducer designed for operation at voice intensity levels is not suited for operation at intensity levels of 160 decibels*. Although microphones exist for high amplitude applications or may be designed for a specific application, it is common to observe a low level microphone being pressed into service within a high amplitude environment. Many transducer (or microphone) manufacturers have been prompt in taking advantage of improved ferroelectric materials and incorporating them into their lines, but they have not informed users of the materials of their change in sensitivity; therefore, the user is sometimes prone to condemn the device on the basis of the change in the observed response to his input signals.

The primary interest in this review is in the non-linear characteristics of the ferroelectric body itself, but in order to prevent any omission of non-linear devices the above type of non-linearity will be discussed in more detail. Figure 17 represents a model device that serves to illustrate the points of the discussion. For convenience, an inexpensive microphone is presented in cross section. Figure 17a shows a typical diaphragm-actuated microphone in which the slight displacements of the diaphragm due to incident sound pressure are coupled to a sensing element of the bender type by means of a coupling rod. The diaphragm is edge clamped, flat in design, and is usually

---

* 0 decibels = 0.0002 dynes/cm^2 = 10^{-16} watts/cm^2

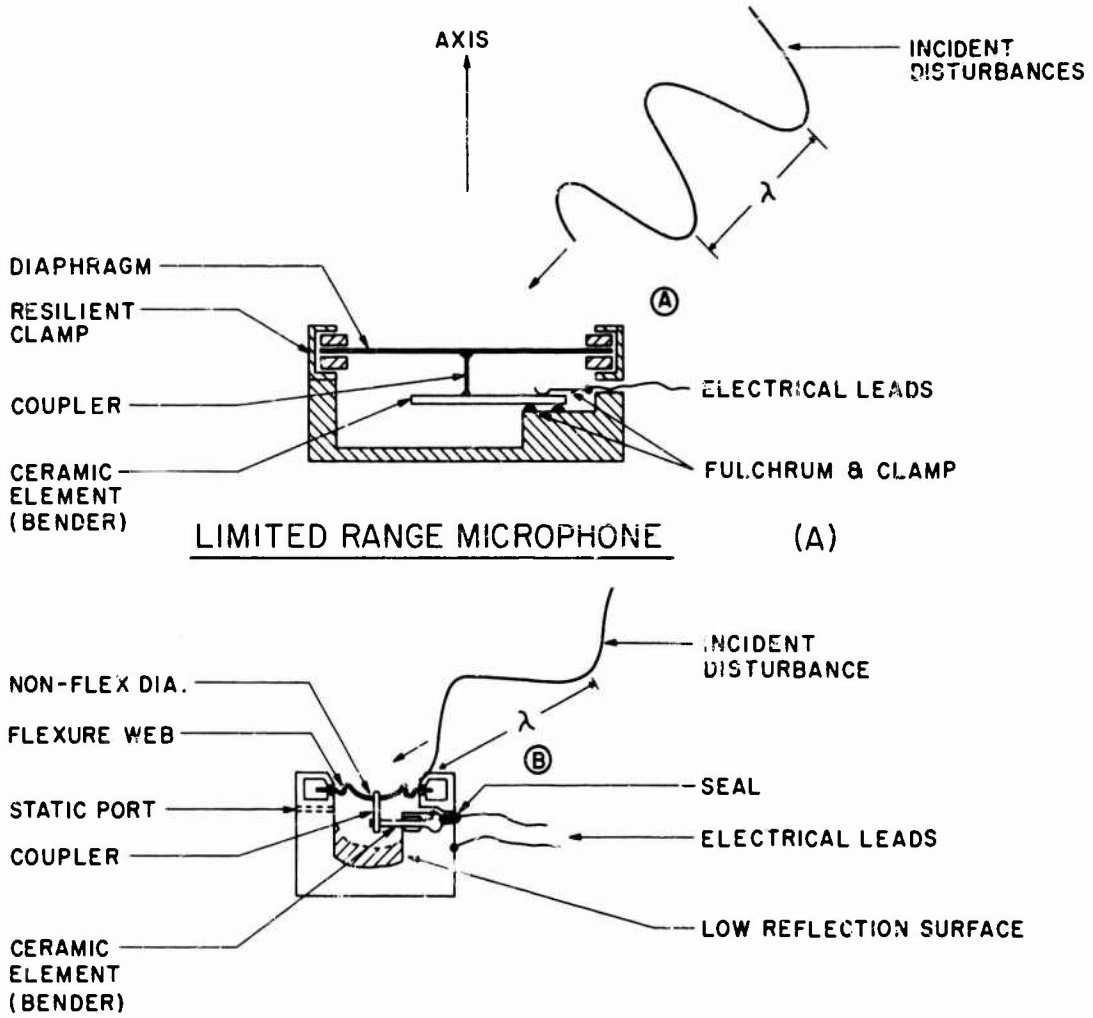

1) NON-FLEXING COUPLER
2) ELIMINATION OF STANDING WAVES RE: DIA./BOTTOM
3) REDUCED ODD HARMONICS IN XTAL
4) MIC $\ll$ WAVELENGTH
5) STATIC PORT CONTROLS LF CUT-OFF
6) EDGE CLAMP AT XTAL
7) FLEX WEB PERMITS EXCURSIONS $\gg$ INCIDENT STRESS
8) XTAL $\ell \gg \omega$ i.e. $f_{\sim} \propto K \frac{t}{\ell^2}$

FIG. 17-ILLUSTRATION OF LIMITED AND EXTENDED RANGE MICROPHONES

made of thin metal. The housing is simple in design, and the bender element may be simply clamped at one edge by a contact spring which also serves as a conductor to one of the electrodes. The housing is usually metal to serve as an electrical shield and ground return for the element. The coupler is usually a non-conductor to permit electrical connections as shown. This simple design represents the cartridge that may be found in many low-cost microphones intended for operation in handheld attitudes at voice-level sound pressures.

Figure 17b is a redesigned counterpart of 17a which illustrates the features that materially eliminate the responses that frequently are judged non-linear. The diaphragm has been stiffened by forming in the central portion to prevent buckling or "oil canning" due to very strong signals. In addition, the periphery of the diaphragm includes a compliant web to permit larger displacements and to extend the linear displacement range of the diaphragm. Due to the larger allowable displacement the edge now may be rigidly clamped, thus obtaining a reproducibility not previously attainable with the yielding edge of 17a. The ceramic element is edge clamped uniformly to permit a more ideal reed support structure and reproducibility in the pass band characteristic. The housing has been modified to prevent high-Q standing waves in the air column between the diaphragm and the rear surface of the housing. A pressure release port has been added to control the static pressure equalization in varying ambient conditions as well as to introduce a reproducible low frequency cutoff response. The coupling rod has been stiffened to prevent flexing due to mechanical drive at high amplitudes. An additional feature of the formed diaphragm is the differential elastic modulus across the surface due to the varying degree of cold work in forming. As an example, the modulus is lower in the region of the web than in the central portion if the diaphragm is fabricated from annealed brass. This causes diffusion of any nodal regions that would tend to present discrete resonance peaks in the response characteristic of the

microphone. Another source of distortion that is sometimes not considered in the operation of a microphone is the size of the device relative to the incident wavelength. This consideration is not important for normal incidence; i.e., where the axis of the device is perpendicular to the wave front. Oblique incidence introduces phase distortion in that as the wavelength approaches the dimension of the microphone a compression and rarefaction can exist simultaneously on the diaphragm resulting in partial cancellation. Other distortion due to refraction about the device causes a departure from linearity.

Nearly all devices of this nature can depart from perfect linearity by virtue of certain design factors. Viscous bonds, resonant support structures, interspersed transmission windows, wind screens, structure-borne vibrations, improperly matched circuit terminations, and many others. High amplitude sounds themselves can become distorted during transmission due to finite amplitude effects which can, in effect, cause the observed wave form to be different at two different positions along the transmission path. These effects are common in sound transmission in fluids and are caused by finite heating in the compression phases which results in increased particle velocity in these regions and subsequent velocity increases relative to the rarefactions. The compressions tend to catch up to the rarefactions and create mild shock fronts. Depending on the frequency of the disturbance, these phenomena may be anticipated at sound pressures exceeding 135 decibels. A microphone exposed to these shock fronts can distort materially the resultant output due to the response of various massive and compliant components within the structure.

The purpose of the foregoing discussion is to acquaint the reader with the non-linear response of an otherwise linear device. It is true that advantage may be taken of certain designed non-linear response characteristics in order to sense or reduce the effect of ambient conditions, or to selectively filter a certain signal component, either to reduce the effect of its presence or to enhance it, as in discrimination against unwanted signals.

C. Non-Linear Devices

Ferroelectric ceramics exhibit certain non-linearities in their response to an electrical input, and it is the purpose of this discussion to present these in some detail.

Since the dielectric susceptibility of a ferroelectric crystal is larger above the Curie temperature than below it, this property of ferroelectrics in their non-polar phase above the Curie temperature (also called the paraelectric phase) has resulted in the development of a group of devices useful in microwave applications. A review of the properties of a common ferroelectric material such as $BaTiO_3$ will be helpful in understanding most of the non-linear devices considered sufficiently developed to be established as useful devices. Many investigations are being carried out to improve these devices and the materials required in their fabrication; hence, more sophistication in the range, stability, and precision of non-linear ferroelectric devices may be anticipated in the near future.

The non-linear devices that have attained a stature of significance may be considered to be:

(a) Dielectric amplifiers
(b) Non-linear capacitors
(c) Phase shifters
(d) Single and Multi-pole switches

1. Dielectric Amplifiers

The dielectric amplifier has not attained the usefulness nor reliability of its counterpart, the magnetic amplifier. Unlike the magnetic amplifier, the dielectric amplifier presents a nearly infinite impedance to dc control signals; this makes it a highly desirable device for many applications where loading of the control circuit must be avoided. The small size and low weight of the dielectric amplifier have great advantages over the magnetic amplifier; however, these are offset seriously by two strong disadvantages: the dielectric is extremely temperature sensitive, and aging of the non-linear

dielectric material causes changes in its operating characteristics. The dielectric amplifier is shown in its simplest form in Figure 18. Its similarity to the magnetic amplifier is quite apparent.

The reason for temperature sensitivity in the dielectric amplifier is that its non-linearity can be obtained from two sources: the field sensitivity of the Curie temperature and the voltage; that is, a change in the ambient temperature has the same effect as a change in control voltage. These remarks (K14) are predicated on existing materials, and in view of the current research activity, the situation can be expected to be improved within the next few years.

When barium titanate- and lead metaniobate-type materials were discovered, it was anticipated they would lead to improved dielectric amplifier devices. The materials possessing square hysteresis loops lead to high gain dielectric amplifiers. It is unfortunate that to date the commercially available ferroelectric materials have a high coercive field and fairly high hysteresis losses as well as being temperature sensitive. As a result, dielectric amplifiers have not had the acceptance that was originally anticipated. Polycrystalline ferroelectric ceramics with less sensitivity to temperature and voltage variations may be used in a variety of applications other than in dielectric amplifiers. Such devices obviously have less controlled variation and do not suffer from the temperature difficulties that limit their use in wide range devices.

2. Non-Linear Capacitors

Polycrystalline ferroelectric ceramics having low voltage variation and temperature sensitivity find a multitude of uses in devices where large input signals are available to drive them. The availability of large driving voltages and a requirement for small non-linear variations are typical of frequency-shift applications in high-frequency oscillators used in radio telemetry and similar applications. Fine frequency tuning of local oscillators in low-powered communications receivers is an

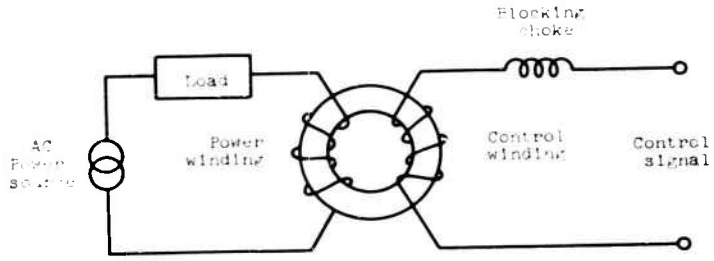

(a) Basic one-core magnetic amplifier

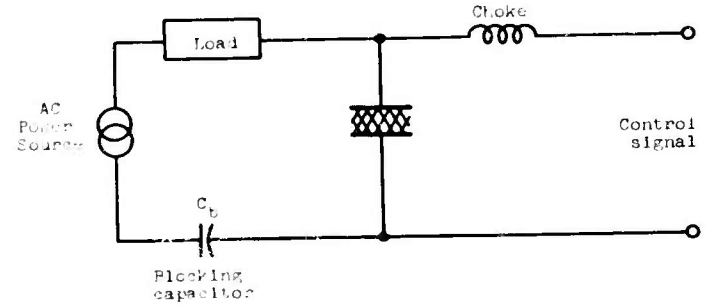

(b) Basic single-capacitor dielectric amplifier

Fig. 18 Basic Magnetic and Dielectric Amplifier Circuits

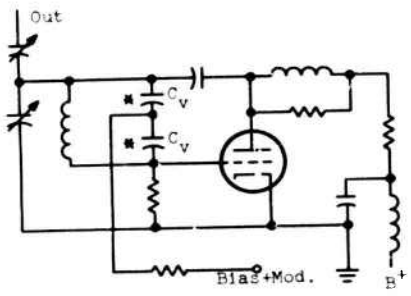

(a) VHF sweep oscillator

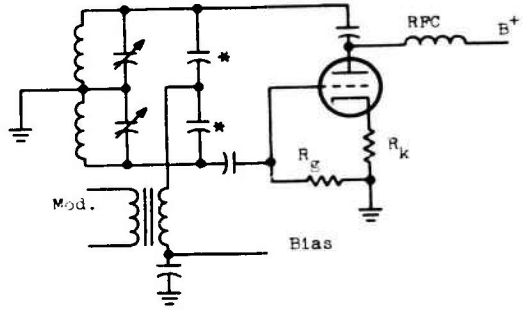

(b) Frequency modulated oscillator

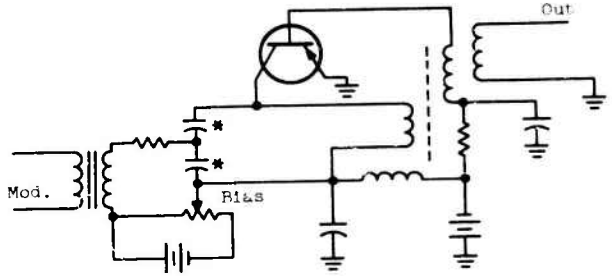

(c) Solid-state FM oscillator

Fig. 19 Frequency Control with Voltage Sensitive Capacitors

application that is rapidly growing. These applications are typical of those where very large space savings are realized through the use of small non-linear capacitors. In general, a large variable bias voltage is present to effect a variation of dielectric constant that may not exceed a tenth of one per cent.

Figure 19 presents several frequency control circuits of the type mentioned above. Component values have been omitted for clarity and the non-linear elements indicated by an asterisk and shown in a paired configuration. Although the dynamic range and linearity of dielectric variation may be better achieved by employing a plurality of capacitors, it is not necessary to utilize the capacitors in pairs. It is also feasible to create a specific non-linear frequency variation by operating several capacitors from different bias voltages.

3. Phase Shifters and Switches

The increase in the susceptibility of barium titanate as the temperature is raised from room temperature to the Curie temperature has led to investigation of its applicability to devices such as phase shifters and microwave switches. It has been shown that its susceptibility increases several magnitudes (T10) at the Curie temperature. Above this temperature there is no hysteresis and no spontaneous polarization. The feasibility of this material for obtaining high isolation by small control voltages has been investigated and isolation approaching 40 decibels was attained. Above the Curie temperature the susceptibility follows a Curie-Weiss law

$$K = \frac{C}{T - T_o} \qquad (1)$$

where T_o is less than the Curie temperature and C is the Curie constant.

Although it is not convenient to operate at temperatures above the Curie temperature of barium titanate, researchers (L5)

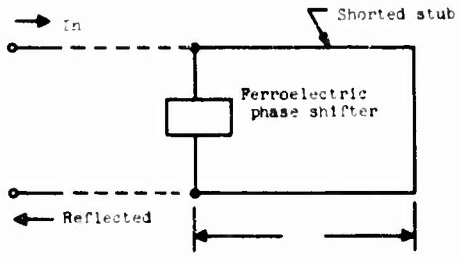

Fig. 20 Ferroelectric Phase Shifter

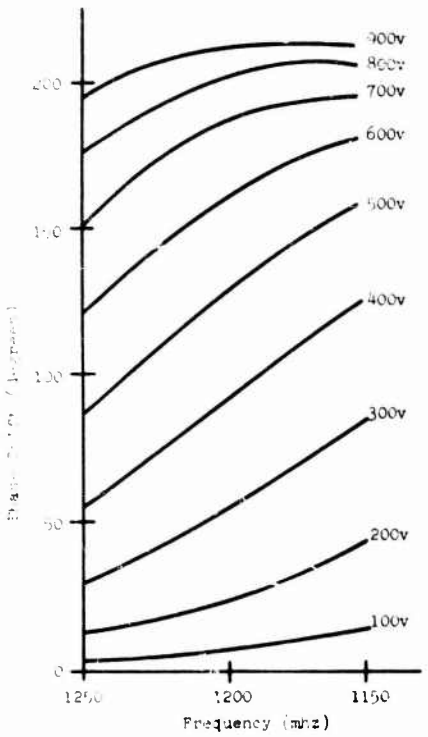

Fig. 21 Phase Shift vs. Frequency for Indicated Bias Voltages

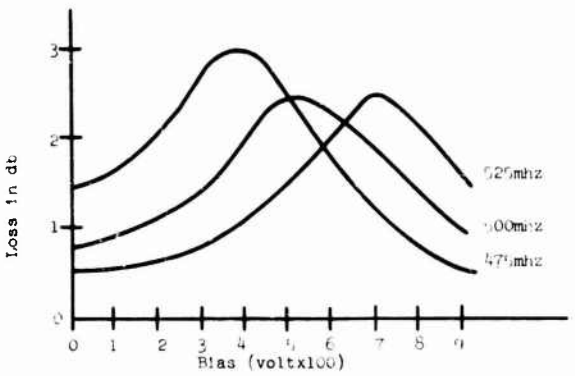

Fig. 22 Insertion Loss as a Function of Bias Voltage for a 180° Phase Shifter in the 500mhz Band

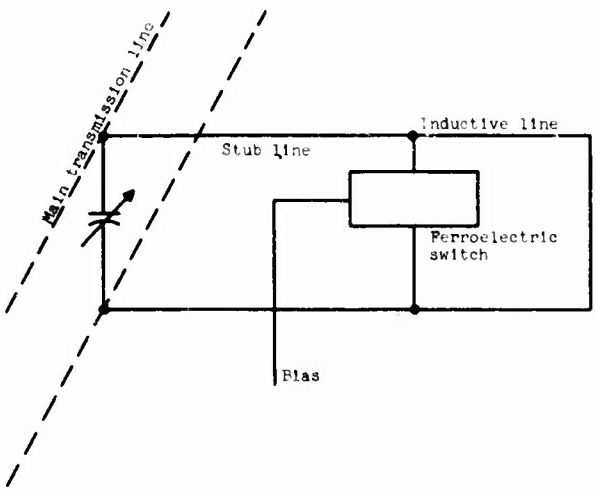

Fig. 23 Ferroelectric Single-pole Stub Switch

have succeeded in lowering the Curie temperature by adding strontium titanate to the barium titanate. The resultant single crystals, although imperfect, have Curie temperatures of approximately 25°C. These crystals have been used to investigate the feasibility of phase shifters and single-pole solid-state switches at microwave frequencies.

The reflection-type phase shifter functions in such a manner as to shift the phase of the reflected signal relative to the incident signal. A voltage applied to the ferroelectric changes the capacitance of the dielectric and hence the phase of the reflected signal. Operation is optimized at a specific narrow band (10%) of frequencies by means of a shorted stub or inductive line. The equivalent circuit is shown in Figure 20. Typical phase shift as a function of frequency for various bias voltages is shown in Figure 21. Insertion loss at the stage of development reached to date is relatively high, but it is anticipated that continued effort to improve the firing and mixing schedules of the materials will result in reduced insertion loss. Representative insertion loss for a 180° phase shifter as a function of bias voltage is shown in Figure 22. This curve depicts the insertion loss for a unit tuned to the 500 mhz band. It is considered that the insertion loss is due to a loss term influenced by a reactive term which increases with frequency from resonance. As the device is operated farther from resonance, the reactive term begins to dominate and the insertion loss is reduced.

4. Single and Multi-pole Switches

Single and multi-pole ferroelectric switches function as reflection-type switches due to their ability to change capacitance upon application of voltage which, when connected across a transmission line, presents a large change in impedance between the two states of the device.

A representative single-pole switch is shown in Figure 23. The switch may be combined with additional switches to

increase the isolation as shown by the response curves of Figure 24. A single-pole switch presents approximately 20 decibels isolation for the specimens shown in Figure 24.

Switches, as discussed here, function in a manner very similar to phase shifters except that they are switched between two states instead of operated in a continuous manner. In general, it is stated that the operation of the switch is less affected by temperature changes, due primarily to its mode of operation. The phase shifter, however, is very sensitive to temperature changes, but adjustment of the Curie temperature of the ferroelectric by changing its composition seems to reduce the temperature control requirements. Operation at higher temperatures should utilize a material having a higher Curie temperature in a thermal enclosure.

D. Loss Phenomena and Effect on Device Operation

Ferroelectric ceramics have experienced perhaps their greatest usefulness as transducer bodies more than in any other application. Since their early development as ferroelectric materials, barium titanate and its varied compositions have represented a breakthrough as a source of stress-sensitive transducer materials compared to single crystal piezoelectric materials such as quartz, Rochelle salt, ADP (ammonium dihydrogen phosphate) and others. This breakthrough is perhaps even more significant when one realizes the ability of these ceramic materials to be readily formed into an extremely varied selection of body shapes. The diversity of this material is obvious if one reviews only a sampling of the many thousands of foreign and domestic patents that have been issued in recent years.

Perhaps the area of greatest concern or question about the piezoelectric ceramic materials is their power-handling capabilities. Certain applications impose high electric drive to these materials with the subsequent development of large mechanical stresses. Under these conditions the dielectric and mechanical losses produce heat energy and reduce electromechani-

cal efficiency. The dielectric losses (B13) are almost entirely due to charge-field hysteresis, while the mechanical losses may be conveniently considered to arise from gross effects such as grain boundary scattering and slippage at crystal boundaries. Both dielectric and mechanical losses increase with increasing temperature.

At this point it is convenient to list the factors (B11) which limit the power-handling capability of the ceramic as follows:

(a) Mechanical strength of the ceramic
(b) Reduction in efficiency* due to dielectric losses
(c) Reduction in efficiency** due to internal mechanical losses
(d) Depolarization of the ceramic due to electric field
(e) Depolarization of ceramic due to temperature rise
(f) Feedback of (e) to (b) and (c).

Item (a) may be nearly eliminated from consideration when one considers design trends employed at the present state of the art. These trends are discussed more extensively in later portions of this report; however, we may infer that mechanical strength considerations are largely reduced by mechanical bias; i.e., pre-loading the ceramic body in a manner that essentially cancels the tensile stresses developed under severe driving conditions.

The reduction in efficiency in the presence of dielectric losses is given to a first approximation by:

---

* Efficiency $= \frac{P_a}{P_a + P_d}$, P_a = Acoustic power delivered to medium
P_d = Power/m^3 dissipated in ceramic by dielectric heating

** Efficiency $= \frac{R}{R + R_c}$, R = Accoustic load resistance
R_c - Resistance due to mechanical losses

$$\text{Efficiency in presence of dielectric loss} = \frac{k}{k + \dfrac{\tan \delta}{\sqrt{1 - k^2}}} \qquad (2)$$

where k is the coupling factor and δ is the phase angle between the electric field and displacement vectors, and $\tan \delta = 1/Q$, where Q is the quality factor related to the transducer bandwidth. The $\tan \delta$ quantity ranges from a value of 0.015 to 0.06 for most ferroelectric ceramics in common use today.

The efficiency of a matched transducer in the presence of BOTH mechanical and dielectric losses is given by:

$$\text{Efficiency} = \frac{k - \dfrac{\sqrt{1 - k^2}}{Q_m}}{k + \dfrac{\tan \delta}{\sqrt{1 - k^2}}} \qquad (3)$$

Q_m is the mechanical quality factor associated with elastic wave propagation in the material, and as in the case of Q_ϵ, $\tan \delta_m = 1/Q_m$ where δ_m is the phase angle between stress and strain. Just as $\tan \delta$ is a function of the applied field, Q_m is a function of the mechanical stress.

The preceding relations are for <u>matched</u> loads where transducer coupling to liquid and solid media is the design objective. Transducer coupling to gaseous loads presents difficult design problems and frequently requires the use of mechanical transformers to obtain adequate efficiencies. In this respect, one can usually neglect the mechanical loss $1/Q_m$ in comparison to $\tan \delta$, since additional mechanical losses are introduced through glue joints, viscous damping in cavities, and losses to supports which also contribute to heat conduction.

A reduction of efficiency accompanies depolarization (B13) of the ceramic due to high ac fields which may occur independent of dielectric heating. During one-half of the ac cycle the field is opposite to the original poling field. Different compositions of piezoelectric ceramic respond differently to

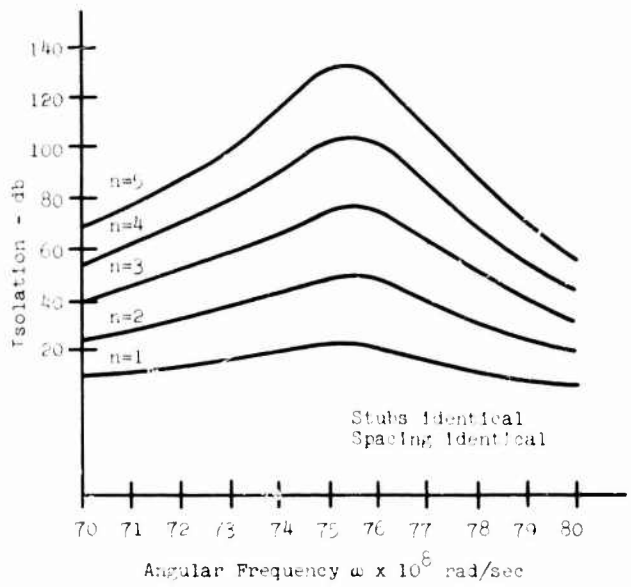

Fig. 24 Isolation Obtained by a Plurality of Single Pole Switches - n = number of switches

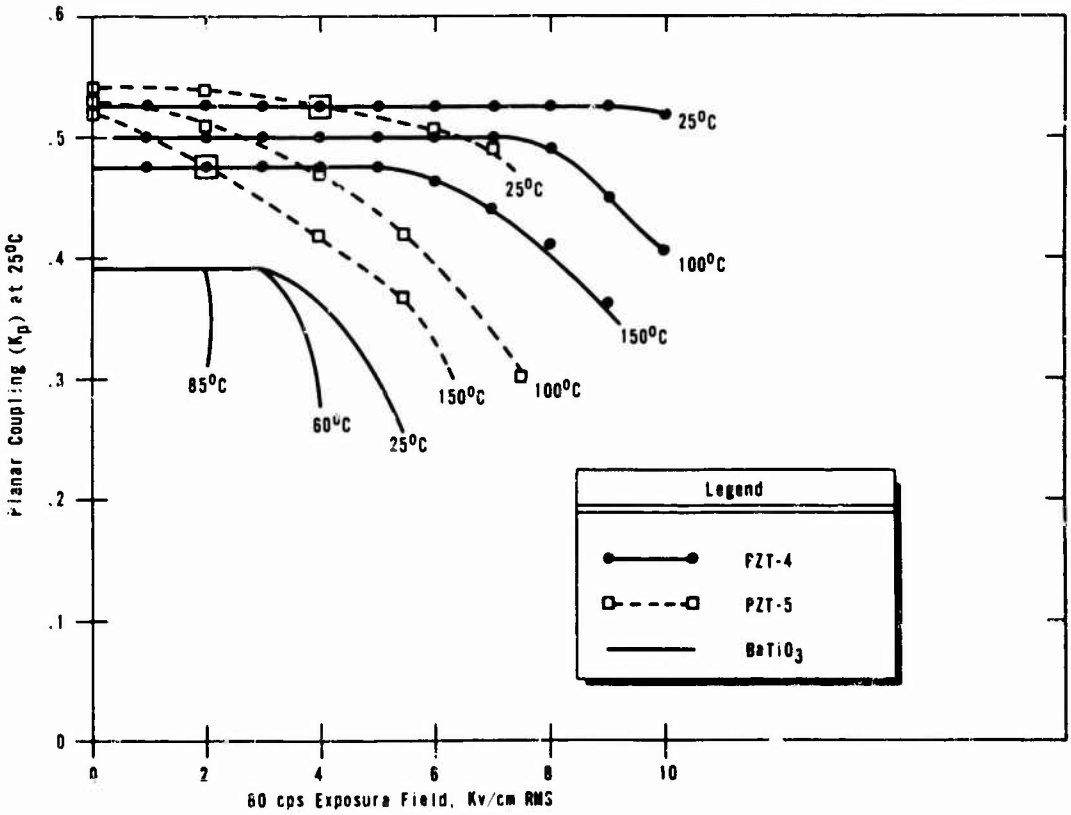

Fig. 25 Depolarization under AC Field for PZT-4, PZT-5 and $BaTiO_3$. Kp Measured at 25°C after Exposure to Indicated Field and Temperature

depoling fields. This is indicated in Figure 25 (B13) for $BaTiO_3$ and two compositions marketed as PZT-4 and PZT-5 (the Clevite Corporation). It is seen that the composition PZT-4 is excellent in its resistance to ac depolarization. One may also infer from Figure 26 that the best material from the standpoint of resisting depolarization under ac drive would be better also from the standpoint of dielectric losses (B13).

Heat energy that is not efficiently conducted from the ceramic causes the temperature of the ceramic to increase and depolarization under high ac drive is accelerated. This also is illustrated in Figure 25. When the effects of this condition (positive feedback) are added to increased dielectric and mechanical losses, the efficiency of the transducer is further reduced. As mentioned elsewhere in this report, an extensive research and development effort has been under way in materials development and design technology in recent years that has contributed tremendously to higher quality ferroelectric bodies and mechanical designs that yield excellent transducers which operate reliably for a long time.

The coupling factor as referred to here is defined by Mason (M9) and is expressed as:

$$k^2 = \frac{\text{mechanical energy stored}}{\text{total energy from battery}}$$

Although a great variety of equations are found for coupling factors, the IRE Standards on Piezoelectric Crystals (I7) summarizes these in the following coefficient:

$$k^2 = 1 - (f_s/f_p)^2 \qquad (4)$$

where f_s is the series resonance and f_p the parallel resonance frequency of the piezoelectric specimen. There is considerable argument (T8) as to whether these coupling factors are realized under normal applications where the design may be for either very high or very low frequency operation.

Considerable planning and correlation study have been devoted to this section on "Devices" to present a comprehensive summary, yet avoid redundancy. One could literally list thousands of devices as revealed in patents scrutiny, trade and scientific journals, and communication with experienced personnel; however, the redundancy becomes cumbersome. The devices have therefore been grouped into a spectral distribution in an attempt to emphasize those physical properties of ferroelectrics that most influence their choice in devices. Certain classical devices have undergone repeated development as new ferroelectric bodies have been developed. These will be discussed in detail as "models" to better present the spectral grouping concept.

E. Spectral Grouping

This presentation of devices emphasizes the piezoelectric properties of the ferroelectric bodies and, if one considers the area of application relative to the acoustic spectrum, it is seen that certain properties are more important than others. This is further amplified with the increasing use of solid-state circuitry as associated with piezoelectric devices. Solid-state accessories to devices such as amplifiers, detectors, etc. require for the most part a low impedance source. The large dielectric constant and high piezoelectric coupling of the ferroelectrics meet this low electrical impedance requirement. Greater sophistication in the design of transducers for a given application produces still lower impedance devices. This trend toward lower impedance transducers has been accompanied by higher driving powers to the ferroelectric bodies. Since all ferroelectric polycrystalline ceramics are subject to somewhat larger dielectric losses which occur under high electric drive than were their single-crystal predecessors, greater consideration must be given to the piezoelectric coupling and mechanically matching the transducer to the load (B13) thus causing

a greater percentage of the input power to be radiated to the loading medium.

In examining the requirements of a particular device for operation within a certain portion of the frequency spectrum and the manner in which certain electrical and physical properties of the transducer material are effective, the various spectral segments will be considered (see Talbe XVII).

DC to 30 CPS: Applications within this portion of the spectrum are predominantly low level, i.e., low amplitude detection of forces acting on various structures or components. The device most commonly used is a strain gauge or accelerometer. In this application, the device is required to present the electrical analogue of the mechanical forces acting on the body. Nearly all transducers designed to do this are inertial driven by the source, and the transducer is a composite mass and spring configuration wherein the ferroelectric material functions as the spring and an added or distributed mass is the accelerated portion of the transducer. This application requires a high capacitance dielectric for low electrical impedance at low frequencies and an electromechanical coupling that is constant over a wide range of temperatures. Dielectric losses and large coupling factors are among the lesser requirements of piezoelectric devices in this portion of the spectrum.

30 to 20,000 CPS: This portion of the spectrum contains the greatest number of devices ranging from low level sensors to high level acoustic transmitters and processing devices. The largest number of devices in this region are microphones, which are low level sensors used in the detection of airborne sounds. These are usually in the form of a diaphragm-actuated sensor in which a thin disc-like film material is displaced by the impinging sound pressure. The displacement is coupled to a thin wafer of ferroelectric, appropriately polarized and supported within a holder. The coupling is usually made by cementing a low-mass rod to the center of the diaphragm and to the sensor element. The sensor is usually operated in a bending

TABLE XVII

Spectral Breakdown of Classical Devices and Related Significant Properties

	Frequency Bands		
DC to 30 cps	30 to 20,000 cps	20 to 1000 kc/s	1000 to 40,000 kc/s
DEVICES			
Accelerometers	Accelerometers	Microphones	Ultrasonic Quality
Strain Gauges	Microphones	Hydrophones	Solid Delay Lines
	Hydrophones	Sonic Processes	Filter(band-pass)
	Sonar Projectors	Sonar	
	Data Process and Storage Devices	Filters(band-pass	
	Filters(band-pass)	Data Process and Storage Devices	
		Ultrasonic Quality	
PROPERTIES*			
Dielectric Constant	Dielectric Cons.	Dielectric Cons.	Dielectric Cons.
Constant Mechanical Coupling with Temperature	Dielectric Loss	Piezo. Coupling	Piezo. Coupling
	Mechanical Loss	Thermal Stability	Thermal Stability
	Piezo. Coupling	Dielectric Loss	Density (Porosity, Impurities, Inclusions)
		Mechanical Loss	Aging

* Significant properties affecting performance and choice of materials

mode and is a composite body of two polarized wafers bonded back-to-back forming what is commonly referred to as a Bimorph. It is interesting to note that at the time polarized ferroelectric elements initially replaced the single crystal elements of Rochelle salts, ADP, etc., full advantage of the higher dielectric material was not taken. Thus, earlier single crystal elements were very high impedance devices (vulnerable to humidity) having a circuit capacitance of only a few picofarads, and ferroelectric bodies were designed to present the same electrical impedance to a circuit. Recently, however, engineers have been utilizing the higher dielectric material and obtaining elements having capacitances ranging up to 50,000 picofarads. Although diaphragm-actuated devices are stiffness controlled in their dynamic response, the increased capacitance of the element has extended the sensitivity to very low frequencies, while the increasing sensitivity of the compliant diaphragm at higher frequencies tends to cancel the high shunt capacitance of the ferroelectric. This practice results in a microphone having an extended bandwidth and utility over a wider range of temperatures and humidity than practical with the popular single crystal elements.

Other low-level acoustic receiving devices used widely in this portion of the spectrum are accelerometers, strain gauges, biological sensors, hydrophones, data-processing and storage devices such as memory elements and dielectric tape-recording components. These devices, as in the case of microphones, are not subjected to high ac driving fields.

F. Memory Devices

Ferroelectric crystals have been investigated for use in memory matrixes of the voltage-coincident type analogous to the current-coincident magnetic matrixes (K14). Barium titanate displays the characteristic square dynamic hysteresis loop required of storage devices, although applied voltages less than the coercive voltage tend to depolarize the crystal. It has

been reported (P11) that one particular memory matrix investigated showed a reduction of remanent charge of 50 per cent after approximately one thousand half-voltage pulses were introduced.

The operation of these materials as memory devices may be seen in Figure 26. If the memory element is at the remanent polarization state indicated as point "a" in Figure 26a and the coincident "write" voltage (c) is applied as in Figure 26b, the state of the polarization is changed to that of position "b" as shown on the hysteresis loop. Although there has been a net change of polarization of 2 p_r, no voltage appears across the load resistor R because of the diode D. If now, however, the "read" voltages shown in (d) are applied to the input, the polarization state is returned to "a" and a voltage appears across R showing that a "one" has been stored. If the state of polarization was at "a" corresponding to a "zero" state and the read voltage was applied, very little voltage would appear across R.

The loss of remanent polarization from continued interrogation of the matrix as mentioned above shows several disadvantages in the use of barium titanate in memory devices. Improvements in thin-film technology as related to single-crystal formation in barium titanate will advance the state of the art in memory devices in the near future. Meanwhile, this undesirable behavior appears to have been eliminated by the application of a new ferroelectric material called triglycine sulfate.

The middle portion of this band and a part extending upwards in frequency into the next band are regions of high power transducers. These transducers are primarily used in sonar and industrial processing applications where high electric drive is common. Piezoelectric coupling and dielectric loss in the transducer material are of major concern. Dielectric losses produce heat energy and subsequently reduce acoustic efficiency (B13)(B11). Until recently, transducers for high power industrial processes and sonar employed large masses of

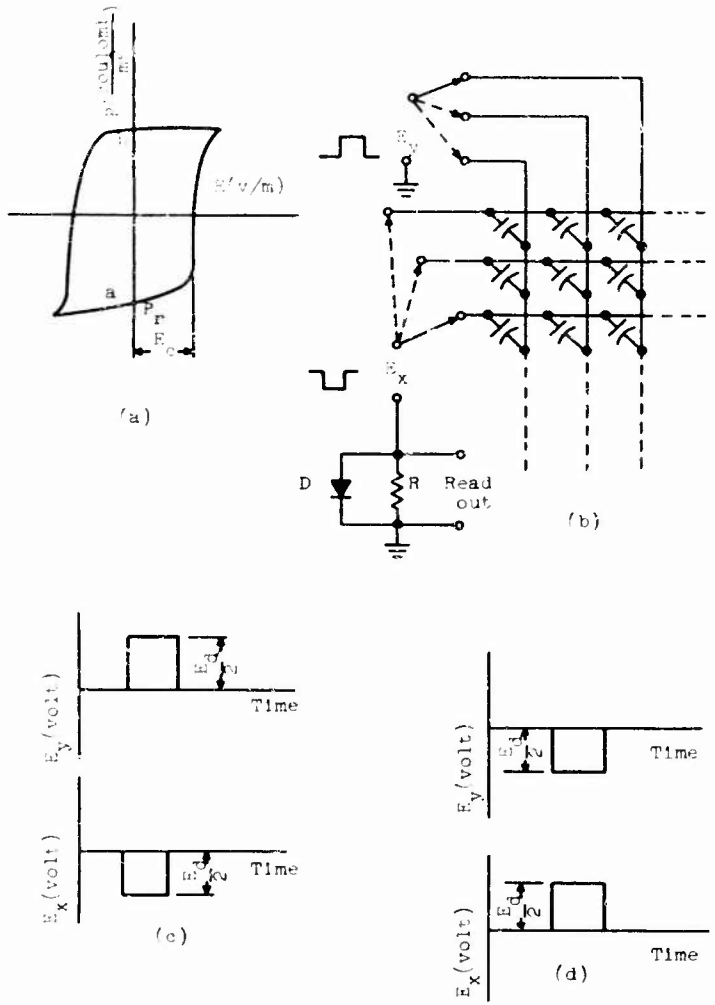

Fig. 26 Ferroelectric Memory Matrix
(a) Hysteresis loop (b) Memory matrix
(c) Write "one" voltages (d) Read voltages

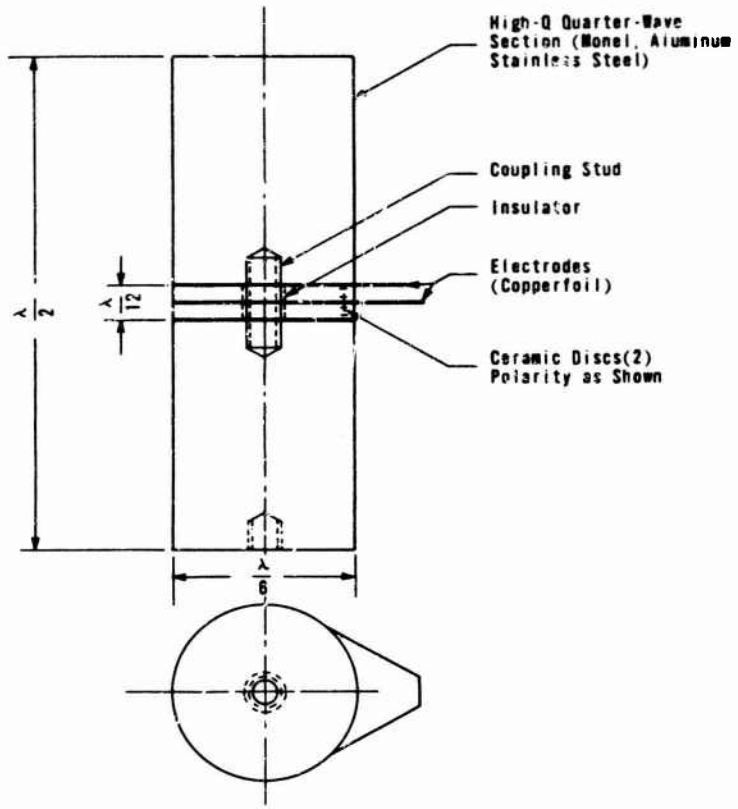

Fig. 27 High-Intensity, Heat Conducting Resonant Transducer

ferroelectric materials having dimensions characteristic of the resonant frequency requirements. Heat energy under high driving fields could not be dissipated sufficiently to prevent temperature rise in the ceramic which caused a degradation and frequently a complete loss of polarization.

This serious limitation of ferroelectric ceramics has largely been overcome by development of the lead-zirconate-titanate group of ferroelectrics together with improved design technology. The latter has resulted in increased heat conductivity to the load (usually water) with a substantial reduction in the operating temperature of the transducer. The basic concept of this design philosophy is shown in Figure 27, and it is adaptable to a wide variety of transducer designs and work loads.

The concept of Figure 27 shows a small sandwich of two discs of ferroelectric ceramic polarized as shown and located at the tension region or nodal region of the composite half wavelength assembly. Quarter-wave sections of high-Q material such as aluminum, Monel*, etc. are bonded and preloaded to each side of the disc by a clamp or bolt as shown. The bolt is also of low-loss material and a clamping pressure equal to or somewhat greater than the maximum tension developed under electrical drive is applied. This assembly is then attached to a coupling section (also resonant) and hence to the load. The bulk of the transducer consists of a high-Q material capable of rapid heat transfer from the ceramic discs to the load or to a suitable heat exchanger. Although amplitudes are small at the disc, they are amplified tremendously in the high-Q sections of the assembly. The basic concept shown in Figure 27 attains amplitudes suitable for ultrasonic machining and similar large amplitude applications. Variations of the concept are applied to sonar transducers, flexural bodies such as microphone elements, and tensional elements such as accelerometers and strain gauges.

---

* Registered Trade Mark of International Nickel Company, Inc.

20 kc/s to 1000 kc/s: This portion of the frequency spectrum is also occupied by a wide variety of transducers. The lower portion of the spectrum is primarily used for microphones, hydrophones, and processing transducers while the upper portion shows a predominance of high-frequency devices such as are used in data processing (Y1), ultrasonic pulse-echo and resonant transducers of the type employed in flaw detection or ultrasonic quality measurements in materials. Some transducers of a type similar to those used in ultrasonic cleaning are used in highly specialized applications in chemical processes. Devices in this portion of the spectrum may be further divided into two categories: (1) low level, and (2) high level.

Low level devices include those transducers which occupy a somewhat passive position in the system and are not subjected to high driving fields, large mechanical stresses, or excessive temperatures. These devices include microphones, hydrophones, pulse-echo transducers, band-pass filters, accelerometers, and other vibration sensors.

High level devices include those transducers used in processing materials such as ultrasonic cleaning, chemical processing, and high power sonar projectors. Greater emphasis is placed on the dielectric and loss properties of the ferroelectric ceramic used in high level capacities. Operation of devices in the higher frequency portion of the spectrum together with generally lowered radiation efficiency requires ferroelectric bodies having superior dielectric and mechanical loss properties.

It may be generally considered that devices used in this portion of the spectrum are "precision" devices, both in design and fabrication as well as in the quality of the ferroelectric material used. Operation at the higher frequencies may require a careful selection of material with many compromises being made between the dielectric properties and the manufacturing processes used in the fabrication of the ceramic body. Surface finish, porosity, electrode configuration and bond strength, density, and the ability to reproduce uniform polarization (M20) from body to body may require the selection of a ceramic which has higher dielectric loss and causes more voltage breakdown.

The design engineer is equally concerned with properties of a quality nature which unfortunately are highly variable and dependent on the technological abilities of ferroelectric manufacturers. These qualities are porosity, dimensional tolerance and stability, equivalent water absorption, electrode bond strength, impurities, and many other characteristics which are predominantly technological.

1000 kc/s to 40,000 kc/s. This region of the frequency spectrum is dominated by devices utilizing the piezoelectric property of ferroelectric ceramics. The lower portion of this segment of the spectrum shows a concentration of transducers operating in a resonant or pulsed mode for ultrasonic quality investigation (A3); that is, high frequency pulsed or continuous ultrasonic energy is transmitted into solid materials (M17) for the purpose of determining the presence of flaws or the response of the material to dynamic stress. Certain physical properties of the material being investigated may also be determined by the propagation of high frequency ultrasound within the body. The most common mode of operation of ferroelectric elements used in these applications utilizes the k_{33} coupling constant; that is, the most convenient form of wave motion for ultrasonic inspection is the compressional mode. Shear waves and Rayleigh or Lamb waves (G8) are used to a lesser degree. Certain materials having laminar or surface characteristics of concern may be more readily examined by shear waves for bulk effects or Rayleigh waves for skin effects.

Delay Lines represent devices which greatly outnumber all other devices utilizing the piezoelectric properties of ferroelectrics in this portion of the spectrum. The extremely rigid tolerances and specifications of these devices make delay lines excellent models for discussion of the majority of electrical and mechanical properties of piezoelectric ceramics.

Delay lines as considered in this discussion are devices in which data are transmitted into a medium where propagation at the velocity of sound occurs. The data are recovered at a later instant of time for processing. The data may be processed with the objectives of distance measurement by radar or sonar or may be used in computer-logic processes to mention

but a few possibilities. Basically, a transducer (M16)(M14) bonded to a portion of suitable delay or propagation medium is driven by an impulse of electrical energy. The resulting acoustic energy is propagated through the medium along a well-defined path and is recovered at the termination of the path length by a second transducer. The time delay is thus a function of the path length and propagation velocity through the medium. It is obvious that a large variety of delay lines may be fabricated from an equally wide variety of materials depending on the end use of the line. For the purpose of this report, that type of line will be considered which is used in conjunction with radar applications wherein the greatest emphasis is placed on extreme precision regarding time delay, thermal environment, electrical and physical performances. These lines employ a transmission medium of fused silica or fused quartz and utilize transducers operating in the transverse mode for the propagation of shear waves through the medium. Shear waves propagate at a lower velocity than compressional waves and suffer no reflection loss at a solid-air interface such as a reflecting facet. Polygon patterns are used to obtain large path lengths and thus long delays. The delay medium is ground in a thin plate-like disc with the propagation path parallel to the plane of the disc. The plane-polarized transverse particle motion is perpendicular to the plane of the disc and the beam width is extremely narrow. The shear waves are reflected without loss at a prescribed facet directing the energy back through the medium to a second facet and so on. This multiple reflection is continued to a receiving transducer which detects the delayed signal.

Typical specifications for a delay line of this type would be:

Transducer frequency	20 mc/s
Transducer bandwidth	60%
Time delay	5000 microseconds
Spurious response	greater than 40 db down
Electrical impedance	50 ohms
Losses (insertion + transmission)	less than 20 db

Other specifications are usually included regarding thermal cycling, thermal coefficients of time delay, vibration cycling, etc., but the advantages of ferroelectric transducer materials may be pointed out by examination of the above listed specifications. The time delay of 5000 microseconds obviously requires a highly pure medium free of stria and having an extremely low absorption of 20 mc/s ultrasonic energy. Such a requirement is met by a transmission medium of fused silica or fused quartz. Spurious responses are caused in part by the transducer, but largely are due to phenomena within the medium such as beam spread and scatter from inhomogeneities and vertical bending due to strain stria or improperly oriented facets. The third-time signal arises by reflection of a percentage of the main signal from the receiving transducer which propagates back through the medium to the input transducer and then undergoes a reversal to return to the receiving transducer with a time delay equal to thrice the main delay. The amplitude of this third-time signal may be attenuated by local absorption coatings and by introducing a controlled amount of absorption during propagation. Additional spurious responses due to side lobes originating at the transducer may be reduced to specifications by transducer area control, reshaping the beam at the reflecting facets by application of absorbers at specific regions, and by careful control of transducer bonding procedures.

The electrical specifications, however, are of particular interest. Until recent years, Y-cut quartz piezoelectric material was used exclusively for the transducers. Although quartz is nearly matched in acoustic impedance to the fused silica medium, the very high electrical impedance (approximately 30,000 ohms) of the transducer resulted in excessive insertion loss when terminated in 50 ohms. The large bandwidth required heavy backing blocks on the transducer together with resistance shunting which resulted in still greater insertion loss. Quartz has certain advantages over most ferroelectric ceramics in its high transition temperature (573°C), zero aging effect, high

voltage breakdown strength, and freedom from pinholes. A direct comparison between a quartz delay line transducer and one fabricated from barium titanate may be seen in the following table:

Characteristic	AC-Cut Quartz	$BaTiO_3$
Load Impedance Radiation	50 ohms	50 ohms
Resistance (electrical)	35,000 ohms	7.5 ohms
Mismatch Loss	54 decibels	4 decibels

The improvement in mismatch loss with the $BaTiO_3$ provides tremendous engineering freedom to overcome the few limitations caused by the application of ferroelectric ceramics to delay line transducers.

The high dielectric constant of the ferroelectric ceramic contributes to low impedance terminations and reduced mismatch losses. At the higher frequencies, however, it presents some difficulty in that impedances become too low and difficult to match with inductors normally used in tuning out the capacitive reactance. This difficulty is reduced by use of a ceramic of the lead zirconate-lead titanate group. The very high electromechanical coupling factor produces a "true" dielectric constant which lies between the free (ϵ^T) dielectric constant and the clamped (ϵ^S) dielectric constant. This is expressed by:

$$\epsilon^S = \epsilon^T (1 - k^2) \tag{5}$$

where k = electromechanical coupling factor. The magnitude of this reduced dielectric constant is seen in the example for lead-zirconate-titanate having the following characteristics:

$$\epsilon^T = 500, \; k = 0.69$$

$$\epsilon^S = 500 \; (1 - (0.69)^2) \approx 262$$

Thus, as the transducer material is loaded with higher acoustic impedance materials and the coupling coefficients approach

unity, the shunt capacitance will become smaller and more practical. These circuit considerations prevail throughout design tasks of high frequency transducers.

Transducers operating in the several megacycles region of the spectrum usually are not subjected to extreme electrical driving powers. Furthermore, transducers of the type illustrated by delay lines exhibit large bandwidths (up to 100%) and frequency drift due to degradation effects is largely insignificant.

The greatest obstacle to high frequency transducers is porosity. In the region of 40 megacycles where the grain size approaches a wavelength in dimension, pin holes become detrimental and electrode diffusion occurs during bonding operations. The resulting holes cause short circuits making the device useless, and costly rework or complete replacement of the transducers is necessary. Filling of the pinholes with a silica compound is sometimes employed where cold bonding techniques are permissible.

Delay line and similar transducers are ground and polished to optical flatness and surface finish. Although polarization in the thickness shear mode may be performed by a fringing technique in the plane of the wafer, the resulting polarization is frequently not uniform and highly variable. At the present state of the art it is more satisfactory to cut the wafers from previously polarized bulk materials. Careful grinding and lapping procedures produce excellent optical-finish wafers with uniform polarization and reproducible coupling factors. Unfortunately, at frequencies above approximately 40 megacycles wafers become exceedingly thin and difficult to fabricate.

Figure 28 is a summarization of the regions of practical applications of ceramic and quartz transducers for ultrasonic delay lines and similar high frequency devices. This type of plot may be created for other regions of the spectrum and serves a very useful purpose in quickly presenting those areas of operation best served by specific transducer materials.

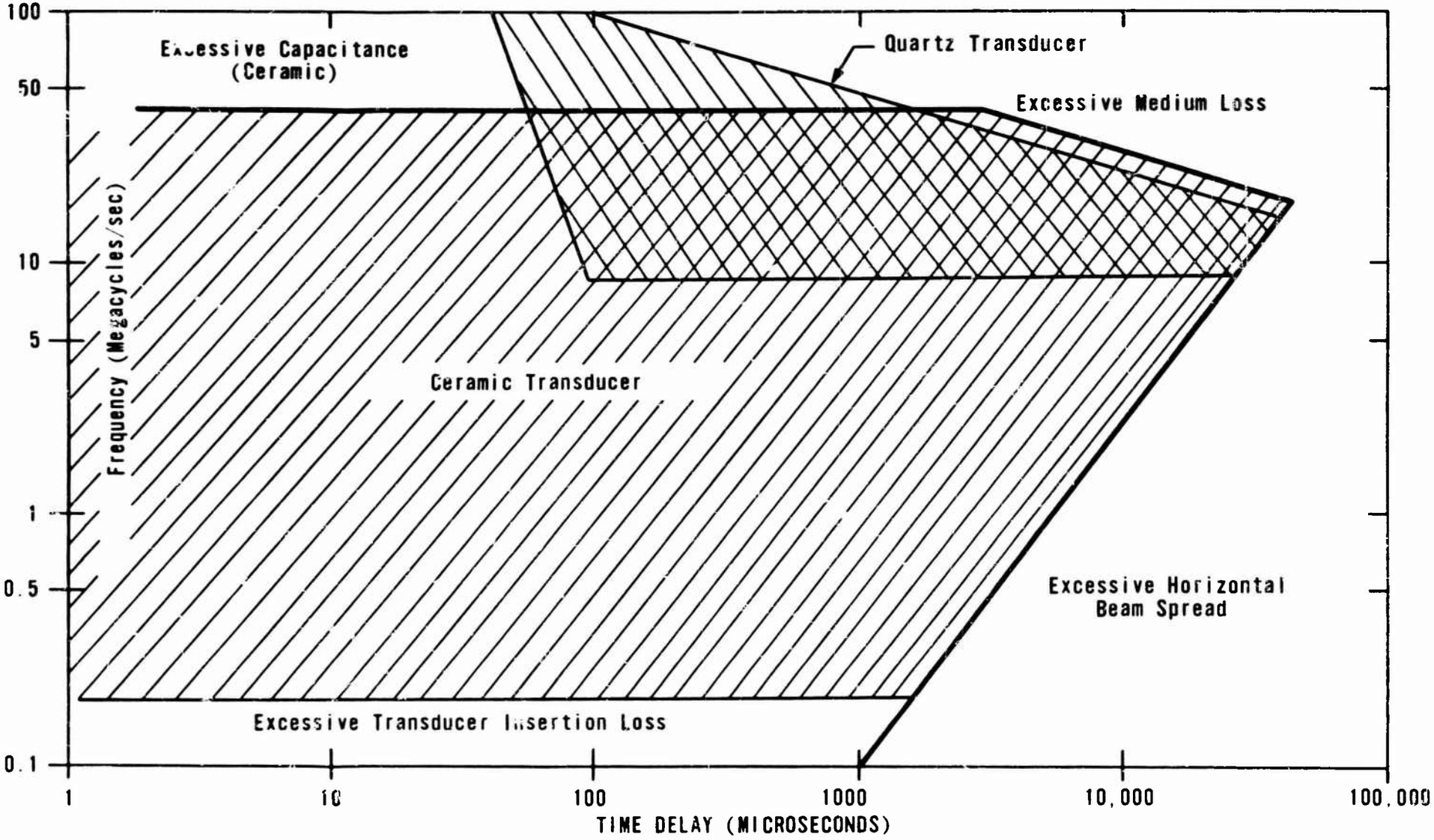

Fig. 2 Regions of Practical Applications of Ceramic and Quartz Transducers for Ultrasonic Solid Delay Lines

At the present, 40 megacycles represent an upper limit to ferroelectric transducers operating in the shear and compressional modes of vibration. This limit is largely due to high leakage currents, pinholes, and difficulty in finishing operations. A 40-megacycle wafer operating in the thickness mode at half-wave resonance is approximately 1 mil thick. Successful and reproducible thin-film type transducers from ferroelectric materials are as yet unavailable. Limited efforts have been made in this respect, but recent developments (F9)(W5)(P7) of piezoelectric semiconductor transducers apparently have caused a restraint on activity toward the development of ferroelectric thin-film transducers.

Included in the portion of the spectrum largely occupied by delay lines is another device that demands attention and in many respects is an outgrowth of delay-line technology. This device is the Photoelastic Delay Line (C5), although its applications may be more diverse than in delay line use. Light modulation by ultrasonic waves was initially discovered by Debye and Sears in 1932 and has later been extended to include ultrasonic transmission in solid media. Although the photoelastic effect in solid media was described by Arenberg (A2) in 1948, the usefulness was tightly limited by lack of electromechanically efficient transducers. This limitation has been largely overcome through the development of ferroelectric transducer materials and improved transducer design.

In the case of ultrasonic waves passing through a liquid, the waves cause periodic changes of the refractive index of the medium and thus of the phase of the light waves traversing it resulting in the formation of diffraction spectra (R6). By separation of the diffracted from the undiffracted light the light output of the device can be made to be proportional to the signal voltage over a wide linear range. Similarly, in the case of high-amplitude ultrasonic waves transmitting in a transparent medium, the instantaneous birefringence produced by the passing wave may be observed at a selected point by polarimetric means. If one arranges two polarizing screens, one on

either side of a transparent medium with their axes mutually perpendicular, essentially no light will be passed. If now, however, a pulse of high amplitude ultrasound is transmitted through the transparent birefringent plate, the phase of one vector component will be delayed with respect to the other and transmission of light occurs. It is obvious that a continuously variable delay line may result merely by displacing the light components along the ultrasonic transmission path. Two such photoelastic delay lines working in tandem have been used to display auto- and cross-correlation functions. Such devices are relatively new to the computer fields, but they have been gaining interest recently in data-processing operations.

G. Model Devices

It is unlikely that any single class of dielectric materials has contributed a greater diversity to the design and application of devices, both active and passive, than ferroelectric ceramics. As vibration transducer materials, they may be found in devices ranging in size from the smallest heart probe sensor to ultrasonic processing systems radiating hundreds of kilowatts of power into cavitating fluids.

It is pointed out that certain regions of the frequency spectrum emphasize certain physical and electrical properties more than others. If one observes this philosophy in the choice and design of devices using piezoelectric ceramics, it is possible to obtain a higher level of performance in ceramic transducers than in many single-crystal type materials. In general, piezoelectric ceramics provide a selection of properties that permits tremendous engineering freedom in the design and fabrication of transducers for most acoustics and sonics applications.

Model devices or transducers are described in the preceding sections of the report to illustrate the more common design features as encountered in the applications of piezoelectric materials. These devices are presented in Figures 27

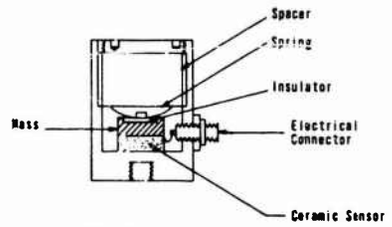

(a) Accelerometer

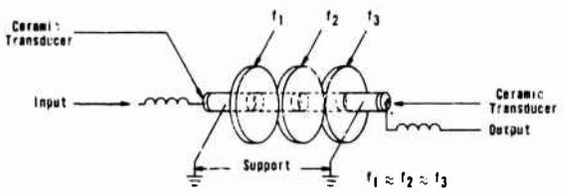

(d) Radial Band-Pass Filter

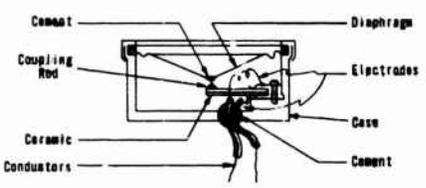

(b) Microphone

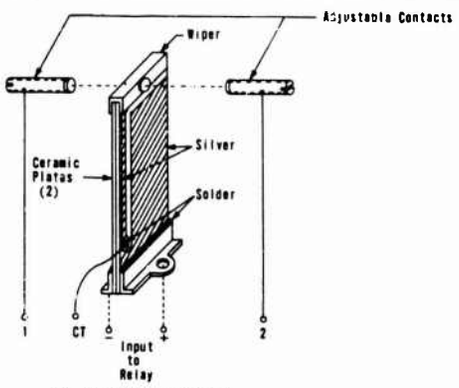

(e) Ceramic Element Relay

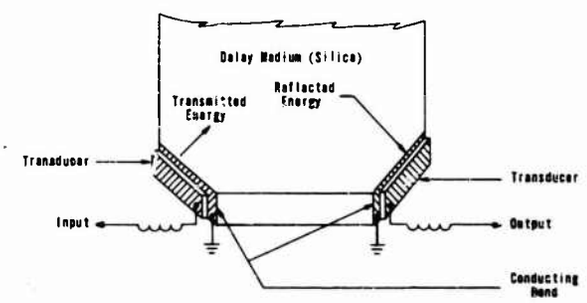

(c) Delay Line

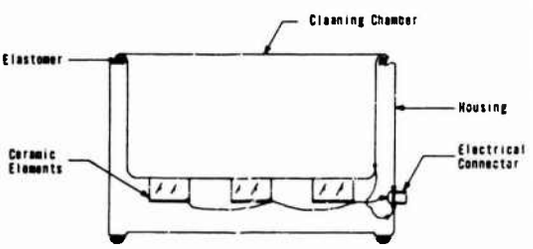

(f) Ultrasonic Cleaner Transducer

FIG FERROELECTRIC DEVICES

and 29a through 29f. Figure 27 represents the use of a design feature wherein high intensity sound is generated by the transducer and, hence, the ceramic is subjected to high ac fields and severe mechanical stress. The destructive effects of this field and mechanical stress are reduced by employing a composite structure which permits rapid heat dissipation from the ceramic. Preloading the composite structure prevents fracture of the ceramic under large mechanical stress. A typical application of this design is also shown in Figure 29f.

Figure 29a is a representative design of an accelerometer, a device normally employed for the detection of forces of low frequency content. Mid-range frequencies are illustrated by the design of Figure 29b, a conventional microphone for audio frequency use. Figure 29c shows a portion of a solid ultrasonic delay line, one of the most precise and costly devices in use today. It is in the fabrication of these devices that piezoelectric ceramics have made large strides, yet considerably more development of improved materials is necessary before complete advantage can be taken of ceramics.

Figure 29d represents an early design of a mechanical bandpass filter, a device providing high selectivity in intermediate frequency amplifiers in communications receivers. The inherent mechanical and dielectric losses of these high electromechanically-efficient materials prevent wide use of filters made entirely from the ceramic; however, ceramic transducers attached to filter elements made from low loss metals yield excellent performance but at greater cost.

Recently, several researchers (C9) have developed mechanical bandpass filters utilizing ferroelectric ceramic bodies in configurations and materials that result in stable well-controlled bandwidths. Piezoelectric ceramics offer resonators and filters that provide small and compact intermediate frequency transformers. The steep selectivity skirts realized by these devices greatly enhance the performance of communications receivers and, in addition to reducing adjacent channel interference, they have permitted an increase in the number

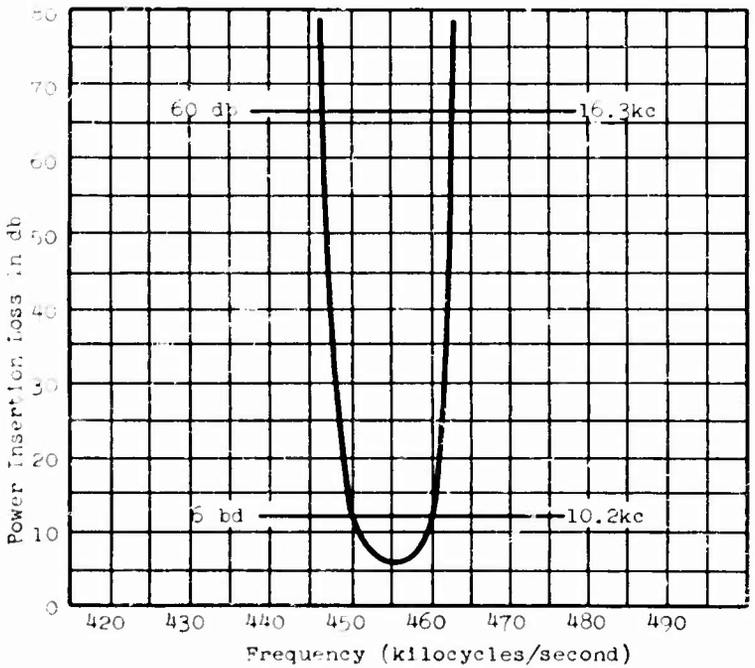

Fig. 30 Frequency Response of Ceramic Ladder Filter

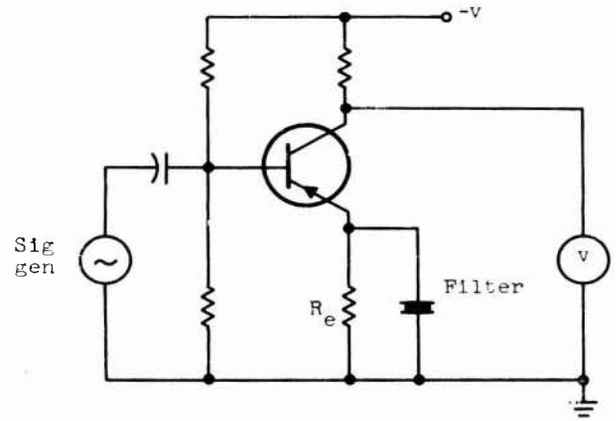

(a) Filter unit used as feedback element

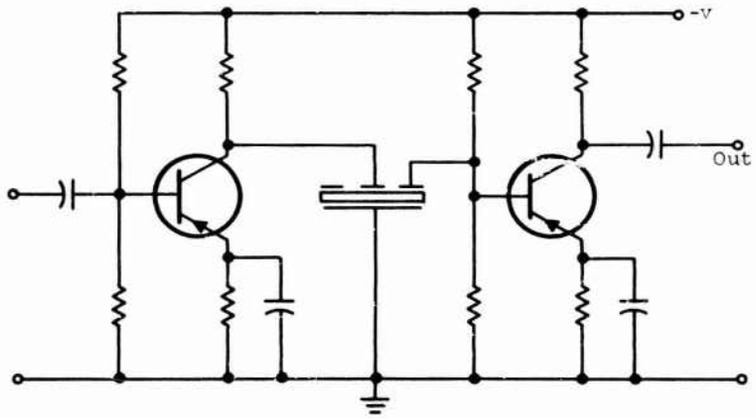

(b) Ceramic filter unit in amplifier

Fig. 31 Ceramic Filter Applications

of channels occupying a given segment of the frequency spectrum.

These filters may utilize one or more of the vibration modes of a ceramic body. These modes include the flexural and folded flexural mode, the length expander mode, radial mode, thickness shear mode and the thickness expander mode. It is not convenient to use more than a single mode in a multi-section filter such as a lattice or ladder filter; however, the terminating sections may use a different mode of vibration for electrical impedance and insertion loss considerations. Low frequency filters or transformers usually use the flexural mode in either the disc or bar configuration. These are convenient geometries in that they may be easily tuned over the frequency range and the frequency skirts altered by electrode positioning. Higher frequency filters; i.e., from approximately 100 kilocycles up to 10 megacycles, utilize the thickness shear and expander modes. The latter modes permit a single disc or wafer to be used in obtaining a multi-section filter. The equivalent stagger tuning obtained on a single wafer by multiple electrodes and series connection yieldsthe steep frequency skirts and flat pass band desired in voice communications.

The steep skirts of the selectivity curve of a typical ceramic ladder filter are shown in Figure 30. Two representative circuit applications are shown in Figure 31. In Figure 31a, the filter element is used to control the negative feedback of an amplifier. When connected as in (a), the emitter resistor provides the negative feedback element and maintains the gain of the stage at a low value. As the frequency of the signal generator is tuned to that of the filter unit, the impedance of the filter being very low at its resonant frequency effectively reduces the emitter resistance and increases manifoldly the gain of the stage resulting in its being very high at the resonant frequency to which the filter is tuned. The ladder filters producing the characteristic as shown in Figure 30 are very small, being no larger than 3/8"x1-1/2", and represent a great reduction in space for the performance gained.

Figure 29e is a somewhat novel device in that the simple armature of a relay is fabricated from a Bimorph element. This design provides a rapid switching contact that is also suitable for resonant reed applications in relay design.

Conclusions. The efficient operation and reproducibility of devices employing piezoelectric ceramics are most dependent on the following factors: (1) loss properties of the material used as the sensor; (2) a particular device to be operated within a certain region of the frequency spectrum must present a certain electrical impedance to the circuit which terminates it; (3) a specific electromechanical insertion loss should not be exceeded; and (4) a desired stress sensitivity is usually specified.

These four factors are determined by the choice of ceramic material, the application to which the device is assigned and the required electrical and mechanical properties to be displayed by the device. High impedance electrical and mechanical loads more frequently use an extensional mode in the material whereas low impedance loads more frequently use a soft (or flexural) mode. The latter mode requires a low electrical impedance where a high dielectric constant is preferred. The normal and transverse piezoelectric coupling factors, generally, should be high and essentially equal. The mechanical compliance should be high to present a low mechanical impedance to the driving force, and if low frequency (up to a few hundred cps) operation is imposed, the dielectric and leakage losses must be low. The latter consideration is most important where thin film materials are used, in perhaps, a laminated structure. Porosity and moisture absorption seriously impair low frequency sensitivity by the electrical shunting effect. Sealing the moisture out by surface doping may effect mechanical compliance, bandwidth, and sensitivity in addition to reducing reproducibility in the performance requirements. The latter usually has negligible effect on the performance of wide band high frequency devices where larger cross sections of material eliminate "through" voids or pores.

Although porosity may be predicted by an equivalent "water absorption" coefficient or by the "percentage of theoretical density" of the ceramic material, this quality is widely variant due to various manufacturers' processes.

The piezoelectric and mechanical properties tabulated in this report serve to provide the design engineer with essentially all the information necessary to effect a design. It is obvious that a required design objective may be met by several ceramic compositions, nevertheless the piezoelectric data presented in this report provide the design engineer with information necessary to specify and select a material to meet the requirements of even the most rigid and exacting device.

VII. BIBLIOGRAPHY

A1 Aurivillius, B. and Fang, P. H., "Ferroelectricity in the Compound $Ba_2Bi_4Ti_5O_{18}$", Phys. Rev. 126 (3) 893-896 (May 1962)

A2 Arenberg, D. L., "Ultrasonic Solid Delay Lines", J. Acoust. Soc. America, 20 (1) (Jan. 1948)

A3 ASTM Special Technical Publication No. 101, Symposium on Ultrasonic Testing, (various authors) (Jan. 1951)

A4 Anderson, R. C. and Friedberg, A. L., "Crystallization of Lead Metaniobate from a Glass", Proceedings of Symposium on Nucleation and Crystallization in Glasses and Melts, Reser, M. K., Smith, G. and Insley, H., Eds., American Ceramic Society, Columbus 14, Ohio (1962) pp. 22-34

A5 Anderson, C. E., Liedl, G. L. and Hruska, S. J., "Reactive Sputtering of Ba-Ti in Oxygen", Progress Report on Materials Science Research, Purdue University (Oct. 1964 - Sept. 1965)

A6 Allsop, H. L. and Gibbs, D. F., "The Electromechanical Properties of Barium Titanate", Phil. Mag. 4 359-370 (1959)

B1 Bradstreet, S. and Harada, Y., "Synthesis of Refractory Mixed Oxide with Perovskite Structure", U.S. Dept. Com., Office Tech. Serv., AD433653 (1960) 14 pp.

B2 Burger, R. M. and Donovan, R. P., "A Broader Choice of Components for Silicon Integrated Circuits", Electronics 38 (9) 48 (1965)

B3 Bratschun, W. R. and Cook, R. L., "Dielectric Properties of Solid Solutions of Sodium Niobate-Lead Zirconate and Sodium Niobate-Lead Titanate", J. Amer. Ceram. Soc. 44 (3) 136-140 (Mar. 1961)

B4 Balygin, I. E. and Porovskii, K. S., "Aging of Ceramic Insulation at High Temperatures" (English trans.), Sov. Phys.-Technical Physics 1 (8) 1663-1669 (1956)

B5 Barrett, H. H., Nutter, P. B., Paladino, A. and Waugh, J. S., "Failure Mechanisms in Ferroelectric and Non-linear Dielectrics", Final Technical Report No. S-543, Contract No. AF 30(602)-2678, Raytheon Company, AD605795 (1 May 1963)

B6 Baxter, P. and Hellicar, N. J., "Electrical Properties of Lead-Barium Niobates and Associated Materials", J. Amer. Ceram. Soc. 43 (11) 578-583 (Nov. 1960)

B7 Baxter, P., Hellicar, N. J. and Lewis, B., "Effect of Additives of Limited Solid Solubility on Ferroelectric Properties of Barium Titanate Ceramics", J. Amer. Ceram. Soc. 42 (10) 465-470 (Oct. 1959)

B8 Bechmann, R., "Elastic, Piezoelectric and Dielectric Constants of Polarized Barium Titanate and Some Applications of the Piezoelectric Equations", J. Acoust. Soc. Amer. 28 (3) 347-350 (May 1956)

B9 Berlincourt, D. A., Curran, D. R. and Jaffe, H., "Piezoelectric and Piezomagnetic Materials", Physical Acoustics Vol. 1 Part A (W. P. Mason, Ed.), Academic Press, New York (1964) pp. 198-269

B10 Berlincourt, D. A., "Failure Mechanisms in Ceramic Dielectrics", Final Report, Contract No. AF 30(602)-2594, Clevite Corp., AD 414353 (30 April 1963)

B11 Berlincourt, D. A., "Power Capacities of Piezoelectric Ceramics in Sonar-Type Acoustic Transducers", Engr. Memo 61-19, Clevite Corp., Cleveland, Ohio, (31 July 1961)

B12 Berlincourt, D. A., and Brunarski, F. T., "Polarization of Titanate Ceramics", U.S. Patent 2,928,163 (Mar. 15, 1960)

B13 Berlincourt, D. A., Jaffe, B., Jaffe, H. and Krueger, H. H. A., "Transducer Properties of Lead Titanate Zirconate Ceramics", IRE Trans. on Ultrasonics Engr. UE-7 (1) 1-6 (Feb. 1960)

B14 Berlincourt, D. A., Cmolik, C. and Jaffe, H., "Piezoelectric Properties of Polycrystalline Lead Titanate Zirconate Compositions", Proc. IRE 48 (2) 220-229 (Feb. 1960)

B15 Berlincourt, D. A. and Krueger, H. H. A., "Domain Processes in Lead Titanate Zirconate and Barium Titanate Ceramics", J. Appl. Phys. 30 (11) 1804-1810 (Nov. 1959)

B16 Berlincourt, D. A., Sandia Corp. Order No. WC 727 (March 1956)

B17 Berlincourt, D. A., "Aging in Barium Titanate Ceramics", Technical Rep. No. 4, ONR Contract No. Nonr-1055(00), Clevite, (March 30, 1955) 19 pp.

B18 Berlincourt, D. A. and Kulcsar, F., "Electromechanical Properties of $BaTiO_3$ Compositions Showing Substantial Shifts in Phase Transition Points", J. Acoust. Soc. Amer. 24 (6) 709-713 (Nov. 1952)

B19 Blood, H. L., Levine, S. and Roberts, N. H., "Anomalous Polarization in Undiluted $BaTiO_3$", J. Appl. Phys. 27 (6) 660-661 (1956)

B20 Bogoroditski, N. P. and Verbitskaja, G. N., "Behavior of Seignetto-ceramics Near the Curie Point", Doklady Akad. Nauk. SSSR 89 447-449 (1953)

B21 Bogoroditski, N. P. and Verbitskaja, G. N., "Electric Properties of Seignetto-ceramics Near the Curie Point", J. Tech. Phys. (USSR) 22 1920-1929 (1952)

B22 Bohun, A., "Thermoemission und Thermoluminezenz bei Flusspat" (in German), Czech. J. Phys. 5 224 (1955)

B23 Branwood, A., Hughes, O. H., Hurd, J. D. and Tredgold, R. H., "Evidence for Space Charge Conduction in Barium Titanate Single Crystals", Proc. Phys. Soc. (London) 79 1161-1165 (1962)

B24 Branwood, A. and Tredgold, R. H., "The Electrical Conductivity of Barium Titanate Single Crystals", Proc. Phys. Soc. (London) 76 93-98 (July 1960)

B25 Bratschun, W. R., "Barium Zirconate-Lead Titanate Ferroelectric Ceramics", J. Amer. Ceram. Soc. 46 (3) 141-144 (Mar. 1963)

B26 Brown, C. S., Kell, R. C., Taylor, R. and Thomas, L. A., "Piezoelectric Materials, A Review of Progress", Proc. Brit. IEE 109B 99-114 (Jan. 1962)

B27 Brown, R. F., "Effect of Two-Dimensional Mechanical Stress on the Dielectric Properties of Poled Ceramic Barium Titanate and Lead Zirconate Titanate", Canad. J. Phys. 39 (5) 741-753 (May 1961)

B28 Buessem, W. R. and Marshall, P. A., Jr., "Crystal Chemistry of Ceramic Dielectrics" (Summary Degradation II), Contract No. DA-28-043 AMC-00170(E), Linden Laboratories, Inc., State College, Pa. (15 June 1965)

B29 Buessem, W. R. and Marshall, P., "Crystal Chemistry of Ceramic Dielectrics", Report No. 16, U.S. Army Electronic Research and Development Lab., Contract No. DA-36-039-SC-78912, Linden Laboratories, Inc., State College, Pa. (Dec. 1962)

B30 Buessem, W. R. and Marshall, P. A., Jr., "High Temperature Ceramic Dielectrics (Summary on Degradation I) Report No. 12, Contract No. DA-36-039-SC-78912, Linden Laboratories, Inc., State College, Pa. (15 Oct. 1961)

B31 Buessem, W. R. and Marshall, P., "Study of Degradation of High K-Ceramic Dielctrics", Report No. 6, U.S. Army Signal Corps Contract No. DA-36-039-SC-75036, Linden Laboratories, Inc., State College, Pa. (31 Dec. 1959)

B32 Buessem, W. R., Marshall, P. A. Jr. and Weyl, W., "Study of the Degradation of High K Ceramic Dielectrics", First Quarterly Report, Contract No. DA-36-039-SC-42679, Linden Laboratories, Inc., State College, Pa. (15 June 1953)

B33 Bunting, E. N., Shelton, G. R., Creamer, A. S. and Jaffe, B., "Properties of Beryllium Barium Titanate Dielectrics", J. Res. Natl. Bur. Standards 47 (1) 15-24 (1951) RP 2222

B34 Bunting, E. N., Shelton, G. R. and Creamer, A. S., "Properties of Calcium-Barium Titanate Dielectrics", J. Res. Natl. Bur. Standards 43 (3) 237-244 (1949)

B35 Bunting, E. N., Shelton, G. R. and Creamer, A. S., "Properties of Barium-Strontium Titanate Dielectrics", J. Amer. Ceram. Soc. 30 (4) 114-125 (1947)

B36 Burdick, G. A. and Lyon, T. J., "Investigation of Large Signal Microwave Effects in Ferroelectric Materials", Third Quarterly Report, Contract No. DA36-039-AMC-03240E, Sperry Microwave Electronics Co., AD602508 (Apr. 1964)

B37 Bhide, V. G. and Multani, M. S., "Effect of Doping Barium Titanate with Manganese Dioxide", Physica 29 23-32 (1963)

B38 Boganov, A. G. and Khomutetskaia, R. A., "Additional Data on Solid Solutions of the $PbTiO_3$-$SrTiO_3$ System", Bull. Acad. Sci. USSR, Phys. Ser. 21 432-436 (1957)

B39 Beam, W. R., Electronics of Solids, McGraw-Hill Book Co., New York (1965)

B40 Brandmayr, R. J., Brown, A. E. and Dunlap, A. M., "Annealing Effects on Microstructure and Dielectric Properties of Hot-Pressed, Ultrafine Grained $BaTiO_3$", Technical Report ECOM-2614, U.S. Army Electronics Command, Fort Monmouth, N. J., AD622970 (May 1965)

B41 Berlincourt, D. A. and Jaffe, H., "Elastic and Piezoelectric Coefficients of Single-Crystal Barium Titanate", Phys. Rev. 111 (1) 143-148 (1958)

B42 Bond, W. L., Mason, W. P. and McSkimin, H. J., "Elastic and Electromechanical Coupling Coefficients of Single-Crystal Barium Titanate", Phys. Rev. 82 442-443 (1951)

B43 Bruggeman, D. A. G., "Berechung verschiedener physikalischer Konstanten von heterogenen Substanzen" Part I, Ann. d. Physik 5 (24) 636-664 (1935)

B44 Bruggeman, D. A. G., "Berechung verschiedener physikalischer Konstanten von heterogenen Substanzen" Part II, Ann. d. Physik 5 (25) 645-672 (1936)

B45 Buessem, W. R., Mechanical Properties of Engineering Ceramics, Interscience Publ., New York (1961)

B46 Buessem, W. R., Cross, L. E. and Goswami, A. K., "Phenomenological Theory of High Permittivity in Fine-Grained Barium Titanate", J. Amer. Ceram. Soc. 49 (1) 33-36 (Jan. 1966)

B47 Benedict, T. S. and Durand, J. L., "Dielectric Properties of Single Domain Crystals of $BaTiO_3$ at Microwave Frequencies", Phys. Rev. 109 1091 (1958)

C1 Cardon, F., "Polarization and Space-Charge-Limited Current in Rutile (TiO_2)", Physica 27 841 (1961)

C2 Christensen, E. G., "The Ferroelectric and Structural Properties of Hafnium Oxide Compounds", DI-82-0377, Boeing Scientific Res. Labs., AD613589 (Sept. 1964)

C3 Coates, R. V., "A Note on the Structure of Non-Ferroelectric Lead Metatantalate", Acta Cryst. 14 84 (1961)

C4 Coates, R. V. and Kay, H. F., "Dielectric Properties of Some Metaniobate and Metatantalate Ceramics", Phil. Mag. 3 (series 8) 1449-1459 (1958)

C5 Corning Glass Works Staff, "Continuously Variable Delay in Photoelastic Line", Electrical Design News, (Nov. 1960)

C6 Cronemeyer, D. E., "Electrical and Optical Properties of Rutile Single Crystals", Phys. Rev. 87 (5) 876-886 (1952)

C7 Cronemeyer, D. C., "Electrical and Optical Properties of Rutile Single Crystals", Report No. 41, Laboratory for Insulation Research, MIT (1951)

C8a Cross, L. E., "High Permittivity Relaxation Dielectrics", Proc. Inst. Electrical Engr. (London) Pt. B109, Suppl. No. 22, Paper No. 3644, 407-411 (1962)

C8b Cross, L. E., "Electric Double Hysteresis in $(K_xNa_{1-x})NbO_3$ Single Crystals:, Nature 181 (4603) 178-179 (1958)

C9 Curran, D. R. and Gerber, W. J., "Ferroelectric Ceramic Filters, IF Transformers and Networks", Sixth Quarterly Report (No. 27), Contract No. DA36-039SC-87275, Clevite Corp., AD418263 (16 July 1963)

C10 Cochran, W., "Crystal Stability and the Theory of Ferroelectricity", Advances in Physics (London) 9 387-423 (1960)

C11 Caspari, M. E. and Merz, W. J., "The Electromechanical Behavior of Barium Titanate Single Domain Crystals", Phys. Rev. 80 1082-1089 (1950)

C12 Cowley, R. A., "Temperature Dependence of a Transverse Optic Mode in Strontium Titanate", Phys. Rev. Letters 9 159-161 (1962)

D1 Dantsiger, A. Ya., "Ferroelectric Properties of Nitrites and Nitrates of Alkali and Alkali Earth Metals", Materialy 4-oi [Chetvertoi] Nauchn. Konf. Aspirantov (Rostov-on-Don, Rostov Univ.) 1962 75-77

D2 DeVries, R. C., "On the Preparation of Thin Single-Crystal Films of $BaTiO_3$", J. Amer. Ceram. Soc. 45 (5) 225-228 (1962)

D3 Dungan, R. H., Barnett, H. M. and Stark, A. H., "Phase Relations and Electrical Parameters in the Ferroelectric-Antiferroelectric Region of the System $PbZrO_3$-$PbTiO_3$-$PbNb_2O_6$", J. Amer. Ceram. Soc. 45 (8) 382-388 (Aug. 1962)

D4 Daniel, W. A. and Gould, B. B., "Activation of Ferroelectric Materials", U.S. Patent 2,928,032 (Mar. 8, 1960)

D5a Devonshire, A. F., "Theory of Barium Titanate. I", Phil. Mag. 40 1040-1063 (1949)

D5b Devonshire, A. F., "Theory of Barium Titanate. II", Phil. Mag. 42 1065-1079 (1951)

D6 Drexler, O. and Ritscher, B., "Ceramic Dielectrics with High K" (In German), Valvo-Berichte (Philips) 7 105-130 (Table 2 on page 113) (Nov. 1961)

D7 Dungan, R. H. and Golding, R. D., "Metastable Ferroelectric Sodium Niobate", J. Amer. Ceram. Soc. 47 (2) 73-76 (Feb. 1964)

D8 DeBretteville, A. P., Jr., Halden, F. A., Vasilos, T. and Reed, L., "Dielectric Studies in the System CdO-Nb_2O_5", J. Amer. Ceram. Soc. 40 (3) 86-89 (1957)

D9 Drexler, O. and Schat, B. R., "Development of Ceramic Materials with a Dielectric Constant of 10,000 at Room Temperature", Science of Ceramics, Volume 1, Academic Press, London (1961)

D10 Dick, B. G. and Overhauser, A. W., "Theory of the Dielectric Constant of Alkali Halide Crystals", Phys. Rev. 112 (1) 90-103 (1958)

D11 Drougard, M. E., Landauer, R. and Young, D. R., "Dielectric Behavior of Barium Titanate in the Paraelectric State", Phys. Rev. 93 1010-1014 (1955)

D12 DeVries, R. C., Nipper, E. F. and Jugle, D. B., "Growth Twinning in Perovskite-Type Ceramics", Final Report, ONR Contract No. Nonr-591(18) Rensselaer Polytechnic Institute (31 Jan. 1966) p. 80

D13 Drougard, M. E. and Young, D. R., "Domain Clamping Effect in Barium Titanate Single Crystals", Phys. Rev. 94 (6) 1561-1564 (1954)

E1 Egerton, L. and Dillon, D. M., "Piezoelectric and Dielectric Properties of Ceramics in the System Potassium-Sodium Niobate", J. Amer. Ceram. Soc. 42 (9) 438-442 (Sept. 1959)

E2 Egerton, L. and Koonce, S. E., "Effect of Firing Cycle on Structure and Some Dielectric and Piezoelectric Properties of Barium Titanate Ceramics", J. Amer. Ceram. Soc. 38 (11) 412-418 (Nov. 1955)

E3 Electronic Properties Information Center, "A Bibliography of Holdings on Ferroelectric Ceramics", EPIC Bibliography No. B-100, Hughes Aircraft Company, Culver City, Cal. (6 Apr. 1965)

F1 Fatuzzo, E., Harbeke, G., Merz, W. J., Nitsche, R., Roetschi, H. and Ruppel, W., "Ferroelectricity in SbSI", Phys. Rev. 127 2036-2037 (1962)

F2 Feldman, C., "Method of Forming Thin Films of $BaTiO_3$", U.S. Patent 2,922,730 (Jan. 1960)

F3 Feldman, C., "Formation of Thin Films of $BaTiO_3$ by Evaporation", Rev. Sci. Instr. 26 (5) 463-466 (1955)

F4 Feuersanger, A. E., Hagenlocher, A. K. and Solomon, A. L., "Preparation and Properties of Thin Barium Titanate Films", J. Electrochem. Soc. 111 (12) 1387-1391 (Dec. 1964)

F5 Fedulov, S. A., "Determining the Curie Point of $BiFeO_3$ Ferroelectric", Doklady Akad. Nauk SSSR 139 (6) 1345-1346 (Aug. 1961); (English trans.) Sov. Phys.-Doklady 6 (8) 729-730 (Feb. 1962)

F6 Fedulov, S. A., Venevtsev, Yu. N., Zhdanov, G. S., Smazhevskaya, E. G. and Rez, I. S., "X-ray and Electrical Studies of the $PbTiO_3$-$BiFeO_3$ System", Kristallografiya 7 (1) 77-83 (Jan.-Feb. 1962); (English trans.) Sov. Phys.-Crystallography 7 (1) 62-66 (July-Aug. 1962)

F7 Fedulov, S. A., Ladyzhenskii, P. B. and Venevtsev, Yu. N., "Study of the $BiFeO_3$-$LaAlO_3$ System", Kristallografiya 9 (4) 516-520 (July-Aug. 1964); (English trans.) Sov. Phys.-Crystallography 9 (4) 428-431 (Jan.-Feb. 1965)

F8 Feldman, C., "Time Changes in Thin Films of $BaTiO_3$", J. Appl. Phys. 27 870-873 (1956)

F9 Foster, N. F., "Ultra-High Frequency Cadmium-Sulphide Transducers", IEEE Trans. on Sonics and Ultrasonics, SU-11 (2) (Nov. 1964)

F10 Francombe, M. H. and Lewis, B., "Structural Dielectric and Optical Properties of Ferroelectric Lead Metaniobate", Acta Cryst. 11 696-703 (1958)

F11 Fousek, J., "The Dielectric Properties of Single Crystals of $BaTiO_3$", Czech. J. Phys. 8 254-255 (1958)

F12 Fousek, J., "On the Problem of the Permittivity Dispersion of Barium Titanate", Czech. J. Phys. 9 (12) 172-185 (1959)

G1 Gerson, R., "Variation in Ferroelectric Characteristics of PZT Ceramics Due to Minor Chemical Modifications", J. Appl. Phys. 31 188-194 (1960)

G2 Glower, D. D. and Heckman, R. C., "Conduction-Ionic or Electronic-in $BaTiO_3$", J. Chem. Phys. 41 (3) 877 (1964)

G3 Goodman, G., "Ferroelectric Ceramic Composition", U.S. Patent 2,729,757 (Jan. 3, 1956)

G4 Goodman, G., "Ferroelectric Properties of Lead Metaniobate", J. Amer. Ceram. Soc. 36 (11) 368-372 (Nov. 1953)

G5 Goswami, A. K., "Dielectric Properties of Fine Grain $BaTiO_3$", Ph.D. Thesis, The Pennsylvania State University (1964)

G6 Gray, A. L. and Herbert, J. M., "The Preparation of Barium Titanate as a Ceramic Transducer Material", Acustica 6 229-234 (1956)

G7 Gray, R. B., "Transducer and Method of Making the Same", U.S. Patent 2,486,560 (Nov. 1, 1949)

G8 Grigsby, T. N. and Tajchman, E. J., "Properties of Lamb Waves Relevant to the Ultrasonic Inspection of Thin Plates", IRE Trans. on Ultrasonics Engr. UE-8, (1) (Mar. 1961)

G9 Gränicher, H. and Jakits, O., "The Dielectric Properties and Phase Transformations of Mixed Crystal Systems of the Perovskite Type", Nuova Cimento Suppl. 11 480-520 (1954)

H1 Hagenlocher, A. K. and Feuersanger, A. E., "Study of Thin Film Compound Formed from Simultaneously Evaporated Constituents", First Quarterly Report, Contract No. DA 36-039 AMC-00105(E), AD425442 (Aug. 1963)

H2 Hall, R. D., "Ferroelectric Bibliography Supplement", AD433653 (Aug. 1963)

H3 Hall, R. D., "Ferroelectric Bibliography", AD255317 (Mar. 1961)

H4 Hall, C. A., Dungan, R. H. and Stark, A. H., "Solid Solutions in Antiferroelectric Region of the System $PbHfO_3$-$PbTiO_3$-$PbSnO_3$-$PbNb_2O_6$", J. Amer. Ceram. Soc. 47 (6) 259-264 (June 1964)

H5 Herczog, A., "Microcrystalline $BaTiO_3$ by Crystallization from Glass", J. Amer. Ceram. Soc. 47 (3) 107-115 (Mar. 1964)

H6 Hass, G. and Thun, R. E., Eds., Physics of Thin Films, Vol. 2, Academic Press, New York (1964)

H7 Hansell, U. G., "Method of Polarizing Transducers", U.S. Patent 2,983,988 (May 16, 1961)

H8 Heuter, T. F. and Bolt, R. H., Sonics, John Wiley and Sons, Inc., New York (1955)

H9 Hill, F. N. and Selwood, P. W., "Structure and Activity of Supported Nickel Catalysts", J. Amer. Chem. Soc. 71 2522-2529 (1949)

H10 Hulm, J. K., "Low-Temperature Dielectric Properties of Cadmium and Lead Niobates", Phys. Rev. 92 504-505 (1953)

H11 Hulm, J. K., Matthias, B. T. and Long, E. A., "A Ferromagnetic Curie Point in $KTaO_3$ at Very Low Temperatures", Phys. Rev. 79 885-886 (1950)

H12 Hurd, J. D., Simpson, A. W. and Tredgold, R. H., "Anomalous Polarization in Ferroelectrics and Other Oxides", Proc. Phys. Soc. (London) 73 448-454 (1959)

H13 Herczog, A. and Stookey, S. D., "Glass and Methods of Devitrifying Same and Making a Capacitor Therefrom", U.S. Patent 3,195,030 (July 1965)

H14 Hagedorn, R., "A Static Model of $BaTiO_3$ at Room Temperature", Z. Phys. 133 394 (1952)

H15 Huibregtse, E. J. and Young, D. R., "Triple Hysteresis Loops and the Free Energy Function in the Vicinity of the 5°C Transition in Barium Titanate", Phys. Rev. 103 1705-1711 (1956)

H16 Huibregtse, E. J., Bessey, W. H. and Drougard, M. E., "Electromechanical Behavior of Single Crystals of Barium Titanate from 25 to 160°C", J. Appl. Phys. 30 (6) 899-905 (1959)

H17 Heywang, W. and Schaefer, R., "On the Influence of Structure on the Hysteresis Behavior of Ceramic $BaTiO_3$" (in German), Z. Angew. Phys. 8 209-213 (1956)

H18 Havinga, E. E., "Ferroelectric Perovskites Containing Manganese Ions", Philips Res. Repts. 21 (1) 49-62 (1966)

I1 Ikeda, T., "A Few Quaternary Systems of Perovskite Type $A^{2+}B^{4+}O_3$ Solid Solutions", J. Phys. Soc. Japan 14 (10) 1286-1294 (Oct. 1959)

I2 Iwasaki, H., "Systems $NaNbO_3$-$NaSbO_3$ and $NaNbO_3$-$KSbO_3$", Japan J. Appl. Phys. 2 737-738 (1963)

I3 Iwasaki, H. and Ikeda, T., "Studies on the System $Na(Nb_{1-x}Ta_x)O_3$", J. Phys. Soc. Japan 18 (2) 157-162 (Feb. 1963)

I4 Ikeda, T. and Okano, T., "Piezoelectric Ceramics of Lead Zirconate-Titanate Modified by Bismuth Ferrite", Japan J. Appl. Phys. 2 63-64 (1963)

I5 Ikeda, T., "Studies on (Ba-Pb)(Ti-Zr)O_3 System", J. Phys. Soc. Japan 14 (2) 168-174 (Feb. 1959)

I6 Ikeda, T., "Some Studies on the Ternary System $(Ba,Pb,Ca)TiO_3$", J. Phys. Soc. Japan 13 (4) 335-340 (Apr. 1958)

I7 "IRE Standards on Piezoelectric Crystals: Measurements of Piezoelectric Ceramics, 1961" (H. Jaffe, Chm.), Proc. IRE 49 1161-1169 (July 1961)

I8 Isupov, V. A., Krainik, N. N., Fridberg, I. D. and Zelenkova, I. E., "Antiferroelectric Properties of Lead Orthovanadate", Fiz. Tverd. Tela 7 (4) 1051-1056 (Apr. 1965); (English trans.) Sov. Phys.-Solid State 7 (4) 844-847 (Oct. 1965)

I9 Iwasaki, H., "Studies on the System (1-x)$NaNbO_3$x$KTaO_3$", J. Phys. Soc. Japan 17 (5) 779-784 (May 1962)

J1 Jona, F. and Shirane, G., Ferroelectric Crystals, The Macmillan Co., New York (1962)

J2 Jaeger, R. E. and Egerton, L., "Hot Pressing of Potassium-Sodium Niobates", J. Amer. Ceram. Soc. 45 (5) 209-213 (May 1962)

J3 Jaffe, H., "Piezoelectric Ceramics", J. Amer. Ceram. Soc. 41 (11) 494-498 (Nov. 1958 Part II)

J4 Jaffe, B., Roth, R. S. and Marzullo, S., "Properties of Piezoelectric Ceramics in the Solid-Solution Series Lead Titanate-Lead Zirconate-Lead Oxide: Tin Oxide and Lead Titanate-Lead Hafnate", J. Res. Natl. Bur. Standards 55 (5) 239-254 (Nov. 1955) R. P. 2626

J5 Jaffe, B., Roth, R. S. and Marzullo, S., "Piezoelectric Properties of Lead Zirconate-Lead Titanate Solid-Solution Ceramics". J. Appl. Phys. 25 809-810 (1954)

J6 Jaffe, B., Roth, R. S., and Marzullo, S., "Improvement of Piezoelectric Ceramics", Rep. No. 6, Natl. Bur. of Standards Off. Ordn. Res., Durham, N. C., Proj. TB2-0001 (January 1, 1954)

J7 Johnson, V. J., Valenta, M. W., Dougherty, J. E., Douglass, R. M. and Meadows, J. W., "$Pb(Sc_{0.5}Nb_{0.5})_x$ $\emptyset_{1-x}O_3$, Perovskite-Type Ferroelectric Solid Solutions Possessing Relatively Large Spontaneous Polarizations", J. Phys. Chem. Solids 24 85-93 (1963)

J8 Jonker, G. H. and Noorlander, W., "Grain Size of Sintered Barium Titanate", Science of Ceramics, Volume I, Academic Press, London (1961) pp. 255-264

J9 Jackson, J. E., Liedl, G. L. and Grace, R. E., "Epitaxial Relations in Thin Films of Barium Titanate and Silver", Progress Report on Materials Science Research, Purdue University (Oct. 1964 - Sept. 1965)

J10 Jackson, J. E., "Epitaxial Relations in Thin Films of Barium Titanate and Silver", M. S. Thesis, Met. E., Purdue University (Jan. 1965)

K1 Kell, R. C. and Hellicar, N. J., "Structural Transitions in Barium Titanate-Zirconate Transducer Materials", Acustica 6 235-238 (1956)

K2 Kodzhespirov, F. F., "The Thermal Conductivity of $BaTiO_3$-Based Solid Solutions of Manganese Niobate", Fiz. Tverd. Tela 3 (3) 781-785 (Mar. 1961); (English trans.) Sov. Phys.-Solid State 3 (3) 567-570 (Sept. 1961)

K3 Krainik, N. N., "Ferroelectric and Antiferroelectric Properties of Solid Solutions of $NaNbO_3$-$PbZrO_3$", Fiz. Tverd. Tela 2 (4) 685-690 (1960). (English trans.) Sov. Phys.-Solid State 2 (4) 633-637 (1960)

K4 Kolkov, S. N., Kunin, V. Ya., Tsikin, A. N., "Calculation of the Defect Density Variation in a Rutile Ceramic During Aging and Regeneration", Sov. Phys.-Solid State 3 (2) 477-481 (English trans.) 1961

K5 Koller, A. and Pospisil, Z., "The Mechanism of Degradation of Titanate Dielectrics", Czech. J. Phys. 8 (3) 315-321 (1958)

K6 Krueger, H. H. A. and Berlincourt, D. A., "Effects of High Static Stress on the Piezoelectric Properties of Transducer Materials", J. Acoust. Soc. Amer. 33 (10) 1339-1344 (Oct. 1961)

K7 Kulcsar, F., "Electromechanical Properties of Lead Titanate Zirconate Ceramics Modified with Tungsten and Thorium", J. Amer. Ceram. Soc. 48 (1) 54 (Jan. 1965)

K8 Kulcsar, F., "Electromechanical Properties of Lead Titanate Zirconate Ceramics Modified with Certain Three- or Five-Valent Additions", J. Amer. Ceram. Soc. 42 (7) 343-349 (July 1959)

K9 Kulcsar, F., "Electromechanical Properties of Lead Titanate Zirconate Ceramics with Lead Partially Replaced by Calcium or Strontium", J. Amer. Ceram. Soc. 42 (1) 49-51 (Jan. 1959)

K10 Kunin, V. Ya., Fomenko, L. N. and Tsikin, A. N., "Changes in the Electrical Conductivity and in the Distribution of Electrical Potential in a Rutile Ceramic During Aging" (English trans.) Sov. Phys.-Solid State 9 (4) 712-715 (1962)

K11 Kunin, V. Ya. and Tsikin, A. N., "Characteristic Variation of the Electrical Conductivity of Rutile Ceramics During the Process of Electrical Aging and Regeneration" (English trans.) Sov. Phys.-Solid State 3 (1) 158-163 (1961)

K12 Kunin, V. Ya. and Tsikin, A. N., "Change of the Dielectric Properties of Rutile Ceramics During Passage of Current and During Heating" (English trans.), Sov. Phys.-Solid State 2 (10) 2101-2106 (1960)

K13 Kunin, V. Ya., Polonskii, Yu. A. and Tsikin, A. N., Izvest. Vuzov, Fizika No. 2, 85 (1960) (Reference cited in K4)

K14 Katz, H. W., Ed., Solid State Magnetic and Dielectric Devices, John Wiley and Sons, Inc., New York (1959)

K15 Kinase, W., "On Interactions among Ions of a $BaTiO_3$ Crystal and on its 180° and 90° Type Domain Boundaries", Progr. Theor. Phys. (Kyoto) 13 (5) 529-539 (1955)

L1 Lewis, B. and White, E. A. D., "Structure and Phase Transitions of Ferroelectric Sodium-Cadmium Niobates", J. Electronics 1 (6) 646-664 (1956)

L2 Longo, T. A., "Thin Films - Active and Passive", Solid State Design 6 8-9 (June 1965)

L3 Liesk, W., "Anomalous Directions of Polarization in Thin Barium Titanate Single Crystals", Appl. Phys. Letters 5 (4) 69-70 (15 Aug. 1964)

L4 Lehovec, K. and Shirn, G. A., "Conductivity Injection and Extraction in Polycrystalline Barium Titanate", J. Appl. Phys. 33 2036-2044 (1962)

L5 Laszlo, F., "Tessellated Stresses - Part V", J. Iron and Steel Inst. (London) 164 (1) 5-26 (Jan. 1950)

L6 Lavedan, L. J. and Donaldson, M. R., "Microwave Ferroelectric Phase Shifters and Switches", Final Report, Contract No. Da 36-039-AMC-02340(E), Sperry Microwave Electronics Co., AD616754 (Mar. 1965)

M1 Merz, W. J., "Ferroelectricity", Progress in Dielectrics, Vol. 4, Birks, J. B. and Hart, J., Eds., Heywood and Co., London (1962) pp. 101-149

M2 Müller, E. K., Nicholson, B. J. and Turner, G. L'E., "The Epitaxy of $BaTiO_3$ Films by Vapour Deposition", Brit. J. Appl. Phys. 13 486 (1962)

M3 Masuno, K., "X-ray and Dielectric Studies of the Systems $(Ba_{1-x}R_{x/3})Nb_2O_6$, Where R is Y, Sm or La", J. Phys. Soc. Japan 19 (3) 323-328 (Mar. 1964)

M4 Müller, E. K., Nicholson, B. J. and Francombe, M. H., "The Vapor Deposition of $BaTiO_3$ by a Grain-by-Grain Evaporation Method", Electrochem. Technology 1 (5-6) 158-163 (May-June 1963)

M5 MacChesney, J. B. and Potter, J. F., "Factors and Mechanisms Affecting the Positive Temperature Coefficient of Resistivity of Barium Titanate", J. Amer. Ceram. Soc. 48 (2) 81-88 (Feb. 1965)

M6 Marks, B. H., "Ceramic Dielectric Materials", Electronics 21 (8) 116-120 (1948)

M7 Marutake, M. and Ikeda, T., "Anisotropy in Polarized Barium Titanate Ceramics", J. Phys. Soc. Japan 12 (3) 233-240 (Mar. 1957)

M8 Marutake, M., "A Calculation of Physical Constants of Ceramic Barium Titanate", J. Phys. Soc. Japan 11 (8) 807-814 (Aug. 1956)

M9 Mason, W. P., Piezoelectric Crystals and Their Application to Ultrasonics, D. Van Nostrand Co., Inc., New York (1950)

M10 Mason, W. P., Physical Acoustics and the Properties of Solids, D. Van Nostrand Co., Inc., Princeton, New Jersey (1958) pp. 76-79

M11 Mason, W. P., "Polarization Process for Pseudocubic Ferroelectrics", U.S. Patent 2,706,326 (Apr. 19, 1955)

M12 Mason, W. P., "Aging of the Properties of Barium Titanate and Related Ferroelectric Ceramics", J. Acoust. Soc. Amer. 27 (1) 73-85 (Jan. 1955)

M13 Mattiat, O. E., "Ceramic IF-Transformers", First Quarterly Report, U.S. Army Signal Corps Contract DA-36-039-SC 64644, Clevite, (28 Sept. 1955) 45 pp.

M14 May, J. E., Jr., "Thickness-Shear Mode $BaTiO_3$ Ceramic Transducers for Ultrasonic Delay Lines", IRE Trans. on Ultrasonic Engr. UE-7 (1) 7-12 (Feb. 1960)

M15 McQuarrie, M. C. and Buessem, W. R., "The Aging Effect in $BaTiO_3$", Bull. Amer. Ceram. Soc. 34 402-406 (Dec. 1955)

M16 McQuarrie, M. C., "Time Effects in the Hysteresis Loop of Polycrystalline Barium Titanate", J. Appl. Phys. 24 1334-1335 (1953)

M17 McSkimin, H. J. and Chambers, R. P., "Methods of Measuring Mechanical Properties of Plastics with High-Frequency Ultrasound", IEEE Trans. on Sonics and Ultrasonics, SU-11 (2) (Nov. 1964)

M18 McSkimin, H. J., "Transducer Design for Ultrasonic Delay Lines", J. Acoust. Soc. America 27 (2) (Mar. 1955)

M19 Mitsui, T. and Westphal, W. B., "Dielectric and X-ray Studies of $Ca_x Ba_{1-x}TiO_3$ and $Ca_xSr_{1-x}TiO_3$", Phys. Rev. 124 (5) 1354-1359 (Dec. 1961)

M20 Mosely, D. S., "Anisotropy of Polarized Polycrystalline $BaTiO_3$", J. Acoust. Soc. America, 27 (5) 947-951 (Sept. 1955)

M21a Megaw, H. D., "Origin of Ferroelectricity in Barium Titanate and Other Perovskite-Type Crystals", Acta Cryst. 5 739-749 (1952)

M21b Megaw, H. D., "Ferroelectricity and Crystal Structure II", Acta Cryst. 7 187-193 (1954)

M22 Mueller, H., "Properties of Rochelle Salt", Phys. Rev. 47 175-191 (1935)

M23 Mueller, H., "The Dielectric Anomalies of Rochelle Salt", Annals of the N. Y. Acad. Sci. 40 321-356 (1960)

M24 Merz, W. J., "Double Hysteresis Loop of Barium Titanate at the Curie Point", Phys. Rev. 91 513-517 (1953)

M25 Meyerhofer, D., "Transition to the Ferroelectric State in Barium Titanate", Phys. Rev. 112 413-423 (1958)

N1 Nomura, S., "Dielectric Properties of Titanates Containing Sn^{4+} Ions I", J. Phys. Soc. Japan 10 (2) 112-119 (Feb. 1955)

N2 Nomura, S. and Kawakubo, T., "Dielectric Properties of $Pb(Fe,Ta)_{0.5}O_3$-$PbTiO_3$ and $Pb(Fe,Ta)_{0.5}O_3$-$PbZrO_3$ Systems", J. Phys. Soc. Japan 17 573-574 (1962)

N3 Nekrasov, M. M. and Poplavko, Yu. M., "Ferroelectric Properties of Solid Solutions in the Trinary System $Ba(Ti,Zr,Sn)O_3$", Fiz. Tverd. Tela 2 (8) 1681-1684 (Aug. 1960); (English trans.) Sov. Phys.-Solid State 2 (8) 1521-1523 (Feb. 1961)

N4 Nomura, S. and Sawada, S., "Dielectric Properties of Lead-Strontium Titanate", J. Phys. Soc. Japan 10 (2) 108-111 (Feb. 1955)

N5 Nomura, S. and Sawada, S., "Dielectric and Thermal Properties of Barium-Lead Titanates", J. Phys. Soc. Japan 6 (1) 36-39 (1951)

N6 Northrip, J. W., "High-Temperature Discharge in Ferroelectric Ceramics", J. Appl. Phys. 31 (12) 2293-2296 (Dec. 1960)

N7 Novosil'tsev, N. S., Khodakov, A. L. and Schulman, M. S., "Metastable States of $BaTiO_3$", Doklady Akad. Nauk, SSSR 83 829-831 (1952)

N8 Niesel, W., "Dielectric Constants of Heterogeneous Mixtures of Isotropic and Anisotropic Solids" (in German), Ann. d. Physik 6 (10) 336-348 (1952)

O1 Oshry, H. I., "Ceramic High-K Titanate Improvement Evaluation", Final Report, Contract No. W36-039-SC44534, U.S. Army Signal Corps Engr. Labs., Erie Resistor Corporation (31 Jan. 1951)

O2 Ouchi, H., Nagano, K. and Hayakawa, S., "Piezoelectric Properties of $Pb(Mg_{1/3}Nb_{2/3})O_3$-$PbTiO_3$-$PbZrO_3$ Solid Solution Ceramics", J. Amer. Ceram. Soc. 48 (12) 630-635 (Dec. 1965)

P1 Pepinsky, R., "Studies in Crystal Preparation and Structural Mechanisms for New Physical Properties of Solids", Final Report, AD285512 (Mar. 1962)

P2 Pajak, Z., "Dielectric Investigation of Perovskite-Type Ferroelectrics. Part I: Ferroelectric Systems with Small Temperature Coefficient of Permittivity", Acta Phys. Polon. 19 473-506 (1959)

P3 Pajak, Z., "Dielectric Investigation of Perovskite-Type Ferroelectrics II. Aging Process", Acta Phys. Polon 19 507-520 (1959)

P4 Payne, W. H. and Tennery, V. J., "Dielectric and Structural Investigations of the System $BaTiO_3$-$BaHfO_3$", J. Amer. Ceram. Soc., 48 (8) 413-417 (Aug. 1965)

P5 Plessner, K. W., "Aging of Dielectric Properties of Barium Titanate Ceramics", Proc. Phys. Soc. (London) 69 1261-1268 (1956)

P6 Plessner, K. W. and West, R., "Replacement of Ti in $BaTiO_3$ Ceramic by Si and Ge", Proc. Phys. Soc. (London) 68B 1150-1152 (1955)

P7 Pomerantz, N., "Propagation of Microwave Phonons in Germanium", IEEE Trans. on Sonics and Ultrasonics SU-11 (2) (Nov. 1964)

P8 Powles, J. G., "Dielectric Properties of Titanates at Ultra-High Frequencies", Nature 162 614 (Oct. 1948)

P9 Prokopowicz, T. I. and Kennedy, P. M., "Research and Development Program Intrinsic Reliability Subminiature Ceramic Capacitors", Twelfth Quarterly Report, Contract No. DA-36-039-SC-90705, U.S. Army Signal Research and Development, Sprague Electric Co., AD 468839 (14 July 1961)

P10 Pulvari, C. F., "Ferrielectricity", Phys. Rev. 120 (5) 1670-1673 (1960)

P11 Pulvari, C. F., "Ferroelectrics and Their Memory Applications" IRE Trans. on Component Parts CP-3 (1) 3-11 (Mar. 1956)

P12 Powles, J. G. and Jackson, W., "Measurement of Dielectric Properties of High Permittivity Materials at Centimeter Wave Lengths", Proc. Inst. Electrical Engrs. (London) 96 383-389 (1949)

R1 Roginskaya, Yu. E., Venevtsev, Yu. N., Fedulov, S. A. and Zhdanov, G. S., "An X-ray Diffraction Investigation of the Magnetic and Electric Properties of the System $BiFeO_3$-$LaFeO_3$", Kristallografiya 8 (4) 610-616 (1963); (English trans.) Sov. Phys.-Cryst. 8 (4) 490-494 (1964)

R2 Reisman, A. and Banks, E., "Reactions of the Group VB Pentoxides. VIII. Thermal, Density and X-ray Studies of the Systems $KNbO_3$-$NaNbO_3$ and $KTaO_3$-$KNbO_3$", J. Amer. Chem. Soc. 80 1877-1882 (20 Apr. 1958)

R3 Rhys-Roberts, C. and Tredgold, R. H., "A Note on the Theory of Space-Charge-Limited Currents", Proc. Phys. Soc. (London) 76 497 (1960)

R4 Roberts, S., "Dielectric Properties of Lead Zirconate and Barium-Lead Zirconate", J. Amer. Ceram. Soc. 33 (2) 63-66 (Feb. 1950)

R5 Roberts, S., "Dielectric and Piezoelectric Properties of Barium Titanate", Phys. Rev. 71 (12) 890-895 (June, 1947)

R6 Rosenthal, A. H., "Application of Ultrasonic Light Modulation to Signal Recording Display, Analysis and Communication", IRE Trans. on Ultrasonic Engr. UE-8 (1) (Mar. 1961)

S1 Shelton, G. R., Bunting, E. N. and Kopell, L., "Development of Inorganic Films with High Dielectric Constant", First Quarterly Report, NBS Report 2024, Dept. of Army Proj. No. 3-93-00-503, AD1819 (1952)

S2 Shibata, H. and Toyoda, H., "Thickness Dependence of Polarization Reversal in $BaTiO_3$ Single Crystals", J. Phys. Soc. Japan 17 (2) 404-405 (1962)

S3 Singh, B., "Ferroelectricity and the Structural Mechanism of the Ammonium Sulfate Transition", Ph. D. Thesis, The Pennsylvania State University (1962)

S4 Subbarao, E. C. Shirane, G. and Jona, F., "X-ray, Dielectric and Optical Study of Ferroelectric Lead Metatantalate and Related Compounds", Acta Cryst. 13 226-231 (1960)

S5 Srikanta, S., Tare, V. B., Sinha, A. P. B. and Biswas, A. B., "Structural Properties of $(Ba, Pb)_{1-\sigma}(Ti,Nb)O_3$ Systems", Acta Cryst. 15 255-258 (1962)

S6 Sawaguchi, E. and Charters, M. L., "Aging and the Double Hysteresis Loop of $Pb_xCa_{1-x}TiO_3$ Ceramics", J. Amer. Ceram. Soc. 42 (4) 157-164 (Apr. 1959)

S7 Sawaguchi, E., "Ferroelectricity versus Antiferroelectricity in the Solid Solutions of $PbZrO_3$ and $PbTiO_3$", J. Phys. Soc. Japan 8 (5) 615-629 (Sept.-Oct. 1953)

S8 Schofield, D. and Brown, R. F., "An Investigation of Some Barium Titanate Compositions for Transducer Applications", Canad. J. Phys. 35 594-607 (1957)

S9 Schofield, D. and Brown, R. F., "Improved Barium Titanate Composition", J. Acoust. Soc. Amer. 29 394-395 (1957)

S10 Selwood, P. W., Ellis, M. and Wethington, K., "Support Oxides of Iron", J. Amer. Chem. Soc.. 71 2181-2184 (1949)

S11 Shelton, G. R., Creamer, A. S. and Bunting, E. N., "Properties of Barium-Magnesium Titanate Dielectrics", J. Res. Natl. Bur. Standards 41 17-26 (1948) RP 1899

S12 Shirane, G. and Pepinsky, R., "Dielectric Properties and Phase Transitions of $Cd_2Nb_2O_7$ and $Pb_2Nb_2O_7$", Phys. Rev. 92 504 (1953)

S13 Shirane, G., "Ferroelectricity and Antiferroelectricity in Ceramic $PbZrO_3$ Containing Ba or Sr", Phys. Rev. 86 (2) 219-227 (Apr. 1952)

S14 Shirane, G. and Suzuki, K., "On the Phase Transition in Barium-Lead Titanate (1)", J. Phys. Soc. Japan 6 (4) 274-278 (July-Aug. 1951)

S15 Shirn, C. A. and Smyth, D. M., "Some Failure Mechanisms at Insulator-Conductor Junctions", Physics of Failure in Electronics, Volume 2, Goldberg, N. F. and Vaccaro, J., Eds., RADC Series in Reliability, AD434329 (1964) pp. 154-162

S16 Smith, R. W. and Rose, A., "Space-Charge-Limited Current in Single Crystals of Cadmium Sulfide", Phys. Rev. 97 1531 (1955)

S17 Smolenskii, G. A., Isupov, V. A. and Agranovskaia, A. I., "High Dielectric Constants of Niobates and Tantalates of Divalent Metals" (English trans.), Sov. Phys.-Doklady 1 300-302 (1957)

S18 Subbarao, E. C. and Hrizo, J., "Solid Solutions Based on Ferroelectric $PbNb_2O_6$", J. Amer. Ceram. Soc. 45 (11) 528-531 (Nov. 1962)

S19 Subbarao, E. C., "A Family of Ferroelectric Bismuth Compounds", J. Phys. Chem. Solids 23 665-676 (1962)

S20 Subbarao, E. C., "Ferroelectricity in $Bi_4Ti_3O_{12}$ and Its Solid Solutions", Phys. Rev. 122 (3) 804-807 (May 1961)

S21 Subbarao, E. C., "Ferroelectricity in Mixed Bismuth Oxides with Layer-Type Structure", J. Chem. Phys. 34 (2) 695-696 (1961)

S22 Subbarao, E. C., "X-ray Study of Phase Transitions in Ferroelectric $PbNb_2O_6$ and Related Materials", J. Amer. Ceram. Soc. 43 (9) 439-442 (Sept. 1960)

S23 Subbarao, E. C., "Studies on Lead Titanate Ceramics Containing Niobium or Tantalum", J. Amer. Ceram. Soc. 43 (3) 119-122 (Mar. 1960)

S24 Subbarao, E. C. and Shirane, G., "Dielectric and Structural Studies in the Systems $Ba(Ti,Nb)O_3$ and $Ba(Ti,Ta)O_3$", J. Amer. Ceram. Soc. 42 (6) 279-284 (June 1959)

S25 Slater, J. C., "The Lorentz Correction in Barium Titanate", Phys. Rev. 78 (6) 748-761 (1950)

S26 Smolenskii, G. A., "On the Occurrence of Spontaneous Polarization in Crystals", Zh. Tekh. Fiz. 27 1778-1783 (1957); (English trans.) Sov. Phys.-Technical Physics 2 1652-1656 (1957)

S27 Smolenskii, G. A., "Survey of Some of the Results of Recent Investigations of Ferroelectric Materials", Izvest. Akad. Nauk SSSR, Ser. Fiz. 21 235-265 (1957)

S28 Szigeti, B., "Polarizability and Dielectric Constant of Ionic Crystals", Trans. Faraday Soc. 45 155-166 (1949)

S29 Szigeti, B., "Compressibility and Absorption Frequency of Ionic Crystals", Proc. Roy. Soc. (London) A204 51-62 (1950)

S30 Silverman, B. D. and Joseph, R. I., "Temperature Dependence of the Dielectric Constant of Paraelectric Materials", Phys. Rev. 129 (5) 2062-2068 (1963)

S31 Subbarao, E. C., McQuarrie, M. C. and Buessem, W. R., "Domain Effects in Polycrystalline Barium Titanate", J. Appl. Phys. 28 (10) 1194-1200 (1957)

T1 Tennery, V. J., "Defect Structure Ferroelectrics", Technical Report No. 1, ONR Contract Nonr 1834 (38), University of Illinois (20 June 1964)

T2 Tien, T.-Y., "X-ray and Dielectric Studies of Strontium Titanate Solid Solutions", Ph.D. Thesis, The Pennsylvania State University (Dec. 1965)

T3 Tien, T.-Y, Subbarao, E. C. and Hrizo, J., "Ferroelectric Phase Transitions in the System $PbTiO_3$-$KNbO_3$", J. Amer. Ceram. Soc. 45 (12) 572-575 (Dec. 1962)

T4 Tomashpal'skii, Yu. Ya., Venevtsev, Yu. N. and Beznozdrev, V. N., "Ferroelectricity and Magnetism in Ferroelectric-Ferromagnetic Systems", Fiz. Tverd. Tela 7 (9) 2763-2767 (Sept. 1965); (English trans.) Sov. Phys.-Solid State 7 (9) 2235-2239 (Mar. 1966)

T5 Terhune, N. A. and Charlton, J. J., Personal Communication (1965)

T6 Terhune, N. A. and Charlton, J. J., "Some Effects of the Replacement of Lattice Elements by Foreign Ions in $BaTiO_3$ and PZT", Fall Meeting, Amer. Ceram. Soc. (Sept. 1957)

T7 Tien, T.-Y., and Carlson, W. G., "Effect of Additives on Properties of Lead Titanate", J. Amer. Ceram. Soc. 45 (12) 567-571 (Dec. 1962)

T8 Toulis, W. J., "Electromechanical Coupling and Composite Transducers", J. Acoust. Soc. America 35 (1) 74 (Jan. 1963)

T9 Triebwasser, S. F., "Ferroelectric Materials", Modern Materials; Advances in Development and Applications. Volume 3, Hausner, H. H., Ed., Academic Press, N. Y. (1960)

T10 Triebwasser, S. F., "Free Energy, Internal Fields and Ionic Polarizabilities in $BaTiO_3$", J. Phys. Chem. Solids 3 53-62 (1957)

T11 Tagaki, Y., "Ferroelectricity and Antiferroelectricity of Some Ionic Crystals", Proc. Intern. Conf. Theor. Phys. Kyoto and Tokyo, 824-836 (1953)

T12 Texas Instruments Co. (prepared by)"Solid-State Techniques for Modulation and Demodulation of Optical Waves", Fifth Quarterly Progress Report, Contract No. DA 36-039-AMC-03250(E), AD457311 (1 July 1964 - 30 Sept. 1964)

V1 von Ardenne, M., Schiller, S. and Heisig, U., "Automated Electron Beams Process Thin-Film Components", Electronics 39 (5) 110-115 (7 Mar. 1966)

V2 von Hippel, A., "Ferroelectricity, Domain Structure and Phase Transitions of $BaTiO_3$", Revs. Modern Phys. 22 221 (1950)

W1 Wilcox, D. L. and Cook, R. L., "Dielectric Behavior in the Systems $PbHfO_3$-$BaHfO_3$ and $PbHfO_3$-$SrHfO_3$", J. Amer. Ceram. Soc. 46 (7) 343-348 (July 1963)

W2 Wainer, E. and Wentworth, C., "Niobate and Tantalate Dielectrics", J. Amer. Ceram. Soc. 35 (8) 207-214 (Aug. 1952)

W3 Wagner, C., "Proceedings of the Seventh Meeting of the International Conference on Electrochemical Thermodynamics and Kinetics, 1955", Butterworth's Scientific Publications, Ltd., London (1957)

W4 Weyl, W. and Terhune, N., "Crystal Chemistry Applied to Foreign Atoms in Titanate Ceramics", Ceramic Age 62 (2) 22-27, 40-41 (1953)

W5 White, D. L., "The Depletion Layer Transducer", IRE Trans. on Ultrasonics Engr. UE-9 (1) (July 1962)

W6 Williams, A. L. W., "Method of Polarizing Ceramic Transducers", U.S. Patent 2,646,610 (July 28, 1953)

Y1 Yu, T. S., "Ferroelectric Tape Recording and Reproducing Processes", Report No. 11, Cont. Nonr 1224 (22) NR 049-122, Communication Sciences Lab., Univ. of Mich., AD 608119 (June 1964)

REFERENCES (added in proof)

A7 Abrahams, S. C., Reddy, J. M. and Bernstein, J. L.,"Ferroelectric Lithium Niobate. 3. Single Crystal X-ray Diffraction Study at 24°C", J. Phys. Chem. Solids 27 997-1012 (1966)

A8 Abrahams, S. C., Levinstein, H. J. and Reddy, J. M., "Ferroelectric Lithium Niobate. 5. Polycrystal X-ray Diffraction Study Between 24° and 1200°C", J. Phys. Chem. Solids 27 1019-1026 (1966)

C13 Cirkler, W. and Lobl, H., "Method for Making a Barrier Layer Capacitor", U.S. Patent 3,124,478 (July 18, 1960)

C14 Cirkler, W. and Lobl, H., "Ceramic Blocking Layer Capacitor", U.S. Patent 3,157,835 (Nov. 17, 1964)

E4 Emtage, P. R., Tantraporn, W., "Schottky Emission Through Thin Insulating Films", Phys. Rev. Letters 8 (7) 267-268 (1962)

M26 Martin, H. J., Die Ferroelektrika, Akademische Verlagsgesellschaft, Leipzig (1964)

VIII. RECOMMENDATIONS FOR FURTHER STUDY

Very little information is reported on the study of ferroelectrics subjected to microwave frequencies. It is suggested that a study to determine the properties of ferroelectrics at various microwave frequencies be made.

A problem in using ferroelectric transducers is to determine the degree of poling necessary to produce the desired piezoelectric properties. It would be helpful to be able to determine the degree of poling during the poling process, for example, by measuring the broad band noise. By this it is implied that the noise density may be related to the rate of domain switching and could conceivably be used as a monitor during the poling process.

Responsibility for content and wording in this report is distributed as follows:

Gruver - I, III, V B
Buessem - II, IV, V C
Dickey - V A, VI
Anderson - V B

Unclassified
Security Classification

DOCUMENT CONTROL DATA - R&D

(Security classification of title, body of abstract and indexing annotation must be entered when the overall report is classified)

1. ORIGINATING ACTIVITY (Corporate author)
Linden Laboratories, Inc.
P. O. Box 920
State College, Pa. 16801

2a. REPORT SECURITY CLASSIFICATION
Unclassified

2b GROUP

3. REPORT TITLE

"STATE-OF-THE-ART REVIEW ON FERROELECTRIC CERAMIC MATERIALS"

4. DESCRIPTIVE NOTES (Type of report and inclusive dates)
Final Technical Report (February 1965-May 1966)

5. AUTHOR(S) (Last name, first name, initial)
Gruver, R. M.
Buessem, W. R. Anderson, J. W.
Dickey, C. W.

6. REPORT DATE	7a. TOTAL NO. OF PAGES	7b. NO. OF REFS
May 1966	223	277

8a. CONTRACT OR GRANT NO.	9a. ORIGINATOR'S REPORT NUMBER(S)
AF 33(615)-2432	AFML-TR-66-164
b. PROJECT NO.	
c.	9b. OTHER REPORT NO(S) (Any other numbers that may be assigned this report)
d.	None

10. AVAILABILITY/LIMITATION NOTICES Qualified requesters may obtain copies of this report from DDC. This document is subject to special export controls and each transmittal to foreign nationals may be made only with prior approval of the Applications Division (MAA), Air Force Materials Lab., Wright-Patterson Air Force Base, Ohio

11. SUPPLEMENTARY NOTES

12. SPONSORING MILITARY ACTIVITY
Air Force Materials Laboratory
Research and Technology Division
Wright-Patterson AFB, Ohio

13. ABSTRACT This report presents a survey of ceramic systems exhibiting ferroelectricity together with fundamental data on ferroelectric crystals. A review of the basic reasons for the occurrence of ferroelectricity as well as for the dependence of the ferroelectric transitions and the properties of ferroelectric materials on the intensive parameters follows. The dielectric, piezoelectric and elastic properties of experimental and commercially available ceramic ferroelectrics are listed. The interpretation of dielectric properties of ceramic ferroelectrics as modified single-crystal properties includes a discussion of dielectric constant, stability, non-linear behavior and domain effects. Techniques for poling and special forming methods for ferroelectrics are described followed by a discussion of the linear and non-linear devices employing ferroelectric materials.

DD FORM 1 JAN 64 1473

Unclassified
Security Classification

Unclassified
Security Classification

14. KEY WORDS	LINK A		LINK B		LINK C	
	ROLE	WT	ROLE	WT	ROLE	WT
Ferroelectric Ceramic Materials Theory of Ceramic Ferroelectrics Piezoelectric and Dielectric Properties of Ceramic Ferroelectrics Interpretation of Dielectric Properties of Ceramic Ferroelectrics Thin Film Ferroelectrics Devitrified Ceramic Ferroelectrics Poling Techniques for Ferroelectric Ceramics Ferroelectric Devices						

INSTRUCTIONS

1. ORIGINATING ACTIVITY: Enter the name and address of the contractor, subcontractor, grantee, Department of Defense activity or other organization *(corporate author)* issuing the report.

2a. REPORT SECURITY CLASSIFICATION: Enter the overall security classification of the report. Indicate whether "Restricted Data" is included. Marking is to be in accordance with appropriate security regulations.

2b. GROUP: Automatic downgrading is specified in DoD Directive 5200.10 and Armed Forces Industrial Manual. Enter the group number. Also, when applicable, show that optional markings have been used for Group 3 and Group 4 as authorized.

3. REPORT TITLE: Enter the complete report title in all capital letters. Titles in all cases should be unclassified. If a meaningful title cannot be selected without classification, show title classification in all capitals in parenthesis immediately following the title.

4. DESCRIPTIVE NOTES: If appropriate, enter the type of report, e.g., interim, progress, summary, annual, or final. Give the inclusive dates when a specific reporting period is covered.

5. AUTHOR(S): Enter the name(s) of author(s) as shown on or in the report. Enter last name, first name, middle initial. If military, show rank and branch of service. The name of the principal author is an absolute minimum requirement.

6. REPORT DATE: Enter the date of the report as day, month, year, or month, year. If more than one date appears on the report, use date of publication.

7a. TOTAL NUMBER OF PAGES: The total page count should follow normal pagination procedures, i.e., enter the number of pages containing information.

7b. NUMBER OF REFERENCES: Enter the total number of references cited in the report.

8a. CONTRACT OR GRANT NUMBER: If appropriate, enter the applicable number of the contract or grant under which the report was written.

8b, 8c, & 8d. PROJECT NUMBER: Enter the appropriate military department identification, such as project number, subproject number, system numbers, task number, etc.

9a. ORIGINATOR'S REPORT NUMBER(S): Enter the official report number by which the document will be identified and controlled by the originating activity. This number must be unique to this report.

9b. OTHER REPORT NUMBER(S): If the report has been assigned any other report numbers *(either by the originator or by the sponsor)*, also enter this number(s).

10. AVAILABILITY/LIMITATION NOTICES: Enter any limitations on further dissemination of the report, other than those imposed by security classification, using standard statements such as:

(1) "Qualified requesters may obtain copies of this report from DDC."

(2) "Foreign announcement and dissemination of this report by DDC is not authorized."

(3) "U. S. Government agencies may obtain copies of this report directly from DDC. Other qualified DDC users shall request through

_____."

(4) "U. S. military agencies may obtain copies of this report directly from DDC. Other qualified users shall request through

_____."

(5) "All distribution of this report is controlled. Qualified DDC users shall request through

_____."

If the report has been furnished to the Office of Technical Services, Department of Commerce, for sale to the public, indicate this fact and enter the price, if known.

11. SUPPLEMENTARY NOTES: Use for additional explanatory notes.

12. SPONSORING MILITARY ACTIVITY: Enter the name of the departmental project office or laboratory sponsoring *(paying for)* the research and development. Include address.

13. ABSTRACT: Enter an abstract giving a brief and factual summary of the document indicative of the report, even though it may also appear elsewhere in the body of the technical report. If additional space is required, a continuation sheet shall be attached.

It is highly desirable that the abstract of classified reports be unclassified. Each paragraph of the abstract shall end with an indication of the military security classification of the information in the paragraph, represented as *(TS), (S), (C), or (U)*.

There is no limitation on the length of the abstract. However, the suggested length is from 150 to 225 words.

14. KEY WORDS: Key words are technically meaningful terms or short phrases that characterize a report and may be used as index entries for cataloging the report. Key words must be selected so that no security classification is required. Identifiers, such as equipment model designation, trade name, military project code name, geographic location, may be used as key words but will be followed by an indication of technical context. The assignment of links, rules, and weights is optional.

Unclassified
Security Classification